From 3D elastic and poroelastic media to 2D ones : asymptotic modeling and applications

Bing He

THÈSE DE DOCTORAT DE L'UNIVERSITÉ GUSTAVE EIFFEL

École doctorale Sciences, Ingénierie et Environnement

présentée par

Bing HE

pour obtenir le grade de

DOCTEUR DE L'UNIVERSITÉ GUSTAVE EIFFEL

Sujet de la thèse

From 3D elastic and poroelastic media to 2D ones: asymptotic modeling and applications

Soutenue le 2 octobre 2024 devant le jury composé de

Rapporteur	Rodrigue DESMORAT	Professeur Université Paris-Saclay
Rapporteur	Jean LERBET	Professeur Université Paris-Saclay
Examinateur	Xiaojing GONG	Professeure Université de Technologie Tarbes Occitanie Pyrénées
Examinateur	Hamid ZAHROUNI	Professeur Université de Lorraine
Directeur de thèse	Qi-Chang HE	Professeur Université Gustave Eiffel
Co-directeur de thèse	Hung LE QUANG	Maître de conférences Université Gustave Eiffel

Abstract

Three-dimension (3D) continuum media with one dimension being much smaller than the two others are omnipresent and play an important role in engineering, including, for example, plates, shells, coatings and thin interphases in civil, mechanical and materials engineerings. One problem of primary importance and lasting interest in mechanics is that of replacing a 3D continuum medium of weak thickness by a two-dimension (2D) continuum medium of null thickness which is equivalent to the 3D one to within an acceptable error. In spite of the fact that a great number of works dedicated to this problem have been reported, the present thesis aims to propose a novel approach which is capable of treating it in a unified coordinate-free way and whose applications lead to new results.

To achieve the aforementioned objective, a shell-like continuum medium of uniform thickness is first considered. After recalling the main elements of a coordinate-free differential geometry theory and the Hadamard relations for a curved interface, a scalar or a vector field defined over the 3D shell-like continuum medium in question is then expressed in terms of the relevant 2D field defined on its middle surface by using the Taylor expansion with any desired degree of accuracy in the sense of asymptotic analysis. When transport phenomena and elasticity are concerned, the Taylor expansions in terms of the corresponding fields on the middle surface are detailed in a coordinate-free way, making appear naturally some important orthogonal projection operators. When elastic plates are concerned, using the obtained Taylor expansion expression of the displacement vector field and a variational principle, a general plate model is derived, including the well-known Mindlin plate model as a particular one and holding for any elastic symmetry. When an elastic laminate plate is considered, the orthogonal projection operators are employed to homogenizing it and the simple Kirchhoff-Love plate model applied to the homogenized plate gives the results comparable to those provided by the widely used complicated zigzag model. Finally, a general imperfect poroelastic interface model is established by using the Taylor ex-

pansion technique together with some appropriate orthogonal projection operators. This general model is numerically implemented by the extended finite element method and applied to the homogenization of poroelastic composites.

Key words : Shell; Plate; Interphase; Imperfect interface; Coordinate-free differential geometry; Asymptotic analysis; Homogenization; XFEM.

Résumé

Les milieux continus tridimensionnel (3D) avec une dimension beaucoup plus petite que les deux autres sont omniprésents et jouent un rôle important dans l'ingénierie, y compris, par exemple, des plaques, des coques, des revêtements et des interphases minces en génie civil, en génie mécanique et en génie des matériaux. Un problème de première importance et de grand intérêt en mécanique est celui de remplacer un milieu continu 3D d'une faible épaisseur par un milieu continu bidimensionnel (2D) d'épaisseur nulle qui est équivalent au milieu 3D à une erreur acceptable près. Malgré le fait qu'un grand nombre de travaux dédiés à ce problème ont été rapportés, la présente thèse a pour objectif de proposer une approche novatrice qui est capable de traiter le problème d'une façon unifiée et indépendante de tout système des coordonnées et dont les applications conduisent à de nouveaux résultats.

Pour atteindre l'objectif susmentionné, un milieu continu en forme d'une coque d'épaisseur uniforme est d'abord considéré. Après avoir rappelé les éléments principaux d'une théorie de géométrie différentielle sans utiliser un système de coordonnées et les relations Hadamard pour une interface courbée, un champ scalaire ou vectoriel défini dans la coque en question est ensuite exprimé en fonction du champ 2D correspondant défini sur sa surface médiane en utilisant le développement de Taylor avec un degré de précision quelconque au sens de l'analyse asymptotique. Lorsque les phénomènes de transport et d'élasticité sont concernés, les développements de Taylor en fonction des champs correspondants sur la surface médiane sont détaillés sans utiliser un système de coordonnées, faisant apparaître naturellement certains opérateurs de projection orthogonaux importants. Quand les plaques élastiques sont en jeu, en utilisant l'expression du développement de Taylor du champ des déplacements et en faisant appel à un principe variationnel, un modèle général de plaques est dérivé, incluant le modèle de plaques de Mindlin comme un cas particulier et étant valable pour toute symétrie élastique. Lorsqu'une plaque stratifiée élastique est en question, les opérateurs de projection orthogonaux sont utilisés pour

son homogénéisation et le simple modèle de plaques de Kirchhoff-Love appliqué à la plaque homogénéisée donne les résultats comparables à ceux fournis par le modèle zigzag compliqué largement utilisé. Enfin, un modèle général d'interface poroélastique imparfaite est établi en utilisant la technique du développement de Taylor et certains opérateurs de projection orthogonaux appropriés. Ce modèle général est implémenté numériquement par la méthode d'éléments finis étendus et appliqué à l'homogénéisation des composites poroélastiques.

Mots clés : Coque; Plaque; Interphase; Interface imparfaite; Géométrie différentielle intrinsèque; Analyse asymptotique; Homogénéisation; XFEM.

Acknowledgement

The journey through my Ph.D. has swiftly passed in what feels like no time at all. Reflecting on these three years, I am profoundly aware of the immense support I have received from various individuals, without whom the completion of this thesis would have been impossible.

Firstly, I extend my heartfelt thanks to Mr. Rodrigue DESMORAT and Mr. Jean LERBET for their roles as my thesis reviewers. Their valuable insights and constructive feedback have significantly contributed to the refinement of my research. I am also grateful to my jury members, Ms. Xiaojing GONG and Mr. Hamid ZAHROUNI , for their willingness to participate in my defense and for their thorough assessment of my work.

I am deeply indebted to my thesis advisor, Mr. Qi-Chang HE. His remarkable commitment to research and academic excellence has been an ongoing source of inspiration. His patience and enthusiasm have greatly supported my growth throughout this process. Additionally, I would like to thank my co-supervisor, Mr. Hung LE QUANG, for his meticulous guidance and patient assistance, which have been crucial in overcoming various obstacles.

My gratitude also goes to my fellow colleagues who have shared this journey with me. Their engaging discussions and unwavering support have been incredibly motivating and instrumental in my progress. The MSME laboratory has felt like a close-knit community, where the collaborative spirit and supportive atmosphere have been essential to my success. The time spent here will always be a cherished part of my doctoral experience.

Lastly, I want to express my appreciation to my family and friends. Their emotional support has provided me with strength during times of uncertainty. I am especially thankful to my parents for instilling in me an appreciation for life itself, which is a gift beyond measure.

Contents

Notations

• Tensorial Notations

a	scalar,	$\cdot$	contracted product of order one,
$\mathbf{a}$	vector,	$:$	contracted product of order two,
$\mathbf{A}$	second-order tensor,	$\otimes$	tensor product,
$\mathfrak{A}$	third-order tensor,	∇	gradient operator,
$\mathbb{A}$	fourth-order tensor,	div	divergence operator,
$\mathbf{I}$	identity tensor of order two,	$\mathbf{P}$	tangential projection operator,
$\mathbb{I}$	identity tensor of order four,	$\mathbf{P}^{\perp}$	normal projection operator,
δ_{ij}	Kronecker symbol,	$\mathbf{n}$	unit normal vector,
$\mathbf{W}$	Weingarten tensor,	$\mathbf{t}$	unit tangent vector,
$\mathbb{P}$	fourth-order tangential projection operator,	$\mathbb{P}^{\perp}$	fourth-order normal projection operator.

• Tensor Calculations

$$\mathbf{a}\cdot\mathbf{b} = a_i b_i, \qquad (\mathbf{A}\mathbf{b})_i = A_{ij} b_j, \qquad (\mathbf{A}\mathbf{B})_{ij} = A_{ik} B_{kj},$$

$$\mathbf{A}:\mathbf{B} = A_{ij} B_{ji}, \qquad (\mathbb{A}:\mathbf{B}) = A_{ijkl} B_{lk}, \qquad (\mathbb{A}\mathbb{B})_{ijkl} = A_{ijmn} B_{nmkl},$$

$$(\mathbf{a}\otimes\mathbf{b})_{ij} = a_i b_j, \qquad (\mathbf{A}\otimes\mathbf{B})_{ijkl} = A_{ij} B_{kl}, \qquad (\mathbb{A}\diamond\mathbf{B})_{ik} = A_{ijkl} B_{jl},$$

$$(\mathbf{A}\overline{\otimes}\mathbf{a})_{ijk} = A_{ik} a_j, \qquad (\mathbf{A}\underline{\otimes}\mathbf{a})_{ijk} = A_{jk} a_i, \qquad (\mathbf{A}\overline{\underline{\otimes}}\mathbf{a})_{ijk} = \tfrac{1}{2}(A_{ik} a_j + A_{ik} a_i),$$

$$(\mathbf{A}\overline{\otimes}\mathbf{B})_{ijkl} = A_{ik} B_{jl}, \qquad (\mathbf{A}\underline{\otimes}\mathbf{B})_{ijkl} = A_{il} B_{jk}, \qquad (\mathbf{A}\overline{\underline{\otimes}}\mathbf{B})_{ijkl} = \tfrac{1}{2}(A_{ik} B_{jl} + A_{il} B_{jk}).$$

• Material Parameters

$\mathbb{C}$	stiffness tensor,	$\mathbf{K}$	permeability tensor,
$\mathbb{S}$	compliance tensor,	K	permeability,
$\lambda,\ \mu$	Lam*é* constants,	$\boldsymbol{\theta}$	Biot-Willis tensor,
$\mathbb{C}^*$	homogenized stiffness tensor,	$\boldsymbol{\theta}^*$	homogenized Biot-Willis tensor.

• Mathematical notations

$T_{\boldsymbol{x}}\mathrm{S}$	tangent space of the surface S at the point $\boldsymbol{x}$,
$N_{\boldsymbol{x}}\mathrm{S}$	normal subspace of the surface S at the point $\boldsymbol{x}$,
$\delta(\cdot)_{\mathbf{v}}(\boldsymbol{x})$	directional derivative along direction $\mathbf{v}$,
$\nabla_S(\cdot)$	tangential gradient,
$\nabla_N(\cdot)$	normal gradient,
$\mathrm{div}_S(\cdot)$	tangential divergence,
$\mathrm{div}_N(\cdot)$	normal divergence,
$\triangle_S(\cdot)$	surface Laplacian operator,
$\langle\cdot\rangle$	volume average operator,
$\nabla_{\mathbf{n}}(\cdot)$	directional derivative along normal vector $\mathbf{n}$.

• Additional notations

$\mathbf{u}$	displacement vector,
ε	strain tensor,
σ	stress tensor,
$\mathbf{w}$	velocity vector,
p	pressure.

General Introduction

The Background and Significance

In a three-dimensional (3D) Euclidean space $\mathbb{R}^3$, when one dimension of a structure is significantly smaller than the two others, this dimension is typically referred to as its thickness, and the structure in question can be modeled as a plate-like or shell-like structure. Such structures are fundamental elements in civil, mechanical and aerospace engineerings [115, 130, 135, 5] [130, 4, 90, 19]. They are also involved in others fields like medicine, biology [137, 32, 91], and nanotechnology [131, 107, 47].

In the analysis of plate-like and shell-like structures, the concept of the midplane or midsurface is crucial. The midplane or midsurface is an imaginary plane or surface that divides the thickness h of a plate-like or shell-like structure, running parallel to its surfaces (see Figure 2.2). It is commonly known as the middle surface or median plane of the structure. Due to the weak thickness of a plate-like or shell-like structure, the distribution of the internal physical fields can be accurately described by the relevant physical fields defined on the middle place or surface. This simplification effectively transforms the originally complex three-dimensional partial differential equations into a two-dimensional framework, significantly streamlining the mathematical representation and computational complexity. It importantly retains essential details about the structure's geometry and mechanical responses, proving especially effective for analyzing thin-walled structures and composite material shell-like configurations.

When focusing on the distribution of the internal fields and the overall mechanical behavior of the structure, with an emphasis on its geometric properties and global deformations, it simplifies to the plate and shell theory. In specific terms, a plate theory is employed when the mid-surface starts with a flat configuration [114, 118, 134, 113], whereas shell theory is utilized when the mid-surface begins with curvature, reflecting structures with initially curved

mid-surfaces [114, 134, 113, 5, 28]. When emphasizing the interaction between a shell-like structure and surrounding materials with diverse properties, or when assessing its mechanical influence on the overall structure, the analysis is streamlined to interface theory. For instance, in composite materials composed of a matrix and particle or fiber reinforcements, the connection between the matrix and the heterogeneous materials (particles or fibers) is typically maintained through an extremely thin transition zone, which can be effectively modeled as an imperfect interface [48, 145, 117, 147, 83, 84]. By simplifying complex three-dimensional problems into two-dimensional analyses, these theories provide critical insights and practical solutions for ensuring structural integrity and performance. Therefore, it is essential to strengthen the theoretical foundations of the relevant theories to ensure accurate modeling and analysis in engineering practice.

Overview of Plate Theories

The development of plate theories spans centuries, starting with Euler's pioneering work in 1776 [39] on plate vibrations. Germain and Lagrange made significant contributions by formulating the Germain-Lagrange plate equation, with Lagrange [81] correcting Germain's initial formulations in 1813 [44]. Cauchy [20] and Poisson [111] further advanced the theory in the early 19th century by applying elasticity principles and deriving the governing differential equations for plate deflections. These foundational contributions laid the groundwork for modern plate theories.

In 1850, Kirchhoff [78] introduced fundamental hypotheses and energy principles that revolutionized plate bending theory. His work clarified the conditions for static equilibrium and introduced the concept of Kirchhoff's hypotheses, simplifying the analysis of plate behavior. These hypotheses enabled Love [97] to establish the thin plate theory for homogeneous and isotropic plates, commonly referred to as the Kirchhoff-Love plate theory. Throughout the 19th and early 20th centuries, Kelvin and Tait [76], Timoshenko [127], and others [67, 70, 75, 136] expanded the theory to include diverse loading conditions and material properties, solidifying plate theory as essential in structural engineering and physics.

Reissner [115] introduced a new theory in 1945, known as Reissner plate theory or Reissner-Mindlin [98] plate theory. This theory incorporates additional shear deformations and derives the thick plate model using the principle of minimum complementary energy. This approach

enables a more accurate description of the plate's bending behavior and shear stress distribution, particularly in addressing real-world applications extensively used in engineering practice. Timoshenko's [130] studies on large deformations expanded the scope of plate theory, accommodating complex real-world scenarios and laying the groundwork for advanced numerical methods. This summary outlines the historical evolution and significant contributions to plate theory. For deeper insights, readers are directed to specialized monographs [128, 133] on the topic.

Plate modeling methods can be broadly categorized into two approaches: axiomatic and asymptotic [118, 3]. Axiomatic methods start with assumptions about the three-dimensional displacement field of the plate and derive models using minimum potential energy principles, constrained by challenges in accurately guessing microstructural field distributions. Asymptotic methods follow axiomatic approaches and introduce a scaling parameter, typically the plate thickness-to-span ratio, which tends to zero in the equations. These methods, employing asymptotic expansions and Γ-convergence, facilitate model derivation, validate axiomatic approaches post facto, and underpin convergence results. However, they are limited by potential deviations from asymptotic assumptions in practical scenarios, affecting model accuracy despite rapid convergence rates. Moreover, both methods face theoretical challenges when dealing with plates composed of materials exhibiting high degrees of anisotropy.

Overview of Laminated Plate Theories

Laminates are extensively utilized in a diverse range of industries owing to their exceptional mechanical properties and high strength-to-weight ratio [43]. However, the presence of transverse anisotropy in multilayered structures, influenced by factors such as layer orientation, arrangement, material properties, and processing conditions, leads to complex phenomena like the zigzag form of the displacement field and interfacial discontinuities in in-plane stresses, while ensuring transverse stress continuity to maintain system stability and equilibrium [16, 17, 19].

The mechanical properties of laminated composites are complex and challenging to fully understand and characterize, requiring a multidisciplinary approach. Pagano [108, 109] established analytical and three-dimensional elasticity solutions for laminates with isotropic or orthotropic layers subjected to cylindrical bending and pinned edges, providing reference standards for simpler laminates and serving as a basis for validating and comparing other methods, including numerical simulations and experimental measurements. However, despite some algorithmic im-

provements, the computational complexity of determining the unknowns in Pagano's solutions remains significant and prohibitive as the number of laminate layers increases [40]. Classical Plate Theory (CPT) [109, 40, 113, 6], based on Kirchhoff assumptions, is a widely used method for analyzing laminated composite plates, but it neglects shear deformation and transverse shear stresses, leading to inaccuracies for thicker laminates. To improve accuracy, refined plate theories, such as High-Order Shear Deformation Theories (HSDT) [96, 106, 74] and Zigzag theories [30, 103, 26], address these limitations by accounting for transverse shear deformation more accurately. HSDT incorporates higher-order terms in the shear deformation, while Zigzag theories capture the zigzag phenomenon observed in the in-plane displacement fields due to material heterogeneity across the laminate's thickness [17, 16, 30, 103, 26, 116, 86, 85, 18]. Despite providing more accurate results, these advanced theories come with increased computational complexity, especially as the number of layers increases [18].

Homogenization theory provides a macroscopic view of laminates by analyzing their microscopic constituents, offering a way to determine effective material properties for use in numerical simulations. This approach has been instrumental in deriving closed-form expressions for the effective properties of composite materials with complex microstructures, including elastic, dielectric, magnetic, piezoelectric, and magneto-electric properties [25, 88, 14, 140, 77, 46]. Research by Gu and He presents a comprehensive study on the effective properties of layered composites, utilizing homogenization methods to address linear uncoupled and coupled phenomena, graded properties, and the impact of stiffeners and softeners [49].

Overview of the Imperfect Interface

Composite materials consist typically of a matrix phase, an inclusion phase, and a transition layer. During manufacturing and service, the matrix and inclusion phases are often connected through a transition layer. The formation of the transition layer involves complex physical and chemical reactions, making its microscopic structure and physical properties markedly different from those of the surrounding material phases. Generally, the transition layer, which plays a critical role in load transfer, is one of the most vulnerable and essential components of composites. This transition layer is typically modeled as an imperfect interface [55, 104, 53, 66, 83, 48, 94, 117, 145] and influences the mechanical behavior of materials and structures. Particularly, with the advancement of nanotechnology, there has been a growing

interest in imperfect interfaces. This is attributed to the substantial ratio of interface (or surface) area to volume in nanoscale materials or structures. At this scale, the expansive interface and surface area in relation to the material volume result in heightened susceptibility to interface and surface effects. These effects exert a significant influence on the mechanical and functional behaviors exhibited by the materials or structures [35, 29, 142].

Despite a significant amount of research, the modeling of interfaces and surfaces and their impact on the mechanical and physical behavior of materials and structures remains a broadly open topic [2, 73]. Gurtin and Murdoch [55] utilized modern geometric concepts to construct a precise and concise theoretical framework, systematically investigating the kinematics, dynamics, and constitutive relations of material surfaces and interfaces based on modern continuum mechanics . This theory has undergone significant refinement and expansion by Gurtin, Murdoch, their collaborators [104, 53, 52, 21, 56, 54, 105], and other researchers (e.g., [125], [132], [141]), demonstrating its substantial utility in modeling interface and surface effects in nanoscale materials and structures.

An alternative method to systematically and rigorously model imperfect interfaces consists in using asymptotic analysis. Sanchez-Palencia [119], Pham-Huy, and Sanchez-Palencia [72] introduced this mathematical technique to establish the Kapitza interface thermal resistance model and the high thermal conductivity interface model. These models accurately represent discontinuous interface relationships present in thin transition layers between adjacent phases, characterized by either extremely low or high thermal conductivity. Subsequently, other researchers have further developed and expanded upon these models [15, 87, 79, 13, 42, 80, 45, 61, 62, 12, 9, 10, 11, 82, 83, 84]. Hashin [61, 62] established the equivalent imperfect interface model for transition layers with arbitrary conductivity or rigidity based on Taylor series expansions.

Gu and He [48] developed a unified and compact general imperfect interface model for analyzing coupled multifield phenomena, utilizing coordinate-free interfacial operators, Hadamard's relation (Hadamard, 1903), and Taylor expansion applied to a 3D curved thin interphase perfectly bonded to its two adjacent phases. This general imperfect interface model can be applied to transition layers with arbitrary electrical conductivity and stiffness, and in extreme cases, it can degenerate into widely used spring imperfect interface model [8, 1, 58, 59, 60, 62, 112] and membrane-type imperfect interface model [122, 121, 120, 34, 36, 31, 37, 22, 23, 24, 82, 83, 84, 101, 101, 145, 144, 99, 102]. Gu et al. [51] derived the weak form of the boundary val-

ue problem for composite materials with general imperfect interfaces in the context of coupled multifield phenomena, marking a crucial step towards implementing imperfect interface effects within the Finite Element Method (FEM) [41] framework. Combining this approach with the XFEM [7, 126, 100] is a highly effective strategy for studying the influence of imperfect interfaces on the mechanical behavior of composite materials and structures. He, Gu and their collaborators have significantly contributed to advancing, expanding, and applying this methodology [145, 146, 143, 144, 147, 94, 117, 50, 138, 93, 95].

The Works of This Thesis

The objective of this thesis is threefold. Firstly, inspired by the works of Gurtin and Murdoch [55], He [66], Gu and He [48], and based on differential geometry, it aims to develop an effective asymptotic analysis method that is independent of any coordinate system for the analysis of plate-like and shell-like structures. Mathematically, by using Hadamard's relations, and some continuity and discontinuity conditions of physical quantities across perfect interfaces, this study introduces conjugate fields that remain continuous across interfaces of different materials. This approach facilitates an arbitrary-order expansion of scalar or vector functions at any point of shell-like structures, encompassing the intrinsic material properties of these structures. The capability to expand functions arbitrarily at any point underscores the method's broad applicability for modeling plate-like, shell-like structures and interfaces. Secondly, employing variational methods, this study formulates the general governing equations of motion and corresponding boundary conditions for plates in a unified and concise manner. Building upon an asymptotic analysis that is independent of any coordinate system and grounded in differential geometry methods, this approach ensures both mathematical rigor and clarity in its physical implications. By utilizing specific operators, particularly in the asymptotic expansion process, the method effectively addresses the challenges posed by high degrees of material anisotropy in plates and broadens its applicability to plates with interfaces of various shapes. This advancement significantly enhances the modeling capabilities of classical plate theory. Furthermore, by utilizing these operators, a homogenization method for laminated plates is established, and analytical expressions for the effective moduli of transversely isotropic materials are derived. Thirdly, a general imperfect interface model with an accuracy of $O(h^2)$ for poroelastic composite materials is established. This model is then integrated with the XFEM and the GSCS for numerical and

homogenization analyses.

This thesis is organized into two parts. The first part comprises two chapters that explore the coordinate-free transition from 3D media to 2D ones. In Chapter 1, the fundamental elements of differential geometry are discussed independently of specific curvilinear coordinate systems. Additionally, the Hadamard relations for scalar, vector, and tensor functions are summarized. In Chapter 2, by utilizing the groundwork laid out in Chapter 1, a shell is constructed and its geometric properties are analyzed. Taylor series expansions for scalar and vector fields within the shell are derived, enabling the modeling of plates, shells, and interfaces by transitioning from three-dimensional to two-dimensional frameworks. This chapter constitutes the central component of this thesis. The second part focuses on asymptotic modeling, analysis, and applications of plates and interfaces, spanning three chapters. In Chapter 3, building upon the Taylor expansions presented in Chapter 2, the governing equations of motion and boundary conditions for plates are derived using variational methods. This chapter initiates with a general case study and subsequently delves into significant special cases. Chapter 4 focuses on the theory of laminated plates, where a homogenization approach is established using operators introduced in Chapter 2 and the continuity relations discussed therein for perfect interfaces. Additionally, a comprehensive comparative analysis with other classical theories of laminated plates is conducted. In Chapter 5, a generalized model for imperfect interfaces in poroelastic composites is established, and several significant special cases are examined. Specifically, these include the extreme cases of the transition layer material and the scenarios where the constituent materials are isotropic. Numerical analysis and homogenization calculations of models containing spherical inclusions are conducted using XFEM and GSCS.

Part I

Coordinate-Free Reduction of a 3D Medium to a 2D One

Chapter 1

Fundamental Elements of Coordinate-Free Differential Geometry and Hadamard's Relations

The objective of this chapter is twofold. First, we introduce the main mathematical tools necessary for the study of surfaces or planar curves in an Euclidean space $\mathbb{R}^k$ of dimension k ($k = 2, 3$). This includes revisiting fundamental concepts from differential geometry, with a particular focus on defining surface differential operators that play a crucial role in subsequent chapters of this thesis. Second, Hadamard's relations are given and proved. Thes relations relations hold for any function which is continuous but piecewise continuously differentable over its definition domain. Following Gu and He [48], the fundamental elements of coordinate-free differential geometry and Hadamard's relations are presented in a coordinate-free way.

1.1 Definitions

Given a differentiable function $\phi : U \subset \mathbb{R}^k \to \mathbb{R}$ and $a \in \phi(U)$ as a regular value of ϕ, the set $\phi^{-1}(a)$ represents a regular surface (or regular planar curve) in $\mathbb{R}^k$ with $k = 2$ or 3 [33], defined as:

$$\mathrm{S} = \{\boldsymbol{x} \in U \mid \phi(\boldsymbol{x}) = a\}. \tag{1.1}$$

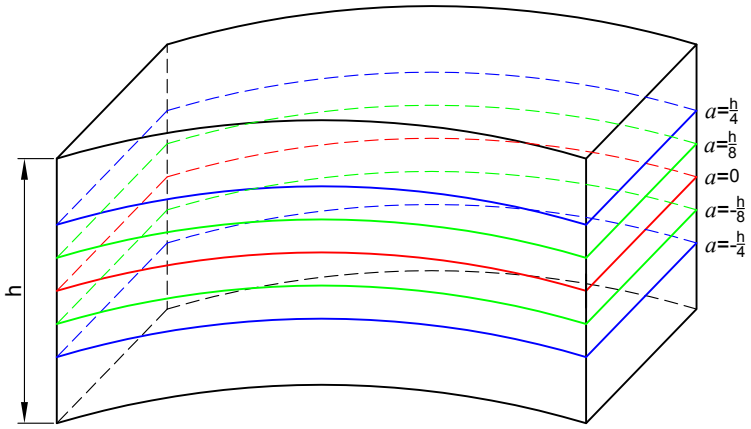

Figure 1.1: *Geometry of a series of stacked regular surfaces.*

Using this definition offers several significant advantages. Firstly, it enables a unified description of 1D and 2D interfacial problems. Secondly, it is directly linked to the "level set" numerical method, which is highly efficient in dealing with surfacial and interfacial phenomena. In subsequent chapters, we will use this numerical method. Thirdly, the continuous variation of the regular value a facilitates the dynamic evolution of S within a k-dimensional space. This dynamic evolution can characterize more intricate geometric objects, such as higher-dimensional manifolds, especially pertinent when $k = 3$. As shown in **Fig.** 1.1, when the regular value a changes continuously, S can represent different parallel surfaces. By varying these values systematically, it is possible to construct a detailed 3D structure.

1.1.1 Normal Vector and Tangent Space

Given definition (1.1), which defines a regular surface S in terms of a differentiable function ϕ and a regular value a, it follows that S is orientable. For a point $\boldsymbol{x} \in \mathrm{S}$, the unit vector $\mathbf{n}(x)$ normal to S can be defined as

$$\mathbf{n}(\boldsymbol{x}) = \frac{\nabla\phi(\boldsymbol{x})}{\| \nabla\phi(\boldsymbol{x}) \|}, \tag{1.2}$$

where $\nabla\phi(\boldsymbol{x})$ represents the gradient of φ at $\boldsymbol{x}$, and $\| \cdot \|$ denotes the Euclidean norm. The set of all tangent vectors to the surface S at a point $\boldsymbol{x}$ forms a $(k-1)$-dimension vector subspace, which is referred to as the space tangent to the surface S at the point $\boldsymbol{x}$, denoted as $T_{\boldsymbol{x}}\mathrm{S}$. It is defined by

$$T_{\boldsymbol{x}}\mathrm{S} = \{\mathbf{t} \in \mathbb{R}^k \mid \mathbf{t} \cdot \mathbf{n}(\boldsymbol{x}) = 0\}. \tag{1.3}$$

In the case where S is a planar curve ($k = 2$), the tangent space $T_{\boldsymbol{x}}\mathrm{S}$ corresponds to the tangent line to S at $\boldsymbol{x}$. If S is a surface ($k = 3$), the tangent space $T_{\boldsymbol{x}}\mathrm{S}$ represents the tangent plane to S at $\boldsymbol{x}$. These two situations are illustrated in **Fig.** 1.2.

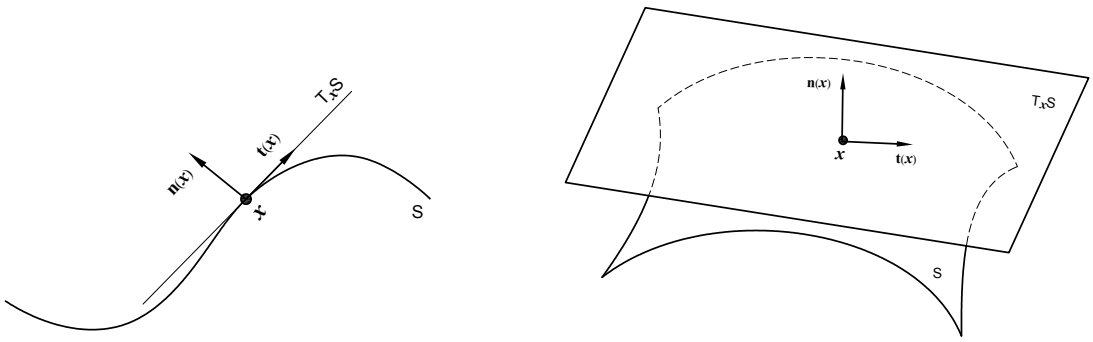

(a) (b)

Figure 1.2: *(a) A plane curve in* $\mathbb{R}^2$. *(b) A surface in* $\mathbb{R}^3$.

1.1.2 Orthogonal Projection Operators

Now, we introduce two complementary orthogonal projection operators defined at every point $\boldsymbol{x}$ on S as:

$$\mathbf{P}^{\perp}(\boldsymbol{x}) = \mathbf{n}(\boldsymbol{x}) \otimes \mathbf{n}(\boldsymbol{x}), \quad \mathbf{P}(\boldsymbol{x}) = \mathbf{I} - \mathbf{P}^{\perp}(\boldsymbol{x}), \tag{1.4}$$

where $\mathbf{I}$ is the second-order identity tensor. These two operators play a fundamental role in our studies. Geometrically, $\mathbf{P}(\boldsymbol{x})$ projects any vector $\mathbf{v} \in \mathbb{R}^k$ onto the tangent space $T_{\boldsymbol{x}}\mathrm{S}$ of S at $\boldsymbol{x}$, while $\mathbf{P}^{\perp}(\boldsymbol{x})$ projects $\mathbf{v}$ onto the normal subspace of S at $\boldsymbol{x}$, denoted as $N_{\boldsymbol{x}}\mathrm{S}$. Geometrically, by employing the two projection operators, a k-dimensional space $\mathbb{R}^k$ can be partitioned into $(k-1)$-dimensional tangent subspaces $T_{\boldsymbol{x}}\mathrm{S}$ and 1-dimensional normal subspace $N_{\boldsymbol{x}}\mathrm{S}$ of the surface S at the point $\boldsymbol{x}$, expressed as:

$$\mathbb{R}^k = T_{\boldsymbol{x}}\mathrm{S} \oplus N_{\boldsymbol{x}}\mathrm{S}, \tag{1.5}$$

where $\oplus$ signifies the direct sum, indicating that the subspaces $T_{\boldsymbol{x}}\mathrm{S}$ and $N_{\boldsymbol{x}}\mathrm{S}$ are mutually orthogonal complements. Therefore, any vector $\mathbf{v} \in \mathbb{R}^k$ can be uniquely decomposed into its tangential component $\mathbf{v}_T \in T_{\boldsymbol{x}}\mathrm{S}$ and its normal component $\mathbf{v}_N \in N_{\boldsymbol{x}}\mathrm{S}$:

$$\mathbf{v} = \mathbf{v}_N + \mathbf{v}_T, \quad \mathbf{v}_N = \mathbf{P}^{\perp}\mathbf{v}, \quad \mathbf{v}_T = \mathbf{P}\mathbf{v}. \tag{1.6}$$

The orthogonal projection operators $\mathbf{P}^{\perp}$ and $\mathbf{P}$ exhibit several fundamental properties. Firstly, they demonstrate idempotence and symmetry expressed by

$$(\mathbf{P}^{\perp})^2 = \mathbf{P}^{\perp}, \quad \mathbf{P}^2 = \mathbf{P}, \quad (\mathbf{P}^{\perp})^T = \mathbf{P}^{\perp}, \quad \mathbf{P}^T = \mathbf{P}. \tag{1.7}$$

These expressions indicate that successive projections of a vector onto the same subspace result in an unchanged projection, illustrating the idempotent nature of the operators, and highlight the symmetry inherent in orthogonal projection. In addition, the orthogonal projection operators also demonstrate orthogonal complementarity, as described by the equations:

$$\mathbf{P}^{\perp}\mathbf{P} = \mathbf{P}\mathbf{P}^{\perp} = \mathbf{0}, \quad \mathbf{P}^{\perp} + \mathbf{P} = \mathbf{I}. \tag{1.8}$$

This property emphasizes that the mutual exclusivity and completeness of projections onto a subspace and its orthogonal complementarity, thereby facilitating the comprehensive decomposition of vectors into components along orthogonal subspaces. These properties can be easily verified using the definitions in equation (1.4).

1.1.3 Tangential and Normal Gradients

Let φ be a scalar-valued field defined over U. Its variation at a point $\boldsymbol{x} \in U$ along any direction $\mathbf{v} \in \mathbb{R}^k$ is defined as

$$\delta\varphi_{\mathbf{v}}(\boldsymbol{x}) = \lim_{\tau \to 0} \frac{\varphi(\boldsymbol{x} + \tau\mathbf{v}) - \varphi(\boldsymbol{x})}{\tau}, \quad \tau \in \mathbb{R}. \tag{1.9}$$

If φ is at least once continuously differentiable, the directional derivative $\delta\varphi_{\mathbf{v}}(\boldsymbol{x})$ can be expressed as:

$$\delta\varphi_{\mathbf{v}}(\boldsymbol{x}) = \nabla\varphi(\boldsymbol{x}) \cdot \mathbf{v}, \tag{1.10}$$

where $\nabla\varphi$ denotes the gradient of φ. As previously mentioned, utilizing the two projection operators allows for the unique decomposition of any vector into its tangential and normal components. Therefore, equation (1.10) can be rewritten as:

$$\delta\varphi_{\mathbf{v}}(\boldsymbol{x}) = \nabla\varphi(\boldsymbol{x}) \cdot (\mathbf{P}^{\perp}\mathbf{v} + \mathbf{P}\mathbf{v}) = (\nabla\varphi(\boldsymbol{x}) \cdot \mathbf{P}^{\perp} + \nabla\varphi(\boldsymbol{x}) \cdot \mathbf{P}) \cdot \mathbf{v}. \tag{1.11}$$

To facilitate our analysis, let us define the tangential gradient of φ at point $\boldsymbol{x}$ as $\nabla_S\varphi(\boldsymbol{x})$ and the normal gradient as $\nabla_N\varphi(\boldsymbol{x})$:

$$\nabla_S\varphi(\boldsymbol{x}) = \nabla\varphi(\boldsymbol{x})\cdot\mathbf{P}, \tag{1.12a}$$

$$\nabla_N\varphi(\boldsymbol{x}) = \nabla\varphi(\boldsymbol{x})\cdot\mathbf{P}^{\perp}. \tag{1.12b}$$

Note that $\nabla_S\varphi(\boldsymbol{x})$ quantifies how the scalar field changes along the tangential direction to the surface (or curve) S at $\boldsymbol{x}$. In other words, $\nabla_S\varphi(\boldsymbol{x})$ captures the rate of change of φ in the direction parallel to S. The gradient $\nabla_S\varphi(\boldsymbol{x})$ also called the surface gradient or curve gradient depending on whether S is a surface or a curve. It is clear that $\nabla_S\varphi(\boldsymbol{x})$ is a surface field. On the other hand, $\nabla_N\varphi(\boldsymbol{x})$ characterizes how the scalar field varies along the normal direction to S at $\boldsymbol{x}$. Thus, $\nabla_N\varphi(\boldsymbol{x})$ measures the rate of change of φ along the direction perpendicular to the surface (or curve). Similarly, the gradient of a vector field $\mathbf{f}$ and a second-order tensor field $\mathbf{T}$ can be decomposed into the tangential gradient and the normal gradient. Precisely, we have

$$\begin{aligned}\nabla\mathbf{f} &= \nabla\,\mathbf{f}\cdot\mathbf{P} + \nabla\mathbf{f}\cdot\mathbf{P}^{\perp} = \nabla_S\mathbf{f} + \nabla_N\mathbf{f},\\ \nabla\mathbf{T} &= \nabla\mathbf{T}\cdot\mathbf{P} + \nabla\mathbf{T}\cdot\mathbf{P}^{\perp} = \nabla_S\mathbf{T} + \nabla_N\mathbf{T}.\end{aligned} \tag{1.13}$$

The operators ∇_S and ∇_N provide valuable insights into how fields behave with respect to the geometry of S, facilitating a detailed analysis of the spatial variations relative to the surface (or curve) direction and enhancing our comprehension of relevant physical phenomena.

1.1.4 Tangential and Normal Divergences

Similarly, the divergence of a vector field $\mathbf{f}$ or a second-order tensor field $\mathbf{T}$ can be decomposed into tangential and normal components defined on a manifold (surface or plane curve) S. These decompositions are essential for our studies as they provide a deeper understanding of the behavior of vector and tensor fields in relation to the manifold. Specifically, the tangential divergence measures the rate at which a vector or tensor field spreads out or converges within the tangent plane of S. This provides insight into how the field changes in a direction parallel to the surface. In a similar way, the normal divergence quantifies the rate of change of a field in the direction orthogonal to S, illustrating its behavior perpendicular to the surface. The divergences

of $\mathbf{f}$ and $\mathbf{T}$ can be decomposed as follows:

$$\begin{aligned} \mathrm{div}\mathbf{f} &= \nabla\mathbf{f}\colon \mathbf{I} = \nabla\mathbf{f}\colon (\mathbf{P}+\mathbf{P}^{\perp}), \\ \mathrm{div}\mathbf{T} &= \nabla\mathbf{T}\colon \mathbf{I} = \nabla\mathbf{T}\colon (\mathbf{P}+\mathbf{P}^{\perp}). \end{aligned} \tag{1.14}$$

Let $\mathrm{div}_S\mathbf{f}$ and $\mathrm{div}_N\mathbf{f}$ represent the tangential and normal divergences of $\mathbf{f}$ and let $\mathrm{div}_S\mathbf{T}$ and $\mathrm{div}_N\mathbf{T}$ denote the tangential and normal divergences of $\mathbf{T}$. Then, we have

$$\begin{aligned} \mathrm{div}_S\mathbf{f} &= \nabla\mathbf{f}\colon \mathbf{P}, \quad \mathrm{div}_N\mathbf{f} = \nabla\mathbf{f}\colon \mathbf{P}^{\perp}, \\ \mathrm{div}_S\mathbf{T} &= \nabla\mathbf{T}\colon \mathbf{P}, \quad \mathrm{div}_N\mathbf{T} = \nabla\mathbf{T}\colon \mathbf{P}^{\perp}. \end{aligned} \tag{1.15}$$

The tangential and normal divergences of a vector field $\mathbf{f}(\boldsymbol{x})$, are also related to its tangential and normal gradients by

$$\begin{aligned} \mathrm{div}_S\mathbf{f}(\boldsymbol{x}) &= \mathrm{tr}[\nabla_S\mathbf{f}(\boldsymbol{x})], \\ \mathrm{div}_N\mathbf{f}(\boldsymbol{x}) &= \mathrm{tr}[\nabla_N\mathbf{f}(\boldsymbol{x})], \end{aligned} \tag{1.16}$$

where $\mathrm{tr}[\cdot]$ represents the trace operation.

1.1.5 Tangential Derivatives of Composite Functions and Divergence Theorem

Carrying out the decomposition of gradient and divergence into tangential and normal components via orthogonal projection operators, the operations involving the tangential (or normal) gradient and tangential (or normal) divergence for composite functions of scalars, vectors, and tensors adhere to the same rules as those governing ordinary gradient and divergence operations [55, 104]. Employing tangential gradient and divergence as illustrative instances, we can rigorously derive the following formulas:

$$\nabla_S(\varphi\mathbf{f}) = \varphi\nabla_S\mathbf{f} + \mathbf{f}\otimes\nabla_S\varphi, \tag{1.17}$$

$$\mathrm{div}_S(\varphi \mathbf{f}) = \varphi \mathrm{div}_S \mathbf{f} + \mathbf{f} \cdot \nabla_S \varphi, \tag{1.18}$$

$$\mathrm{div}_S(\varphi \mathbf{T}) = \varphi \mathrm{div}_S \mathbf{T} + \mathbf{T} \cdot \nabla_S \varphi, \tag{1.19}$$

$$\mathrm{div}_S(\mathbf{f} \otimes \mathbf{g}) = \mathbf{f} \mathrm{div}_S \mathbf{g} + \nabla_S \mathbf{f} \cdot \mathbf{g}, \tag{1.20}$$

$$\mathrm{div}_S(\mathbf{T}\mathbf{f}) = \mathbf{f} \cdot \mathrm{div}_S \mathbf{T}^T + \mathbf{T} : \nabla_S \mathbf{f}, \tag{1.21}$$

where $\otimes$ signifies the tensor product and $\mathbf{g}$ represents a vector, while $(\cdot)^T$ denotes the transpose operation.

Let $\mathbf{g}$ denote a vector field defined on S, which is tangential such that $\mathbf{g}(\boldsymbol{x}) \cdot \mathbf{n}(\boldsymbol{x}) = 0$ for all $\boldsymbol{x} \in E$. Additionally, consider $\mathbf{T}$ as a tangential surface tensor field defined on S. Applying the divergence theorem to $\mathbf{g}$ and $\mathbf{T}$, we examine any subdomain $\Sigma \subseteq$ S with its boundary denoted by $\partial\Sigma$. Denoting by $\nu(\boldsymbol{x})$ the unit tangent vector to Σ but normal to $\partial\Sigma$ at $\boldsymbol{x} \in \partial\Sigma$, the divergence theorem applied to $\mathbf{g}$ and $\mathbf{T}$ is expressed as:

$$\int_{\partial\Sigma} \mathbf{g} \cdot \nu \, d\sigma = \int_{\Sigma} \mathrm{div}_S \mathbf{g} \, dS, \tag{1.22}$$

$$\int_{\partial\Sigma} \mathbf{T} \cdot \nu \, d\sigma = \int_{\Sigma} \mathrm{div}_S \mathbf{T} \, dS. \tag{1.23}$$

When considering Σ as a surface, each equation's left-hand side represents a line integral, capturing the field's flux across the boundary $\partial\Sigma$, while the right-hand side denotes a surface integral, assessing the field's divergence over the entire surface Σ. Conversely, if Σ is a plane curve, the left-hand side of each equation converts into a definite integral, bounded by the curve's endpoints, still reflecting the field's flux along the curve. Meanwhile, the right-hand side remains a line integral, signifying the field's divergence along the surface. Notably, when Σ forms a closed plane curve or surface, the left-hand side of each equation evaluates to zero, indicating equilibrium in the flux across the entire boundary.

1.2 Weingarten Tensor and Curvatures

1.2.1 Variation of the Unit Normal Vector

When studying curves or surfaces S, we are particularly interested in their local properties at a point $\boldsymbol{x} \in \mathrm{S}$. These local properties can be effectively described by examining the variation of the unit normal vectors $\mathbf{n}$, which are intrinsically linked to fundamental characteristics such as curvature and the normal acceleration of the curve or surface. To analyze this variation, we first compute the gradient of the normal vector $\mathbf{n}(x)$. By employing the definitions provided in equations (1.2) and (1.4), we derive the following expression:

$$\nabla \mathbf{n}(\boldsymbol{x}) = \frac{\nabla^2 \varphi(\boldsymbol{x})}{\|\nabla \varphi(\boldsymbol{x})\|} - \frac{(\nabla \varphi(\boldsymbol{x}) \otimes \nabla \varphi(\boldsymbol{x}))\nabla^2 \varphi(\boldsymbol{x})}{\|\nabla \varphi(\boldsymbol{x})\|} = \mathbf{P}\frac{\nabla^2 \varphi(\boldsymbol{x})}{\|\nabla \varphi(\boldsymbol{x})\|}. \tag{1.24}$$

Under the assumption that $\varphi \in C^2(\mathbb{R}^k, \mathbb{R})$, the Hessian matrix $\nabla^2 \varphi$ of φ is symmetric. Next, in the neighborhood of the point $\boldsymbol{x} \in \mathrm{S}$, we consider an infinitesimal increment $\delta \boldsymbol{x}$ along the direction tangent to the curve or surface, i.e, $\delta \boldsymbol{x} \in T_{\boldsymbol{x}}\mathrm{S})$. We aim to comprehend how the unit normal vector $\mathbf{n}$ changes under this small increment $\delta \boldsymbol{x}$. Describing this change in terms of the directional derivative of $\mathbf{n}$ is natural and yields the expression:

$$\delta \mathbf{n}(\boldsymbol{x}; \delta \boldsymbol{x}) = \nabla \mathbf{n}(\boldsymbol{x}) \delta \boldsymbol{x} = \mathbf{P}\frac{\nabla^2 \varphi(\boldsymbol{x})}{\|\nabla \varphi(\boldsymbol{x})\|}\delta \boldsymbol{x} = \mathbf{P}\frac{\nabla^2 \varphi(\boldsymbol{x})}{\|\nabla \varphi(\boldsymbol{x})\|}\mathbf{P}\delta \boldsymbol{x}, \tag{1.25}$$

where the equality $\mathbf{P}\delta \boldsymbol{x} = \delta \boldsymbol{x}$ is employed due to $\delta \boldsymbol{x} \in T_{\boldsymbol{x}}\mathrm{S}$. Introducing the Weingarten tensor $\mathbf{W}(\boldsymbol{x})$ as defined by (see, for example, He et al. [66] and [63]): as follows

$$\mathbf{W}(\boldsymbol{x}) = -\mathbf{P}\frac{\nabla^2 \varphi(\boldsymbol{x})}{\|\nabla \varphi(\boldsymbol{x})\|}\mathbf{P}, \tag{1.26}$$

the directional derivative $\delta \mathbf{n}(\boldsymbol{x}; \delta \boldsymbol{x})$ can be simply expressed as

$$\delta \mathbf{n}(\boldsymbol{x}; \delta \boldsymbol{x}) = -\mathbf{W}(\boldsymbol{x}) \delta \boldsymbol{x}. \tag{1.27}$$

The Weingarten tensor $\mathbf{W}(\boldsymbol{x})$ is in fact the tangential gradient of the unit normal vector $\mathbf{n}(\boldsymbol{x})$, albeit with an opposite sign:

$$\mathbf{W}(\boldsymbol{x}) = -\nabla_S \mathbf{n}(\boldsymbol{x}). \tag{1.28}$$

The explicit and concise expression (1.26) of the Weingarten tensor $\mathbf{W}(\boldsymbol{x})$ clearly indicates that: (i) it is symmetric; (ii) it is a tangential surface tensor field. Using the definition of the Weingarten tensor $\mathbf{W}(\boldsymbol{x})$, we can easily establish relationships between the tangential gradients and divergences of $\mathbf{P}$ and $\mathbf{W}(\boldsymbol{x})$. These relationships are expressed concisely as follows:

$$\nabla\mathbf{P}\cdot\mathbf{P} = \mathbf{W}\overline{\otimes}\mathbf{n} + \mathbf{n}\otimes\mathbf{W}, \tag{1.29a}$$

$$\nabla\mathbf{P}\colon\mathbf{P} = \mathbf{n}\mathrm{tr}[\mathbf{W}], \tag{1.29b}$$

$$\nabla\mathbf{W}\cdot\mathbf{P} = \mathbf{n}\otimes\mathbf{W}^2 + \mathbf{P}\cdot\nabla\mathbf{W}\cdot\mathbf{P}, \tag{1.29c}$$

$$\nabla\mathbf{W}\colon\mathbf{P} = \mathbf{n}\mathrm{tr}[\mathbf{W}^2] + \mathbf{P}\cdot\nabla\mathbf{W}\colon\mathbf{P}. \tag{1.29d}$$

where the tensor product $\mathbf{W}\overline{\otimes}\mathbf{n}$ is defined as $(\mathbf{W}\overline{\otimes}\mathbf{n})_{ijk} = W_{ik}n_j$.

1.2.2 Curvature of a Plane Curve and a Surface

The Weingarten tensor plays a fundamental role in differential geometry, particularly in characterizing the local properties of a curve or surface S. It provides crucial insights into the geometric shape and curvature of surfaces. Specifically, the Weingarten tensor signifies the rate of variation of the curve's (or surface's) normal vectors along its tangential directions. This variation rate is indispensable for understanding the curve's (or surface's) curvature and the directional alterations of its normal vectors. Consequently, analyzing the Weingarten tensor is essential to comprehending the local geometric attributes of curves and surfaces, such as curvature and convexity.

For a plane curve S , the Weingarten tensor $\mathbf{W}(\boldsymbol{x})$ of the curve is a rank-1 tensor. The curvature $\kappa(\boldsymbol{x})$ of S is calculated as follows:

$$\kappa(\boldsymbol{x}) = \mathrm{tr}[\mathbf{W}(\boldsymbol{x})] = \frac{\nabla^2\varphi(\boldsymbol{x})}{\|\nabla\varphi(\boldsymbol{x})\|} : \mathbf{P}(\boldsymbol{x}). \tag{1.30}$$

In reality, $\mathbf{W}(\boldsymbol{x})$ has the simple representation:

$$\mathbf{W}(\boldsymbol{x}) = \kappa(\boldsymbol{x})\mathbf{P}(\boldsymbol{x}). \tag{1.31}$$

For a surface S immersed in Euclidean space, its local geometric properties at a point $\boldsymbol{x} \in$ S are

characterized by the concepts of mean curvature and Gaussian curvature, both of which provide essential information about the surface's curvature characteristics. The mean curvature $\bar{\kappa}(\boldsymbol{x})$ at a point $\boldsymbol{x}$ on S is defined as half the trace of the Weingarten tensor $\mathbf{W}(\boldsymbol{x})$:

$$\bar{\kappa}(\boldsymbol{x}) = \frac{1}{2}\mathrm{tr}[\mathbf{W}(\boldsymbol{x})]. \tag{1.32}$$

Geometrically, it quantifies the average rate of change of the unit normal vector along directions tangent to the surface. The Gaussian curvature $\bar{K}(\boldsymbol{x})$ is an intrinsic measure of the curvature of S and can be expressed through the determinant of $\mathbf{W}(\boldsymbol{x})$ by the relationship:

$$[\mathbf{W}(\boldsymbol{x})\mathbf{a}] \times [\mathbf{W}(\boldsymbol{x})\mathbf{b}] = \bar{K}(\boldsymbol{x})(\mathbf{a} \times \mathbf{b}), \quad \text{for all} \quad \mathbf{a}, \mathbf{b} \in T_{\boldsymbol{x}}\mathrm{S}, \tag{1.33}$$

where $\mathbf{a}$ and $\mathbf{b}$ are arbitrary tangent vectors at $\boldsymbol{x}$. This equation signifies that the Gaussian curvature represents the product of the principal curvatures and characterizes the local deviation of the surface from being flat.

The principal curvatures $\bar{c}_1(\boldsymbol{x})$ and $\bar{c}_2(\boldsymbol{x})$ at $\boldsymbol{x}$ are related to $\bar{\kappa}(\boldsymbol{x})$ and $\bar{K}(\boldsymbol{x})$ through the following formulas:

$$\bar{c}_1(\boldsymbol{x}) = \bar{\kappa}(\boldsymbol{x}) - \sqrt{\bar{\kappa}^2(\boldsymbol{x}) - \bar{K}(\boldsymbol{x})}, \tag{1.34a}$$

$$\bar{c}_2(\boldsymbol{x}) = \bar{\kappa}(\boldsymbol{x}) + \sqrt{\bar{\kappa}^2(\boldsymbol{x}) - \bar{K}(\boldsymbol{x})}. \tag{1.34b}$$

These principal curvatures provide insights into the maximum and minimum curvatures at the point $\boldsymbol{x}$. Moreover, the principal curvature radii $\bar{r}_1(\boldsymbol{x}) = 1/\bar{c}_1(\boldsymbol{x})$ and $\bar{r}_2(\boldsymbol{x}) = 1/\bar{c}_2(\boldsymbol{x})$ offer a quantitative measure of the curvature at $\boldsymbol{x}$, providing valuable information about the local geometric behavior of the surface S.

1.3 Hadamard's Relation

In subsequent studies, we will frequently encounter functions that are continuous everywhere but differentiable only almost everywhere. A prototype of such functions is a continuous function Ψ (scalar, vector, or tensor) defined in a domain $\Omega \subset \mathbb{R}^3$, whose derivative exists and is continuous at every point in Ω except on a surface $\Gamma \subset \Omega$. The objective of this section is to pro-

vide an explicit expression for the jump in the derivative of Ψ across Γ, depending on whether Ψ is a scalar, vector, or tensor function. This expression for the jump in the derivative of Ψ is termed the "Hadamard's relation", as it was first established by Hadamard [57] in his renowned treatise "Leçons sur la propagation des ondes et les équations de l'hydrodynamique". In mechanics, an excellent English reference on this subject, in our opinion, is a review article written by Hill [68] 63 years ago. The presentation and proof methods of Hadamard's relation in this section are largely inspired by the work of Gu and He [48].

In accordance with the previous chapter, the surface Γ separating Ω into two subdomains $\Omega^{(1)}$ and $\Omega^{(2)}$ (see **Fig.** 1.3) is characterized by a scalar function ϕ defined in $\mathbb{R}^3$:

$$\Gamma = \{\boldsymbol{x} \in \mathbb{R}^3 \,|\, \phi(\boldsymbol{x}) = 0\}. \tag{1.35}$$

The unit normal vector to Γ at point $\boldsymbol{x}$ is determined by equation (1.2).

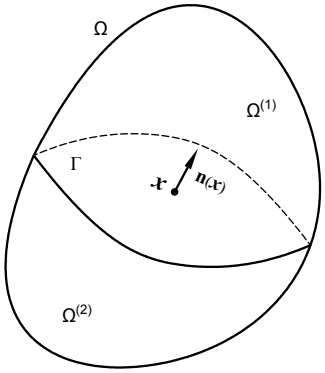

Figure 1.3: *Geometry of domain* Ω.

1.3.1 Jump of the Derivative of a Scalar Function

Let $\varphi : \Omega \subset \mathbb{R}^k \to \mathbb{R}$ be a scalar function defined piecewise by:

$$\varphi(\boldsymbol{x}) = \begin{cases} \varphi^{(1)}(\boldsymbol{x}) & \text{if } \boldsymbol{x} \in \Omega^{(1)} \\ \varphi^{(2)}(\boldsymbol{x}) & \text{if } \boldsymbol{x} \in \Omega^{(2)} \end{cases}, \tag{1.36}$$

with the continuity condition on Γ:

$$\varphi(\boldsymbol{x}) = \varphi^{(1)}(\boldsymbol{x}) = \varphi^{(2)}(\boldsymbol{x}), \quad \text{if } \boldsymbol{x} \in \Gamma, \tag{1.37}$$

where $\varphi^{(i)} : \Omega^{(i)} \subset \Omega \to \mathbb{R}$ (for $i = 1,2$) are continuously differentiable on their respective domains. The domain Ω is the union of the subdomains $\Omega^{(1)}$ and $\Omega^{(2)}$ along with their common boundary Γ, i.e., $\Omega = \Omega^{(1)} \cup \Omega^{(2)} \cup \Gamma$.

For all $\boldsymbol{x} \in \Gamma$, there exists a neighborhood $U \subset \Gamma$ such that for all $\boldsymbol{y} \in \Gamma$, the Taylor expansions of the scalar functions $\varphi^{(1)}$ and $\varphi^{(2)}$ around $\boldsymbol{x}$ are given by:

$$\varphi^{(1)}(\boldsymbol{y}) = \varphi^{(1)}(\boldsymbol{x}) + \nabla\varphi^{(1)}(\boldsymbol{x}) \cdot (\boldsymbol{y} - \boldsymbol{x}) + 0(\|\boldsymbol{y} - \boldsymbol{x}\|^2) \tag{1.39a}$$

$$\varphi^{(2)}(\boldsymbol{y}) = \varphi^{(2)}(\boldsymbol{x}) + \nabla\varphi^{(2)}(\boldsymbol{x}) \cdot (\boldsymbol{y} - \boldsymbol{x}) + 0(\|\boldsymbol{y} - \boldsymbol{x}\|^2) \tag{1.39b}$$

where $0(\|\boldsymbol{y} - \boldsymbol{x}\|^2)$ represents the higher-order terms in the expansions. Taking into account the continuity condition (1.37), the difference $\varphi^{(2)}(\boldsymbol{y}) - \varphi^{(1)}(\boldsymbol{y})$ can be expressed as:

$$[\nabla\varphi^{(2)}(\boldsymbol{x}) - \nabla\varphi^{(1)}(\boldsymbol{x})] \cdot (\boldsymbol{y} - \boldsymbol{x}) = 0(\|\boldsymbol{y} - \boldsymbol{x}\|^2). \tag{1.39}$$

Dividing both sides of this equality by $\|\boldsymbol{y} - \boldsymbol{x}\|$ results in:

$$[\nabla\varphi^{(2)}(\boldsymbol{x}) - \nabla\varphi^{(1)}(\boldsymbol{x})] \cdot \frac{\boldsymbol{y} - \boldsymbol{x}}{\|\boldsymbol{y} - \boldsymbol{x}\|} = 0\|\boldsymbol{y} - \boldsymbol{x}\|. \tag{1.40}$$

Taking the limit as $\boldsymbol{y} \to \boldsymbol{x}$, we obtain:

$$[\nabla\varphi^{(2)}(\boldsymbol{x}) - \nabla\varphi^{(1)}(\boldsymbol{x})] \cdot \mathbf{t}(\boldsymbol{x}) = 0 \quad \text{for } \forall \boldsymbol{x} \in \Gamma, \tag{1.41}$$

where

$$\mathbf{t}(\boldsymbol{x}) = \lim_{\boldsymbol{y} \to \boldsymbol{x}} \frac{\boldsymbol{y} - \boldsymbol{x}}{\|\boldsymbol{y} - \boldsymbol{x}\|}, \tag{1.42}$$

is the unit tangent vector to the surface Γ at $\boldsymbol{x}$. Considering that $\mathbf{t} \in T_{\boldsymbol{x}}\Gamma$, where $T_{\boldsymbol{x}}\Gamma$ is the tangent space of Γ at $\boldsymbol{x}$, we infer that the difference in gradients, $\nabla\varphi^{(2)}(\boldsymbol{x}) - \nabla\varphi^{(1)}(\boldsymbol{x})$ belongs to the normal subspace of Γ at $\boldsymbol{x}$; that is,

$$\nabla\varphi^{(2)}(\boldsymbol{x}) - \nabla\varphi^{(1)}(\boldsymbol{x}) \in N_{\boldsymbol{x}}\Gamma \quad \text{for } \forall \boldsymbol{x} \in \Gamma. \tag{1.43}$$

Thus, we have

$$\nabla\varphi^{(2)}(\boldsymbol{x}) - \nabla\varphi^{(1)}(\boldsymbol{x}) = \alpha\mathbf{n}(\boldsymbol{x}) \quad \text{if } \boldsymbol{x} \in \Gamma, \tag{1.44}$$

where $\mathbf{n}(\boldsymbol{x})$ is the unit normal vector of the interface Γ at $\boldsymbol{x}$ and α is a scalar. When $\alpha \neq 0$, this equation establishes the Hadamard jump relation for a scalar function continuous but not differentiable across Γ, confirming that the gradient jump aligns with the normal vector to the surface. Additionally, the observation that the gradient jump belongs the normal subspace of Γ at $\boldsymbol{x}$ leads to:

$$\nabla_S \varphi^{(2)}(\boldsymbol{x}) - \nabla_S \varphi^{(1)}(\boldsymbol{x}) = \mathbf{0} \quad \text{if } \boldsymbol{x} \in \Gamma. \tag{1.45}$$

This expression reveals the continuity of the surface gradient $\nabla_S \varphi(\boldsymbol{x})$ across the interface Γ.

1.3.2 Jump of the Derivative of a Vector Function

Let's extend our analysis to a vector function $\mathbf{f} : \Omega \subset \mathbb{R}^k \to \mathbb{R}^k$, defined similarly to the scalar function φ. Specifically, $\mathbf{f}(\boldsymbol{x})$ is defined piecewise as:

$$\mathbf{f}(\boldsymbol{x}) = \begin{cases} \mathbf{f}^{(1)}(\boldsymbol{x}) & \text{if } \boldsymbol{x} \in \Omega^{(1)} \\ \mathbf{f}^{(2)}(\boldsymbol{x}) & \text{if } \boldsymbol{x} \in \Omega^{(2)} \end{cases}, \tag{1.46}$$

subject to the continuity condition on Γ:

$$\mathbf{f}(\boldsymbol{x}) = \mathbf{f}^{(1)}(\boldsymbol{x}) = \mathbf{f}^{(2)}(\boldsymbol{x}), \text{ if } \boldsymbol{x} \in \Gamma, \tag{1.47}$$

where $\mathbf{f}^{(i)} : \Omega^{(i)} \subset \Omega \to \mathbb{R}^k$ (for $i = 1, 2$) are continuously differentiable on their respective domains. The domain Ω is composed of the subdomains $\Omega^{(1)}$ and $\Omega^{(2)}$ along with their shared boundary Γ, i.e., $\Omega = \Omega^{(1)} \cup \Omega^{(2)} \cup \Gamma$.

For every $\boldsymbol{x} \in \Gamma$, we can find a neighborhood $U \subset \Gamma$ such that for all $\boldsymbol{y} \in \Gamma$, the Taylor expansions of $\mathbf{f}^{(1)}$ and $\mathbf{f}^{(2)}$ around $\boldsymbol{x}$ are given by:

$$\mathbf{f}^{(1)}(\boldsymbol{y}) = \mathbf{f}^{(1)}(\boldsymbol{x}) + \nabla \mathbf{f}^{(1)}(\boldsymbol{x}) \cdot (\boldsymbol{y} - \boldsymbol{x}) + \mathbf{0}(\|\boldsymbol{y} - \boldsymbol{x}\|^2), \tag{1.48a}$$

$$\mathbf{f}^{(2)}(\boldsymbol{y}) = \mathbf{f}^{(2)}(\boldsymbol{x}) + \nabla \mathbf{f}^{(2)}(\boldsymbol{x}) \cdot (\boldsymbol{y} - \boldsymbol{x}) + \mathbf{0}(\|\boldsymbol{y} - \boldsymbol{x}\|^2). \tag{1.48b}$$

Here, $\mathbf{0}(|\boldsymbol{y} - \boldsymbol{x}|^2)$ represents higher-order terms in the expansions.Considering the continuity

condition (1.47), the difference $\mathbf{f}^{(2)}(\boldsymbol{y}) - \mathbf{f}^{(1)}(\boldsymbol{y})$ can be expressed as:

$$[\nabla \mathbf{f}^{(2)}(\boldsymbol{x}) - \nabla \mathbf{f}^{(1)}(\boldsymbol{x})] \cdot (\boldsymbol{y} - \boldsymbol{x}) = \mathbf{0}(\|\boldsymbol{y} - \boldsymbol{x}\|^2) \tag{1.49}$$

Similarly, by dividing both sides of this equality by $|\boldsymbol{y} - \boldsymbol{x}|$ and taking their limits as as $\boldsymbol{y} \to \boldsymbol{x}$, we obtain

$$[\nabla \mathbf{f}^{(2)}(\boldsymbol{x}) - \nabla \mathbf{f}^{(1)}(\boldsymbol{x})] \cdot \mathbf{t} = \mathbf{0} \quad \text{for } \forall \boldsymbol{x} \in \Gamma, \tag{1.50}$$

where the vector $\mathbf{t}$ is a unit tangent vector to Γ at $\boldsymbol{x}$, as defined in the preceding paragraph (i.e., $\mathbf{t} \in T_{\boldsymbol{x}}\Gamma$).It follows that the tangent plane $T_{\boldsymbol{x}}\Gamma$ is entirely equivalent to the kernel space $\text{Ker}[\nabla \mathbf{f}^{(2)}(\boldsymbol{x}) - \nabla \mathbf{f}^{(1)}(\boldsymbol{x})]$ of the tensor $\nabla \mathbf{f}^{(2)}(\boldsymbol{x}) - \nabla \mathbf{f}^{(1)}(\boldsymbol{x})$. Therefore, the image space $\text{Im}[\nabla \mathbf{f}^{(2)}(\boldsymbol{x}) - \nabla \mathbf{f}^{(1)}(\boldsymbol{x})]$ should be the one-dimensional space orthogonal to the tangent plane, which is spanned by the normal vectors to the tangent plane $T_{\boldsymbol{x}}\Gamma$. Consequently, $\nabla \mathbf{f}^{(2)}(\boldsymbol{x}) - \nabla \mathbf{f}^{(1)}(\boldsymbol{x})$ takes the form:

$$\nabla \mathbf{f}^{(2)}(\boldsymbol{x}) - \nabla \mathbf{f}^{(1)}(\boldsymbol{x}) = \mathbf{a} \otimes \mathbf{n}(\boldsymbol{x}) \quad \text{if } \boldsymbol{x} \in \Gamma, \tag{1.51}$$

where $\mathbf{a}$ is a vector. If $\mathbf{a} \neq \mathbf{0}$, $\mathbf{f}$ is not differentiable on Γ, and (1.51) represents the Hadamard's relation for a vector function. It is evident that even when $\nabla \mathbf{f}^{(2)}(\boldsymbol{x}) \neq \nabla \mathbf{f}^{(1)}(\boldsymbol{x})$ on Γ, the surface gradient is continuous:

$$\nabla_S \mathbf{f}^{(1)}(\boldsymbol{x}) = \nabla_S \mathbf{f}^{(2)}(\boldsymbol{x}) \quad \text{if } \boldsymbol{x} \in \Gamma, \tag{1.52}$$

which also implies:

$$\text{div}_S \mathbf{f}^{(1)}(\boldsymbol{x}) = \text{div}_S \mathbf{f}^{(2)}(\boldsymbol{x}) \quad \text{if } \boldsymbol{x} \in \Gamma. \tag{1.53}$$

These expressions indicate that even if $\nabla \mathbf{f}^{(2)}(\boldsymbol{x})$ and $\nabla \mathbf{f}^{(1)}(\boldsymbol{x})$ differ across Γ, the continuity of the surface gradient and divergence is preserved.

1.3.3 Jump of the Derivative of a Tensor Function

The approach utilized to establish the Hadamard's relation for scalar and vector functions can be extended to derive analogous relations for higher-order tensor functions. Let's consider a second-order tensor function $\mathbf{T} : \Omega \subset \mathbb{R}^k \to \mathbb{R}^k \times \mathbb{R}^k$, defined analogously to the scalar and

vector function. Specifically, $\mathbf{T}(\boldsymbol{x})$ is defined piecewise as follows:

$$\mathbf{T}(\boldsymbol{x}) = \begin{cases} \mathbf{T}^{(1)}(\boldsymbol{x}) & \text{if } \boldsymbol{x} \in \Omega^{(1)} \\ \mathbf{T}^{(2)}(\boldsymbol{x}) & \text{if } \boldsymbol{x} \in \Omega^{(2)} \end{cases}, \tag{1.54}$$

subject to the continuity condition on Γ:

$$\mathbf{T}(\boldsymbol{x}) = \mathbf{T}^{(1)}(\boldsymbol{x}) = \mathbf{T}^{(2)}(\boldsymbol{x}) \quad \text{if } \boldsymbol{x} \in \Gamma, \tag{1.55}$$

where $\mathbf{T}^{(i)} : \Omega^{(i)} \subset \Omega \to \mathbb{R}^k \times \mathbb{R}^k$ (for $i = 1, 2$) are continuously differentiable on their respective domains. According to the previous derivation, we can deduce that:

$$\nabla \mathbf{T}^{(2)}(\boldsymbol{x}) - \nabla \mathbf{T}^{(1)}(\boldsymbol{x}) = \mathbf{A} \otimes \mathbf{n}(\boldsymbol{x}) \quad \text{if } \boldsymbol{x} \in \Gamma, \tag{1.56}$$

where $\mathbf{A}$ is a second-order tensor. When $\mathbf{A} \neq \mathbf{0}$, F is not differentiable on Γ, and (1.56) corresponds to the Hadamard relation for a tensor function. From this relation, we directly infer that:

$$\nabla_S \mathbf{T}^{(1)}(\boldsymbol{x}) = \nabla_S \mathbf{T}^{(2)}(\boldsymbol{x}) \quad \text{if } \boldsymbol{x} \in \Gamma, \tag{1.57}$$

$$\operatorname{div}_S \mathbf{T}^{(1)}(\boldsymbol{x}) = \operatorname{div}_S \mathbf{T}^{(2)}(\boldsymbol{x}) \quad \text{if } \boldsymbol{x} \in \Gamma. \tag{1.58}$$

These expressions illustrate the preservation of surface gradient and divergence continuity, even in the presence of potential differences between $\nabla \mathbf{T}^{(2)}(\boldsymbol{x})$ and $\nabla \mathbf{T}^{(1)}(\boldsymbol{x})$ across Γ. Additionally, extending this methodology to higher-order tensor functions allows for the consistent derivation of analogous Hadamard relations, while also maintaining the continuity of surface gradient and divergence properties.

1.3.4 Jumps of High Derivatives

The established relations illustrate that while the derivative of a continuous function across a surface Γ may exhibit discontinuities, its surface derivative remains continuous. By iteratively exploiting this observation, we can generalize the continuity of the tangential (or surface) derivative of any order for continuous functions (scalar, vector, or tensor) across Γ. For exam-

ple, considering the scalar function φ defined by (1.36) and (1.37), where φ is assumed to be twice continuously differentiable in Ω, we can formulate:

$$\nabla_S[\nabla_S \boldsymbol{\varphi}^{(1)}(\boldsymbol{x})] = \nabla_S[\nabla_S \boldsymbol{\varphi}^{(2)}(\boldsymbol{x})] \quad \text{for } \forall \boldsymbol{x} \in \Gamma, \tag{1.59}$$

which implies further:

$$\triangle_S \boldsymbol{\varphi}^{(1)}(\boldsymbol{x}) = \triangle_S \boldsymbol{\varphi}^{(2)}(\boldsymbol{x}) \quad \text{for } \forall \boldsymbol{x} \in \Gamma, \tag{1.60}$$

Here, $\triangle_S$ represents the surface Laplacian, defined as:

$$\triangle_S \boldsymbol{\varphi}^{(i)}(\boldsymbol{x}) = \nabla_S[\nabla_S \boldsymbol{\varphi}^{(1)}(\boldsymbol{x})] \quad \text{for } \forall \boldsymbol{x} \in \Gamma. \tag{1.61}$$

Chapter 2

Taylor Expansions of 3D Fields About a Curved Surface

In a three-dimension (3D) Euclidean space $\mathbb{R}^3$, when one dimension of a structure is significantly smaller than the other two dimensions, this dimension is typically referred to as the thickness of the structure, and the structure itself can be modeled as a plate-like or shell-like entity. Given that the thickness of a (plate or) shell is considerably smaller than its other dimensions, the internal field of the shell can be effectively approximated in terms of its distribution on its median surface.

In this chapter, we first employ the surface definition of Chapter 1 to construct a shell and analyze the geometric properties of this shell. Building on this foundation, and taking into consideration the influence of the material properties of the shell on the continuity of the field, we derive the Taylor series expansions for both scalar and vector fields within the shell. These results are instrumental in subsequent analyses, enabling a transition from a 3D medium to a 2D ones, thus facilitating the estabilishment of plate and shell theories as well as interface theories. By reducing dimensions, we can more effectively analyze and predict the behavior of plates and shells under various conditions. Furthermore, the expansions aid in the formulation of boundary conditions and continuity requirements that are essential for the accurate modeling of physical phenomena in thin-walled structures.

2.1 Parallel Curves and Surfaces

Given a plane curve or surface S defined by (1.1), we can construct a parallel plane curve or surface S_d as follows:

$$\mathrm{S}_d = \{\boldsymbol{y} \in \mathbb{R}^k \,|\, \boldsymbol{y} = \boldsymbol{x} + d\mathbf{n}(\boldsymbol{x}),\, \boldsymbol{x} \in \mathrm{S}, d \in \mathbb{R}\}, \tag{2.1}$$

where $\mathbf{n}(\boldsymbol{x})$ denotes the unit normal vector to the curve or surface S at the point $\boldsymbol{x}$. The parallel curve or surface S_d is defined by translating each point $\boldsymbol{x} \in \mathrm{S}$ a distance d in the direction of the normal vector $\mathbf{n}(\boldsymbol{x})$. Therefore, the set S_d represents all points $\boldsymbol{y} \in \mathbb{R}^k$ that are at a distance d along the normal vector from the corresponding points on S. This construction ensures that S_d is parallel to S, with an oriented distance d (see **Fig.** 2.1). The local geometrical properties of

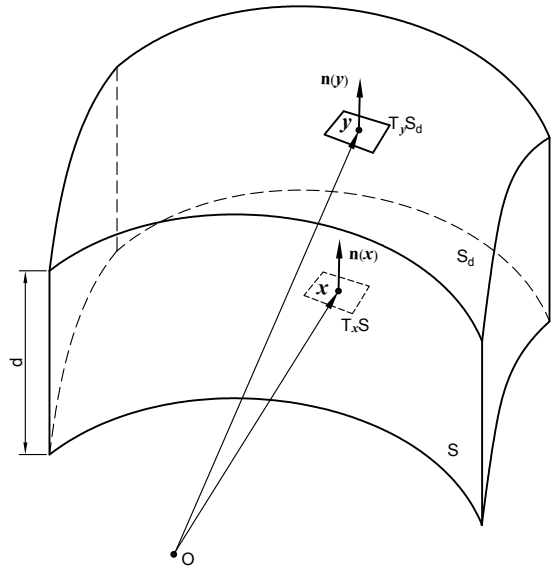

Figure 2.1: *Geometry of parallel surfaces.*

S_d are determined by those of S and the distance d. Specifically, for $\forall \boldsymbol{y} \in \mathrm{S}_d$, $\exists \boldsymbol{x} \in \mathrm{S}$ such that $\boldsymbol{y} = \boldsymbol{x} + d\mathbf{n}(\boldsymbol{x})$, and the unit normal vector $\mathbf{n}(\boldsymbol{y})$ is collinear to the unit normal vector $\mathbf{n}(\boldsymbol{x})$. To demonstrate this, consider the definition of S_d and compute the variation of $\boldsymbol{y} \in \mathrm{S}_d$ due to an increment $\delta\boldsymbol{x} \in T_{\boldsymbol{x}}\mathrm{S}$:

$$\delta\boldsymbol{y} = \delta\boldsymbol{x} + d\delta\mathbf{n}(\boldsymbol{x}; \delta\boldsymbol{x}) = \delta\boldsymbol{x} - d\mathbf{W}(\boldsymbol{x})\delta\boldsymbol{x} = [\mathbf{P}(\boldsymbol{x}) - d\mathbf{W}(\boldsymbol{x})]\delta\boldsymbol{x}. \tag{2.2}$$

Since $\mathbf{W}(\boldsymbol{x})$ is a tangential surface tensor field, it follows from the aforementioned equation that the vector $\boldsymbol{\delta y}$, tangent to S_d at $\boldsymbol{y} \in \mathrm{S}_d$, is parallel to the vector $\boldsymbol{\delta x}$, tangent to S at $\boldsymbol{x} \in \mathrm{S}$. In other words, the tangent spaces $T_{\boldsymbol{y}}\mathrm{S}_d$ and $T_{\boldsymbol{x}}\mathrm{S}$ are parallel manifolds. From the above equation, it is evident that the following condition must hold to ensure that the normal vectors remain well-defined and non-degenerate as we construct the parallel surface S_d using the aforementioned method:

$$1 - d\hat{c}_i(\boldsymbol{x}) \neq 0 \quad (i = 1, 2), \tag{2.3}$$

where $\hat{c}_i(\boldsymbol{x})$ are the principal curvatures of S at the point $\boldsymbol{x}$. Furthermore, if the condition is satisfied, there exists a unique correspondence between $\boldsymbol{\delta y}$ and $\boldsymbol{\delta x}$. Thus, for $\forall \boldsymbol{y} \in \mathrm{S}_d$, $\exists \boldsymbol{x} \in \mathrm{S}$ related by $\boldsymbol{y} = \boldsymbol{x} + d\mathbf{n}(\boldsymbol{x})$, we can write:

$$\mathbf{n}(\boldsymbol{y}) = \mathbf{n}(\boldsymbol{x}). \tag{2.4}$$

An important implication of above equation is that:

$$\nabla \mathbf{n}(\boldsymbol{x}) \cdot \mathbf{n}(\boldsymbol{x}) = \mathbf{0}. \tag{2.5}$$

To establish this, observe that $\nabla \mathbf{n}(\boldsymbol{x}) \cdot \mathbf{n}(\boldsymbol{x})$ represents the directional derivative of $\mathbf{n}(\boldsymbol{x})$ in the direction of $\mathbf{n}(\boldsymbol{x})$, which can be written as:

$$\nabla \mathbf{n}(\boldsymbol{x}) \cdot \mathbf{n}(\boldsymbol{x}) = \lim_{d \to 0} \frac{\mathbf{n}[\boldsymbol{x} + d\mathbf{n}(\boldsymbol{x})] - \mathbf{n}(\boldsymbol{x})}{d} \tag{2.6}$$

Substituting equation (2.4) into the right-hand side of above equation immediately gives relation (2.5). This result indicates that the normal directional derivative of the unit normal vector field within a domain consisting of parallel surfaces or curves is zero. This fundamental property will be consistently utilized in our subsequent analyses. Similarly, the fact that $T_{\boldsymbol{y}}\mathrm{S}_d = T_{\boldsymbol{x}}\mathrm{S}$ implies that:

$$\mathbf{P}(\boldsymbol{y}) = \mathbf{P}(\boldsymbol{x}), \tag{2.7a}$$

$$\nabla \mathbf{P}(\boldsymbol{x}) \cdot \mathbf{n}(\boldsymbol{x}) = \mathbf{0}. \tag{2.7b}$$

Combining equations (1.28) and (2.5), we derive the directional derivative of $\mathbf{W}(\boldsymbol{x})$ in the direction of $\mathbf{n}(\boldsymbol{x})$ as:

$$\nabla\mathbf{W}(\boldsymbol{x})\cdot\mathbf{n}(\boldsymbol{x}) = \mathbf{W}^2, \tag{2.8}$$

which can be further developed as:

$$\nabla\mathbf{W}^r(\boldsymbol{x})\cdot\mathbf{n}(\boldsymbol{x}) = r\mathbf{W}^{r+1}, \quad r\in\mathbb{Z}_+. \tag{2.9}$$

We now propose to establish the expression of the Weingarten tensor $\mathbf{W}(\boldsymbol{y})$ of S_d at $\boldsymbol{y}$ in terms of $\mathbf{W}(\boldsymbol{x})$ and d. By definition, we have

$$\mathbf{W}(\boldsymbol{x}) = -\nabla_{\boldsymbol{x}}\mathbf{n}(\boldsymbol{x})\cdot\mathbf{P}(\boldsymbol{x}), \quad \mathbf{W}(\boldsymbol{y}) = -\nabla_{\boldsymbol{y}}\mathbf{n}(\boldsymbol{y})\cdot\mathbf{P}(\boldsymbol{y}). \tag{2.10}$$

Taking into account relations (2.4), (2.7b), we can write

$$\mathbf{W}(\boldsymbol{x}) = -\nabla_{\boldsymbol{x}}\mathbf{n}(\boldsymbol{y})\cdot\mathbf{P}(\boldsymbol{y}) = -\nabla_{\boldsymbol{y}}\mathbf{n}(\boldsymbol{y})\cdot\left(\frac{\partial\boldsymbol{y}}{\partial\boldsymbol{x}}\right)\cdot\mathbf{P}(\boldsymbol{y}). \tag{2.11}$$

According to definition (2.1), we have $\frac{\partial\boldsymbol{y}}{\partial\boldsymbol{x}} = \mathbf{I} + d\nabla_{\boldsymbol{x}}\mathbf{n}(\boldsymbol{x})$, which leads to:

$$\mathbf{W}(\boldsymbol{x}) = -\nabla_{\boldsymbol{y}}\mathbf{n}(\boldsymbol{y})\cdot[\mathbf{I} + d\nabla_{\boldsymbol{x}}\mathbf{n}(\boldsymbol{x})]\cdot\mathbf{P}(\boldsymbol{y}) = \mathbf{W}(\boldsymbol{y})[\mathbf{P}(\boldsymbol{x}) - d\mathbf{W}(\boldsymbol{x})]. \tag{2.12}$$

If condition (2.3) is satisfied, the tensor $\mathbf{P}(\boldsymbol{x}) - d\mathbf{W}(\boldsymbol{x})$ becomes an invertible transformation from $T_{\boldsymbol{x}}\mathrm{S}$ to $T_{\boldsymbol{x}}\mathrm{S}$, enabling us to express:

$$\mathbf{W}(\boldsymbol{y}) = \mathbf{W}(\boldsymbol{x})[\mathbf{P}(\boldsymbol{x}) - d\mathbf{W}(\boldsymbol{x}))]^{-1}. \tag{2.13}$$

This relation implies that $\mathbf{W}(\boldsymbol{y})$ shares the same principal directions as $\mathbf{W}(\boldsymbol{x})$. In other words, the principal curvature directions of $\mathbf{W}(\boldsymbol{y})$ are identical to those of $\mathbf{W}(\boldsymbol{x})$. When S and S_d are two parallel plane curves, we deduce from (2.13) the relationship between the curvatures $\kappa(\boldsymbol{x})$ and $\kappa(\boldsymbol{y})$:

$$\kappa(\boldsymbol{y}) = \frac{\kappa(\boldsymbol{x})}{1 - d\kappa(\boldsymbol{x})}. \tag{2.14}$$

When S and S_d are two parallel surfaces, it follows from (2.13) that

$$\hat{c}_1(\boldsymbol{y}) = \frac{\hat{c}_1(\boldsymbol{x})}{1 - d\hat{c}_1(\boldsymbol{x})}, \quad \hat{c}_2(\boldsymbol{y}) = \frac{\hat{c}_2(\boldsymbol{x})}{1 - d\hat{c}_2(\boldsymbol{x})}, \tag{2.15}$$

which provide relations between the principal curvatures of S and S_d.

2.2 Taylor Expansion of 3D Fields About a Curved Surface

Let Ω_h be the domain in $\mathbb{R}^3$ occupied by a shell of uniform thickness, which is bounded by the top surface S^+ and the bottom surface S^-. The distance between these surfaces is small in comparison to the other dimensions of the shell (see **Fig.** 2.2). The distance between the top and bottom curved surfaces is defined as the thickness of the shell and is denoted by h. The middle surface S_0 of the shell is defined as the set of points that are equidistant from the top surface S^+ and the bottom surface S^-. We assume that the shell has a uniform thickness, meaning that the distance between the top surface S^+ and the bottom surface S^- is constant at every point. Consequently, the middle surface S_0 is parallel to both S^+ and S^-. Let $\boldsymbol{x}_0$ denote an arbitrary point on the middle surface S_0, as defined by the equation (1.1), where the regularization parameter a is set to 0. Based on the construction of the parallel surfaces described previously in equation (2.1), the surfaces S^+ and S^- can be expressed as follows:

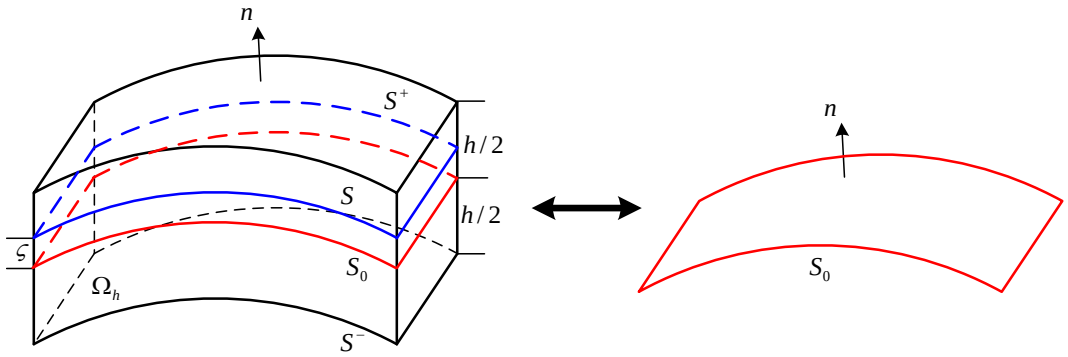

Figure 2.2: *Configuration of a shell formed by stacked parallel surfaces.*

$$S^+ = \{\boldsymbol{x} \in \mathbb{R}^3 \mid \boldsymbol{x} = \boldsymbol{x}_0 + \frac{h}{2}\mathbf{n}(\boldsymbol{x}_0), \ \ \boldsymbol{x}_0 \in S_0\}, \tag{2.16}$$

$$S^- = \{\boldsymbol{x} \in \mathbb{R}^3 \mid \boldsymbol{x} = \boldsymbol{x}_0 - \frac{h}{2}\mathbf{n}(\boldsymbol{x}_0),\ \ \boldsymbol{x}_0 \in S_0\}, \tag{2.17}$$

while the domain Ω_h bounded by S^+ and S^- be characterized as

$$\Omega_h = \{\boldsymbol{x} \in \mathbb{R}^3 \mid \boldsymbol{x} = \boldsymbol{x}_0 + d\mathbf{n}(\boldsymbol{x}_0),\ \ \boldsymbol{x}_0 \in S_0,\ \ -\frac{h}{2} \le d \le \frac{h}{2}\}, \tag{2.18}$$

where $\mathbf{n}$ is the unit vector normal to the surfaces S_0, S^+ and S^-.

Let $\Psi : \Omega_h \subset \mathbb{R}^k \to \mathbb{R}$ or $\mathbb{R}^k$ represent a scalar field or a component of a vector field that is sufficiently smooth. Considering that the thickness of the shell Ω_h is much smaller than its other dimensions, the fields within this three-dimensional shell can be approximated using a Taylor series expansion about the mid-surface S_0. Specifically, for any point $\boldsymbol{x} \in \Omega_h$, $\Psi(\boldsymbol{x})$ can be expanded in terms of $\Psi(\boldsymbol{x}_0)$ as follows:

$$\Psi(\boldsymbol{x}) = \Psi(\boldsymbol{x}_0) + \varsigma\nabla_{\mathbf{n}}\Psi(\boldsymbol{x}_0) + \frac{\varsigma^2}{2!}\nabla_{\mathbf{n}}^2\Psi(\boldsymbol{x}_0) + \frac{\varsigma^3}{3!}\nabla_{\mathbf{n}}^3\Psi(\boldsymbol{x}_0) + \cdots + \frac{\varsigma^N}{N!}\nabla_{\mathbf{n}}^N\Psi(\boldsymbol{x}_0) + \cdots, \tag{2.19}$$

where ς is the normal distance between $\boldsymbol{x}$ and the mid-surface S_0 and given by

$$\varsigma = (\boldsymbol{x} - \boldsymbol{x}_0) \cdot \mathbf{n}. \tag{2.20}$$

Note that

$$\nabla_{\mathbf{n}}\varsigma = \nabla\varsigma \cdot \mathbf{n} = \mathbf{n}. \tag{2.21}$$

Here, $\nabla_{\mathbf{n}}$ denotes the normal derivative with respect to S_0, capturing the rate of change of a field in the direction normal to the mid-surface. Additionally, ∇_n^N $(N = 1, 2, 3, \cdots)$ represents denotes the Nth normal derivative, defined recursively by

$$\nabla_{\mathbf{n}}^N\Psi = \nabla\left(\nabla_{\mathbf{n}}^{N-1}\Psi\right) \cdot \mathbf{n}, \tag{2.22}$$

indicating the N-fold differentiation along the normal direction to the surface S_0. Formula (2.19) allows for a field Ψ in the shell Ω_h to be expressed in terms of its values and derivatives on the mid-surface S_0, thus reducing of a 3D problem to a 2D one.

However, in some situations, the function Ψ may not exhibit sufficient smoothness. For instance, consider the middle surface S_0 dividing the domain Ω_h into two distinct subdomains

$\Omega_h^{(-)}$ and $\Omega_h^{(+)}$, each comprised of different materials. Even if $\Omega_h^{(-)}$ and $\Omega_h^{(+)}$ are perfectly bonded, the field Ψ within Ω_h may be continuous in Ω_h but not continuously differentiable on S_0. In such an instance where Ψ is piecewise smooth, the application of Taylor series expansion and the concept of normal derivatives may remain applicable within individual subdomains $\Omega_h^{(-)}$ and $\Omega_h^{(+)}$. This is expressed by:

$$\Psi(\boldsymbol{x}) = \begin{cases} \Psi(\boldsymbol{x}_0) + \varsigma \nabla_{\mathbf{n}} \Psi^{(+)}(\boldsymbol{x}_0) + \frac{\varsigma^2}{2!} \nabla_{\mathbf{n}}^2 \Psi^{(+)}(\boldsymbol{x}_0) + \frac{\varsigma^3}{3!} \nabla_{\mathbf{n}}^3 \Psi^{(+)}(\boldsymbol{x}_0) + \cdots, & \text{if } \boldsymbol{x} \in \Omega_h^{(+)} \\ \Psi(\boldsymbol{x}_0) + \varsigma \nabla_{\mathbf{n}} \Psi^{(-)}(\boldsymbol{x}_0) + \frac{\varsigma^2}{2!} \nabla_{\mathbf{n}}^2 \Psi^{(-)}(\boldsymbol{x}_0) + \frac{\varsigma^3}{3!} \nabla_{\mathbf{n}}^3 \Psi^{(-)}(\boldsymbol{x}_0) + \cdots, & \text{if } \boldsymbol{x} \in \Omega_h^{(-)} \end{cases}, \tag{2.23}$$

where

$$\nabla_{\mathbf{n}} \Psi^{(\pm)}(\boldsymbol{x}_0) = \lim_{t \to 0^{\pm}} \frac{\Psi(\boldsymbol{x}_0 + t\mathbf{n}) - \Psi(\boldsymbol{x}_0)}{t} \tag{2.24}$$

and higher-order normal derivatives can be defined in a similar way. The observed discontinuity can be attributed to the inherent properties of the material. Additionally, as discussed previously in the context of Hadamard's relations, even though Ψ is not differentiable at the point $\boldsymbol{x}_0 \in S_0$, its surface gradient remains continuous, i.e.,:

$$\nabla_S \Psi^{(+)}(\boldsymbol{x}_0) = \nabla_S \Psi^{(-)}(\boldsymbol{x}_0). \tag{2.25}$$

Moreover, if S_0 is a perfect interface, the normal components of the conjugate fields Φ of $\nabla\Psi$ are continuous across the interface, i.e.,

$$\Phi^{(+)} \cdot \mathbf{n} = \Phi^{(-)} \cdot \mathbf{n}. \tag{2.26}$$

Considering the influence of material properties on the distribution of the field, and utilizing these two complementary continuous fields, we express the Taylor series expansion in an alternative manner. Reviewing equation (2.19), for the sake of generalization, the Taylor series expansion of $\Psi(\boldsymbol{x})$ can be reformulated as follows:

$$\Psi(\boldsymbol{x}) = \mathscr{A}_0 + \varsigma \mathscr{A}_1 + \frac{\varsigma^2}{2!} \mathscr{A}_2 + \frac{\varsigma^3}{3!} \mathscr{A}_3 + \cdots + \frac{\varsigma^N}{N!} \mathscr{A}_N + \cdots, \tag{2.27}$$

where

$$\mathscr{A}_N = \nabla_{\mathbf{n}}^N \Psi \quad \text{for } N = 0, 1, 2, 3, \ldots, \tag{2.28}$$

with each $\mathscr{A}_N$ being recursively deducible from $\mathscr{A}_{N-1}$ and $\mathscr{B}_{N-1} = \nabla_{\mathbf{n}}^{N-1}(\Phi \cdot \mathbf{n})$. Simultaneously, $\mathscr{B}_{N-1}$ can be iteratively derived from $\mathscr{A}_{N-2}$ and $\mathscr{B}_{N-2}$. It is worth noting that $\mathscr{A}_N$ and $\mathscr{B}_N$ denote scalar or vector functions defined on $S_0 \subset \Omega_h$, depending on whether Ψ is a scalar or vector field, respectively. For clarity, the derivation of $\mathscr{A}_N$ and $\mathscr{B}_N$ is detailed in the following subsection.

2.2.1 Taylor Expansion of a Scalar Field Involved in a Transport-Like Phenomenon

Let Ψ represent a scalar field such as temperature, pressure, or electric potential, while Φ denotes the associated flux like heat flux, velocity vector, or electric current density, depending on the specific physical nature of Ψ in question. In relation to these transport phenomena, when $\Omega_h^{(-)}$ and $\Omega_h^{(+)}$ are perfectly connected by the interface S_0, the scalar field Ψ within Ω_h may exhibit continuity throughout Ω_h but may lack differentiability at a point $\boldsymbol{x}_0 \in S_0$. However, according to the Hadamard relations for scalar fields, we have:

$$\nabla_S \Psi^{(+)} = \nabla_S \Psi^{(-)}. \tag{2.29}$$

On the other hand, the normal flux across the interface S_0 is continuous, i.e.,

$$(\Phi \cdot \mathbf{n})^{(+)} = (\Phi \cdot \mathbf{n})^{(-)}. \tag{2.30}$$

In this scenario, let us delineate the explicit recursive formulas for $\mathscr{A}_N$ and $\mathscr{B}_N$ of scalar fields, focusing on fluid flow through porous media as an illustrative example. To ensure precision in our notation, we adhere to classical conventions, representing the scalar field p in place Ψ and the vector flux field $\mathbf{w}$ instead of Φ. This physical context encompasses diverse applications such as groundwater flow, oil and gas reservoir engineering, and soil mechanics. Assuming that material forming Ω_h is linear, the relationship between the velocity vector $\mathbf{w}$ and the pore pressure p in Ω_h, as described by Darcy's law, is given by

$$\mathbf{w} = -\mathbf{K} \cdot \nabla p. \tag{2.31}$$

Here, the second-order tensor $\mathbf{K}$, which is symmetric and positive definite, represents the permeability tensor characterizing the ability of the medium to transmit fluid This relationship is widely used for predicting and managing fluid flow in various natural and engineered porous media systems. Under steady-state conditions, and in the absence of any mass sources or sinks, the mass conservation equation takes the form

$$\operatorname{div} \mathbf{w} = 0. \tag{2.32}$$

In this case, $\mathscr{A}_N$ and $\mathscr{B}_N$ denote scalar functions defined on $S_0 \subset \Omega_h$. These functions are rewritten as follows:

$$\mathscr{A}_N = \nabla_{\mathbf{n}}^N p, \quad \mathscr{B}_N = \nabla_{\mathbf{n}}^N (\mathbf{w} \cdot \mathbf{n}). \tag{2.33}$$

2.2.2 Cases Where $N = 0$ and $N = 1$

Substituting $N = 0$ into equations (2.33), we obtain:

$$\mathscr{A}_0 = p, \quad \mathscr{B}_0 = \mathbf{w} \cdot \mathbf{n}. \tag{2.34}$$

When $N = 1$, to derive the explicit expressions of the operators $\mathscr{A}_1$ and $\mathscr{B}_1$, we recall that for any given surface S, the gradient of the pore pressure field ∇p evaluated on S admits the unique decomposition:

$$\nabla p = \nabla_S p + \nabla_N p. \tag{2.35}$$

Applying Darcy's law, the normal velocity vector is related to ∇p by

$$w_n = \mathbf{w} \cdot \mathbf{n} = -(\mathbf{K} \cdot \nabla p) \cdot \mathbf{n}.$$

Using the foregoing two equation, we obtain

$$\mathbf{w} \cdot \mathbf{n} = w_n = -(\mathbf{K} \cdot \nabla_S p) \cdot \mathbf{n} - (\mathbf{K} \cdot \nabla_N p) \cdot \mathbf{n}, \tag{2.36}$$

$$(\mathbf{K} \cdot \nabla_N p) \cdot \mathbf{n} = (\mathbf{K} \cdot \mathbf{P}^{\perp} \cdot \nabla p) \cdot \mathbf{n} = (\mathbf{n} \cdot \mathbf{K} \cdot \mathbf{n}) \nabla p \cdot \mathbf{n}. \tag{2.37}$$

Since the conductivity tensor $\mathbf{K}$ is a second-order positive-definite tensor, substituting equation (2.37) into equation (2.36) and dividing both sides by $\mathbf{n}\cdot\mathbf{K}\cdot\mathbf{n}$, we obtain

$$\mathscr{A}_1 = \nabla_{\mathbf{n}} p = -\frac{w_n}{\mathbf{n}\cdot\mathbf{K}\cdot\mathbf{n}} - \mathbf{s}\cdot\nabla_S p \tag{2.38}$$

where $\mathbf{s}$ is defined by

$$\mathbf{s} = \frac{\mathbf{n}\cdot\mathbf{K}}{\mathbf{n}\cdot\mathbf{K}\cdot\mathbf{n}}. \tag{2.39}$$

It is worth noting that w_n and $\nabla_S p$ are both continuous across any perfect interface.

Regarding the derivation of the expression for $\mathscr{B}_1$, we first recall that the unit normal vector $\mathbf{n}$ defined in a domain formed by parallel sheets has the specific property

$$\nabla\mathbf{n}\cdot\mathbf{n} = 0. \tag{2.40}$$

Thus, we have:

$$\nabla_{\mathbf{n}} w_n = \nabla(w_n)\cdot\mathbf{n} = \nabla\mathbf{w} : \mathbf{P}^{\perp} = \mathrm{div}_N\mathbf{w}. \tag{2.41}$$

This equation implies that the directional derivative of w_n in the normal direction is equal to the normal divergence of the flux vector $\mathbf{w}$. Simultaneously, the decomposition

$$\mathrm{div}\mathbf{w} = \nabla\mathbf{w} : \mathbf{P} + \nabla\mathbf{w} : \mathbf{P}^{\perp} = \mathrm{div}_S\mathbf{w} + \mathrm{div}_N\mathbf{w} \tag{2.42}$$

holds. Substituting this equation into the equilibrium equation (2.32) leads to

$$\mathrm{div}_N\mathbf{w} = -\mathrm{div}_S\mathbf{w}. \tag{2.43}$$

Using Darcy's law (2.31) and the decomposition (2.35), we calculate

$$\mathrm{div}_S\mathbf{w} = \nabla\mathbf{w} : \mathbf{P} = -\nabla(\mathbf{K}\cdot\nabla p) : \mathbf{P} = -\nabla(\mathbf{K}\cdot\mathbf{P}\cdot\nabla p) : \mathbf{P} - \nabla(\mathbf{K}\cdot\mathbf{P}^{\perp}\cdot\nabla p) : \mathbf{P}. \tag{2.44}$$

In this formula,

$$\nabla(\mathbf{K}\cdot\mathbf{P}^{\perp}\cdot\nabla p) = \nabla[\mathbf{K}\cdot\mathbf{n}(\nabla p\cdot\mathbf{n})]. \tag{2.45}$$

Taking into account the definition of $\nabla p \cdot \mathbf{n}$, above equation becomes

$$\nabla(\mathbf{K}\cdot\mathbf{P}^{\perp}\cdot\nabla p) = -\nabla\left[\frac{\mathbf{K}\cdot\mathbf{n}}{\mathbf{n}\cdot\mathbf{K}\cdot\mathbf{n}}w_n + \frac{(\mathbf{K}\cdot\mathbf{n})\otimes(\mathbf{n}\cdot\mathbf{K})}{\mathbf{n}\cdot\mathbf{K}\cdot\mathbf{n}}\cdot\mathbf{P}\cdot\nabla p\right]. \tag{2.46}$$

Substituting (2.46) into (2.44) and considering (2.43) leads to

$$\mathscr{B}_1 = \nabla_{\mathbf{n}}(\mathbf{w}\cdot\mathbf{n}) = \mathrm{div}_S(\mathbf{S}\cdot\nabla_S p) - \mathrm{div}_S(\mathbf{s}w_n) \tag{2.47}$$

where the tensor $\mathbf{S}$ is defined by

$$\mathbf{S} = \mathbf{K} - \frac{(\mathbf{K}\cdot\mathbf{n})\otimes(\mathbf{n}\cdot\mathbf{K})}{\mathbf{n}\cdot\ \mathbf{K}\cdot\mathbf{n}}. \tag{2.48}$$

It is evident that $\mathbf{S}$ is a symmetric second-order tensor.

2.2.3 Case Where $N = 2$

Applying the first formula of (2.33), we calculate $\mathscr{A}_2$ as follows:

$$\mathscr{A}_2 = \nabla\mathscr{A}_1\cdot\mathbf{n} = \nabla\left(-\frac{w_n}{\mathbf{n}\cdot\mathbf{K}\cdot\mathbf{n}} - \mathbf{s}\cdot\nabla_s p\right)\cdot\mathbf{n} \tag{2.49}$$

where the expression (2.38) for $\mathscr{A}_1$ is used in the second equality. Given that $\nabla\mathbf{n}\cdot\mathbf{n} = 0$, we have:

$$\nabla\left(\frac{1}{\mathbf{n}\cdot\mathbf{K}\cdot\mathbf{n}}\right)\cdot\mathbf{n} = 0, \quad \nabla\mathbf{s}\cdot\mathbf{n} = 0. \tag{2.50}$$

Consequently,

$$\mathscr{A}_2 = -\frac{1}{\mathbf{n}\cdot\mathbf{K}\cdot\mathbf{n}}\nabla w_n\cdot\mathbf{n} - \mathbf{s}\cdot\nabla(\nabla_S p)\cdot\mathbf{n}. \tag{2.51}$$

In this expression,

$$\nabla(\nabla_S p)\cdot\mathbf{n} = \nabla(\nabla p\cdot\mathbf{P})\cdot\mathbf{n} = \nabla p\cdot\nabla\mathbf{P}\cdot\mathbf{n} + (\nabla^2 p\cdot\mathbf{n})\cdot\mathbf{P}. \tag{2.52}$$

However, $\nabla\mathbf{P}\cdot\mathbf{n} = -(\nabla\mathbf{n}\cdot\mathbf{n})\otimes\mathbf{n} - \mathbf{n}\otimes(\nabla\mathbf{n}\cdot\mathbf{n}) = 0$. Thus,

$$\nabla(\nabla_S p)\cdot\mathbf{n} = (\nabla^2 p\cdot\mathbf{n})\cdot\mathbf{P} = [\nabla(\nabla p\cdot\mathbf{n}) - \nabla p\cdot\nabla\mathbf{n}]\cdot\mathbf{P} = \nabla_S(\nabla p\cdot\mathbf{n}) + \mathbf{W}\cdot\nabla_S p. \tag{2.53}$$

Taking into account the definitions of $\mathscr{A}_1$ and $\mathscr{B}_1$, we arrive at the final form of $\mathscr{A}_2$:

$$\mathscr{A}_2 = -\frac{\mathscr{B}_1}{\mathbf{n}\cdot\mathbf{K}\cdot\mathbf{n}} - \mathbf{s}\cdot(\nabla_S\mathscr{A}_1 + \mathbf{W}\cdot\nabla_S\mathscr{A}_0). \tag{2.54}$$

Applying the second formula of (2.33), we calculate $\mathscr{B}_2$ as follows

$$\mathscr{B}_2 = \nabla\mathscr{B}_1\cdot\mathbf{n} = \nabla\left[\nabla(\mathbf{S}\cdot\nabla_S p)\colon\mathbf{P} - \nabla(\mathbf{s}w_n)\colon\mathbf{P}\right]\cdot\mathbf{n}. \tag{2.55}$$

Given that $\nabla\mathbf{P}\cdot\mathbf{n} = 0$, we consider the first term on the right-hand side of the above equation:

$$\begin{aligned}\nabla\left[\nabla(\mathbf{S}\cdot\nabla_S p)\colon\mathbf{P}\right]\cdot\mathbf{n} &= \left[\nabla\nabla(\mathbf{S}\cdot\nabla_S p)\cdot\mathbf{n}\right]\colon\mathbf{P}\\ &= \nabla\nabla\left[(\mathbf{S}\cdot\nabla_S p)\cdot\mathbf{n}\right]\colon\mathbf{P} - \left[\nabla(\mathbf{S}\cdot\nabla_S p)\cdot\nabla\mathbf{n}\right]\colon\mathbf{P}.\end{aligned} \tag{2.56}$$

The term $\nabla\nabla\left[(\mathbf{S}\cdot\nabla_S p)\cdot\mathbf{n}\right]\colon\mathbf{P}$ can be expanded as:

$$\nabla\nabla\left[(\mathbf{S}\cdot\nabla_S p)\cdot\mathbf{n}\right]\colon\mathbf{P} = \nabla_S[\mathbf{S}\cdot\nabla_S(\nabla p\cdot\mathbf{n})]\colon\mathbf{I} + \nabla_S[\mathbf{S}\cdot\mathbf{W}\cdot\nabla_S p]\colon\mathbf{I} \tag{2.57}$$

The term $-\left[\nabla(\mathbf{S}\cdot\nabla_S p)\cdot\nabla\mathbf{n}\right]\colon\mathbf{P}$ can be rewritten as:

$$-\left[\nabla(\mathbf{S}\cdot\nabla_S p)\cdot\nabla\mathbf{n}\right]\colon\mathbf{P} = \nabla_S(\mathbf{S}\cdot\nabla_S p)\colon\mathbf{W}. \tag{2.58}$$

For the second term on the right-hand side of equation (2.55), given that $\nabla\mathbf{P}\cdot\mathbf{n} = 0$, we have:

$$-\left[\nabla(\mathbf{s}w_n)\colon\mathbf{P}\right]\cdot\mathbf{n} = \left[\nabla(\nabla\mathbf{s}w_n)\cdot\mathbf{n}\right]\colon\mathbf{P}. \tag{2.59}$$

This can be further decomposed as:

$$\left[\nabla(\nabla\mathbf{s}w_n)\cdot\mathbf{n}\right]\colon\mathbf{P} = -\nabla\left[\nabla(\mathbf{s}w_n)\cdot\mathbf{n}\right]\colon\mathbf{P} + \left[\nabla(\mathbf{s}w_n)\cdot\nabla\mathbf{n}\right]\colon\mathbf{P}. \tag{2.60}$$

The first term on the right-hand side, $-\nabla\left[\nabla(\mathbf{s}w_n)\cdot\mathbf{n}\right]\colon\mathbf{P}$, can be expanded as follows

$$-\nabla\left[\nabla(\mathbf{s}w_n)\cdot\mathbf{n}\right]\colon\mathbf{P} = -\nabla_S\left[\mathbf{s}(\nabla w_n\cdot\mathbf{n})\right]\colon\mathbf{I}. \tag{2.61}$$

The second term, $[\nabla(\mathbf{s}q_n)\cdot\nabla\mathbf{n}]:\mathbf{P}$, can be rewritten as:

$$[\nabla(\mathbf{s}w_n)\cdot\nabla\mathbf{n}]:\mathbf{P}=-\nabla_S(\mathbf{s}w_n):\mathbf{W}, \tag{2.62}$$

Taking into account the definitions of $\mathscr{A}_1$ and $\mathscr{B}_1$, we arrive at the final form of $\mathscr{B}_2$:

$$\begin{aligned}\mathscr{B}_2 =&\nabla_S[\mathbf{S}\cdot\nabla_S\mathscr{A}_1]:\mathbf{I}+\nabla_S[\mathbf{S}\cdot\mathbf{W}\cdot\nabla_S\mathscr{A}_0]:\mathbf{I}+\nabla_S(\mathbf{S}\cdot\nabla_S\mathscr{A}_0):\mathbf{W}\\&-2\nabla_S(\mathbf{s}\mathscr{B}_1):\mathbf{I}-2\nabla_S(\mathbf{s}\mathscr{B}_0):\mathbf{W}.\end{aligned} \tag{2.63}$$

2.2.4 Case Where N is Arbitrary

By systematically extending the prior computations to $N=3,4,5,\ldots$, we have deduced the general recurrence relations for $\mathscr{A}_N$ and $\mathscr{B}_N$. These recursive expressions offer a concise and effective means to compute $\mathscr{A}_N$ and $\mathscr{B}_N$ for any integer N. They are given as follows:

$$\mathscr{A}_N=-\frac{\mathscr{B}_{N-1}}{\mathbf{n}\cdot\mathbf{K}\cdot\mathbf{n}}-\mathbf{s}\cdot\sum_{r=0}^{N-1}\frac{(N-1)!}{(N-1-r)!}\mathbf{W}^r\cdot\nabla_S\mathscr{A}_{N-1-r}, \tag{2.64}$$

$$\begin{aligned}\mathscr{B}_N=&\sum_{r=0}^{N-1}\frac{(N-1)!}{(N-1-r)!}\left[\sum_{k=0}^{N-1-r}\frac{(N-1-r)!}{(N-1-r-k)!}\nabla_S\left(\mathbf{S}\cdot\mathbf{W}^k\cdot\nabla_S\mathscr{A}_{N-1-r-k}\right):\mathbf{W}^r\right]\\&-\sum_{r=0}^{N-1}\frac{(N-1)!}{(N-1-r)!}\left[\nabla_S(\mathbf{s}\mathscr{B}_{N-1-r}):\mathbf{W}^r\right].\end{aligned} \tag{2.65}$$

By substituting $N=0,1,2$ into the explicit recursive formulas (2.64) and (2.65) for $\mathscr{A}_N$ and $\mathscr{B}_N$, respectively, we obtain results consistent with our earlier derivations. This process serves to validate the accuracy of the explicit recursion formulas for $\mathscr{A}_N$ and $\mathscr{B}_N$.

A rigorous proof of these formulas necessitates a step-by-step derivation, starting from the base cases and iteratively progressing to higher values of N. While conventionally, one would extend the recursion from $\mathscr{A}_{N-1}$ and $\mathscr{B}_{N-1}$ to obtain $\mathscr{A}_N$ and $\mathscr{B}_N$, this procedure primarily entails technical computations that closely parallel the subsequent validation process for the recursion for vector field. Subsequently, a detailed exposition of the derivation process for$\mathscr{A}_N$ and $\mathscr{B}_N$ from $\mathscr{A}_{N-1}$ and $\mathscr{B}_{N-1}$ within the vector framework will be provided. This comprehensive treatment aims to furnish a scholarly reference for the verification of the recursion formulas,

elucidating the underlying logic and methodology employed in ensuring the accuracy of the mathematical expressions.

Combining equations (2.27), (2.64), and (2.65), we have presented the complete Taylor series expansion of the pore pressure field in this section. This explicit expression of the Taylor series incorporates crucial information about the material properties, which are embedded in the operators $\mathbf{S}$ and $\mathbf{s}$. This Taylor series expansion is applicable to other types of transport phenomena and exhibits a similar structure for $\mathscr{A}_N$ and $\mathscr{B}_N$. For instance, when addressing heat conduction problems, Darcy's law is substituted with Fourier's law, and the mass conservation principle is replaced by the corresponding energy conservation principle. Despite these variations, the equations maintain a comparable form, resulting in $\mathbf{S}$ and $\mathbf{s}$ also have analogous expressions. This comprehensive examination of the Taylor series expansion highlights its broad applicability across diverse domains, making it a versatile tool for modeling various transport phenomena.

2.3 Taylor Expansion of a Vector Field Involved in an Elastic Problem

Now, we are placed in the context of linear elasticity. Then, Ψ represents the displacement vector field, while $\Phi \cdot \mathbf{n}$ denotes the traction vector field. It is conveninet to adopt conventional symbols: denote the displacement vector field by $\mathbf{u}$ instead of Ψ and symbolize the traction vector field by $\mathbf{t}$ rather than $\Phi \cdot \mathbf{n}$. According to the Cauchy theorem, the traction vector $\mathbf{t}$ is given by $\mathbf{t} = \boldsymbol{\sigma} \cdot \mathbf{n}$ with $\boldsymbol{\sigma}$ being the second-order Cauchy stress tensor.

The material constituting Ω_h is assumed to be linearly elastic and generally anisotropic. The material constitutive law is specified by Hooke's law:

$$\boldsymbol{\sigma} = \mathbb{C} : \boldsymbol{\varepsilon}, \tag{2.66}$$

where $\mathbb{C}$ is the fourth-order elastic stiffness tensor and has the usual minor and major symmetries

$$C_{ijkl} = C_{jikl} = C_{klij}. \tag{2.67}$$

The tensor $\mathbb{C}$ is positive-definite. The infinitesimal strain tensor $\boldsymbol{\varepsilon}$ is a symmetric second-order

tensor and defined by

$$\varepsilon = \frac{1}{2}\left[\nabla \mathbf{u} + (\nabla \mathbf{u})^T\right]. \tag{2.68}$$

On the other hand, the stress-strain relationship reads

$$\varepsilon = \mathbb{S} : \sigma, \tag{2.69}$$

where the elastic compliance tensor $\mathbb{S}$ is related to $\mathbb{C}$ by $\mathbb{S} = \mathbb{C}^{-1}$. Thus, $\mathbb{S}$ has also the usual minor and major and is positive definite. In the static situation and in the absence of body forces, the stress tensor σ satisfies the equilibrium equations

$$\mathrm{div}\sigma = 0. \tag{2.70}$$

If $S_0 \subset \Omega_h$ is a perfect interface partitioning Ω_h into two distinct subdomains $\Omega_h^{(-)}$ and $\Omega_h^{(+)}$, the displacement vector $\mathbf{u}$ and the traction $\mathbf{t}$ are both continuous across S_0:

$$\mathbf{u}^{(+)}(x_0) = \mathbf{u}^{(-)}(x_0) \quad \text{for } x_0 \in S_0, \tag{2.71}$$

$$\mathbf{t}^{(+)}(x_0) = \mathbf{t}^{(-)}(x_0) \quad \text{for } x_0 \in S_0. \tag{2.72}$$

Applying the Cauchy theorem, we have $\mathbf{t}^{(\pm)}(x_0) = \sigma^{(\pm)}(x_0)\mathbf{n}(x_0)$. So, the above traction continuity condition can be further written as

$$\sigma^{(+)}(x_0)\mathbf{n}(x_0) = \sigma^{(-)}(x_0)\mathbf{n}(x_0) \quad \text{for } x_0 \in S_0. \tag{2.73}$$

Applying the Hadamard relation (1.51) for a vector-valued function given in the first chapter to the displacement vector, we have

$$\nabla \mathbf{u}^{(+)}(x_0) - \nabla \mathbf{u}^{(-)}(x_0) = \mathbf{a} \otimes \mathbf{n}(x_0) \quad \text{for } x_0 \in S_0 \tag{2.74}$$

which implies that

$$\nabla_S \mathbf{u}^{(+)}(x_0) = \nabla_S \mathbf{u}^{(-)}(x_0) \quad \text{for } x_0 \in S_0. \tag{2.75}$$

Further, accounting for the strain tensor definition (2.68), the relation (2.74) gives rise to

$$\boldsymbol{\varepsilon}^{(+)}(\boldsymbol{x}_0) - \boldsymbol{\varepsilon}^{(-)}(\boldsymbol{x}_0) = \frac{1}{2}[\mathbf{a}(\boldsymbol{x}_0) \otimes \mathbf{n}(\boldsymbol{x}_0) + \mathbf{n}(\boldsymbol{x}_0) \otimes \mathbf{a}(\boldsymbol{x}_0)] \quad \text{for } \boldsymbol{x}_0 \in S_0. \tag{2.76}$$

This relation implies that

$$\boldsymbol{\varepsilon}_s^{(+)}(\boldsymbol{x}_0) = \boldsymbol{\varepsilon}_s^{(-)}(\boldsymbol{x}_0) \quad \text{for } \boldsymbol{x}_0 \in S_0, \tag{2.77}$$

where $\boldsymbol{\varepsilon}_s$ is the surface (or tangential) strain tensor defined on $S \subset \Omega_h$ by

$$\boldsymbol{\varepsilon}_s(\boldsymbol{x}) = \mathbf{P}(\boldsymbol{x}) \cdot \boldsymbol{\varepsilon}(\boldsymbol{x}) \cdot \mathbf{P}(\boldsymbol{x}). \tag{2.78}$$

The relations (2.76) or (2.77) formulates the well-known fact in mechanics: across a perfect interface S_0, the tangential components of the strain tensor are continuous while its normal components are discontinuous.

It is useful to introduce two fourth-order complementary orthogonal projection operators [69, 64] as follows:

$$\mathbb{P} = \mathbf{P}\underline{\otimes}\mathbf{P} = \mathbb{I} - \mathbf{P}^{\perp}\underline{\otimes}\mathbf{I} - \mathbf{I}\underline{\otimes}\mathbf{P}^{\perp} + \mathbf{P}^{\perp}\underline{\otimes}\mathbf{P}^{\perp}, \tag{2.79}$$

$$\mathbb{P}^{\perp} = \mathbb{I} - \mathbb{P} = \mathbf{P}^{\perp}\overline{\otimes}\mathbf{I} + \mathbf{I}\overline{\otimes}\mathbf{P}^{\perp} - \mathbf{P}^{\perp}\overline{\otimes}\mathbf{P}^{\perp}. \tag{2.80}$$

Above, $\mathbb{I}$ denotes the fourth-order identity tensor for the space of symmetric second-order tensors and is defined by:

$$\mathbb{I} = \mathbf{I}\overline{\otimes}\mathbf{I} = \frac{1}{2}(\mathbf{I}\underline{\otimes}\mathbf{I} + \mathbf{I}\overline{\otimes}\mathbf{I}). \tag{2.81}$$

In the foregoing formulae, $\underline{\otimes}$ and $\overline{\otimes}$ denote the Kronecker tensor product defined by

$$(\mathbf{X}\underline{\otimes}\mathbf{Y})_{ijkl} = A_{ik}B_{jl}, \quad (\mathbf{X}\overline{\otimes}\mathbf{Y})_{ijkl} = A_{il}B_{jk}, \tag{2.82}$$

where $\mathbf{X}$ and $\mathbf{Y}$ are any two second-order tensors, and

$$\mathbf{X}\overline{\otimes}\mathbf{Y} = \frac{1}{2}(\mathbf{X}\underline{\otimes}\mathbf{Y} + \mathbf{X}\overline{\otimes}\mathbf{Y}). \tag{2.83}$$

We can verify tha $\mathbb{P}$ and $\mathbb{P}^{\perp}$ are two complementary orthogonal projection operators in the sense that

$$\mathbb{P}+\mathbb{P}^{\perp}=\mathbb{I}, \quad \mathbb{P}\mathbb{P}=\mathbb{P}, \quad \mathbb{P}^{\perp}\mathbb{P}^{\perp}=\mathbb{P}^{\perp}, \quad (\mathbb{P})^{T}=\mathbb{P}, \quad (\mathbb{P}^{\perp})^{T}=\mathbb{P}^{\perp}, \quad \mathbb{P}\mathbb{P}^{\perp}=\mathbb{P}^{\perp}\mathbb{P}=\mathbb{O}, \tag{2.84}$$

where $(\cdot)^{T}$ represents the transposition and $\mathbb{O}$ denotes the fourth-order zero tensor.

With the aid of the introduced projection operators, the relation (2.77) can be compactly written as

$$\mathbb{P}(\boldsymbol{x}_0)\boldsymbol{\varepsilon}^{(+)}(\boldsymbol{x}_0)=\mathbb{P}(\boldsymbol{x}_0)\boldsymbol{\varepsilon}^{(-)}(\boldsymbol{x}_0) \quad \text{for} \quad \boldsymbol{x}_0\in S_0. \tag{2.85}$$

Furthermore, the traction continuity condition (2.73) is equivalent to

$$\mathbb{P}^{\perp}(\boldsymbol{x}_0)\boldsymbol{\sigma}^{(+)}(\boldsymbol{x}_0)=\mathbb{P}^{\perp}(\boldsymbol{x}_0)\boldsymbol{\sigma}^{(-)}(\boldsymbol{x}_0) \quad \text{for} \quad \boldsymbol{x}_0\in S_0. \tag{2.86}$$

Note that the continuity relations (2.85) and (2.86) are complementary. Indeed, equations (2.85) and (2.86) reflect that the important fact that the strain components parallel to the plane tangent to a perfect interface S_0 are continuous across S_0 while the stress components normal to the plane tangent to the perfect interface S_0 are continuous across S_0. This fact holds independently of material constituting Ω_h.

In the case in question, $\mathscr{A}_N$ and $\mathscr{B}_N$ denote two vector functions defined on $S_0\subset\Omega_h$. Precisely, we have

$$\mathscr{A}_N=\nabla^N_{\mathbf{n}}\mathbf{u}, \quad \mathscr{B}_N=\nabla^N_{\mathbf{n}}\mathbf{t}. \tag{2.87}$$

2.3.1 Cases Where $N=0$ and $N=1$

Substituting $N=0$ into (2.87) yields

$$\mathscr{A}_0=\mathbf{u}, \quad \mathscr{B}_0=\mathbf{t}. \tag{2.88}$$

When $N=1$, to obtain the explicit expressions of the operator $\mathscr{A}_1$, we first note that $\nabla\mathbf{u}$ evaluated on S admits the following decomposition:

$$\nabla\mathbf{u}=\nabla\mathbf{u}\cdot\mathbf{P}+\nabla\mathbf{u}\cdot\mathbf{P}^{\perp}=\nabla_S\mathbf{u}+\nabla_{\mathbf{n}}\mathbf{u}\otimes\mathbf{n}. \tag{2.89}$$

Substituting this decomposition into the expression of $\mathbf{t}$ and considering the symmetry of tensor $\mathbb{C}$, we obtain

$$\mathbf{t} = \boldsymbol{\sigma} \cdot \mathbf{n} = (\mathbb{C} : \nabla \mathbf{u}) \cdot \mathbf{n} = \mathbb{C} : \nabla_S \mathbf{u} \cdot \mathbf{n} + (\mathbf{n} \cdot \mathbb{C} \cdot \mathbf{n}) \cdot \nabla_{\mathbf{n}} \mathbf{u}. \tag{2.90}$$

The fourth-order tensor $\mathbb{C}$ is positive definite, namely $\boldsymbol{\varepsilon} : (\mathbb{C}\boldsymbol{\varepsilon}) > 0$ for all $\boldsymbol{\varepsilon} \neq 0$. This ensures the positivity and invertibility of $\mathbf{n} \cdot \mathbb{C} \cdot \mathbf{n}$. Indeed, posing $\boldsymbol{\varepsilon} = \mathbf{a} \otimes \mathbf{n}$ with any $\mathbf{a} \in \mathbb{R}^k$ being a non-zero vector, we have

$$(\mathbf{a} \otimes \mathbf{n}) : [\mathbb{C} : (\mathbf{a} \otimes \mathbf{n})] > 0, \tag{2.91}$$

because $\mathbb{C}$ is positive definite. This amounts to

$$\mathbf{a} \cdot (\mathbf{n} \cdot \mathbb{C} \cdot \mathbf{n}) \cdot \mathbf{a} > 0, \tag{2.92}$$

showing that $\mathbf{n} \cdot \mathbb{C} \cdot \mathbf{n}$ is positive definite and therefore invertible. Let us define $\mathbf{G} = \mathbf{n} \cdot \mathbb{C} \cdot \mathbf{n}$ and denote its inverse as $\mathbf{F} = \mathbf{G}^{-1}$. By substituting this definition into equation (2.90), we obtain:

$$\nabla_{\mathbf{n}} \mathbf{u} = \mathbf{F} \cdot \mathbf{t} - \mathfrak{D} : \nabla_S \boldsymbol{u} \tag{2.93}$$

where $\mathfrak{D}$ is the third-order tensor defined by

$$\mathfrak{D} = \mathbf{F} \cdot (\mathbf{n} \cdot \mathbb{C}). \tag{2.94}$$

Using the decomposition (1.14), the equilibrium equation (2.70) can be rewritten as

$$\nabla \boldsymbol{\sigma} : \mathbf{P} + \nabla \boldsymbol{\sigma} : \mathbf{P}^{\perp} = 0. \tag{2.95}$$

Given the fact that the unit normal vector $\mathbf{n}$ defined in a domain formed by parallel sheets satisfies $\nabla \mathbf{n} \cdot \mathbf{n} = 0$, we can write

$$\nabla \boldsymbol{\sigma} : \mathbf{P}^{\perp} = \nabla(\boldsymbol{\sigma} \cdot \mathbf{n}) \cdot \mathbf{n} - \boldsymbol{\sigma} \cdot \nabla \mathbf{n} \cdot \mathbf{n} = \nabla_{\mathbf{n}} \mathbf{t}. \tag{2.96}$$

Accounting for this result, it follows from (2.95) that

$$\nabla_{\mathbf{n}} \mathbf{t} = -\mathrm{div}_S \boldsymbol{\sigma}. \tag{2.97}$$

Using Hooke's law and the formula (2.89) in (2.97), we get

$$\nabla_{\mathbf{n}}\mathbf{t} = -\mathrm{div}_S(\mathbb{C} : (\nabla_S \mathbf{u}) - \mathrm{div}_S[(\mathbb{C}\cdot\mathbf{n})\cdot\nabla_{\mathbf{n}}\mathbf{u}] = -\mathrm{div}_S(\mathbb{C} : (\nabla_s \mathbf{u}) - \mathrm{div}_S[(\mathbb{C}\cdot\mathbf{n})\cdot\mathscr{A}_1].$$

By substituting equation (2.93) into the preceding equation, we derive:

$$\nabla_{\mathbf{n}}\mathbf{t} = -\mathrm{div}_S(\mathbb{A} : \nabla_S \mathbf{u}) - \mathrm{div}_S(B\cdot\mathbf{t}), \tag{2.98}$$

where the tensors $\mathbb{A}$ and $\mathfrak{B}$ are defined by

$$\mathbb{A} = \mathbb{C} - (\mathbb{C}\cdot\mathbf{n})\cdot\mathbf{F}\cdot(\mathbf{n}\cdot\mathbb{C}), \tag{2.99}$$

$$\mathfrak{B} = (\mathbb{C}\cdot\mathbf{n})\cdot\mathbf{F}. \tag{2.100}$$

It can be verified that $\mathbb{A}$ is the fourth-order symmetric having the minor and major symmetries:

$$A_{ijkl} = A_{jikl} = A_{klij}. \tag{2.101}$$

Additionally, it can be shown that $\mathbb{A}$ possesses the following properties:

$$\mathbb{A}(\mathbb{PSP}) = (\mathbb{PSP})\mathbb{A} = \mathbb{P}, \quad \mathbb{AP} = \mathbb{PA} = \mathbb{A}. \tag{2.102}$$

Furthermore, the second term in the expression of $\mathbb{A}$ can be expressed by

$$(\mathbb{C}\cdot\mathbf{n})\cdot\mathbf{F}\cdot(\mathbf{n}\cdot\mathbb{C}) = \mathbb{C}\colon\mathbb{B}\colon\mathbb{C} \tag{2.103}$$

where the fourth-order $\mathbb{B}$ is given by

$$\mathbb{B} = \frac{1}{2}(\mathbf{F}\underline{\otimes}\mathbf{P}^{\perp} + \mathbf{P}^{\perp}\underline{\otimes}\mathbf{F}). \tag{2.104}$$

The fourth-order tensor $\mathbb{B}$ relates the stress tensor to the normal component of the displacement gradient, facilitating the expression of the anisotropic behavior of the material. Additionally, it

can be verified that

$$\mathbb{B}(\mathbb{P}^{\perp}\mathbb{C}\mathbb{P}^{\perp}) = (\mathbb{P}^{\perp}\mathbb{C}\mathbb{P}^{\perp})\mathbb{B} = \mathbb{P}^{\perp}, \quad \mathbb{B}\mathbb{P}^{\perp} = \mathbb{P}^{\perp}\mathbb{B} = \mathbb{B}. \tag{2.105}$$

2.3.2 Case Where $N = 2$

When $N = 2$, we can figure out $\mathscr{A}_2$ by

$$\mathscr{A}_2 = \nabla\mathscr{A}_1 \cdot \mathbf{n} = (\nabla\mathbf{F}\cdot\mathbf{n})\cdot\mathbf{t} + \mathbf{F}\cdot(\nabla\mathbf{t}\cdot\mathbf{n}) - (\nabla D\cdot\mathbf{n}) : \nabla_S\mathbf{u} - D : \nabla(\nabla_S\mathbf{u})\cdot\mathbf{n}. \tag{2.106}$$

To address the first term of equation (2.106), consider the inverse relationship between the tensors $\mathbf{G}$ and $\mathbf{F}$, implying that

$$\nabla(\mathbf{F}\cdot\mathbf{G})\cdot\mathbf{n} = \nabla\mathbf{I}\cdot\mathbf{n}.$$

This leads to

$$(\nabla\mathbf{F}\cdot\mathbf{n})\cdot\mathbf{G} + \mathbf{F}\cdot(\nabla\mathbf{G}\cdot\mathbf{n}) = \mathbf{0}. \tag{2.107}$$

Exploiting the property $\nabla\mathbf{n}\cdot\mathbf{n} = \mathbf{0}$, we deduce:

$$\nabla\mathbf{G}\cdot\mathbf{n} = \nabla(\mathbf{n}\cdot\mathbb{C}\cdot\mathbf{n})\cdot\mathbf{n} = \mathbf{0}, \tag{2.108}$$

implying $(\nabla\mathbf{F}\cdot\mathbf{n})\cdot\mathbf{G} = \mathbf{0}$. Since $\mathbf{G}$ is invertible, it follows:

$$\nabla\mathbf{F}\cdot\mathbf{n} = \mathbf{0}. \tag{2.109}$$

For the second term of equation (2.106), it can be transformed into

$$\mathbf{F}\cdot(\nabla\mathbf{t}\cdot\mathbf{n}) = \mathbf{F}\cdot\mathscr{B}_1. \tag{2.110}$$

For the third term of equation (2.106), we consider the property $\nabla(\mathbf{n}\cdot\mathbb{C})\cdot\mathbf{n} = 0$, so that

$$\nabla D\cdot\mathbf{n} = \nabla[\mathbf{F}\cdot(\mathbf{n}\cdot\mathbb{C})]\cdot\mathbf{n} = (\nabla\mathbf{F}\cdot\mathbf{n})\cdot(\mathbf{n}\cdot\mathbb{C}) + \mathbf{F}\cdot[\nabla(\mathbf{n}\cdot\mathbb{C})\cdot\mathbf{n}] = \mathbf{0}. \tag{2.111}$$

Now, for the last term of equation (2.106), considering $\nabla\mathbf{P}\cdot\mathbf{n}=0$, we proceed with the calculation:

$$\mathfrak{D}:\nabla(\nabla_S\mathbf{u})\cdot\mathbf{n}=\mathfrak{D}:\nabla(\nabla\mathbf{u}\cdot\mathbf{P})\cdot\mathbf{n}=\mathfrak{D}:[\nabla(\nabla\mathbf{u}\cdot\mathbf{n})\cdot\mathbf{P}-\nabla\mathbf{u}\cdot\nabla\mathbf{n}\cdot\mathbf{P}] \tag{2.112}$$

Taking into account the definitions of $\mathscr{A}_1$ and $\mathscr{B}_1$, we arrive at the final form of $\mathscr{A}_2$:

$$\mathscr{A}_2=\mathbf{F}\cdot\mathscr{B}_1-\mathfrak{D}:(\nabla_S\mathscr{A}_1+\nabla_S\mathscr{A}_0\cdot\mathbf{W}). \tag{2.113}$$

Applying the second formula of (2.87), $\mathscr{B}_2$ can be figured out by:

$$\mathscr{B}_2=\nabla\mathscr{B}_1\cdot\mathbf{n}=-\nabla[(\mathbb{A}:\nabla_S\mathbf{u})+div_S(\mathfrak{B}\cdot\mathbf{t})]\cdot\mathbf{n}. \tag{2.114}$$

The first term of equation (2.114) can be expanded as follows: given $\nabla\mathbf{P}\cdot\mathbf{n}=0$, then

$$\begin{aligned}\nabla[div_S(\mathbb{A}:\nabla_S\mathbf{u})]\cdot\mathbf{n}&=\nabla[\nabla(\mathbb{A}:\nabla_S\mathbf{u}):\mathbf{P}]\cdot\mathbf{n}\\&=\nabla[\nabla(\mathbb{A}:\nabla_S\mathbf{u})\cdot\mathbf{n}]:\mathbf{P}-\nabla(\mathbb{A}:\nabla_S\mathbf{u})\cdot\nabla\mathbf{n}\cdot\mathbf{P}.\end{aligned} \tag{2.115}$$

In the above expression, the first term can be further expanded as

$$\nabla[\nabla(\mathbb{A}:\nabla_S\mathbf{u})\cdot\mathbf{n}]:\mathbf{P}=\nabla[(\nabla\mathbb{A}\cdot\mathbf{n}):\nabla_S\mathbf{u}+\mathbb{A}:(\nabla\nabla_S\mathbf{u})\cdot\mathbf{n}]:\mathbf{P}, \tag{2.116}$$

and the second term can be rewritten as

$$-\nabla(\mathbb{A}:\nabla_S\mathbf{u})\cdot\nabla\mathbf{n}\cdot\mathbf{P}=\nabla(\mathbb{A}:\nabla_S\mathbf{u}):\mathbf{W}. \tag{2.117}$$

By adding the two foregoing expressions and taking into account the definitions of $\mathscr{A}_0$ and $\mathscr{A}_1$, we obtain:

$$\nabla[div_S(\mathbb{A}:\nabla_S\mathbf{u})]\cdot\mathbf{n}=\nabla[\mathbb{A}:(\nabla_S\mathscr{A}_1+\nabla_S\mathscr{A}_0\cdot\mathbf{W})]:\mathbf{P}+[\nabla(\mathbb{A}:\nabla_S\mathscr{A}_0)\cdot\mathbf{P}]:\mathbf{W}. \tag{2.118}$$

As demonstrated by equation (1.15), $\nabla(\cdot):\mathbf{P}=\nabla_S(\cdot):\mathbf{I}$, we have

$$\nabla[div_S(\mathbb{A}:\nabla_S\mathbf{u})]\cdot\mathbf{n}=\nabla_S(\mathbb{A}:\nabla_S\mathscr{A}_1):\mathbf{I}+\nabla_S(\mathbb{A}:\nabla_S\mathscr{A}_0\cdot\mathbf{W}):\mathbf{I}+\nabla_S(\mathbb{A}:\nabla_S\mathscr{A}_0):\mathbf{W}. \tag{2.119}$$

For the second term of equation (2.114), its expansion process and the properties used in the expansion are similar to those employed in the expansion of the first term of equation (2.114) (i.e., the expansion process mentioned above). To enhance clarity and coherence in the process, we present the expansion process in a single continuous equation as follows:

$$\begin{aligned}
\nabla[div_S(\mathfrak{B}\cdot\mathbf{t})]\cdot\mathbf{n} =& \nabla[\nabla(\mathfrak{B}\cdot\mathbf{t}):\mathbf{P}]\cdot\mathbf{n}\\
=& \nabla(\mathfrak{B}\cdot\mathbf{t}):(\nabla\mathbf{P}\cdot\mathbf{n})+[\nabla\nabla(\mathfrak{B}\cdot\mathbf{t})\cdot\mathbf{n}]:\mathbf{P}\\
=& \nabla[\nabla(\mathfrak{B}\cdot\mathbf{t})\cdot\mathbf{n}]:\mathbf{P}-\nabla(\mathfrak{B}\cdot\mathbf{t}):(\nabla\mathbf{n}\cdot\mathbf{P})\\
=& \nabla[(\nabla\mathfrak{B}\cdot\mathbf{t})\cdot\mathbf{n}+\mathfrak{B}\cdot\nabla\mathbf{t}\cdot\mathbf{n}]:\mathbf{P}+\nabla(\mathfrak{B}\cdot\mathbf{t})\cdot\mathbf{W}]\\
=& \nabla(\mathfrak{B}\cdot\mathscr{B}_1):\mathbf{P}+\nabla(B\cdot\mathscr{B}_0)\cdot\mathbf{W}\\
=& \nabla_S(\mathfrak{B}\cdot\mathscr{B}_1):\mathbf{I}+\nabla_S(\mathfrak{B}\cdot\mathscr{B}_0):\mathbf{W}.
\end{aligned} \tag{2.120}$$

Combining the results obtained from equations (2.119) and (2.120), the expression of $\mathscr{B}_2$ takes the form

$$\begin{aligned}
\mathscr{B}_2 =& -\nabla_S(\mathbb{A}:\nabla_S\mathscr{A}_1):\mathbf{I}-\nabla_S(\mathbb{A}:\nabla_s\mathscr{A}_0\cdot\mathbf{W}):\mathbf{I}-\nabla_S(\mathbb{A}:\nabla_s\mathscr{A}_0):\mathbf{W}\\
&-\nabla_S(\mathfrak{B}\cdot\mathscr{B}_1):\mathbf{I}-\nabla_S(\mathfrak{B}\cdot\mathscr{B}_0):\mathbf{W}.
\end{aligned} \tag{2.121}$$

2.3.3 Case Where N is Arbitrary

By systematically continuing our computations for $N=3,4,5,\ldots$, we can establish the general recurrence expressions for $\mathscr{A}_N$ and $\mathscr{B}_N$. These recursive expressions provide a succinct and efficient method for calculating $\mathscr{A}_N$ and $\mathscr{B}_N$ for any integer N. Precisely, they can be expressed as follows:

$$\mathscr{A}_N = \boldsymbol{F}\cdot\mathscr{B}_{N-1}-\mathfrak{D}:\left[\sum_{r=0}^{N-1}\frac{(N-1)!}{(N-1-r)!}\nabla_S\mathscr{A}_{N-1-r}\cdot\mathbf{W}^r\right], \tag{2.122}$$

$$\begin{aligned}
\mathscr{B}_N =& -\left[\sum_{r=0}^{N-1}\frac{(N-1)!}{(N-1-r)!}\sum_{r=0}^{N-1-r}\frac{(N-1-r)!}{(N-1-r-k)!}\nabla_s\left[\mathbb{A}:\left(\nabla_S\mathscr{A}_{N-1-r-k}\cdot\mathbf{W}^k\right)\right]:\mathbf{W}^r\right]\\
&-\sum_{r=0}^{N-1}\frac{(N-1)!}{(N-1-r)!}\nabla_S(\mathfrak{B}\cdot\mathscr{B}_{N-1-r}):\mathbf{W}^r.
\end{aligned} \tag{2.123}$$

To validate the derivation from $N-1$ to N, we will detail the steps to derive $\mathscr{A}_N$ and $\mathscr{B}_N$ from $\mathscr{A}_{N-1}$ and $\mathscr{B}_{N-1}$, based on the previously established recurrence relations. Assuming we have

$\mathscr{A}_{N-1}$ and $\mathscr{B}_{N-1}$, the recurrence formula for $\mathscr{A}_N$ is

$$\mathscr{A}_N = \nabla_{\mathbf{n}} \mathscr{A}_{N-1}. \tag{2.124}$$

Given

$$\mathscr{A}_{N-1} = \boldsymbol{F} \cdot \mathscr{B}_{N-2} - \mathfrak{D} : \left[\sum_{r=0}^{N-2} \frac{(N-2)!}{(N-2-r)!} \nabla_S \mathscr{A}_{N-2-r} \cdot \mathbf{W}^r \right], \tag{2.125}$$

we calculate the normal derivative of $\mathscr{A}_{N-1}$:

$$\mathscr{A}_N = \nabla \left[\boldsymbol{F} \cdot \mathscr{B}_{N-2} - \mathfrak{D} : \sum_{r=0}^{N-2} \frac{(N-2)!}{(N-2-r)!} (\nabla_S \mathscr{A}_{N-2-r} \cdot \mathbf{W}^r) \right] \cdot \mathbf{n}. \tag{2.126}$$

Considering the aforementioned fact that $\nabla \mathbf{F} \cdot \mathbf{n} = \mathbf{0}$, the first term of the above equation can be reformulated as

$$\nabla(\mathbf{F} \cdot \mathscr{B}_{N-2}) \cdot \mathbf{n} = (\nabla \mathbf{F} \cdot \mathbf{n}) \cdot \mathscr{B}_{N-2} - \mathbf{F} \cdot (\nabla \mathscr{B}_{N-2} \cdot \mathbf{n}) = \mathbf{F} \cdot \mathscr{B}_{N-1}. \tag{2.127}$$

Taking into account the fact that $\nabla \mathfrak{D} \cdot \mathbf{n} = \mathbf{0}$ as proved in equation (2.111), the second term can be expressed as follows:

$$\nabla_{\mathbf{n}} \left(-\mathfrak{D} : \sum_{r=0}^{N-2} \frac{(N-2)!}{(N-2-r)!} (\nabla_S \mathscr{A}_{N-2-r} \cdot \mathbf{W}^r) \right) = -\mathfrak{D} : \sum_{r=0}^{N-2} \frac{(N-2)!}{(N-2-r)!} \nabla_{\mathbf{n}} (\nabla_S \mathscr{A}_{N-2-r} \cdot \mathbf{W}^r). \tag{2.128}$$

Utilizing the previously provided rule that $\nabla \mathbf{W}^r(\boldsymbol{x}) \cdot \mathbf{n}(\boldsymbol{x}) = r \mathbf{W}^{r+1}$, we can rewrite the equation as:

$$-\mathfrak{D} : \sum_{r=0}^{N-2} \frac{(N-2)!}{(N-2-r)!} \nabla_S \mathscr{A}_{N-2-r} \cdot (\nabla \mathbf{W}^r \cdot \mathbf{n}) = -\mathfrak{D} : \sum_{r=0}^{N-2} \frac{(N-2)!}{(N-2-r)!} r \nabla_S \mathscr{A}_{N-2-r} \cdot \mathbf{W}^{r+1}. \tag{2.129}$$

Taking into account the fact that $\nabla \mathbf{P} \cdot \mathbf{n} = \mathbf{0}$, we can proceed as follows:

$$\begin{aligned}
&-\mathfrak{D} : \sum_{r=0}^{N-2} \frac{(N-2)!}{(N-2-r)!} \nabla(\nabla_S \mathscr{A}_{N-2-r}) \cdot \mathbf{n} \cdot \mathbf{W}^r \\
&= -\mathfrak{D} : \sum_{r=0}^{N-2} \frac{(N-2)!}{(N-2-r)!} [\nabla(\nabla \mathscr{A}_{N-2-r} \cdot \mathbf{n}) - \nabla \mathscr{A}_{N-2-r} \cdot \nabla \mathbf{n}] \cdot \mathbf{P} \cdot \mathbf{W}^r \\
&= -\mathfrak{D} : \sum_{r=0}^{N-2} \frac{(N-2)!}{(N-2-r)!} (\nabla \mathscr{A}_{N-1-r} \cdot \mathbf{P} \cdot \mathbf{W}^r + \nabla \mathscr{A}_{N-2-r} \cdot \mathbf{P} \cdot \mathbf{W}^{r+1}) \\
&= -\mathfrak{D} : \sum_{r=0}^{N-2} \frac{(N-2)!}{(N-2-r)!} (\nabla_S \mathscr{A}_{N-1-r} \cdot \mathbf{W}^r + \nabla_S \mathscr{A}_{N-2-r} \cdot \mathbf{W}^{r+1}).
\end{aligned} \tag{2.130}$$

Combining equations (2.127), (2.128) and (2.130), we can express $\mathscr{A}_N$ as follows:

$$\mathscr{A}_N = \boldsymbol{F} \cdot \mathscr{B}_{N-1} - \mathfrak{D} : \sum_{r=0}^{N-2} \frac{(N-2)!}{(N-2-r)!} \left[\nabla_S \mathscr{A}_{N-1-r} \cdot \mathbf{W}^r + (r+1) \nabla_S \mathscr{A}_{N-2-r} \cdot \mathbf{W}^{r+1} \right].$$

The above equation can be reduced to

$$\mathscr{A}_N = \boldsymbol{F} \cdot \mathscr{B}_{N-1} - \mathfrak{D} : \left[\sum_{r=0}^{N-1} \frac{(N-1)!}{(N-1-r)!} \nabla_S \mathscr{A}_{N-1-r} \cdot \mathbf{W}^r \right], \tag{2.131}$$

which is consistent with equation (2.122). Hence, the recursion formula for $\mathscr{A}_N$ has been validated.

Similarly, $\mathscr{B}_N$ can be calculated by

$$\mathscr{B}_N = \nabla \mathscr{B}_{N-1} \cdot \mathbf{n}.$$

Given the expression

$$\begin{aligned}
\mathscr{B}_{N-1} = &-\left[\sum_{r=0}^{N-2} \frac{(N-2)!}{(N-2-r)!} \sum_{r=0}^{N-2-r} \frac{(N-2)!}{(N-2-r-k)!} \nabla_S \left[\mathbb{A} : \left(\nabla_S \mathscr{A}_{N-2-r-k} \cdot \mathbf{W}^k \right) \right] : \mathbf{W}^r \right] \\
&- \left[\sum_{r=0}^{N-2} \frac{(N-2)!}{(N-2-r)!} \nabla_S (\mathfrak{B} \cdot \mathscr{B}_{N-2-r}) : \mathbf{W}^r \right],
\end{aligned} \tag{2.132}$$

we compute the normal derivative of $\mathscr{B}_{N-1}$:

$$\begin{aligned}\mathscr{B}_N = &-\nabla\left[\sum_{r=0}^{N-2}\frac{(N-2)!}{(N-2-r)!}\sum_{r=0}^{N-2-r}\frac{(N-2)!}{(N-2-r-k)!}\nabla_S\left[\mathbb{A}:\left(\nabla_S\mathscr{A}_{N-2-r-k}\cdot\mathbf{W}^k\right)\right]:\mathbf{W}^r\right]\cdot\mathbf{n}\\ &-\nabla\left[\sum_{r=0}^{N-2}\frac{(N-2)!}{(N-2-r)!}\nabla_S(\mathfrak{B}\cdot\mathscr{B}_{N-2-r}):\mathbf{W}^r\right]\cdot\mathbf{n}.\end{aligned} \tag{2.133}$$

Since that the derivation process has already made use of the properties mentioned earlier, for the sake of clarity and coherence, the complete derivation steps for both terms will be directly presented in a unified manner. This approach aims to provide a comprehensive understanding of the derivation process. For the first term, derivation proceeds as follows:

$$\begin{aligned}&\nabla[\nabla_S[\mathbb{A}:(\nabla_S\mathscr{A}_{N-2-r-k}\cdot\mathbf{W}^k)]:\mathbf{W}^r]\cdot\mathbf{n}\\ =&\nabla[\nabla[\mathbb{A}:(\nabla_S\mathscr{A}_{N-2-r-k}\cdot\mathbf{W}^k)]\cdot\mathbf{P}:\mathbf{W}^r]\cdot\mathbf{n}\\ =&\nabla[\mathbb{A}:(\nabla_S\mathscr{A}_{N-2-r-k}\cdot\mathbf{W}^k)]\cdot(\nabla\mathbf{P}\cdot\mathbf{n}):\mathbf{W}^r+[(\nabla\nabla(\mathbb{A}:(\nabla_S\mathscr{A}_{N-2-r-k}\cdot\mathbf{W}^k))\cdot\mathbf{n})\cdot\mathbf{P}]:\mathbf{W}^r\\ &+[\nabla(\mathbb{A}:(\nabla_S\mathscr{A}_{N-2-r-k}\cdot\mathbf{W}^k))\cdot\mathbf{P}]:(\nabla\mathbf{W}^r\cdot\mathbf{n})\\ =&[(\nabla\nabla(\mathbb{A}:(\nabla_S\mathscr{A}_{N-2-r-k}\cdot\mathbf{W}^k))\cdot\mathbf{n})\cdot\mathbf{P}]:\mathbf{W}^r-[\nabla(\mathbb{A}:(\nabla_S\mathscr{A}_{N-2-r-k}\cdot\mathbf{W}^k))\cdot(\nabla\mathbf{n}\cdot\mathbf{P})]:\mathbf{W}^r\\ &+[\nabla(\mathbb{A}:(\nabla_S\mathscr{A}_{N-2-r-k}\cdot\mathbf{W}^k))\cdot\mathbf{P}]:(\nabla\mathbf{W}^r\cdot\mathbf{n})\\ =&(r+1)\nabla_S[\mathbb{A}:\nabla_S(\mathscr{A}_{N-2-r-k}\cdot\mathbf{W}^k)]:\mathbf{W}^r+\nabla_s[\mathbb{A}:(\nabla_S\mathscr{A}_{N-1-r-k}\cdot\mathbf{W}^k)]:\mathbf{W}^r\\ &+(k+1)\nabla_S[\mathbb{A}:(\nabla_S\mathscr{A}_{N-2-r-k}\cdot\mathbf{W}^{k+1})]:\mathbf{W}^r.\end{aligned} \tag{2.134}$$

For the derivation of the second term, the following steps are taken:

$$\begin{aligned}&\nabla[\nabla_S(\mathfrak{B}\cdot\mathscr{B}_{N-2-r}):\mathbf{W}^r]\cdot\mathbf{n}\\ =&\nabla[\nabla(\mathfrak{B}\cdot\mathscr{B}_{N-2-r})\cdot\mathbf{P}:\mathbf{W}^r]\cdot\mathbf{n}\\ =&[\nabla(\mathfrak{B}\cdot\mathscr{B}_{N-2-r})\cdot(\nabla\mathbf{P}\cdot\mathbf{n})]:\mathbf{W}^r+[(\nabla\nabla(\mathfrak{B}\cdot\mathscr{B}_{N-2-r})\cdot\mathbf{n})\cdot\mathbf{P}]:\mathbf{W}^r+[\nabla(\mathfrak{B}\cdot\mathscr{B}_{N-2-r})\cdot\mathbf{P}]:(\nabla\mathbf{W}^r\cdot\mathbf{n})\\ =&[\nabla(\mathfrak{B}\cdot(\nabla\mathscr{B}_{N-2-r}\cdot\mathbf{n}))\cdot\mathbf{P}]:\mathbf{W}^r+[\nabla(\mathfrak{B}\cdot\nabla\mathscr{B}_{N-2-r})\cdot\mathbf{P}\cdot\mathbf{W}]:\mathbf{W}^r+[\nabla(\mathfrak{B}\cdot\mathscr{B}_{N-2-r})\cdot\mathbf{P}]:(r\mathbf{W}^{r+1})\\ =&\nabla_S(\mathfrak{B}\cdot\mathscr{B}_{N-1-r}):\mathbf{W}^r+\nabla_S(\mathfrak{B}\cdot\mathscr{B}_{N-2-r}):\mathbf{W}^{r+1}+r\nabla_S(\mathfrak{B}\cdot\mathscr{B}_{N-2-r}):\mathbf{W}^{r+1}\\ =&\nabla_S(\mathfrak{B}\cdot\mathscr{B}_{N-1-r}):\mathbf{W}^r+(r+1)\nabla_S(\mathfrak{B}\cdot\mathscr{B}_{N-2-r}):\mathbf{W}^{r+1}.\end{aligned} \tag{2.135}$$

The addition of the outcomes derived from equations (2.134) and (2.135) yields:

$$\begin{aligned}\mathscr{B}_N = -[&\sum_{r=0}^{N-2}\frac{(N-2)!}{(N-2-r)!}\sum_{r=0}^{N-2-r}\frac{(N-2)!}{(N-2-r-k)!}[(r+1)\nabla_S[\mathbb{A}:\nabla_S(\mathscr{A}_{N-2-r-k}\cdot\mathbf{W}^k)]:\mathbf{W}^r\\ &+\nabla_S[\mathbb{A}:(\nabla_S\mathscr{A}_{N-1-r-k}\cdot\mathbf{W}^k)]:\mathbf{W}^r+(k+1)\nabla_S[\mathbb{A}:(\nabla_S\mathscr{A}_{N-2-r-k}\cdot\mathbf{W}^{k+1})]:\mathbf{W}^r]]\\ &-\sum_{r=0}^{N-2}\frac{(N-2)!}{(N-2-r)!}[\nabla_S(\mathfrak{B}\cdot\mathscr{B}_{N-1-r}):\mathbf{W}^r+(r+1)\nabla_S(\mathfrak{B}\cdot\mathscr{B}_{N-2-r}):\mathbf{W}^{r+1}].\end{aligned} \tag{2.136}$$

The above equation can be reduced as

$$\begin{aligned}\mathscr{B}_N = -&\left[\sum_{r=0}^{N-1}\frac{(N-1)!}{(N-1-r)!}\sum_{r=0}^{N-1-r}\frac{(N-1-r)!}{(N-1-r-k)!}\nabla_S\left[\mathbb{A}:\left(\nabla_S\mathscr{A}_{N-1-r-k}\cdot\mathbf{L}^k\right)\right]:\mathbf{W}^r\right]\\ &-\sum_{r=0}^{N-1}\frac{(N-1)!}{(N-1-r)!}\nabla_S(\mathfrak{B}\cdot\mathscr{B}_{N-1-r}):\mathbf{W}^r\end{aligned} \tag{2.137}$$

which is consistent with equation (2.123). Therefore, the validity of the recursion formula for $\mathscr{B}_N$ has been confirmed.

2.4 Particular Cases of Isotropic and Transversely Isotropic Materials

2.4.1 Scalar Fields with Isotropic Materials

When the material forming the domain Ω_h is isotropic, the permeability is direction-independent. In this case, the permeability tensor $\mathbf{K}$ is isotropic and takes the simplest form:

$$\mathbf{K} = K\mathbf{I}, \tag{2.138}$$

where K is a positive scalar coefficient. As a result, the operators involved in the Taylor series expansion of the scalar field possess explicit and simplified expressions. By substituting the above expression of $\mathbf{K}$ into the definition (2.39) of $\mathbf{s}$, we obtain

$$\mathbf{s} = \mathbf{n}. \tag{2.139}$$

This indicates that $\mathbf{s}$ equals the unit normal vector $\mathbf{n}$. Similarly, substituting (2.138) into the definition (2.48) of $\mathbf{S}$, it follows that

$$\mathbf{S} = K\mathbf{P}^{\perp}. \tag{2.140}$$

2.4.2 Vector Fields with Transversely Isotropic Materials

When the elastic material constituting Ω_h is transversely isotropic about the axis normal to the middle surface, the elastic stiffness tensor $\mathbb{C}$ has the expression

$$\mathbb{C} = (C_{11} - C_{12})\mathbb{P} + 2C_{44}\mathbb{P}^{\perp} + C_{12}\mathbf{P}\otimes\mathbf{P} + C_{13}(\mathbf{P}\otimes\mathbf{P}^{\perp} + \mathbf{P}^{\perp}\otimes\mathbf{P}) + (C_{33} - 2C_{44})\mathbf{P}^{\perp}\otimes\mathbf{P}^{\perp}. \tag{2.141}$$

where the fourth-order tensors $\mathbb{P}$, $\mathbb{P}^{\perp}$, $\mathbf{P}\otimes\mathbf{P}$, $\mathbf{P}\otimes\mathbf{P}^{\perp} + \mathbf{P}^{\perp}\otimes\mathbf{P}$, $\mathbf{P}^{\perp}\otimes\mathbf{P}^{\perp}$ form a complete set of transversely isotropic tensor generators. In Voigt notation, the matrix representation of $\mathbb{C}$ for the transversely isotropic material in question is given by

$$[\mathbb{C}] = \begin{bmatrix} C_{11} & C_{12} & C_{13} & 0 & 0 & 0 \\ C_{12} & C_{11} & C_{23} & 0 & 0 & 0 \\ C_{13} & C_{23} & C_{33} & 0 & 0 & 0 \\ 0 & 0 & 0 & C_{44} & 0 & 0 \\ 0 & 0 & 0 & 0 & C_{44} & 0 \\ 0 & 0 & 0 & 0 & 0 & \frac{1}{2}(C_{11} - C_{12}) \end{bmatrix}. \tag{2.142}$$

In the case under consideration, the operators appearing in the Taylor series expansion of the displacement vector admit explicit expressions. Before proceeding with the derivation of these explicit expressions, it is necessary to present a technique for computing the inverse of a tensor having the form $(\mathbf{U} + \alpha\mathbf{a}\otimes\mathbf{b})$, as outlined by He and Feng [65]. Here, $\mathbf{U}$ denotes an inversible tensor, and the secalar α and the vectors $\mathbf{a}$ and $\mathbf{b}$ are such that $1 + \alpha(\mathbf{b}\cdot\mathbf{U}\mathbf{a}) \neq 0$. Then, the following formula holds:

$$(\mathbf{U} + \alpha\mathbf{a}\otimes\mathbf{b})^{-1} = \mathbf{U}^{-1} - \frac{\alpha}{1 + \alpha(\mathbf{b}\cdot\mathbf{U}\mathbf{a})}(\mathbf{U}^{-1}\mathbf{a})\otimes(\mathbf{U}^{-1}\mathbf{b}). \tag{2.143}$$

Given the expression (2.141) of the elastic stiffness tensor $\mathbb{C}$ for a transversely isotropic

material, we can write

$$\mathbf{G} = \mathbf{n} \cdot \mathbb{C} \cdot \mathbf{n} = C_{44}\mathbf{I} + (C_{33} - C_{44})\mathbf{P}^{\perp}. \tag{2.144}$$

Applying (2.143), we can deduce the inverse of $\mathbf{G}$ as follows:

$$\mathbf{F} = \frac{1}{C_{44}}\mathbf{I} - \frac{C_{33} - C_{44}}{C_{33}C_{44}}\mathbf{P}^{\perp}. \tag{2.145}$$

Utilizing the properties of operators $\mathbb{P}^{\perp}$ and $\mathbb{P}$ as described in (2.84), respectively, we obtain:

$$\mathbb{P}^{\perp}\mathbb{C}\mathbb{P}^{\perp} = 2C_{44}\mathbb{P}^{\perp} + (C_{33} - 2C)\mathbf{P}^{\perp} \otimes \mathbf{P}^{\perp}. \tag{2.146}$$

Taking into account that $\mathbb{B}(\mathbb{P}^{\perp}\mathbb{C}\mathbb{P}^{\perp}) = (\mathbb{P}^{\perp}\mathbb{C}\mathbb{P}^{\perp})\mathbb{B} = \mathbb{P}^{\perp}$, indicating that the inversion formula (2.143) is applicable to $\mathbb{P}\mathbb{C}\mathbb{P}$ as well, we can consequently infer:

$$\mathbb{B} = \frac{1}{2C_{44}}\left(\mathbb{P}^{\perp} - \frac{C_{33} - 2C_{44}}{C_{33}}\mathbf{P}^{\perp} \otimes \mathbf{P}^{\perp}\right). \tag{2.147}$$

We proceed by computing $\mathbb{C} : \mathbb{B} : \mathbb{C}$, a crucial step in determining $\mathbb{A}$. It can be verified that

$$\mathbb{C} : \mathbb{B} : \mathbb{C} = 2C_{44}\mathbb{P}^{\perp} + \frac{C_{13}^2}{C_{33}}\mathbf{P} \otimes \mathbf{P} + C_{13}(\mathbf{P} \otimes \mathbf{P}^{\perp} + \mathbf{P}^{\perp} \otimes \mathbf{P}) + (C_{33} - 2C_{44})\mathbf{P}^{\perp} \otimes \mathbf{P}^{\perp}. \tag{2.148}$$

By substituting the above equation into equations (2.99) and (2.103), we derive the expression for $\mathbb{A}$ as:

$$\mathbb{A} = (C_{11} - C_{12})\mathbb{P} + \left(C_{12} - \frac{C_{13}^2}{C_{33}}\right)\mathbf{P} \otimes \mathbf{P}. \tag{2.149}$$

Given equation (2.141) and combining it with the definitions of $\mathfrak{B}$ and $\mathfrak{D}$ provided in equations (2.94) and (2.100) respectively, we obtain

$$\mathfrak{D} = \frac{C_{13}}{C_{33}}\mathbf{n} \otimes \mathbf{I} + \left(\frac{C_{33} - C_{13}}{C_{33}}\right)\mathbf{n} \otimes \mathbf{n} \otimes \mathbf{n} + 2\mathbf{n}\underline{\otimes}\mathbf{P}, \tag{2.150}$$

$$\mathfrak{B} = \frac{C_{13}}{C_{33}}\mathbf{I} \otimes \mathbf{n} + \left(\frac{C_{33} - C_{13}}{C_{33}}\right)\mathbf{n} \otimes \mathbf{n} \otimes \mathbf{n} + 2\mathbf{P}\underline{\otimes}\mathbf{n}. \tag{2.151}$$

2.4.3 Vector Fields within Isotropic Materials

When the material forming Ω_h exhibits isotropy, the elastic stiffness tensor $\mathbb{C}$ takes the classic form:

$$\mathbb{C} = \lambda \boldsymbol{I} \otimes \boldsymbol{I} + 2\mu \mathbb{I}, \tag{2.152}$$

where, λ and μ denote the Lamé elastic coefficients. The expression (5.77) is a particular case of (2.141). Indeed, it suffices to note that the parameters $C_{11} - C_{12}$ and $2C_{44}$ are both equivalent to 2μ, whereas C_{12}, C_{13}, and $C_{33} - 2C_{44}$ all correspond to λ. Then, accounting for these relationships in equations (2.144)-(2.151), we can readily obtain

$$\mathbf{G} = \mu \mathbf{I} + (\mu + \lambda)\mathbf{P}^{\perp}, \tag{2.153}$$

$$\boldsymbol{F} = \frac{1}{\lambda + 2\mu}\mathbf{P}^{\perp} + \frac{1}{\mu}\mathbf{P}, \tag{2.154}$$

$$\mathbb{B} = \frac{1}{2\mu}\left(\mathbb{P}^{\perp} - \frac{\lambda}{\lambda + 2\mu}\mathbf{P}^{\perp} \otimes \mathbf{P}^{\perp}\right), \tag{2.155}$$

$$\mathbb{A} = 2\mu\mathbb{P} + \frac{2\mu\lambda}{\lambda + 2\mu}\mathbf{P} \otimes \mathbf{P}, \tag{2.156}$$

$$\mathfrak{D} = \frac{\lambda}{\lambda + 2\mu}\mathbf{n} \otimes \mathbf{I} + \frac{2\mu}{\lambda + 2\mu}\mathbf{n} \otimes \mathbf{n} \otimes \mathbf{n} + 2\mathbf{n}\underline{\otimes}\mathbf{P}, \tag{2.157}$$

$$\mathfrak{B} = \frac{\lambda}{\lambda + 2\mu}\mathbf{I} \otimes \mathbf{n} + \frac{2\mu}{\lambda + 2\mu}\mathbf{n} \otimes \mathbf{n} \otimes \mathbf{n} + 2\mathbf{P}\underline{\otimes}\mathbf{n}. \tag{2.158}$$

2.5 Conclusion

In this chapter, we have explored the theoretical framework for analyzing thin-walled structures within three-dimensional Euclidean space, focusing particularly on shells modeled as entities with significantly smaller thickness compared to their other dimensions. By developing Taylor series expansions for scalar and vector fields within these shells, we transitioned from three-dimensional to two-dimensional frameworks, facilitating the application of plate and shell

theories as well as interface theories. In the context of interfaces where scalar or vector functions exhibit piecewise continuity between distinct regions, traditional Taylor series expansions are typically conducted separately on each side of the interface. Specifically, assuming the interface divides two distinct domains in space, the function's expansion near the interface is segmented into two parts: one originating from one side of the interface and another from the opposite side, as shown in equation (2.23). It is noteworthy that this piecewise discontinuity arises due to material properties. Taking this into consideration, we introduce continuous dual variables across this interface and establish recursive formulas in a unified format akin to the Taylor series expansion, as shown in equation (2.27). Moreover, we have provided the form of the recursive formula and detailed derivations demonstrating the correctness of this recursive formula for the Taylor series expansion of scalar and vector functions.

This form of Taylor series expansion is widely applied in the field of mechanics. Indeed, when investigating the distribution of fields within thin-walled structures, this Taylor series enables the derivation of a comprehensive framework encompassing various plate and shell theories. In the subsequent chapter, we will present a detailed exposition of this concept. When our focus is solely on the mechanical influence of thin-walled structures on the overall structure rather than the distribution of internal physical fields, we can utilize this Taylor series expansion to establish imperfect interface models. This topic will be presented in Chapter 5. During the derivation of the Taylor series expansion, certain operators were introduced. This chapter also extensively discusses their explicit expressions under transversely isotropic and isotropic conditions. Utilizing these operators, we can homogenize laminated plates, a topic that will be addressed in the procedural section of Chapter 4.

In conclusion, the analytical tools developed in this study not only simplify the dimensional complexity but also facilitate accurate predictions of shell behavior under diverse conditions. Looking ahead, these findings lay the groundwork for further refining these models, investigating additional material properties, and broadening applications to fields like aerospace engineering and structural mechanics. Our study underscores the critical role of dimensional reduction in advancing the comprehension and predictive capabilities of shell structures. The methodologies and results presented herein establish a robust foundation for future advancements in the analysis and design of thin-walled structures.

Part II

Asymptotic Modeling, Analysis, and Applications

Chapter 3

Derivation of Compact Coordinate-Free Plate Theory from Taylor Expansions of Strain Energy via Variational Analysis

When studying surfaces in differential geometry, the geometric properties are often characterized by the surface's position vector $\mathbf{r}$. The first fundamental form, involving $d\mathbf{r}$, provides metric information such as lengths and angles on the surface. On the other hand, the second fundamental one, involving $d^2\mathbf{r}$, offers curvature information that aids in understanding the degree of curvature and variation of curvature across the surface. Thus, by examining $d\mathbf{r}$ and $d^2\mathbf{r}$, we obtain fundamental geometric insights into the surface, including its metric properties and curvature characteristics. These insights are pivotal for comprehending the shape, structure, and evolution of the surface, serving as the foundation for a thorough exploration of its geometric attributes. Such an expansion for the gradient of displacement holds significance; indeed, it encompasses $\nabla\mathbf{u}$ and $\nabla^2\mathbf{u}$, analogous to $d\mathbf{r}$ and $d^2\mathbf{r}$ in the context of differential geometry.

Drawing inspiration from this differential geometric framework, we apply the Taylor series expansion of displacements from Chapter 2 to establish a general expression for the strain energy of plate-shell structures in terms of the deformation metrics of the mid-surface. Subsequently, we derive stress measures conjugate to the deformation metrics of the mid-surface. Employing a variational approach, we systematically derive the dynamic governing equations and corresponding boundary conditions for plate-shell structures in a concise and rigorous manner.

Additionally, we thoroughly investigate scenarios where coupling effects are neglected, pro-

viding detailed analyses of the corresponding stress measures, constitutive equations, and boundary conditions. In cases where the structure starts as a flat plate (zero curvature) and undergoes small deflections and rotations, this theoretical framework simplifies to the Mindlin plate theory (2D) and Timoshenko beam theory (1D). Furthermore, we conduct a comprehensive exploration of scenarios neglecting both coupling effects and shear forces, including detailed examinations of stress measures, constitutive equations, and boundary conditions. Under the assumption of a flat initial configuration and small deflections and rotations, this theoretical framework aligns with the Kirchhoff plate theory (2D) and the Bernoulli-Euler beam theory (1D).

It is important to notice that these theoretical frameworks are applicable to plate-shell structures composed of anisotropic materials, reflecting their wide-ranging practical utility. Furthermore, we extensively investigate their explicit formulations for both transversely isotropic and isotropic cases, enhancing their applicability across different material compositions and structural configurations.

3.1 General Taylor Expansions of Strain Energy

Let Ξ_h denote the strain energy, which quantifies the elastic potential energy stored in a thin plate-shell structure Ω_h due to deformation under applied loads. Specifically, the strain energy Ξ_h of the thin plate-shell structure is expressed as:

$$\Xi_h = \frac{1}{2}\int_{\Omega_h} \sigma : \varepsilon dv, \tag{3.1}$$

where σ denotes the stress tensor and ε signifies the strain tensor. By substituting Hooke's law (2.66) and the definition (2.68) of ε into the equation above, and accounting for the symmetry of the elastic stiffness tensor $\mathbb{C}$, the strain energy Ξ_h can be reformulated in terms of the displacement gradient $\nabla\mathbf{u}$ as follows:

$$\Xi_h = \frac{1}{2}\int_{\Omega_h} (\nabla\mathbf{u} : \mathbb{C} : \nabla\mathbf{u})\, dv. \tag{3.2}$$

Assuming the domain Ω_h is structured as described in Chapter 2, we define a coordinate system (x_1, x_2, x_3) such that the x_3-axis is aligned with the unit normal vector $\mathbf{n}$ to the mid-surface S_0 at each point $\boldsymbol{x}_0 \in S_0$. Specifically, S_0 is parameterized by (x_1, x_2) coordinates, and x_3 measures

the perpendicular distance from S_0 along the direction of $\mathbf{n}$. In this context, applying the decomposition (2.89) and combining it with the Taylor expansion (2.19) of the displacement $\mathbf{u}$, the gradient of $\mathbf{u}$ is written as follows:

$$\nabla\mathbf{u} = \left[\nabla_S\left(\mathbf{u}|_{x_0}\right) + \nabla_{\mathbf{n}}\mathbf{u}|_{x_0} \otimes \mathbf{n}\right] + x_3\left[\nabla_S\left(\nabla_{\mathbf{n}}\mathbf{u}|_{x_0}\right) + \nabla^2_{\mathbf{n}}\mathbf{u}|_{x_0} \otimes \mathbf{n}\right] + \mathbf{0}\left(\left|x_3^2\right|\right). \tag{3.3}$$

The term $\mathbf{0}(|x_3|)$ indicates that in the gradient expansion, we have considered only the zero and first-order terms associated with x_3, while neglecting higher-order terms. Substituting this gradient expansion into the strain energy expression (3.2), we obtain:

$$\begin{aligned}
\Xi_h =& \frac{1}{2}\int_{S_0}\int_{-\frac{h}{2}}^{\frac{h}{2}} \left[\nabla_S\mathbf{u} + \nabla_{\mathbf{n}}\mathbf{u} \otimes \mathbf{n}\right] : \mathbb{C} : \left[\nabla_S\mathbf{u} + \nabla_{\mathbf{n}}\mathbf{u} \otimes \mathbf{n}\right] dx_3 ds \\
&+ \int_{S_0}\int_{-\frac{h}{2}}^{\frac{h}{2}} x_3\left[\nabla_S\left(\nabla_{\mathbf{n}}\mathbf{u}\right) + \nabla^2_{\mathbf{n}}\mathbf{u} \otimes \mathbf{n}\right] : \mathbb{C} : \left[\nabla_S\mathbf{u} + \nabla_{\mathbf{n}}\mathbf{u} \otimes \mathbf{n}\right] dx_3 ds \\
&+ \frac{1}{2}\int_{S_0}\int_{-\frac{h}{2}}^{\frac{h}{2}} x_3^2\left[\nabla_S\left(\nabla_{\mathbf{n}}\mathbf{u}\right) + \nabla^2_{\mathbf{n}}\mathbf{u} \otimes \mathbf{n}\right] : \mathbb{C} : \left[\nabla_S\left(\nabla_{\mathbf{n}}\mathbf{u}\right) + \nabla^2_{\mathbf{n}}\mathbf{u} \otimes \mathbf{n}\right] dx_3 ds + 0\left(h^4\right).
\end{aligned} \tag{3.4}$$

Hence, on one hand, we decompose the original integral expression for energy from a volume integral into a line integral along the thickness direction (i.e., x_3) and a surface integral along the mid-surface (i.e., S_0). On the other hand, it is evident that substituting the Taylor expansion in the form of equation (3.3) into the energy integral formula results in an energy expression that is a third-order approximation in terms of the thickness.

Building upon the groundwork established in Chapter 2, we can now proceed to analyze each integral term separately. For the first term, we can further expand it as follows:

$$\begin{aligned}
&\left[\nabla_S\mathbf{u} + \nabla_{\mathbf{n}}\mathbf{u} \otimes \mathbf{n}\right] : \mathbb{C} : \left[\nabla_S\mathbf{u} + \nabla_{\mathbf{n}}\mathbf{u} \otimes \mathbf{n}\right] \\
&= \nabla_S\mathbf{u} : \mathbb{C} : \nabla_S\mathbf{u} + \nabla_S\mathbf{u} : \mathbb{C} : \left(\nabla_{\mathbf{n}}\mathbf{u} \otimes \mathbf{n}\right) + \left(\nabla_{\mathbf{n}}\mathbf{u} \otimes \mathbf{n}\right) : \mathbb{C} : \nabla_S\mathbf{u} + \left(\nabla_{\mathbf{n}}\mathbf{u} \otimes \mathbf{n}\right) : \mathbb{C} : \left(\nabla_{\mathbf{n}}\mathbf{u} \otimes \mathbf{n}\right)
\end{aligned} \tag{3.5}$$

As shown in (2.93), $\nabla_n\mathbf{u}$ is given by:

$$\nabla_n\mathbf{u} = \boldsymbol{F}\cdot\mathbf{t} - \mathfrak{D} : \nabla_s\mathbf{u}. \tag{3.6}$$

Moreover, due to the fact that $\mathbf{F}$ is invertible as discussed in Chapter 2, we can dot-multiply both sides of the equation by $\mathbf{F}^{-1} = \mathbf{n}\cdot\mathbb{C}\cdot\mathbf{n}$. Consequently, the above expression can be reformulated

as:

$$\mathbf{t} = (\mathbf{n}\cdot\mathbb{C}\cdot\mathbf{n})\cdot\nabla_{\mathbf{n}}\mathbf{u} + (\mathbf{n}\cdot\mathbb{C})\colon\nabla_S\mathbf{u}. \tag{3.7}$$

We can consolidate therefore the last two terms on the right-hand side of equation (3.5) as follows:

$$\begin{aligned}(\nabla_{\mathbf{n}}\mathbf{u}\otimes\mathbf{n})\colon\mathbb{C}\colon\nabla_S\mathbf{u} + (\nabla_{\mathbf{n}}\mathbf{u}\otimes\mathbf{n})\colon\mathbb{C}\colon(\nabla_{\mathbf{n}}\mathbf{u}\otimes\mathbf{n}) &= \nabla_{\mathbf{n}}\mathbf{u}\cdot[(\mathbf{n}\cdot\mathbb{C})\colon\nabla_S\mathbf{u} + (\mathbf{n}\cdot\mathbb{C}\cdot\mathbf{n})\cdot\nabla_{\mathbf{n}}\mathbf{u}] \\ &= \nabla_{\mathbf{n}}\mathbf{u}\cdot\mathbf{t}\end{aligned} \tag{3.8}$$

By introducing two operators $\mathbf{P}$ and $\mathbf{P}^{\perp}$ which have been defined in Chapter 1, we rewrite the above equation as:

$$\begin{aligned}\nabla_S\mathbf{u}\colon\mathbb{C}\colon(\nabla_{\mathbf{n}}\boldsymbol{u}\otimes\mathbf{n}) &= \nabla_S\mathbf{u}\colon(\mathbb{C}\cdot\mathbf{n})\cdot(\mathbf{F}\cdot\mathbf{t}) - \nabla_S\mathbf{u}\colon(\mathbb{C}\cdot\mathbf{n})\cdot\mathfrak{D}\colon\nabla_S\mathbf{u}) \\ &= \nabla_S\mathbf{u}\colon\mathfrak{B}\cdot\mathbf{t} - \nabla_S\mathbf{u}\colon[(\mathbb{C}\cdot\mathbf{n})\cdot\mathbf{F}\cdot(\mathbf{n}\cdot\mathbb{C})]\colon\nabla_S\mathbf{u}.\end{aligned} \tag{3.9}$$

Expanding upon this, by introducing operators $\mathbf{P}$ and $\mathbf{P}^{\perp}$, we can reframe the above equation as:

$$\begin{aligned}\nabla_S\mathbf{u}\colon\mathbb{C}\colon(\nabla_{\mathbf{n}}\boldsymbol{u}\otimes\mathbf{n}) &= \nabla_S\mathbf{u}\colon(\mathbf{P}+\mathbf{P}^{\perp})\cdot B\cdot\mathbf{t} - \nabla_S\mathbf{u}\colon[(\mathbb{C}\cdot\mathbf{n})\cdot\mathbf{F}\cdot(\mathbf{n}\cdot\mathbb{C})]\colon\nabla_S\mathbf{u} \\ &= \mathbf{P}\cdot\nabla_S\mathbf{u}\colon\mathfrak{B}\cdot\mathbf{t} + \nabla_S(\mathbf{u}\cdot\mathbf{n})\cdot\mathbf{t} - \nabla_S\mathbf{u}\colon[(\mathbb{C}\cdot\mathbf{n})\cdot\mathbf{F}\cdot(\mathbf{n}\cdot\mathbb{C})]\colon\nabla_S\mathbf{u}\end{aligned} \tag{3.10}$$

By combining equations (3.5) and (3.8) with (3.10), equation (3.5) can be simplified to:

$$\begin{aligned}&[\nabla_S\mathbf{u} + \nabla_{\mathbf{n}}\mathbf{u}\otimes\mathbf{n}]\colon\mathbb{C}\colon[\nabla_S\mathbf{u} + \nabla_{\mathbf{n}}\mathbf{u}\otimes\mathbf{n}] \\ &= \nabla_S\mathbf{u}\colon\mathbb{A}\colon\nabla_S\mathbf{u} + \nabla_S\mathbf{u}\colon\mathfrak{B}\cdot\mathbf{t} + \nabla_S(\mathbf{u}\cdot\mathbf{n})\cdot\mathbf{t} + \nabla_{\mathbf{n}}\mathbf{u}\cdot\mathbf{t}.\end{aligned} \tag{3.11}$$

The expansion of the second integral term of equation (3.4) yields:

$$\begin{aligned}&\nabla_S(\nabla_{\mathbf{n}}\mathbf{u})\colon\mathbb{C}\colon(\nabla_{\mathbf{n}}\mathbf{u}\otimes\mathbf{n}) \\ &= \nabla_S(\nabla_{\mathbf{n}}\mathbf{u})\colon(\mathbb{C}\cdot\mathbf{n})\cdot(\mathbf{F}\cdot\mathbf{t}) - \nabla_S(\nabla_{\mathbf{n}}\mathbf{u})\colon(\mathbb{C}\cdot\mathbf{n})\cdot(\mathfrak{D}\colon\nabla_S\mathbf{u}) \\ &= \nabla_S(\nabla_{\mathbf{n}}\mathbf{u})\colon\mathfrak{B}\cdot\mathbf{t} - \nabla_S(\nabla_{\mathbf{n}}\mathbf{u})\colon[(\mathbb{C}\cdot\mathbf{n})\cdot\mathbf{F}\cdot(\mathbf{n}\cdot\mathbb{C})]\colon\nabla_S\mathbf{u}\end{aligned} \tag{3.12}$$

At this point, we make the assumption that each layer parallel to the mid-surface of the plate

experiences no compression from adjacent layers, while the cross-section of the plate remains planar after deformation. Hence, we have:

$$\mathbf{t}\cdot\mathbf{n}=0,\quad \nabla_{\mathbf{n}}^{N}\mathbf{t}=\mathbf{0}\quad (N=1,2,3,4,5,\ldots). \tag{3.13}$$

Therefore, equation (2.113) can be simplified as follows:

$$\nabla_{\mathbf{n}}^{2}\mathbf{u}=-\mathfrak{D}:(\nabla_S(\nabla_{\mathbf{n}}\mathbf{u})+\nabla_S\mathbf{u}\cdot\mathbf{W}), \tag{3.14}$$

In the case where the cross-section of the plate maintains planarity post-deformation, we will subsequently introduce $\nabla_S(\nabla_{\mathbf{n}}\mathbf{u})$ as a representation of the curvature of the mid-plane. Within the context of infinitesimal deformations, the term $\nabla_S\mathbf{u}\cdot\mathbf{W}$ is small compared to $\nabla_S(\nabla_{\mathbf{n}}\mathbf{u})$. Consequently, the aforementioned equation can be further expressed as:

$$\nabla_{\mathbf{n}}^{2}\mathbf{u}=-\mathfrak{D}:\nabla_S(\nabla_{\mathbf{n}}\mathbf{u}), \tag{3.15}$$

Hence, the second integral term can be simplified to:

$$\begin{aligned}&\left[\nabla_S(\nabla_{\mathbf{n}}\mathbf{u})+\nabla_{\mathbf{n}}^{2}\mathbf{u}\otimes\mathbf{n}\right]:\mathbb{C}:\left[\nabla_S\mathbf{u}+\nabla_{\mathbf{n}}\mathbf{u}\otimes\mathbf{n}\right]\\&=\nabla_S(\nabla_{\mathbf{n}}\mathbf{u}):\mathbb{A}:\nabla_S\mathbf{u}+\nabla_S(\nabla_{\mathbf{n}}\mathbf{u}):\mathfrak{B}\cdot\mathbf{t}-\mathfrak{D}:\nabla_S(\nabla_{\mathbf{n}}\mathbf{u})\cdot\mathbf{t}\end{aligned} \tag{3.16}$$

Similarly, the third integral term can be simplified to:

$$\left[\nabla_S(\nabla_{\mathbf{n}}\mathbf{u})+\nabla_{\mathbf{n}}^{2}\mathbf{u}\otimes\mathbf{n}\right]:\mathbb{C}:\left[\nabla_S(\nabla_{\mathbf{n}}\mathbf{u})+\nabla_{\mathbf{n}}^{2}\mathbf{u}\otimes\mathbf{n}\right]=\nabla_S(\nabla_{\mathbf{n}}\mathbf{u}):\mathbb{A}:\nabla_S(\nabla_{\mathbf{n}}\mathbf{u}) \tag{3.17}$$

By introducing the surface strain, denoted by ε_s and defined by:

$$\varepsilon_s=\frac{1}{2}\mathbf{P}\cdot[\nabla\mathbf{u}+(\nabla\mathbf{u})^{T}]\cdot\mathbf{P}, \tag{3.18}$$

we obtain with the aid of the symmetric properties of $\mathbb{A}$

$$\frac{1}{2}\int_{S_0}\int_{-\frac{h}{2}}^{\frac{h}{2}}\nabla_S\mathbf{u}:\mathbb{A}:\nabla_S\mathbf{u}dx_3ds=\frac{1}{2}\int_{S_0}\int_{-\frac{h}{2}}^{\frac{h}{2}}\varepsilon_s:\mathbb{A}:\varepsilon_s dx_3ds. \tag{3.19}$$

Finally, with (3.11)-(3.17) and (3.19), we have

$$\begin{aligned}\Xi_h =& \frac{1}{2}\int_{S_0}\int_{-\frac{h}{2}}^{\frac{h}{2}} [\varepsilon_s : \mathbb{A} : \varepsilon_s + \varepsilon_s : \mathfrak{B}\cdot\mathbf{t} + \nabla_S(\mathbf{u}\cdot\mathbf{n})\cdot\mathbf{t} + \nabla_{\mathbf{n}}\mathbf{u}\cdot\mathbf{t}]\, dx_3 ds \\ &+ \int_{S_0}\int_{-\frac{h}{2}}^{\frac{h}{2}} x_3 [\nabla_S(\nabla_{\mathbf{n}}\mathbf{u}) : \mathbb{A} : \nabla_S\mathbf{u} + \nabla_S(\nabla_{\mathbf{n}}\mathbf{u}) : \mathfrak{B}\cdot\mathbf{t} - \mathfrak{D} : \nabla_S(\nabla_{\mathbf{n}}\mathbf{u})\cdot\mathbf{t}]\, dx_3 ds \\ &+ \frac{1}{2}\int_{S_0}\int_{-\frac{h}{2}}^{\frac{h}{2}} x_3^2 [\nabla_S(\nabla_{\mathbf{n}}\mathbf{u}) : \mathbb{A} : \nabla_S(\nabla_{\mathbf{n}}\mathbf{u})]\, dx_3 ds + 0\left(h^4\right).\end{aligned} \tag{3.20}$$

The integral (3.19) exhibits a quadratic form of metric tensors related to the displacement field of the mid-surface. This displacement field is intricately connected to the formulation of membrane energy, representing the elastic energy associated with the deformations in the mid-surface of the structure. Hence, we can write

$$\Xi_{membrane} = \frac{1}{2}\int_{S_0}\int_{-\frac{h}{2}}^{\frac{h}{2}} (\varepsilon_s : \mathbb{A} : \varepsilon_s) dx_3 ds. \tag{3.21}$$

As previously assumed, the neglect of normal stresses in the thickness direction (i.e., $\mathbf{t}\cdot\mathbf{n} = 0$) implies that the vector $\mathbf{t}$ solely represents shear forces along the thickness direction. Consequently, the term $\nabla_S(\mathbf{u}\cdot\mathbf{n})\cdot\mathbf{t} + \nabla_{\mathbf{n}}\mathbf{u}\cdot\mathbf{t}$ signifies the work done by shear forces along the thickness direction. Therefore, we denote

$$\Xi_{shear} = \frac{1}{2}\int_{S_0}\int_{-\frac{h}{2}}^{\frac{h}{2}} (\nabla_S(\mathbf{u}\cdot\mathbf{n})\cdot\mathbf{t} + \nabla_{\mathbf{n}}\mathbf{u}\cdot\mathbf{t}) dx_3 ds. \tag{3.22}$$

Utilizing operators $\mathbf{P}$ and $\mathbf{P}^{\perp}$, equation (3.7) can be expressed as follows:

$$\begin{aligned}\mathbf{t} =& (\mathbf{n}\cdot\mathbb{C}\cdot\mathbf{n})\cdot\nabla_{\mathbf{n}}\mathbf{u} + (\mathbf{n}\cdot\mathbb{C}) : \nabla_S\mathbf{u} \\ =& (\mathbf{n}\cdot\mathbb{C}\cdot\mathbf{n})\cdot\nabla_{\mathbf{n}}\mathbf{u} + (\mathbf{n}\cdot\mathbb{C}\cdot(\mathbf{P}+\mathbf{P}^{\perp})) : \nabla_S\mathbf{u} \\ =& (\mathbf{n}\cdot\mathbb{C}\cdot\mathbf{n})\cdot\nabla_{\mathbf{n}}\mathbf{u} + (\mathbf{n}\cdot\mathbb{C}\cdot\mathbf{n})\cdot\nabla_S(\mathbf{u}\cdot\mathbf{n}) + (\mathbf{n}\cdot\mathbb{C}) : \varepsilon_s.\end{aligned} \tag{3.23}$$

Physically, the term $(\mathbf{n}\cdot\mathbb{C}) : \varepsilon_s$ denotes the projection the stress field within the curved surface onto the normal direction of this surface. Notably, the outcome of this projection is evidently zero. This implies that the stress vector $\mathbf{t}$ given by (3.23) is reduced to

$$\mathbf{t} = (\mathbf{n}\cdot\mathbb{C}\cdot\mathbf{n})\cdot\nabla_{\mathbf{n}}\mathbf{u} + (\mathbf{n}\cdot\mathbb{C}\cdot\mathbf{n})\cdot\nabla_S(\mathbf{u}\cdot\mathbf{n}). \tag{3.24}$$

Therefore, the shear energy (3.22) can be expressed as the following symmetric quadratic form:

$$\Xi_{shear} = \frac{1}{2}\int_{S_0}\int_{-\frac{h}{2}}^{\frac{h}{2}} [\nabla_S(\mathbf{u}\cdot\mathbf{n}) + \nabla_{\mathbf{n}}\mathbf{u}]\cdot\mathbf{G}\cdot[\nabla_S(\mathbf{u}\cdot\mathbf{n}) + \nabla_{\mathbf{n}}\mathbf{u}]\,dx_3 ds. \tag{3.25}$$

The third integral term of equation (3.20) can be expressed as:

$$\Xi_{bending} = \frac{1}{2}\int_{S_0}\int_{-\frac{h}{2}}^{\frac{h}{2}} x_3^2\,[\nabla_S(\nabla_n\mathbf{u}) : \mathbb{A} : \nabla_S(\nabla_n\mathbf{u})]\,dx_3 ds. \tag{3.26}$$

Indeed, $\nabla_S(\nabla_{\mathbf{n}}\mathbf{u}) : \mathbb{A} : \nabla_S(\nabla_{\mathbf{n}}\mathbf{u})$ constitutes a quadratic form involving the components of the variation in the curvature tensor associated with a displacement field of the mid-surface of the shell or plate. Prior to undertaking the variation derivation of pure bending energy, we introduce a symmetric curvature tensor defined by

$$\boldsymbol{\kappa} = \frac{1}{2}\left[\nabla_S(\nabla_{\mathbf{n}}\mathbf{u}) + (\nabla_S(\nabla_{\mathbf{n}}\mathbf{u}))^T\right]. \tag{3.27}$$

The curvature tensor $\boldsymbol{\kappa}$ holds significant geometric importance on a curved surface, providing essential information about the curvature radius and direction of the surface. By computing the principal curvatures and their corresponding directions, insights into the degree and orientation of curvature at a given point on the surface can be obtained. The symmetric curvature tensor $\boldsymbol{\kappa}$ is instrumental in simplifying subsequent derivations, contributing to a more rigorous and compact mathematical framework. Indeed, due to the symmetry of the tensor $\mathbb{A}$, the expression for the pure bending energy (3.26) can be further simplified as:

$$\begin{aligned}\Xi_{bending} &= \frac{1}{2}\int_{S_0}\int_{-\frac{h}{2}}^{\frac{h}{2}} x_3^2\,[\nabla_S(\nabla_{\mathbf{n}}\mathbf{u}) : \mathbb{A} : \nabla_S(\nabla_{\mathbf{n}}\mathbf{u})]\,dx_3 ds \\ &= \frac{1}{2}\int_{S_0}\int_{-\frac{h}{2}}^{\frac{h}{2}} x_3^2\,[\boldsymbol{\kappa} : \mathbb{A} : \boldsymbol{\kappa}]\,dx_3 ds.\end{aligned} \tag{3.28}$$

The remaining terms of the strain energy in equation (3.20) can be expressed as:

$$\Xi_{couple} = \Xi_{couple1} + +\Xi_{couple2} + \Xi_{couple3} \tag{3.29}$$

where $\Xi_{couple1}$, $\Xi_{couple2}$ and $\Xi_{couple3}$, representing the coupling effects between membrane, s-

hear, and bending deformations, are given by

$$\Xi_{couple1} = \frac{1}{2}\int_{S_0}\int_{-\frac{h}{2}}^{\frac{h}{2}} [\varepsilon_s : \mathfrak{B}\cdot\mathbf{t}]\, dx_3 ds, \tag{3.30}$$

$$\Xi_{couple2} = \int_{S_0}\int_{-\frac{h}{2}}^{\frac{h}{2}} x_3\,[\nabla_S(\nabla_{\mathbf{n}}\mathbf{u}) : \mathfrak{B}\cdot\mathbf{t} - \mathfrak{D} : \nabla_S(\nabla_{\mathbf{n}}\mathbf{u})\cdot\mathbf{t}]\, dx_3 ds, \tag{3.31}$$

$$\Xi_{couple3} = \int_{S_0}\int_{-\frac{h}{2}}^{\frac{h}{2}} x_3\,[\nabla_S(\nabla_{\mathbf{n}}\mathbf{u}) : \mathbb{A} : \varepsilon_s]\, dx_3 ds. \tag{3.32}$$

As before, $\varepsilon_s : (\mathbb{C}\cdot\mathbf{n})$, denoting the projection of the stress field within the curved surface onto its normal direction, notably vanishes. Consequently, introducing equation (3.7) into equation (3.30), it can be shown that

$$\Xi_{couple1} = \frac{1}{2}\int_{S_0}\int_{-\frac{h}{2}}^{\frac{h}{2}} [\varepsilon_s : (\mathbb{C}\cdot\mathbf{n})\cdot\nabla_{\mathbf{n}}\mathbf{u} + \varepsilon_s : (\mathbb{C}\cdot\mathbf{n})\cdot\nabla_S(\mathbf{u}\cdot\mathbf{n})]\, dx_3 ds = 0. \tag{3.33}$$

By substituting equation (3.7) into equation (3.31), the expression of $\Xi_{couple2}$ is given by:

$$\Xi_{couple2} = \int_{S_0}\int_{-\frac{h}{2}}^{\frac{h}{2}} x_3\,[\nabla_S(\nabla_{\mathbf{n}}\mathbf{u}) : \mathfrak{B} - \mathfrak{D} : \nabla_S(\nabla_{\mathbf{n}}\mathbf{u})]\cdot\mathbf{G}\cdot[(\nabla_S(\mathbf{u}\cdot\mathbf{n}) + \nabla_{\mathbf{n}}\mathbf{u})]\, dx_3 ds. \tag{3.34}$$

Due to the symmetries $B_{ijk} = B_{jik}$ and $D_{ijk} = D_{ikj}$ of $\mathfrak{B}$ and $\mathfrak{D}$, the above equation can be rewritten as:

$$\Xi_{couple2} = \int_{S_0}\int_{-\frac{h}{2}}^{\frac{h}{2}} x_3\,(\kappa : \mathfrak{B} - \mathfrak{D} : \kappa)\cdot\mathbf{G}\cdot[(\nabla_S(\mathbf{u}\cdot\mathbf{n}) + \nabla_{\mathbf{n}}\mathbf{u})]\, dx_3 ds. \tag{3.35}$$

In addition, $\Xi_{couple3}$ can take the equivalent expression as follows:

$$\Xi_{couple3} = \int_{S_0}\int_{-\frac{h}{2}}^{\frac{h}{2}} x_3\,(\kappa : \mathbb{A} : \varepsilon_s)\, dx_3 ds. \tag{3.36}$$

Finally, the strain energy is can be decomposed into four parts as

$$\Xi_h = \Xi_{membrane} + \Xi_{bending} + \Xi_{shear} + \Xi_{couple} \tag{3.37}$$

where $\Xi_{membrane}$, $\Xi_{bending}$ and Ξ_{shear} are respectively the elastic energies associated with the

membrane, pure bending and pure shear deformations while Ξ_{couple} is related to their coupled effects.

3.2 Strain Energy for Special Cases

3.2.1 Case of Transversely Isotropic Materials

When the material constituting of Ω_h is assumed to be transversely isotropic, the tensors involved in energy expressions are represented more succinctly, as demonstrated in equations (2.144)-(2.151). By substituting these tensors into the previous energy computation formulas, a more concise formulation can be derived. Upon examining these streamlined energy expressions, it becomes evident that specific geometric features are intricately linked to particular types of energy in the system. Specifically, the energy associated with membrane deformation, denoted by $\Xi_{membrane}$, can be described as follows:

$$\Xi_{membrane} = \frac{1}{2}\int_{S_0}\int_{-\frac{h}{2}}^{\frac{h}{2}} \left\{ \left(C_{12} - \frac{C_{13}^2}{C_{33}} \right) [tr(\boldsymbol{\varepsilon}_s)]^2 + C_1 \left(\boldsymbol{\varepsilon}_s : \boldsymbol{\varepsilon}_s \right) \right\} dx_3 ds, \tag{3.38}$$

where, $tr(\cdot)$ is the trace of the tensor and $\boldsymbol{\varepsilon}_s$ is a surface strain tensor characterizing the overall deformation in the mid-surface area of the plate. The elastic energy associated with bending, denoted as $\Xi_{bending}$, is given by:

$$\Xi_{bending} = \frac{1}{2}\int_{S_0}\int_{-\frac{h}{2}}^{\frac{h}{2}} x_3^2 \left\{ \left(C_{12} - \frac{C_{13}^2}{C_{33}} \right) [tr(\boldsymbol{\kappa})]^2 + C_1 \left(\boldsymbol{\kappa} : \boldsymbol{\kappa} \right) \right\} dx_3 ds. \tag{3.39}$$

As previously mentioned, $\boldsymbol{\kappa}$ represents the curvature tensor of the mid-surface. The energy expression above is specifically associated with the curvature of the mid-surface, indicating the energy exclusively arising from pure bending. The shear energy Ξ_{shear} characterizing the energy associated with shear deformation takes the following expression:

$$\Xi_{shear} = \frac{1}{2}\int_{S_0}\int_{-\frac{h}{2}}^{\frac{h}{2}} C_{44} \left\{ [\nabla_S(\mathbf{u}\cdot\mathbf{n}) + \nabla_{\mathbf{n}}\mathbf{u}] \cdot [\nabla_S(\mathbf{u}\cdot\mathbf{n}) + \nabla_{\mathbf{n}}\mathbf{u}] \right\} dx_3 ds. \tag{3.40}$$

As illustrated in **Fig.** 3.2, when the cross-section of the plate remains planar after deformation, the term $\nabla_S(\mathbf{u}\cdot\mathbf{n}) + \nabla_{\mathbf{n}}\mathbf{u}$ signifies a shear deformation. Consequently, the energy expression

above characterizes the energy arising solely from shear deformation.

In the context of transversely isotropic plates, the coupled effect $\Xi_{couple2}$ between bending and shear deformation, specified by equation (3.35), takes the following simple expression:

$$\Xi_{couple2} = \int_{S_0} \int_{-\frac{h}{2}}^{\frac{h}{2}} x_3 \left(C_{44} + \frac{C_{44}C_{13}}{C_{33}} \right) \left\{ \frac{1}{2} \left[\mathbf{n} \cdot \kappa + \kappa \cdot \mathbf{n} \right] \cdot \left[\nabla_S (\mathbf{u} \cdot \mathbf{n}) + \nabla_{\mathbf{n}} \mathbf{u} \right] \right\} dx_3 ds. \tag{3.41}$$

The coupled effect $\Xi_{couple3}$ between membrane and bending deformation, given by equation (3.36), is now reduced to

$$\Xi_{couple3} = \int_{S_0} \int_{-\frac{h}{2}}^{\frac{h}{2}} x_3 \left\{ \left(C_{12} - \frac{C_{13}^2}{C_{33}} \right) \left[tr(\varepsilon_s) tr(\kappa) \right] + C_1 \left(\varepsilon_s : \kappa \right) \right\} dx_3 ds. \tag{3.42}$$

3.2.2 Case of Isotropic Materials

Similarly, in the context of isotropic materials, there is a notable streamlining of the tensors present in energy expressions, as shown by equations (2.153)-(2.158). By introducing these tensors into the previous energy computation formulas, the expressions for $\Xi_{membrane}$, $\Xi_{bending}$, Ξ_{shear}, $\Xi_{couple2}$, and $\Xi_{couple3}$ can be obtained in a more concise manner as follows:

$$\Xi_{membrane} = \frac{1}{2} \int_{S_0} \int_{-\frac{h}{2}}^{\frac{h}{2}} \left\{ \frac{2\mu\lambda}{\lambda + 2\mu} \left[tr(\varepsilon_s) \right]^2 + 2\mu \left(\varepsilon_s : \varepsilon_s \right) \right\} dx_3 ds, \tag{3.43}$$

$$\Xi_{bending} = \frac{1}{2} \int_{S_0} \int_{-\frac{h}{2}}^{\frac{h}{2}} x_3^2 \left\{ \frac{2\mu\lambda}{\lambda + 2\mu} \left[tr(\kappa) \right]^2 + 2\mu \left(\kappa : \kappa \right) \right\} dx_3 ds, \tag{3.44}$$

$$\Xi_{shear} = \frac{1}{2} \int_{S_0} \int_{-\frac{h}{2}}^{\frac{h}{2}} \mu \left\{ \left[\nabla_S (\mathbf{u} \cdot \mathbf{n}) + \nabla_{\mathbf{n}} \mathbf{u} \right] \cdot \left[\nabla_S (\mathbf{u} \cdot \mathbf{n}) + \nabla_{\mathbf{n}} \mathbf{u} \right] \right\} dx_3 ds, \tag{3.45}$$

$$\Xi_{couple2} = \int_{S_0} \int_{-\frac{h}{2}}^{\frac{h}{2}} x_3 \left(\mu + \frac{\lambda\mu}{\lambda + 2\mu} \right) \left\{ \frac{1}{2} \left[\mathbf{n} \cdot \kappa + \kappa \cdot \mathbf{n} \right] \cdot \left[\nabla_s (\mathbf{u} \cdot \mathbf{n}) + \nabla_n \mathbf{u} \right] \right\} dx_3 ds, \tag{3.46}$$

$$\Xi_{couple3} = \int_{S_0} \int_{-\frac{h}{2}}^{\frac{h}{2}} x_3 \left\{ \frac{2\mu\lambda}{\lambda + 2\mu} \left[tr(\varepsilon_s) tr(\kappa) \right] + 2\mu \left(\varepsilon_s : \kappa \right) \right\} dx_3 ds. \tag{3.47}$$

3.3 Variational Analysis for Equations of Motion and Boundaries in Energy Functionals

To study the motion and mechanical response of dynamical systems, we often rely on energy functionals to describe the behavior of the system. Energy functionals provide a convenient way to capture the energy distribution and evolutionary trends of the system. However, merely knowing the energy functional is insufficient to fully understand the dynamical characteristics of the system. We also need to derive the appropriate equations of motion and boundary conditions from these energy functionals to comprehensively understand the system's behavior. In this challenging task, the variational method becomes an important tool. The core idea of the variational method is to find the extremum of an energy functional. By performing variational operations on the functional, we can find the functions that make the functional extremal, which describe the optimal behavior of the system. In dynamical systems, this optimal behavior typically manifests as functions that satisfy the system's equations of motion and boundary conditions.

Therefore, through the variational method, we can systematically derive the governing equations that describe the system's motion and the constraints at the boundaries. In this part, we will delve into how to use the variational method to analyze energy functionals and derive the equations of motion and boundary conditions from them. In this process, we will also introduce the energy density function and thereby derive the stress resultants, moment resultants, and shear resultants. Through such analysis, we will gain a more comprehensive understanding of the dynamical behavior of the system, providing robust theoretical support and guidance for solving practical problems

3.3.1 Strain Energy Density Function and Constitutive Equations of Plates

Let's introduce the strain energy density function, denoted by E. When studying a structure's strain energy, we're often interested in how it varies across different locations. This spatial distribution is captured by the strain energy density function, which provides a detailed picture of energy distribution within the system. By analyzing the fluctuations of this density function, we can understand how strain energy varies across different regions, aiding in structural design and optimization.

Furthermore, the total strain energy of a structure can be calculated by integrating the strain

energy density function over the entire surface. By taking partial derivatives of this function with respect to the fields ε_s, κ, and $\nabla_S(\mathbf{u}\cdot\mathbf{n})+\nabla_{\mathbf{n}}\mathbf{u}$, we can determine their corresponding physical quantities: in-surface stress resultants, moment resultants, and shear resultants, respectively. The strain energy density can be expressed as:

$$\begin{aligned} E =& \frac{1}{2}\int_{-\frac{h}{2}}^{\frac{h}{2}}(\varepsilon_s :\, \mathbb{A} :\, \varepsilon_s)dx_3 + \frac{1}{2}\int_{-\frac{h}{2}}^{\frac{h}{2}} x_3^2(\kappa :\, \mathbb{A} :\, \kappa)dx_3 \\ &+ \frac{1}{2}\int_{-\frac{h}{2}}^{\frac{h}{2}}(\nabla_S(\mathbf{u}\cdot\mathbf{n})+\nabla_{\mathbf{n}}\mathbf{u})\cdot\mathbf{G}\cdot(\nabla_S(\mathbf{u}\cdot\mathbf{n})+\nabla_n\mathbf{u})dx_3 \\ &+ \int_{-\frac{h}{2}}^{\frac{h}{2}} x_3[(\kappa :\, \mathfrak{B}-\mathfrak{D} :\, \kappa)\cdot(\nabla_S(\mathbf{u}\cdot\mathbf{n})+\nabla_{\mathbf{n}}\mathbf{u})]dx_3 + \int_{-\frac{h}{2}}^{\frac{h}{2}} x_3[\kappa :\, \mathbb{A} :\, \varepsilon_s]dx_3. \end{aligned} \tag{3.48}$$

Consequently, the constitutive equations can be obtained as follows:

Firstly, when we differentiate the energy density function with respect to ε_s, we derive the resulting in-plane stress resultant $\mathbf{N}_s$

$$\mathbf{N}_s = \frac{\partial E}{\partial \varepsilon_s} = \int_{-\frac{h}{2}}^{\frac{h}{2}}(\mathbb{A} :\, \varepsilon_s + x_3\mathbb{A} :\, \kappa)dx_3. \tag{3.49}$$

Secondly, differentiating with respect to κ, yields the moment resultant, $\mathbf{M}$:

$$\begin{aligned} \mathbf{M} = \frac{\partial E}{\partial \kappa} = \int_{-\frac{h}{2}}^{\frac{h}{2}}\{x_3^2(\mathbb{A} :\, \kappa) + x_3\mathbb{A} :\, \varepsilon_s + x_3[\mathfrak{B}\cdot\mathbf{G}\cdot(\nabla_S(\mathbf{u}\cdot\mathbf{n})+\nabla_{\mathbf{n}}\mathbf{u}) \\ -(\nabla_S(\mathbf{u}\cdot\mathbf{n})+\nabla_{\mathbf{n}}\mathbf{u})\cdot\mathbf{G}\cdot\mathfrak{D}]\}dx_3. \end{aligned} \tag{3.50}$$

Finally, the shear force resultant, $\mathbf{Q}$, is obtained by differentiating with respect to $(\nabla_S(\mathbf{u}\cdot\mathbf{n})+\nabla_{\mathbf{n}}\mathbf{u})$:

$$\begin{aligned} \mathbf{Q} = \frac{\partial E}{\partial(\nabla_S(\mathbf{u}\cdot\mathbf{n})+\nabla_{\mathbf{n}}\mathbf{u})} &= \int_{-\frac{h}{2}}^{\frac{h}{2}}[\mathbf{G}\cdot(\nabla_S(\mathbf{u}\cdot\mathbf{n})+\nabla_{\mathbf{n}}\mathbf{u}) + x_3(\kappa :\, \mathfrak{B}-\mathfrak{D} :\, \kappa)]dx_3 \\ &= \int_{-\frac{h}{2}}^{\frac{h}{2}}(\mathbf{t}+x_3\kappa :\, (\mathbb{C}\cdot\mathbf{n}))dx_3. \end{aligned} \tag{3.51}$$

Consequently, the strain energy density can be rewritten in the following equivalent form

$$E = \frac{1}{2}[\varepsilon_s :\, \mathbf{N}_s + \kappa :\, \mathbf{M} + (\nabla_S(\mathbf{u}\cdot\mathbf{n})+\nabla_{\mathbf{n}}\mathbf{u})\cdot\mathbf{Q}]. \tag{3.52}$$

3.3.2 Equilibrium Equations and Boundary Conditions of plates

Given the general expressions for the total strain energy in equations (3.21) to (3.36), we will apply a variational analysis to each term individually. Starting with the membrane energy expression in equation (3.21), we expand this term using the chain rule and the symmetries of the tensor $\mathbb{A}$. This yields the following detailed variation of the membrane energy:

$$\delta\Xi_{membrane} = \int_{S_0}\int_{-\frac{h}{2}}^{\frac{h}{2}} [\nabla\cdot[(\varepsilon_s : \mathbb{A})\cdot\delta(\mathbf{P}\cdot\mathbf{u})] - \nabla\cdot(\varepsilon_s : \mathbb{A})\cdot\delta(\mathbf{P}\cdot\mathbf{u})]dx_3 ds, \tag{3.53}$$

where δ denotes the variation operator. Next, we consider the variation of the pure bending energy as given in equation (3.26). By taking into account the definition of the curvature tensor κ from equation (3.27) and the symmetry of the tensor $\mathbb{A}$, we can systematically expand the variational derivative of the pure bending energy as follows:

$$\delta\Xi_{bending} = \int_{S_0}\int_{-\frac{h}{2}}^{\frac{h}{2}} \left[\nabla\cdot(x_3^2\mathbf{P}\cdot(\kappa\colon\mathbb{A})\cdot\delta\nabla_{\mathbf{n}}\mathbf{u}) - \nabla\cdot(x_3^2\kappa\colon\mathbb{A}\cdot\mathbf{P})\cdot\delta\nabla_{\mathbf{n}}\mathbf{u}\right] dx_3 ds. \tag{3.54}$$

Given the shear energy in equation (3.25), we can express its variation as follows:

$$\delta\Xi_{shear} = \int_{S_0}\int_{-\frac{h}{2}}^{\frac{h}{2}} [\nabla\cdot(\mathbf{P}\cdot\mathbf{t}\delta(\mathbf{u}\cdot\mathbf{n})) - \nabla\cdot(\mathbf{P}\cdot\mathbf{t})\delta(\mathbf{u}\cdot\mathbf{n}) + \mathbf{t}\cdot\delta(\nabla_{\mathbf{n}}\mathbf{u})]dx_3 ds. \tag{3.55}$$

The variational formulation for Ξ_{couple2} given by equation (3.35) reads:

$$\begin{aligned}\delta\Xi_{couple2} = \int_{S_0}\int_{-\frac{h}{2}}^{\frac{h}{2}} \{&x_3(\kappa\colon\mathfrak{B}-\mathfrak{D}\colon\kappa)\cdot\mathbf{G}\cdot\delta(\nabla_{\mathbf{n}}\mathbf{u}) + \nabla\cdot[x_3(\kappa\colon\mathfrak{B}-\mathfrak{D}\colon\kappa)\cdot\mathbf{G}\cdot\mathbf{P}\delta(\mathbf{u}\cdot\mathbf{n})]\\ &+\nabla\cdot[x_3\mathbf{P}\cdot(\mathfrak{B}\cdot\mathbf{G}\cdot(\nabla_S(\mathbf{u}\cdot\mathbf{n})+\nabla_{\mathbf{n}}\mathbf{u}) - (\nabla_S(\mathbf{u}\cdot\mathbf{n})+\nabla_{\mathbf{n}}\mathbf{u})\cdot\mathbf{G}\cdot\mathfrak{D})\cdot\delta(\nabla_{\mathbf{n}}\mathbf{u})]\\ &-\nabla\cdot[x_3(\mathfrak{B}\cdot\mathbf{G}\cdot(\nabla_S(\mathbf{u}\cdot\mathbf{n})+\nabla_{\mathbf{n}}\mathbf{u}) - (\nabla_S(\mathbf{u}\cdot\mathbf{n})+\nabla_{\mathbf{n}}\mathbf{u})\cdot\mathbf{G}\cdot\mathfrak{D})\cdot\mathbf{P}]\cdot\delta(\nabla_{\mathbf{n}}\mathbf{u})\\ &-\nabla\cdot[x_3(\kappa\colon\mathfrak{B}-\mathfrak{D}\colon\kappa)\cdot\mathbf{G}\cdot\mathbf{P}]\delta(\mathbf{u}\cdot\mathbf{n})\}dx_3 ds.\end{aligned} \tag{3.56}$$

Similarly, the variational formulation for Ξ_{couple3} provided by equation (3.32) implies:

$$\begin{aligned}\delta\Xi_{couple3} = \int_{S_0}\int_{-\frac{h}{2}}^{\frac{h}{2}} [&\nabla\cdot(x_3\varepsilon_s\colon\mathbb{A}\cdot\delta(\nabla_{\mathbf{n}}\mathbf{u})) - \nabla\cdot(x_3\varepsilon_s\colon\mathbb{A})\cdot\delta(\nabla_{\mathbf{n}}\mathbf{u})\\ &+\nabla\cdot(x_3\kappa\colon\mathbb{A}\cdot\delta(\mathbf{P}\cdot\mathbf{u})) - \nabla\cdot(x_3\kappa\colon\mathbb{A})\cdot\delta(\mathbf{P}\cdot\mathbf{u})]dx_3 ds.\end{aligned} \tag{3.57}$$

Through this detailed variational analysis, we systematically derive the governing equations

of motion and their corresponding boundary conditions. By combining the variational expressions and integrating the constitutive relations (equations (3.49)-(3.51)), we obtain the variational derivative of the total strain energy as follows:

$$\begin{aligned}\delta\Xi = \int_{S_0} \{&\nabla\cdot[\mathbf{N}_s\cdot\delta(\mathbf{P}\cdot\mathbf{u})] - (\nabla\cdot\mathbf{N}_s)\cdot\delta(\mathbf{P}\cdot\mathbf{u}) + \nabla\cdot[\mathbf{P}\cdot\mathbf{M}\cdot\delta(\nabla_{\mathbf{n}}\mathbf{u})] \\ &- \nabla\cdot(\mathbf{M}\cdot\mathbf{P})\cdot\delta(\nabla_{\mathbf{n}}\mathbf{u}) + \mathbf{Q}\cdot\delta(\nabla_{\mathbf{n}}\mathbf{u}) + \nabla\cdot[\mathbf{P}\cdot\mathbf{Q}\delta(\mathbf{u}\cdot\mathbf{n})] - \nabla\cdot(\mathbf{P}\cdot\mathbf{Q})\delta(\mathbf{u}\cdot\mathbf{n})\}ds.\end{aligned} \tag{3.58}$$

The work done by external forces, denoted by W, is defined as a functional representing the energy exerted by these forces during associated displacements, assuming they remain constant throughout the deformation process. The variation of the work done by external forces is given by:

$$\begin{aligned}\delta W &= \int_{S_0}(\mathbf{f}\cdot\delta\mathbf{u})ds + \int_{\partial S_0}[\bar{\mathbf{N}}\cdot\delta(\mathbf{P}\cdot\mathbf{u}) + \bar{\mathbf{M}}\cdot\delta(\nabla_{\mathbf{n}}\mathbf{u})]dl \\ &= \int_{S_0}[\mathbf{f}_s\cdot\delta(\mathbf{P}\cdot\mathbf{u}) + f_{x_3}\delta(\mathbf{u}\cdot\mathbf{n})]ds + \int_{\partial S_0}[\bar{\mathbf{N}}\cdot\delta(\mathbf{P}\cdot\mathbf{u}) + \bar{\mathbf{M}}\cdot\delta(\nabla_{\mathbf{n}}\mathbf{u})]dl\end{aligned} \tag{3.59}$$

where $\mathbf{f}$ represents the body force resultant acting on the middle surface of the plate S_0, and $\bar{\mathbf{N}}$ and $\bar{\mathbf{M}}$ denote, respectively, the Cauchy traction resultant and moment applied to the boundary of the middle surface of the plate ∂S_0. The kinetic energy of the plate is given by

$$K = \int_{-\frac{h}{2}}^{\frac{h}{2}}\int_{S_0}\frac{1}{2}\rho\dot{\mathbf{u}}^2 dx_3 ds \tag{3.60}$$

where the superimposed dot on a variable denotes the time derivative (e.g., $\dot{\mathbf{u}} = \partial\mathbf{u}/\partial t$). The variation of the kinetic energy can be rewritten as

$$\begin{aligned}\delta K &= \int_{-\frac{h}{2}}^{\frac{h}{2}}\int_{S_0}\rho\ddot{\mathbf{u}}\cdot\delta\mathbf{u}dx_3 ds \\ &= -\int_{S_0}\{[I_0\overline{(\ddot{\mathbf{P}}\cdot\mathbf{u})} + I_1\overline{(\ddot{\nabla}_{\mathbf{n}}\mathbf{u})}]\cdot\delta(\mathbf{P}\cdot\mathbf{u}) + [I_1\overline{(\ddot{\mathbf{P}}\cdot\mathbf{u})} + I_2\overline{(\ddot{\nabla}_{\mathbf{n}}\mathbf{u})}]\delta(\nabla_{\mathbf{n}}\mathbf{u}) + [I_0\overline{(\ddot{\mathbf{u}}\cdot\mathbf{n})}]\delta(\mathbf{u}\cdot\mathbf{n})\}ds,\end{aligned} \tag{3.61}$$

where I_0, I_1 and I_2 are defined by

$$I_0 = \int_{-\frac{h}{2}}^{\frac{h}{2}}\rho dx_3, \quad I_1 = \int_{-\frac{h}{2}}^{\frac{h}{2}}\rho x_3 dx_3, \quad I_2 = \int_{-\frac{h}{2}}^{\frac{h}{2}}\rho x_3^2 dx_3. \tag{3.62}$$

These integrals are determined by the spatial distribution of mass density ρ along the thickness

dimension. The dynamic formulation of the variational principle for total energy, or equivalently, Hamilton's principle, is expressed as:

$$\delta\Pi = \int_0^T (\delta\Xi - \delta W - \delta K)dt = 0 \tag{3.63}$$

where $\delta\Pi$ denotes the variation of the total potential energy over the time interval $[0,T]$, encompassing variations in strain energy $\delta\Xi$, work done by external forces δW, and kinetic energy δK. This formulation ensures the total potential energy is stationary with respect to infinitesimal variations in the deformation field and velocities, reflecting the system's dynamic equilibrium. Substituting equations (3.58), (3.59), and (3.61) into equation (3.63) yields the explicit expression for the variational derivative of the total potential energy:

$$\begin{aligned}
&\int_0^T \int_{S_0} \{[-\mathbf{f}_s - \nabla\cdot\mathbf{N}_s + I_0\overline{(\ddot{\mathbf{P}}\cdot\mathbf{u})} + I_1\overline{(\nabla_{\mathbf{n}}\ddot{\mathbf{u}})}]\cdot\delta(\mathbf{P}\cdot\mathbf{u}) + [-\nabla\cdot(\mathbf{M}\cdot\mathbf{P}) + \mathbf{Q} + I_1\overline{(\ddot{\mathbf{P}}\cdot\mathbf{u})} + I_2\overline{(\nabla_{\mathbf{n}}\ddot{\mathbf{u}})}]\cdot\delta(\nabla_{\mathbf{n}}\mathbf{u}) \\
&+ [-f_{x_3} - \nabla\cdot(\mathbf{P}\cdot\mathbf{Q}) + I_0\overline{(\ddot{\mathbf{u}}\cdot\mathbf{n})}]\delta(\mathbf{u}\cdot\mathbf{n})\}dsdt + \int_0^T \int_{S_0} \{\nabla\cdot[\mathbf{N}_s\cdot\delta(\mathbf{P}\cdot\mathbf{u})] + \nabla\cdot[(\mathbf{P}\cdot\mathbf{Q})\delta(\mathbf{u}\cdot\mathbf{n})] \\
&+ \nabla\cdot[\mathbf{P}\cdot\mathbf{M}\cdot\delta(\nabla_{\mathbf{n}}\mathbf{u})]\}dsdt - \int_0^T \int_{\partial S_0} [\bar{\mathbf{N}}\cdot\delta(\mathbf{P}\cdot\mathbf{u}) + \bar{\mathbf{M}}\cdot\delta\nabla(\mathbf{u}\cdot\mathbf{n})]dldt = 0.
\end{aligned} \tag{3.64}$$

By applying the divergence theorem and Stokes's theorem, equation (3.64) can be reformulated in the following manner:

$$\begin{aligned}
&\int_0^T \int_{S_0} \{[-\mathbf{f}_s - \nabla\cdot\mathbf{N}_s + I_0\overline{(\ddot{\mathbf{P}}\cdot\mathbf{u})} + I_1\overline{(\nabla_{\mathbf{n}}\ddot{\mathbf{u}})}]\cdot\delta(\mathbf{P}\cdot\mathbf{u}) + [-\nabla\cdot(\mathbf{M}\cdot\mathbf{P}) - \mathbf{Q} + I_1\overline{(\ddot{\mathbf{P}}\cdot\mathbf{u})} + I_2\overline{(\nabla_{n}\ddot{\mathbf{u}})}]\cdot\delta(\nabla_{\mathbf{n}}\mathbf{u}) \\
&+ [-f_{x_3} - \nabla\cdot(\mathbf{P}\cdot\mathbf{Q}) + I_0\overline{(\ddot{\mathbf{u}}\cdot\mathbf{n})}]\delta(\mathbf{u}\cdot\mathbf{n})\}dsdt + \int_0^T \int_{\partial S_0} \{[\mathbf{N}_s\cdot\mathbf{m} - \bar{\mathbf{N}}]\cdot\delta(\mathbf{P}\cdot\mathbf{u}) + [\mathbf{P}\cdot\mathbf{Q}\cdot\mathbf{m}]\delta(\mathbf{u}\cdot\mathbf{n}) \\
&+ [\mathbf{P}\cdot\mathbf{M}\cdot\mathbf{m} - \bar{\mathbf{M}}]\cdot\delta(\nabla_{\mathbf{n}}\mathbf{u})\}dldt = 0
\end{aligned} \tag{3.65}$$

where $\mathbf{m}$ denotes the unit normal vector at the edge of the plates, as illustrated in **Fig.** 3.1.

Considering the first integral term in the above equation, since the variables $\delta(\mathbf{P}\cdot\mathbf{u})$, $\delta(\mathbf{u}\cdot\mathbf{n})$, and $\delta(\nabla_{\mathbf{n}}\mathbf{u})$ are arbitrary, we obtain therefore the following equilibrium equations

$$\left.\begin{aligned}
\mathbf{f}_s + \nabla\cdot\mathbf{N}_s &= I_0\overline{(\ddot{\mathbf{P}}\cdot\mathbf{u})} + I_1\overline{(\nabla_{\mathbf{n}}\ddot{\mathbf{u}})} \\
\nabla\cdot(\mathbf{M}\cdot\mathbf{P}) - \mathbf{Q} &= I_1\overline{(\ddot{\mathbf{P}}\cdot\mathbf{u})} + I_2\overline{(\nabla_{\mathbf{n}}\ddot{\mathbf{u}})} \\
f_{x_3} + \nabla\cdot(\mathbf{P}\cdot\mathbf{Q}) &= I_0\overline{(\ddot{\mathbf{u}}\cdot\mathbf{n})}
\end{aligned}\right\}, \tag{3.66}$$

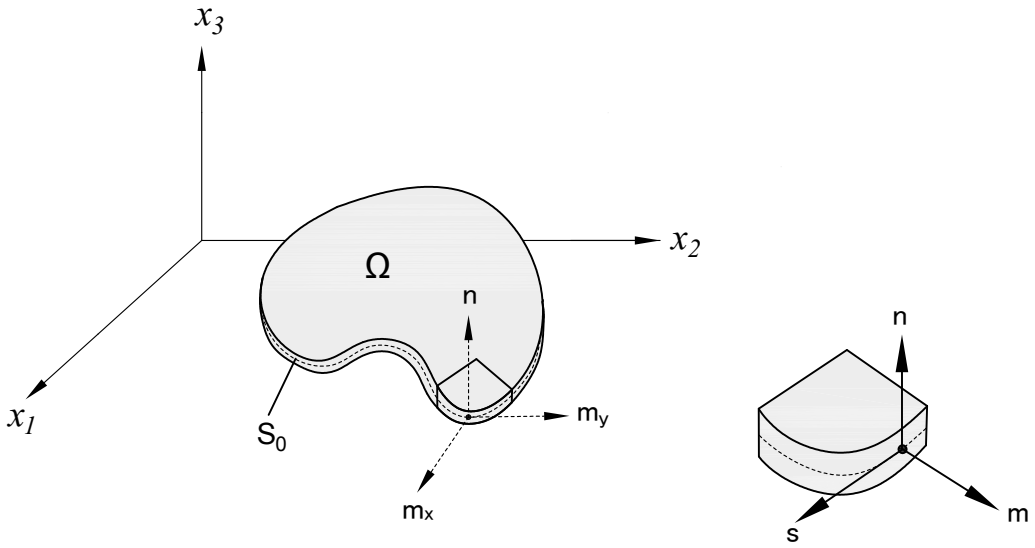

Figure 3.1: *Geometry of a plate with curved boundary.*

where the terms involving I_2 can contribute to higher frequencies of vibration which is called rotary (or rotatory) inertia term. The corresponding boundary conditions can be derived from the second integral term:

$$\left.\begin{aligned} \mathbf{N}_s \cdot \mathbf{m} - \bar{\mathbf{N}} &= \mathbf{0} \\ \mathbf{P} \cdot \mathbf{Q} \cdot \mathbf{m} &= \mathbf{0} \\ \mathbf{P} \cdot \mathbf{M} \cdot \mathbf{m} - \bar{\mathbf{M}} &= \mathbf{0} \end{aligned}\right\}. \tag{3.67}$$

3.3.3 Application to Transverse Isotropic Plates

For plates with transversely isotropic materials, the energy density function in equation (3.48) can be explicitly determined. This can be achieved either by deriving it from the strain energy formula specific to transverse isotropy (equations (3.43) to (3.42)) or by substituting the transverse isotropic operators (equations (2.144)-(2.151) from subsection 2.4.2 into equation (3.48). Importantly, both methods yield equivalent energy density functions. Specifically, for

transverse isotropy, E is expressed as:

$$\begin{aligned}
E =& \frac{1}{2}\int_{-\frac{h}{2}}^{\frac{h}{2}} \left\{ \left(C_{12} - \frac{C_{13}^2}{C_{33}} \right) [tr(\boldsymbol{\varepsilon}_s)]^2 + (C_{11} - C_{12}) (\boldsymbol{\varepsilon}_s : \boldsymbol{\varepsilon}_s) \right\} dx_3 \\
&+ \frac{1}{2}\int_{-\frac{h}{2}}^{\frac{h}{2}} x_3^2 \left\{ \left(C_{12} - \frac{C_{13}^2}{C_{33}} \right) [tr(\boldsymbol{\kappa})]^2 + (C_{11} - C_{12}) (\boldsymbol{\kappa} : \boldsymbol{\kappa}) \right\} dx_3 \\
&+ \frac{1}{2}\int_{-\frac{h}{2}}^{\frac{h}{2}} C_{44} \{ [\nabla_S(\mathbf{u}\cdot\mathbf{n}) + \nabla_{\mathbf{n}}\mathbf{u}] \cdot [\nabla_S(\mathbf{u}\cdot\mathbf{n}) + \nabla_{\mathbf{n}}\mathbf{u}] \} dx_3 \\
&+ \int_{-\frac{h}{2}}^{\frac{h}{2}} x_3 \left(C_{44} + \frac{C_{44}C_{13}}{C_{33}} \right) \left\{ \frac{1}{2} [\mathbf{n}\cdot\boldsymbol{\kappa} + \boldsymbol{\kappa}\cdot\mathbf{n}] \cdot [\nabla_S(\mathbf{u}\cdot\mathbf{n}) + \nabla_{\mathbf{n}}\mathbf{u}] \right\} dx_3 \\
&+ \int_{-\frac{h}{2}}^{\frac{h}{2}} x_3 \left\{ \left(C_{12} - \frac{C_{13}^2}{C_{33}} \right) [tr(\boldsymbol{\varepsilon}_s) tr(\boldsymbol{\kappa})] + (C_{11} - C_{12}) (\boldsymbol{\varepsilon}_s : \boldsymbol{\kappa}) \right\} dx_3 .
\end{aligned} \tag{3.68}$$

The in-plane stress resultants $\mathbf{N}_s$, moment resultants $\mathbf{M}$, and shear resultants $\mathbf{Q}$, obtained by differentiating the energy density function E with respect to the corresponding deformation measures take therefore the following forms:

$$\mathbf{N}_s = \int_{-\frac{h}{2}}^{\frac{h}{2}} \left\{ \left(C_{12} - \frac{C_{13}^2}{C_{33}} \right) [tr(\boldsymbol{\varepsilon}_s) + x_3 tr(\boldsymbol{\kappa})] \mathbf{P} + (C_{11} - C_{12}) (\boldsymbol{\varepsilon}_s + x_3 \boldsymbol{\kappa}) \right\} dx_3, \tag{3.69}$$

$$\begin{aligned}
\mathbf{M} = \int_{-\frac{h}{2}}^{\frac{h}{2}} \Bigg\{ & x_3^2 \left[\left(C_{12} - \frac{C_{13}^2}{C_{33}} \right) \mathrm{tr}(\boldsymbol{\kappa}) \mathbf{P} + (C_{11} - C_{12}) \boldsymbol{\kappa} \right] + x_3 \left[\left(C_{12} - \frac{C_{13}^2}{C_{33}} \right) \mathrm{tr}(\boldsymbol{\varepsilon}_s) \mathbf{P} + (C_{11} - C_{12}) \boldsymbol{\varepsilon}_s \right] \\
& + x_3 \left(\frac{C_{44}}{2} + \frac{C_{44}C_{13}}{2C_{33}} \right) \left[\mathbf{n} \otimes (\nabla_S(\mathbf{u}\cdot\mathbf{n}) + \nabla_{\mathbf{n}}\mathbf{u}) + (\nabla_S(\mathbf{u}\cdot\mathbf{n}) + \nabla_{\mathbf{n}}\mathbf{u}) \otimes \mathbf{n} \right] \Bigg\} dx_3,
\end{aligned} \tag{3.70}$$

$$\mathbf{Q} = \int_{-\frac{h}{2}}^{\frac{h}{2}} \left[C_{44} (\nabla_S(\mathbf{u}\cdot\mathbf{n}) + \nabla_{\mathbf{n}}\mathbf{u}) + x_3 \frac{C_{44}}{2} (\mathbf{n}\cdot\boldsymbol{\kappa} + \boldsymbol{\kappa}\cdot\mathbf{n}) \right] dx_3. \tag{3.71}$$

By substituting the transverse isotropic operators (2.144)-(2.151) into equations (3.49)-(3.51), the same expressions for $\mathbf{N}_s$, $\mathbf{M}$, and $\mathbf{Q}$ as derived above are obtained. Based on the constitutive equations provided above, the strain energy density of transversely isotropic materials can be expressed as:

$$E = \frac{1}{2} [\boldsymbol{\varepsilon}_s : \mathbf{N}_s + \boldsymbol{\kappa} : \mathbf{M} + (\nabla_S(\mathbf{u}\cdot\mathbf{n}) + \nabla_{\mathbf{n}}\mathbf{u}) \cdot \mathbf{Q}], \tag{3.72}$$

which is consistency with that of anisotropic materials in form.

By performing variational differentiation on the strain energy formula specific to transverse isotropy (equations (3.43)-(3.42)) and considering the constitutive relations (equations (3.69)-(3.71)), we derive a total energy variation consistent with that of equation (3.58). Consequently, the resulting governing equations and boundary conditions are formally identical to equations (3.66) and (3.67), respectively. The consistency of the previously derived strain energy density functions confirms that while the expressions for $\mathbf{N}_s$, $\mathbf{M}$, and $\mathbf{Q}$ vary with material properties, the fundamental governing equations and boundary conditions remain invariant.

3.3.4 Application to Isotropic Plates

Similarly, for isotropic materials, the energy density function in equation (3.48) can be explicitly expressed as

$$\begin{aligned} E =& \frac{1}{2}\int_{-\frac{h}{2}}^{\frac{h}{2}} \left\{ \frac{2\mu\lambda}{\lambda+2\mu}\left[tr(\varepsilon_s)\right]^2 + 2\mu\left(\varepsilon_s :\, \varepsilon_s\right)\right\} dx_3 \\ &+ \frac{1}{2}\int_{-\frac{h}{2}}^{\frac{h}{2}} x_3^2 \left\{ \frac{2\mu\lambda}{\lambda+2\mu}\left[tr(\kappa)\right]^2 + 2\mu\left(\kappa :\, \kappa\right)\right\} dx_3 \\ &+ \frac{1}{2}\int_{-\frac{h}{2}}^{\frac{h}{2}} \mu\left\{\left[\nabla_S(\mathbf{u}\cdot\mathbf{n}) + \nabla_{\mathbf{n}}\mathbf{u}\right]\cdot\left[\nabla_s(\mathbf{u}\cdot\mathbf{n}) + \nabla_n\mathbf{u}\right]\right\} dx_3 \\ &+ \int_{-\frac{h}{2}}^{\frac{h}{2}} x_3\left(\mu + \frac{\lambda\mu}{\lambda+2\mu}\right)\left\{\frac{1}{2}\left[\mathbf{n}\cdot\kappa + \kappa\cdot\mathbf{n}\right]\cdot\left[\nabla_S(\mathbf{u}\cdot\mathbf{n}) + \nabla_{\mathbf{n}}\mathbf{u}\right]\right\} dx_3 \\ &+ \int_{-\frac{h}{2}}^{\frac{h}{2}} x_3\left\{\frac{2\mu\lambda}{\lambda+2\mu}\left[tr(\varepsilon_s)tr(\kappa)\right] + 2\mu\left(\varepsilon_s :\, \kappa\right)\right\} dx_3. \end{aligned} \tag{3.73}$$

The expressions for $\mathbf{N}_s$, $\mathbf{M}$, and $\mathbf{Q}$ are derived by differentiating the energy density function E with respect to the corresponding deformation measures as follows:

$$\mathbf{N}_s = \int_{-\frac{h}{2}}^{\frac{h}{2}} \left\{ \frac{2\mu\lambda}{\lambda+2\mu}\left[tr(\varepsilon_s) + x_3 tr(\kappa)\right]\mathbf{P} + 2\mu\left(\varepsilon_s + x_3\kappa\right)\right\} dx_3, \tag{3.74}$$

$$\begin{aligned} \mathbf{M} = \int_{-\frac{h}{2}}^{\frac{h}{2}} \Bigg\{ & x_3^2\left(\frac{2\mu\lambda}{\lambda+2\mu}\,\mathrm{tr}(\kappa)\mathbf{P} + 2\mu\kappa\right) + x_3\left[\frac{2\mu\lambda}{\lambda+2\mu}\,\mathrm{tr}(\varepsilon_s)\mathbf{P} + 2\mu\varepsilon_s\right] \\ & + x_3\left(\frac{\mu}{2} + \frac{\mu\lambda}{2(\lambda+2\mu)}\right)\left[\mathbf{n}\otimes\left(\nabla_S(\mathbf{u}\cdot\mathbf{n}) + \nabla_{\mathbf{n}}\mathbf{u}\right) + \left(\nabla_S(\mathbf{u}\cdot\mathbf{n}) + \nabla_{\mathbf{n}}\mathbf{u}\right)\otimes\mathbf{n}\right]\Bigg\} dx_3, \end{aligned} \tag{3.75}$$

$$\mathbf{Q} = \int_{-\frac{h}{2}}^{\frac{h}{2}} \left[\mu(\nabla_S(\mathbf{u}\cdot\mathbf{n}) + \nabla_{\mathbf{n}}\mathbf{u}) + x_3 \frac{\mu}{2}(\mathbf{n}\cdot\kappa + \kappa\cdot\mathbf{n}) \right] dx_3. \tag{3.76}$$

By inserting the operators for isotropy (2.153)-(2.157) into equations (3.49)-(3.51), one arrives at the same expressions for $\mathbf{N}_s$, $\mathbf{M}$, and $\mathbf{Q}$ as derived above. The strain energy density of isotropic materials maintains consistency with that of anisotropy materials in form, i.e.:

$$E = \frac{1}{2}[\varepsilon_s : \mathbf{N}_s + \kappa : \mathbf{M} + (\nabla_S(\mathbf{u}\cdot\mathbf{n}) + \nabla_{\mathbf{n}}\mathbf{u})\cdot\mathbf{Q}]. \tag{3.77}$$

As previously discussed, the formulations for $\mathbf{N}_s$, $\mathbf{M}$, and $\mathbf{Q}$ vary depending on whether the material is isotropic, transversely isotropic, or anisotropic. Nonetheless, the governing equations of motion and boundary conditions, which are analogous to equations (3.66) and (3.67), respectively, maintain the same structural form for both transversely isotropic and isotropic materials.

3.4 The Dynamic Plate Theory without Coupling Effect

Consider a geometrically symmetric plate constituting of a homogeneous material. Under the assumption of small rotations and deflections, as indicated by equation (2.14) in Chapter 2.1, curvature variations through the thickness are negligible. This aligns with the fundamental principles of classical plate theory.

Given the absence of inter-layer compression and the resulting uniform stress vector $\mathbf{t}$ through the thickness, the integral term in equation (3.31) representing $\Xi_{couple2}$ exhibits odd symmetry with respect to x_3, integrating to zero. Additionally, since ε_s is a surface tensor (equation (3.18)), it remains constant through the thickness. Consequently, the corresponding integral term in equation (3.36) for $\Xi_{couple3}$ also vanishes. Therefore, the coupling effect can be disregarded in this case.

Revisiting the strain energy formulation based on these assumptions, we reintroduce the strain energy density function and employ variational methods to derive the governing equations and associated boundary conditions. This framework reduces to the classical Mindlin plate theory in two dimensions and the Timoshenko beam theory in one dimension.

3.4.1 General Form of Plate Theory without Coupling

By neglecting the coupling effect, the total strain energy Ξ_h comprises the membrane energy $\Xi_{membrane}$, the bending energy $\Xi_{bending}$, and the shear energy Ξ_{shear}, as defined in equations (3.21), (3.28), and (3.25), respectively. Explicitly,

$$\begin{aligned}\Xi_h =& \frac{1}{2}\int_{S_0}\int_{-\frac{h}{2}}^{\frac{h}{2}}(\boldsymbol{\varepsilon}_s\colon \mathbb{A}\colon \boldsymbol{\varepsilon}_s)dx_3ds + \frac{1}{2}\int_{S_0}\int_{-\frac{h}{2}}^{\frac{h}{2}}x_3^2(\boldsymbol{\kappa}\colon \mathbb{A}\colon \boldsymbol{\kappa})dx_3ds \\ &+ \frac{1}{2}\int_{S_0}\int_{-\frac{h}{2}}^{\frac{h}{2}}x_3^2\left[(\nabla_S(\mathbf{u}\cdot\mathbf{n})+\nabla_{\mathbf{n}}\mathbf{u})\cdot\mathbf{G}\cdot(\nabla_S(\mathbf{u}\cdot\mathbf{n})+\nabla_{\mathbf{n}}\mathbf{u})\right]dx_3ds.\end{aligned} \tag{3.78}$$

Correspondingly, the energy density function E is given by:

$$\begin{aligned}E =& \frac{1}{2}\int_{-\frac{h}{2}}^{\frac{h}{2}}(\boldsymbol{\varepsilon}_s\colon \mathbb{A}\colon \boldsymbol{\varepsilon}_s)dx_3 + \frac{1}{2}\int_{-\frac{h}{2}}^{\frac{h}{2}}x_3^2(\boldsymbol{\kappa}\colon \mathbb{A}\colon \boldsymbol{\kappa})dx_3 \\ &+ \frac{1}{2}\int_{-\frac{h}{2}}^{\frac{h}{2}}(\nabla_S(\mathbf{u}\cdot\mathbf{n})+\nabla_{\mathbf{n}}\mathbf{u})\cdot\mathbf{G}\cdot(\nabla_S(\mathbf{u}\cdot\mathbf{n})+\nabla_{\mathbf{n}}\mathbf{u})dx_3.\end{aligned} \tag{3.79}$$

Differentiating the energy density function E with respect to the corresponding deformation measures implies the expressions of the in-surface stress resultants $\mathbf{N}_s$, moment resultants $\mathbf{M}$, and shear resultants $\mathbf{Q}$ as follows:

$$\mathbf{N}_s = \frac{\partial E}{\partial \boldsymbol{\varepsilon}_s} = \int_{-\frac{h}{2}}^{\frac{h}{2}}(\mathbb{A}\colon \boldsymbol{\varepsilon}_s)dx_3, \tag{3.80}$$

$$\mathbf{M} = \frac{\partial E}{\partial \boldsymbol{\kappa}} = \int_{-\frac{h}{2}}^{\frac{h}{2}}x_3^2(\mathbb{A}\colon \boldsymbol{\kappa})dx_3, \tag{3.81}$$

$$\mathbf{Q} = \frac{\partial E}{\partial(\nabla_s(\mathbf{u}\cdot\mathbf{n})+\nabla_n\mathbf{u})} = \int_{-\frac{h}{2}}^{\frac{h}{2}}[\mathbf{K}\cdot(\nabla_S(\mathbf{u}\cdot\mathbf{n})+\nabla_{\mathbf{n}}\mathbf{u})]d\boldsymbol{x}_3 = \int_{-\frac{h}{2}}^{\frac{h}{2}}\mathbf{t}dx_3. \tag{3.82}$$

Building on the derived expressions for for $\mathbf{N}_s$, $\mathbf{M}$, and $\mathbf{Q}$, the energy density function E can be concisely expressed as:

$$E = \frac{1}{2}[\boldsymbol{\varepsilon}_s\colon \mathbf{N}_s + \boldsymbol{\kappa}\colon \mathbf{M} + (\nabla_S(\mathbf{u}\cdot\mathbf{n})+\nabla_{\mathbf{n}}\mathbf{u})\cdot\mathbf{Q}]. \tag{3.83}$$

Substituting equations (3.80), (3.81), and (3.82) into (3.53)-(3.55), the variations of $\Xi_{membrane}$, $\Xi_{bending}$, and Ξ_{shear} are given by:

$$\delta\Xi_{membrane} = \int_{S_0} [\nabla \cdot [\mathbf{N}_s \cdot \delta(\mathbf{P} \cdot \mathbf{u})] - (\nabla \cdot \mathbf{N}_s) \cdot \delta(\mathbf{P} \cdot \mathbf{u})] ds, \tag{3.84}$$

$$\delta\Xi_{bending} = \int_{S_0} [\nabla \cdot (\mathbf{P} \cdot \mathbf{M} \cdot \delta(\nabla_n \mathbf{u})) - \nabla \cdot (\mathbf{M} \cdot \mathbf{P}) \cdot \delta(\nabla_{\mathbf{n}} \mathbf{u})] \, ds, \tag{3.85}$$

$$\delta\Xi_{shear} = \int_{S_0} [\nabla \cdot (\mathbf{P} \cdot \mathbf{Q} \delta(\mathbf{u} \cdot \mathbf{n})) - \nabla \cdot (\mathbf{P} \cdot \mathbf{Q}) \delta(\mathbf{u} \cdot \mathbf{n}) + \mathbf{Q} \cdot \delta(\nabla_{\mathbf{n}} \mathbf{u})] ds. \tag{3.86}$$

Summing the above variations, the variation of the total strain energy Ξ is

$$\begin{aligned} \delta\Xi = \int_{S_0} \{ & \nabla \cdot [\mathbf{N}_s \cdot \delta(\mathbf{P} \cdot \mathbf{u})] - (\nabla \cdot \mathbf{N}_s) \cdot \delta(\mathbf{P} \cdot \mathbf{u}) + \nabla \cdot [\mathbf{P} \cdot \mathbf{M} \cdot \delta(\nabla_{\mathbf{n}} \mathbf{u})] \\ & - \nabla \cdot (\mathbf{M} \cdot \mathbf{P}) \cdot \delta(\nabla_{\mathbf{n}} \mathbf{u}) + \mathbf{Q} \cdot \delta(\nabla_{\mathbf{n}} \mathbf{u}) + \nabla \cdot [\mathbf{P} \cdot \mathbf{Q} \delta(\mathbf{u} \cdot \mathbf{n})] - \nabla \cdot (\mathbf{P} \cdot \mathbf{Q}) \delta(\mathbf{u} \cdot \mathbf{n}) \} ds, \end{aligned} \tag{3.87}$$

which agrees with the form in equation (3.58). Additionally, the variations of the work done by external forces and the kinetic energy correspond to those in equations (3.59) and (3.61), respectively. It can be deduced from the Hamilton's principle (3.63) the following governing equations:

$$\left.\begin{aligned} \mathbf{f}_s + \nabla \cdot \mathbf{N}_s &= I_0 \overline{(\ddot{\mathbf{P}} \cdot \mathbf{u})} + I_1 \overline{(\ddot{\nabla}_{\mathbf{n}} \mathbf{u})} \\ \nabla \cdot (\mathbf{M} \cdot \mathbf{P}) - \mathbf{Q} &= I_1 \overline{(\ddot{\mathbf{P}} \cdot \mathbf{u})} + I_2 \overline{(\ddot{\nabla}_{\mathbf{n}} \mathbf{u})} \\ f_{x_3} + \nabla \cdot (\mathbf{P} \cdot \mathbf{Q}) &= I_0 \overline{(\ddot{\mathbf{u}} \cdot \mathbf{n})} \end{aligned}\right\}, \tag{3.88}$$

and the boundary conditions:

$$\left.\begin{aligned} \mathbf{N}_s \cdot \mathbf{m} - \bar{\mathbf{N}} &= \mathbf{0} \\ \mathbf{P} \cdot \mathbf{Q} \cdot \mathbf{m} &= \mathbf{0} \\ \mathbf{P} \cdot \mathbf{M} \cdot \mathbf{m} - \bar{\mathbf{M}} &= \mathbf{0} \end{aligned}\right\}. \tag{3.89}$$

While the governing equations and boundary conditions match those in equations (3.66) and (3.67), the formulations for $\mathbf{N}_s$, $\mathbf{M}$, and $\mathbf{Q}$ used here differ from previous expressions. These differences were detailed earlier, where specific calculations for $\mathbf{N}_s$, $\mathbf{M}$, and $\mathbf{Q}$ were provided.

Notably, the $\mathbf{N}_s$, $\mathbf{M}$, and $\mathbf{Q}$ introduced in this section exclude coupling effects, unlike those in Chapter 3.3.1.

3.4.2 Mindlin Plate Theory

Consider a plate with uniform thickness h. A rectangular Cartesian coordinate system (x_1, x_2, x_3) is adopted, where the x_1-x_2-plane coincides with the plate's geometric mid-plane and the x_3-coordinate is positive downward. **Fig.** 3.2 illustrates this configuration. The time-dependent displacement field of the middle surface is represented by:

$$\mathbf{u}_0(\mathbf{x},t) = \begin{Bmatrix} u_0(x_1,x_2,t) \\ v_0(x_1,x_2,t) \\ w(x_1,x_2,t) \end{Bmatrix}, \tag{3.90}$$

where:

- $u_0(x_1,x_2,t)$ represents the displacement of a material point in the x_1-direction at the middle surface at time t.
- $v_0(x_1,x_2,t)$ represents the displacement of a material point in the x_2-direction at the middle surface at time t.
- $w(x_1,x_2,t)$ represents the bending deflection of the middle surface at time t.

For simplicity, we denote hereafter the three quantities mentioned above as u_0, v_0 and w. The deformed mid-surface of the plate can be represented by

$$\Gamma = \{\mathbf{x} \in \mathbb{R}^3 \mid g(\mathbf{x}) = x_3 - w = 0\}. \tag{3.91}$$

Substituting the expression for the mid-surface into equation (1.2) yields the expression of the normal vector to the mid-surface:

$$\mathbf{n} = \begin{Bmatrix} n_1 \\ n_2 \\ n_3 \end{Bmatrix} = \frac{1}{\sqrt{(\frac{\partial w}{\partial x_1})^2 + (\frac{\partial w}{\partial x_2})^2 + 1}} \begin{Bmatrix} -\frac{\partial w}{\partial x_1} \\ -\frac{\partial w}{\partial x_2} \\ 1 \end{Bmatrix}. \tag{3.92}$$

The two complementary orthogonal projection operators $\mathbf{P}^{\perp}$ and $\mathbf{P}$ can be obtained as follows:

$$\mathbf{P}^{\perp} = \mathbf{n} \otimes \mathbf{n} = \frac{1}{(\frac{\partial w}{\partial x_1})^2 + (\frac{\partial w}{\partial x_2})^2 + 1} \begin{bmatrix} (\frac{\partial w}{\partial x_1})^2 & \frac{\partial w}{\partial x_1}\frac{\partial w}{\partial x_2} & -\frac{\partial w}{\partial x_1} \\ \frac{\partial w}{\partial x_1}\frac{\partial w}{\partial x_2} & (\frac{\partial w}{\partial x_2})^2 & -\frac{\partial w}{\partial x_2} \\ -\frac{\partial w}{\partial x_1} & -\frac{\partial w}{\partial x_2} & 1 \end{bmatrix}, \tag{3.93}$$

$$\mathbf{P} = \mathbf{I} - \mathbf{P}^{\perp} = \frac{1}{(\frac{\partial w}{\partial x_1})^2 + (\frac{\partial w}{\partial x_2})^2 + 1} \begin{bmatrix} 1 + (\frac{\partial w}{\partial x_2})^2 & -\frac{\partial w}{\partial x_1}\frac{\partial w}{\partial x_2} & \frac{\partial w}{\partial x_1} \\ -\frac{\partial w}{\partial x_1}\frac{\partial w}{\partial x_2} & 1 + (\frac{\partial w}{\partial x_1})^2 & \frac{\partial w}{\partial x_2} \\ \frac{\partial w}{\partial x_1} & \frac{\partial w}{\partial x_2} & (\frac{\partial w}{\partial x_1})^2 + (\frac{\partial w}{\partial x_2})^2 \end{bmatrix}. \tag{3.94}$$

For infinitesimal strains and rotations, the mid-surface deflection (the normal displacement component) is significantly smaller than the plate thickness. This results in an exceptionally small surface curvature, with its square negligible compared to unity. Consequently, the normal vector can be expressed as:

$$\mathbf{n} = \begin{Bmatrix} n_1 \\ n_2 \\ n_3 \end{Bmatrix} = \begin{Bmatrix} -\frac{\partial w}{\partial x_1} \\ -\frac{\partial w}{\partial x_2} \\ 1 \end{Bmatrix}. \tag{3.95}$$

The complementary orthogonal projection operators $\mathbf{P}^{\perp}$ and $\mathbf{P}$ are therefore reduced to

$$\mathbf{P}^{\perp} = \begin{bmatrix} 0 & 0 & -\frac{\partial w}{\partial x_1} \\ 0 & 0 & -\frac{\partial w}{\partial x_2} \\ -\frac{\partial w}{\partial x_1} & -\frac{\partial w}{\partial x_2} & 1 \end{bmatrix}, \tag{3.96}$$

and

$$\mathbf{P} = \begin{bmatrix} 1 & 0 & \frac{\partial w}{\partial x_1} \\ 0 & 1 & \frac{\partial w}{\partial x_2} \\ \frac{\partial w}{\partial x_1} & \frac{\partial w}{\partial x_2} & 0 \end{bmatrix}. \tag{3.97}$$

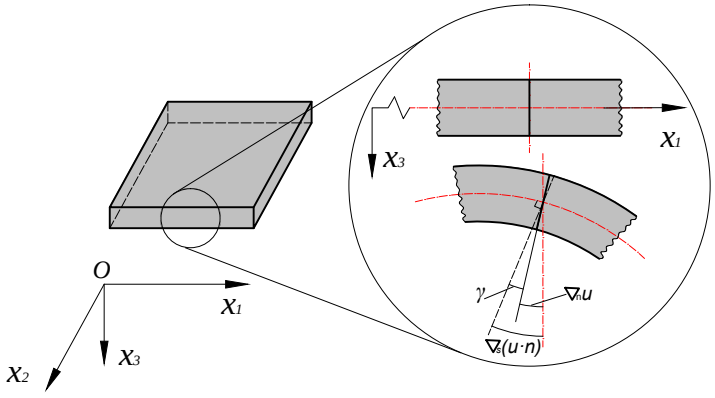

Figure 3.2: *The deformed configuration of a Mindlin plate.*

For infinitesimal deflections and rotations, the normal gradient operator $\nabla_{\mathbf{n}}(\cdot)$ which represents the gradient along the direction normal to the mid-surface can be expressed as:

$$\nabla_{\mathbf{n}}(\cdot) = \frac{\partial(\cdot)}{\partial x_3}. \tag{3.98}$$

Essentially, it describes the change of a scalar or vector function in the direction perpendicular to the mid-surface, represented by the partial derivative with respect to the coordinate x_3. The assumption (3.13) is rewritten as:

$$\nabla_{\mathbf{n}}\mathbf{t} = \nabla_{\mathbf{n}}(\mathbf{G}\cdot[\nabla_S(\mathbf{u}\cdot\mathbf{n}) + \nabla_{\mathbf{n}}\mathbf{u}]) = 0. \tag{3.99}$$

As illustrated in **Fig.** 3.2, the equation above signifies that the gradient of $\gamma = \nabla_S(\mathbf{u}\cdot\mathbf{n}) + \nabla_{\mathbf{n}}\mathbf{u}$ along the direction normal to the midplane is zero. Based on its geometric interpretation, we can derive the following expression:

$$\nabla^2_{\mathbf{n}}\mathbf{u} = \frac{\partial(\nabla_{\mathbf{n}}\mathbf{u})}{\partial x_3} = \mathbf{0}. \tag{3.100}$$

The vanishing partial derivative of the normal gradient $\nabla_{\mathbf{n}}\mathbf{u}$ with respect to x_3 indicates that the normal displacement gradient is independent of the thickness coordinate during deformation. This motivates introducing a concise representation for the normal gradient $\nabla_{\mathbf{n}}\mathbf{u}$ as the vector function $\phi(x_1, x_2, t)$, capturing the displacement characteristics relative to the mid-surface. Thus, $\nabla_{\mathbf{n}}\mathbf{u}$ is expressed as:

$$\nabla_{\mathbf{n}}\mathbf{u} = \phi(x_1, x_2, t), \tag{3.101}$$

where ϕ is a vector function solely dependent on x_1, x_2, and t, with components:

$$\phi(x_1,x_2,t) = \begin{Bmatrix} \phi_1(x_1,x_2,t) \\ \phi_2(x_1,x_2,t) \\ 0 \end{Bmatrix}. \tag{3.102}$$

Similarly, the normal gradient $\nabla_{\mathbf{n}}\mathbf{u}$ of the displacement field $\mathbf{u}$ equals its partial derivative with respect to the thickness direction x_3

$$\nabla_{\mathbf{n}}\mathbf{u} = \frac{\partial \mathbf{u}}{\partial x_3}. \tag{3.103}$$

Accordingly, referring to equation (3.101), the displacement at any point $\mathbf{x}$ within the plate and at time t can be succinctly expressed as:

$$\mathbf{u}(\mathbf{x},t) = \varphi(x_1,x_2,t) + x_3\phi(x_1,x_2,t) \tag{3.104}$$

where φ represents a vector function dependent solely on x_1, x_2, and t. Considering the displacement at the mid-surface, we have:

$$\mathbf{u}|_{x_3=0} = \mathbf{u}_0, \tag{3.105}$$

where $\mathbf{u}_0$ is defined by (3.90). This yields:

$$\varphi(x_1,x_2,t) = \mathbf{u}_0(x_1,x_2,t). \tag{3.106}$$

Hence, a direct correspondence exists between the displacement at any point within the plate and that at its mid-surface. The displacement field at any point within the plate can be expressed as:

$$\mathbf{u}(\mathbf{x},t) = \mathbf{u}_0(x_1,x_2,t) + x_3\phi(x_1,x_2,t). \tag{3.107}$$

Substituting equation (3.107) into equation (3.18) yields the explicit expression of the strain tensor $\boldsymbol{\varepsilon}_s$:

$$\boldsymbol{\varepsilon}_s = \begin{bmatrix} \frac{\partial u_0}{\partial x_1} & \frac{1}{2}\left(\frac{\partial u_0}{\partial x_2} + \frac{\partial v_0}{\partial x_1}\right) & 0 \\ \frac{1}{2}\left(\frac{\partial u_0}{\partial x_2} + \frac{\partial v_0}{\partial x_1}\right) & \frac{\partial v_0}{\partial x_2} & 0 \\ 0 & 0 & 0 \end{bmatrix}. \tag{3.108}$$

Similarly, by introducing equation (3.107) into equation (3.27), we obtain the explicit expression for the curvature tensor $\boldsymbol{\kappa}$:

$$\boldsymbol{\kappa} = \begin{bmatrix} \frac{\partial \phi_1}{\partial x_1} & \frac{1}{2}\left(\frac{\partial \phi_1}{\partial x_2} + \frac{\partial \phi_2}{\partial x_1}\right) & 0 \\ \frac{1}{2}\left(\frac{\partial \phi_1}{\partial x_2} + \frac{\partial \phi_2}{\partial x_1}\right) & \frac{\partial \phi_2}{\partial x_2} & 0 \\ 0 & 0 & 0 \end{bmatrix}. \tag{3.109}$$

Furthermore, the expression of $\nabla_S(\mathbf{u}\cdot\mathbf{n})$ can be specified by:

$$\nabla_S(\mathbf{u}\cdot\mathbf{n}) = \begin{Bmatrix} \frac{\partial w}{\partial x_1} \\ \frac{\partial w}{\partial x_2} \\ 0 \end{Bmatrix}. \tag{3.110}$$

Building on these formulations, explicit expressions for the in-plane stress resultants $\mathbf{N}_s$, moment resultants $\mathbf{M}$, and shear resultants $\mathbf{Q}$ can be derived once the plate's material properties are known. The following subsections detail two important cases: plates with transversely isotropic and isotropic materials.

3.4.3 Transversely Isotropic Material

For a plate made of a transversely isotropic material, the in-plane stress resultants, $\mathbf{N}_s$, moment resultants, $\mathbf{M}$, and shear resultants, $\mathbf{Q}$, can be derived by substituting the operators (2.144)-(2.151) for transverse isotropy into equations (3.80)-(3.82). The specific expressions for $\mathbf{N}_s$, $\mathbf{M}$,

and $\mathbf{Q}$ are as follows:

$$\mathbf{N}_s = \int_{-\frac{h}{2}}^{\frac{h}{2}} \left\{ \left(C_{12} - \frac{C_{13}^2}{C_{33}} \right) tr(\boldsymbol{\varepsilon}_s)\mathbf{P} + (C_{11} - C_{12})\boldsymbol{\varepsilon}_s \right\} dx_3, \tag{3.111}$$

$$\mathbf{M} = \int_{-\frac{h}{2}}^{\frac{h}{2}} \left\{ x_3^2 \left[\left(C_{12} - \frac{C_{13}^2}{C_{33}} \right) \mathrm{tr}(\boldsymbol{\kappa})\mathbf{P} + (C_{11} - C_{12})\boldsymbol{\kappa} \right] \right\} dx_3, \tag{3.112}$$

$$\mathbf{Q} = \int_{-\frac{h}{2}}^{\frac{h}{2}} C_{44}(\nabla_S(\mathbf{u}\cdot\mathbf{n}) + \nabla_{\mathbf{n}}\mathbf{u}) dx_3. \tag{3.113}$$

Using the expressions for $\boldsymbol{\varepsilon}_s$ and $\mathbf{P}$ in equations (3.97) and (3.108), $\mathbf{N}_s$ can be expanded into the following matrix form:

$$\mathbf{N}_s = h\left(C_{12} - \frac{C_{13}^2}{C_{33}} \right) \begin{bmatrix} \frac{\partial u_0}{\partial x_1} + \frac{\partial v_0}{\partial x_2} & 0 & 0 \\ 0 & \frac{\partial u_0}{\partial x_1} + \frac{\partial v_0}{\partial x_2} & 0 \\ 0 & 0 & 0 \end{bmatrix} + h(C_{11} - C_{12}) \begin{bmatrix} \frac{\partial u_0}{\partial x_1} & \frac{1}{2}\left(\frac{\partial u_0}{\partial x_2} + \frac{\partial v_0}{\partial x_1}\right) & 0 \\ \frac{1}{2}\left(\frac{\partial u_0}{\partial x_2} + \frac{\partial v_0}{\partial x_1}\right) & \frac{\partial v_0}{\partial x_2} & 0 \\ 0 & 0 & 0 \end{bmatrix}.$$

In accordance with the fundamental assumption of Mindlin plate theory, which postulates that the thickness of the plate remains invariant during deformation, the modulus C_{33} is considered to be a significantly large quantity. Therefore, the term C_{13}^2/C_{33} approaches zero, leading to the simplification of $\mathbf{N}_s$ as follows:

$$\mathbf{N}_s = h \begin{bmatrix} C_{11}\frac{\partial u_0}{\partial x_1} + C_{12}\frac{\partial v_0}{\partial x_2} & \frac{(C_{11}-C_{12})}{2}\left(\frac{\partial u_0}{\partial x_2} + \frac{\partial v_0}{\partial x_1}\right) & 0 \\ \frac{(C_{11}-C_{12})}{2}\left(\frac{\partial u_0}{\partial x_2} + \frac{\partial v_0}{\partial x_1}\right) & C_{12}\frac{\partial u_0}{\partial x_1} + C_{11}\frac{\partial v_0}{\partial x_2} & 0 \\ 0 & 0 & 0 \end{bmatrix}. \tag{3.114}$$

Using the expressions for $\boldsymbol{\kappa}$ and $\mathbf{P}$ given by equations (3.97) and (3.109), the moment tensor $\mathbf{M}$ provided by (3.112) is rewritten in the following matrix form:

$$\mathbf{M} = \frac{h^3}{24}\left(C_{12} - \frac{C_{13}^2}{C_{33}} \right) \begin{bmatrix} \frac{\partial \phi_1}{\partial x_1} + \frac{\partial \phi_2}{\partial x_2} & 0 & 0 \\ 0 & \frac{\partial \phi_1}{\partial x_1} + \frac{\partial \phi_2}{\partial x_2} & 0 \\ 0 & 0 & 0 \end{bmatrix} + \frac{h^3}{24}(C_{11} - C_{12}) \begin{bmatrix} \frac{\partial \phi_1}{\partial x_1} & \frac{1}{2}\left(\frac{\partial \phi_1}{\partial x_2} + \frac{\partial \phi_2}{\partial x_1}\right) & 0 \\ \frac{1}{2}\left(\frac{\partial \phi_1}{\partial y} + \frac{\partial \phi_2}{\partial x_1}\right) & \frac{\partial \phi_2}{\partial x_2} & 0 \\ 0 & 0 & 0 \end{bmatrix}.$$

Similarly, as C_{13}^2/C_{33} approaches zero, the expression of $\mathbf{M}$ takes the following simple form:

$$\mathbf{M} = \frac{h^3}{24}\begin{bmatrix} C_{11}\frac{\partial \phi_1}{\partial x_1} + C_{12}\frac{\partial \phi_2}{\partial x_2} & \frac{(C_{11}-C_{12})}{2}(\frac{\partial \phi_1}{\partial x_2} + \frac{\partial \phi_2}{\partial x_1}) & 0 \\ \frac{(C_{11}-C_{12})}{2}(\frac{\partial \phi_1}{\partial x_2} + \frac{\partial \phi_2}{\partial x}) & C_{12}\frac{\partial \phi_1}{\partial x} + C_{11}\frac{\partial \phi_2}{\partial x_2} & 0 \\ 0 & 0 & 0 \end{bmatrix}. \tag{3.115}$$

For the shear resultant $\mathbf{Q}$, substituting equations (3.102) and (3.110) into equation (3.113) yields its explicit expression:

$$\mathbf{Q} = hC_{44}\begin{Bmatrix} \frac{\partial w}{\partial x_1} + \phi_1 \\ \frac{\partial w}{\partial x_2} + \phi_2 \\ 0 \end{Bmatrix}. \tag{3.116}$$

3.4.4 Isotropic Material

For an isotropic plate, the in-plane stress resultants $\mathbf{N}_s$, moment resultants $\mathbf{M}$, and shear resultants $\mathbf{Q}$ can be obtained by substituting the isotropy operators (2.153)-(2.157) into equations (3.80)-(3.82). Specifically:

$$\mathbf{N}_s = \frac{\partial E}{\partial \varepsilon_s} = \int_{-\frac{h}{2}}^{\frac{h}{2}} \left\{ \frac{2\mu\lambda}{\lambda+2\mu} tr(\varepsilon_s)\mathbf{P} + 2\mu\varepsilon_s \right\} dx_3, \tag{3.117}$$

$$\mathbf{M} = \frac{\partial E}{\partial \kappa} = \int_{-\frac{h}{2}}^{\frac{h}{2}} x_3^2 \left(\frac{2\mu\lambda}{\lambda+2\mu} \mathrm{tr}(\kappa)\mathbf{P} + 2\mu\kappa \right) dx_3, \tag{3.118}$$

$$\mathbf{Q} = \frac{\partial E}{\partial(\nabla_S(\mathbf{u}\cdot\mathbf{n}) + \nabla_{\mathbf{n}}\mathbf{u})} = \int_{-\frac{h}{2}}^{\frac{h}{2}} \mu(\nabla_S(\mathbf{u}\cdot\mathbf{n}) + \nabla_{\mathbf{n}}\mathbf{u}) dx_3. \tag{3.119}$$

Given the expressions for ε_s and $\mathbf{P}$ in equations (3.97) and (3.108), $\mathbf{N}_s$ can be expressed in matrix form as follows:

$$\mathbf{N}_s = \frac{2h\mu\lambda}{\lambda+2\mu}\begin{bmatrix} \frac{\partial u_0}{\partial x_1} + \frac{\partial v_0}{\partial x_2} & 0 & 0 \\ 0 & \frac{\partial u_0}{\partial x_1} + \frac{\partial v_0}{\partial x_2} & 0 \\ 0 & 0 & 0 \end{bmatrix} + 2h\mu\begin{bmatrix} \frac{\partial u_0}{\partial x_1} & \frac{1}{2}(\frac{\partial u_0}{\partial x_2} + \frac{\partial v_0}{\partial x_1}) & 0 \\ \frac{1}{2}(\frac{\partial u_0}{\partial x_2} + \frac{\partial v_0}{\partial x_1}) & \frac{\partial v_0}{\partial x_2} & 0 \\ 0 & 0 & 0 \end{bmatrix},$$

or equivalently,

$$\mathbf{N}_s = \frac{hE}{1-\nu^2}\begin{bmatrix} \frac{\partial u_0}{\partial x_1}+\nu\frac{\partial v_0}{\partial x_2} & \frac{(1-\nu)}{2}(\frac{\partial u_0}{\partial x_2}+\frac{\partial v_0}{\partial x_1}) & 0 \\ \frac{(1-\nu)}{2}(\frac{\partial u_0}{\partial x_2}+\frac{\partial v_0}{\partial x_1}) & \nu\frac{\partial u_0}{\partial x_1}+\frac{\partial v_0}{\partial x_2} & 0 \\ 0 & 0 & 0 \end{bmatrix}, \tag{3.120}$$

where E is Young's modulus, ν is Poisson's ratio, and their relationship with the Lame coefficients is given by:

$$\lambda = \frac{E\nu}{1-\nu^2}, \quad \mu = \frac{E}{2(1+\nu)}. \tag{3.121}$$

Similarly, the moment tensor $\mathbf{M}$ given by (3.184) takes the following matrix form:

$$\mathbf{M} = \frac{h^3\mu\lambda}{6(\lambda+2\mu)}\begin{bmatrix} \frac{\partial\phi_1}{\partial x_1}+\frac{\partial\phi_2}{\partial x_2} & 0 & 0 \\ 0 & \frac{\partial\phi_1}{\partial x_1}+\frac{\partial\phi_2}{\partial x_2} & 0 \\ 0 & 0 & 0 \end{bmatrix} + \frac{h^3\mu}{6}\begin{bmatrix} \frac{\partial\phi_1}{\partial x} & \frac{1}{2}(\frac{\partial\phi_1}{\partial x_2}+\frac{\partial\phi_2}{\partial x_1}) & 0 \\ \frac{1}{2}(\frac{\partial\phi_1}{\partial x_2}+\frac{\partial\phi_2}{\partial x_1}) & \frac{\partial\phi_2}{\partial x_2} & 0 \\ 0 & 0 & 0 \end{bmatrix}$$

or equivalently,

$$\mathbf{M} = \frac{h^3E}{12(1-\nu^2)}\begin{bmatrix} \frac{\partial\phi_1}{\partial x_1}+\nu\frac{\partial\phi_2}{\partial x_2} & \frac{(1-\nu)}{2}(\frac{\partial\phi_1}{\partial x_2}+\frac{\partial\phi_2}{\partial x_1}) & 0 \\ \frac{(1-\nu)}{2}(\frac{\partial\phi_1}{\partial x_2}+\frac{\partial\phi_2}{\partial x_1}) & \nu\frac{\partial\phi_1}{\partial x_1}+\frac{\partial\phi_2}{\partial x_2} & 0 \\ 0 & 0 & 0 \end{bmatrix}. \tag{3.122}$$

By inserting equations (3.102) and (3.110) into equation (3.119), the explicit expression for the shear resultant $\mathbf{Q}$ can be obtained:

$$\mathbf{Q} = h\nu\begin{Bmatrix} \frac{\partial w}{\partial x_1}+\phi_1 \\ \frac{\partial w}{\partial x_2}+\phi_2 \\ 0 \end{Bmatrix}. \tag{3.123}$$

3.4.5 Timoshenko Beam Theory

When the field in the x_2 direction vanishes and the fields in the x_1-direction and x_3-direction are independent of x_2, the Mindlin plate reduces to a Timoshenko beam. For a beam with uniform thickness h and length L, the coordinates at any point $\mathbf{x}$ within the beam simplify to $\mathbf{x} \in \mathbb{R}^2$. To maintain consistency with the previous Mindlin plate discussion, the coordinate system (x_1, x_3)

is adopted, with x_1 along the beam's centerline and x_3 positive upward. This configuration is shown in **Fig.** 3.3. The time-dependent displacement field of the midline curve is expressed as:

$$\mathbf{u}_0(\mathbf{x},t) = \begin{Bmatrix} u_0(x_1,t) \\ w(x_1,t) \end{Bmatrix}. \tag{3.124}$$

The deformed midline curve of the beam can be represented by

$$\Gamma = \{\mathbf{x} \in \mathbb{R}^2 \mid g(\mathbf{x}) = x_3 - w = 0\}. \tag{3.125}$$

The normal vector perpendicular to the deformed midline curve of the beam is referred to as:

$$\mathbf{n} = \begin{Bmatrix} n_1 \\ n_3 \end{Bmatrix} = \begin{Bmatrix} -\frac{\partial w}{\partial x_1} \\ 1 \end{Bmatrix}. \tag{3.126}$$

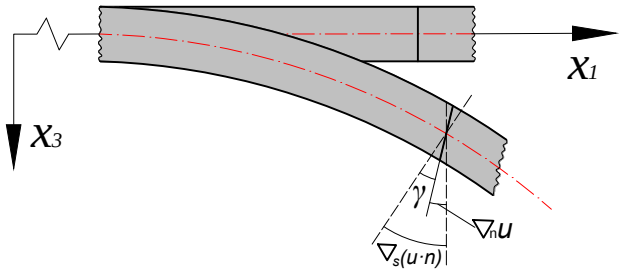

Figure 3.3: *The deformed configuration of a Timoshenko beam.*

The complementary orthogonal projection operators $\mathbf{P}^{\perp}$ and $\mathbf{P}$ can be expressed as:

$$\mathbf{P}^{\perp} = \begin{bmatrix} 0 & -\frac{\partial w}{\partial x_1} \\ -\frac{\partial w}{\partial x_1} & 1 \end{bmatrix}, \tag{3.127}$$

and

$$\mathbf{P} = \begin{bmatrix} 1 & \frac{\partial w}{\partial x_1} \\ \frac{\partial w}{\partial x_1} & 0 \end{bmatrix}. \tag{3.128}$$

Therefore, the displacement is reduced to the following form:

$$\mathbf{u}(\mathbf{x},t) = \mathbf{u}_0(x_1,t) + x_3\phi(x_1,t), \tag{3.129}$$

where $\phi(x_1,t)$ is a vector function given as follows:

$$\phi(x_1,t) = \begin{Bmatrix} \phi_1(x_1,t) \\ 0 \end{Bmatrix}. \tag{3.130}$$

The expressions of ε_s, κ, and $\nabla_S(\mathbf{u}\cdot\mathbf{n})$ takes the following forms:

$$\varepsilon_s = \begin{bmatrix} \frac{\partial u_0}{\partial x_1} & 0 \\ 0 & 0 \end{bmatrix}, \tag{3.131}$$

$$\kappa = \begin{bmatrix} \frac{\partial \phi_1}{\partial x_1} & 0 \\ 0 & 0 \end{bmatrix}, \tag{3.132}$$

$$\nabla_S(\mathbf{u}\cdot\mathbf{n}) = \begin{Bmatrix} \frac{\partial w}{\partial x_1} \\ 0 \end{Bmatrix}. \tag{3.133}$$

The axial force N_s, bending moment M, and the shear force Q can be obtained as:

$$N_s = \frac{Eh}{1-\nu^2}\frac{\partial u_0}{\partial x_1}, \tag{3.134}$$

$$M = \frac{Eh^3}{12(1-\nu^2)}\frac{\partial \phi_1}{\partial x_1}, \tag{3.135}$$

$$Q = \mu h(\phi_1 + \frac{\partial w}{\partial x_1}). \tag{3.136}$$

The equations (3.66) are reduced to:

$$\frac{Eh}{1-\nu^2}\frac{\partial^2 u_0}{\partial x_1^2} + f_s = \rho h\frac{\partial^2 u_0}{\partial t^2}, \tag{3.137a}$$

$$\frac{Eh^3}{12(1-\nu^2)}\frac{\partial^2 \phi_1}{\partial x_1^2} + \mu h(\phi_1 + \frac{\partial w}{\partial x_1}) = \frac{\rho h^2}{12}\frac{\partial^2 \phi_1}{\partial t^2}, \tag{3.137b}$$

$$\mu h(\phi_1 + \frac{\partial w}{\partial x_1}) + f_{x_3} = \rho h\frac{\partial^2 w}{\partial t^2}, \tag{3.137c}$$

for any $x_1 \in (0,L)$ and $t \in (0,T)$. And the boundary conditions (3.67) are simplified to:

$$N_s = \bar{N}_s \quad \text{or} \quad u_0 = \bar{u}_0 \quad \text{at} \quad x_1 = 0 \quad \text{and} \quad x_1 = L, \tag{3.138a}$$

$$M = \bar{M} \quad \text{or} \quad \phi_1 = \bar{\phi}_1 \quad \text{at} \quad x_1 = 0 \quad \text{and} \quad x_1 = L, \tag{3.138b}$$

$$Q = \bar{Q} \quad \text{or} \quad w = \bar{w} \quad \text{at} \quad x_1 = 0 \quad \text{and} \quad x_1 = L. \tag{3.138c}$$

This formulation constitutes a boundary-initial value problem for determining u_0, w , and ϕ_1, governed by the system of differential equations in equations (3.137a-c) and the boundary conditions in equations (3.138a-c), with initial conditions at $t = 0$ and $t = T$. This establishes a non-classical Timoshenko beam model. Unlike the classical Timoshenko beam theory, the equations of motion in (3.137a-c) explicitly incorporate the Poisson effect. While this effect is often negligible for slender beams with significant aspect ratios (by setting $\nu = 0$), it becomes crucial for non-slender beams or materials with pronounced Poisson effects to ensure accurate results. Ignoring the Poisson effect reduces the model to the classical Timoshenko beam. Neglecting axial effects ($u_0 = 0$) simplifies equations (3.137a) and boundary conditions (3.138a) to the classical model in Hutchinson [71]. For time-independent fields $w = w(x_1)$, and $\phi_1 = \phi_1(x_1)$, the model reduces to the quasistatic Timoshenko beam of Wang [139].

3.5 The Dynamic Plate Theory without Coupling Effect and Shear Force

Let us consider a scenario where the plate structure exhibits geometric symmetry about its mid-surface, and the material composing the plate is homogeneous. Given the context of small rotations and deflections, as previously outlined, we will disregard the coupling effect. In the previous case, shear forces were taken into account, which is applicable to moderately thick plates. However, in the case of thin plates, the thickness of the plate is typically much smaller compared to its width and length. Consequently, the stiffness of the plate is primarily determined by its bending stiffness, while the shear stiffness is relatively small. Due to this smaller shear stiffness, the deformation of the plate is primarily bending deformation, with shear deformation being comparatively minor. Therefore, in analysis, the influence of shear forces can typically be neglected.In this section, we revisit the formulation of the strain energy based on

the aforementioned foundations and reintroduce the strain energy density function. Utilizing variational methods, we derive the governing equations and corresponding boundary conditions. This theory simplifies to classical Kirchhoff-Love plate theory in the two-dimensional case and degenerates to Bernoulli-Euler beam theory in the one-dimensional case.

3.5.1 General Form of Plate Theory without Coupling Effect and Shear Force

When neglecting both the coupling effect and shear force (i.e., $\Xi_{\text{couple}} = 0$, and $\Xi_{\text{shear}} = 0$), the total strain energy Ξ_h consists of the membrane energy $\Xi_{membrane}$ and the bending energy $\Xi_{bending}$, as outlined in equations (3.21) and (3.28). Specifically, it can be formulated as:

$$\Xi_h = \frac{1}{2}\int_{S_0}\int_{-\frac{h}{2}}^{\frac{h}{2}} (\boldsymbol{\varepsilon}_s : \mathbb{A} : \boldsymbol{\varepsilon}_s) dx_3 ds + \frac{1}{2}\int_{S_0}\int_{-\frac{h}{2}}^{\frac{h}{2}} x_3^2 [\boldsymbol{\kappa} : \mathbb{A} : \boldsymbol{\kappa}] dx_3 ds. \tag{3.139}$$

Given the previously provided expression for the total strain energy, we can derive the corresponding energy density function E as follows:

$$E = \frac{1}{2}\int_{-\frac{h}{2}}^{\frac{h}{2}} (\boldsymbol{\varepsilon}_s : \mathbb{A} : \boldsymbol{\varepsilon}_s) dx_3 + \frac{1}{2}\int_{-\frac{h}{2}}^{\frac{h}{2}} x_3^2 (\boldsymbol{\kappa} : \mathbb{A} : \boldsymbol{\kappa}) dx_3. \tag{3.140}$$

Based on the energy density function, it is evident that the involved geometric measures are solely $\boldsymbol{\varepsilon}_s$ and $\boldsymbol{\kappa}$. Consequently, the conjugate physical fields, i.e., the in-plane stress resultants $\mathbf{N}_s$ and moment resultants $\mathbf{M}$, can be determined by differentiating the energy density function E with respect to the respective deformation measures. Their expressions are specifically given by:

$$\mathbf{N}_s = \frac{\partial E}{\partial \boldsymbol{\varepsilon}_s} = \int_{-\frac{h}{2}}^{\frac{h}{2}} (\mathbb{A} : \boldsymbol{\varepsilon}_s) dx_3, \tag{3.141}$$

$$\mathbf{M} = \frac{\partial E}{\partial \boldsymbol{\kappa}} = \int_{-\frac{h}{2}}^{\frac{h}{2}} \boldsymbol{x}_3^2 (\mathbb{A} : \boldsymbol{\kappa}) dx_3. \tag{3.142}$$

Utilizing the provided constitutive equations, we can concisely express the energy density function E as follows:

$$E = \frac{1}{2}[\boldsymbol{\varepsilon}_s : \mathbf{N}_s + \boldsymbol{\kappa} : \mathbf{M}]. \tag{3.143}$$

Before we proceed with the variation of the total strain energy Ξ, it is necessary to determine the number and nature of the independent variables involved in the variation process, due to the reduced geometric measurements, as previously mentioned. Specifically, under the condition that $\Xi_{\text{shear}} = 0$ and according to equation (3.25), the following constraint applies:

$$[\nabla_S(\mathbf{u}\cdot\mathbf{n}) + \nabla_{\mathbf{n}}\mathbf{u}]\cdot(\mathbf{n}\cdot\mathbb{C}\cdot\mathbf{n})\cdot[\nabla_S(\mathbf{u}\cdot\mathbf{n}) + \nabla_{\mathbf{n}}\mathbf{u}] = \mathbf{0}. \tag{3.144}$$

Given that $\mathbf{n}\cdot\mathbb{C}\cdot\mathbf{n}$ is positive definite and invertible, as detailed in equations (2.90)-(2.93) of Chapter 3.4, the above equation indicates that:

$$\nabla_{\mathbf{n}}\mathbf{u} + \nabla_S(\mathbf{u}\cdot\mathbf{n}) = \mathbf{0}. \tag{3.145}$$

Based on the preceding explanation, we can deduce that:

$$\delta\nabla_{\mathbf{n}}\mathbf{u} = -\delta\nabla_S(\mathbf{u}\cdot\mathbf{n}). \tag{3.146}$$

In the variational process, it is noteworthy that the variation of $\nabla_S\mathbf{u}$ on a given surface S_0 is not independent of the variation of $\mathbf{u}$. As a result, the independent variables in this variational framework reduce to $\delta(\mathbf{P}\cdot\mathbf{u})$ and $\delta(\mathbf{u}\cdot\mathbf{n})$. This distinction marks a significant departure from the previous variational processes discussed in Chapters 4.5 and 4.6. It will be applied in subsequent analyses of the work done by external forces and kinetic energy.

Now, we proceed to perform a variational analysis of the total strain energy term by term. Based on equations (3.53) and (3.141), we obtain the variation of $\Xi_{membrane}$ as:

$$\delta\Xi_{membrane} = \int_{S_0}[\nabla\cdot[\mathbf{N}_s\cdot\delta(\mathbf{P}\cdot\mathbf{u})] - (\nabla\cdot\mathbf{N}_s)\cdot\delta(\mathbf{P}\cdot\mathbf{u})]ds. \tag{3.147}$$

Considering the definition of the curvature tensor κ given in equation (3.27) and employing the intrinsic symmetry of the tensor $\mathbb{A}$, we can systematically unfold the variational derivative of the pure bending energy in the following manner:

$$\begin{aligned}\delta\Xi_{bending} = \int_{S_0}\{&-\nabla\cdot[\mathbf{P}\cdot\mathbf{M}\cdot\mathbf{P}\cdot\delta(\nabla(\mathbf{u}\cdot\mathbf{n}))] + \nabla\cdot[\nabla_S\cdot(\mathbf{M}\cdot\mathbf{P})\delta(\mathbf{u}\cdot\mathbf{n})]\\ &-\nabla\cdot[\nabla_S\cdot(\mathbf{M}\cdot\mathbf{P})]\delta(\mathbf{u}\cdot\mathbf{n})\}ds.\end{aligned} \tag{3.148}$$

By summing the variations of the membrane and bending energies, we obtain the total variation of the strain energy Ξ as follows:

$$\begin{aligned}\delta\Xi = &\int_{S_0} [\nabla\cdot[\mathbf{N}_s\cdot\delta(\mathbf{P}\cdot\mathbf{u})] - (\nabla\cdot\mathbf{N}_s)\cdot\delta(\mathbf{P}\cdot\mathbf{u}) - \nabla\cdot[\mathbf{P}\cdot\mathbf{M}\cdot\mathbf{P}\cdot\delta(\nabla(\mathbf{u}\cdot\mathbf{n}))] \\ &+\nabla\cdot[\nabla_S\cdot(\mathbf{M}\cdot\mathbf{P})\delta(\mathbf{u}\cdot\mathbf{n})] - \nabla\cdot[\nabla_S\cdot(\mathbf{M}\cdot\mathbf{P})]\delta(\mathbf{u}\cdot\mathbf{n})]ds.\end{aligned} \tag{3.149}$$

The potential energy of external forces, denoted as W, quantifies the work exerted by these forces through corresponding displacements, under the assumption of force constancy during deformation. The variation in external work is expressed as:

$$\begin{aligned}\delta W &= \int_{S_0}(\mathbf{f}\cdot\delta\mathbf{u})ds + \int_{\partial S_0}[\bar{\mathbf{N}}\cdot\delta(\mathbf{P}\cdot\mathbf{u}) + \bar{\mathbf{M}}\cdot\delta\nabla(\mathbf{u}\cdot\mathbf{n})]dl \\ &= \int_{S_0}[\mathbf{f}_s\cdot\delta(\mathbf{P}\cdot\mathbf{u}) + f_{x_3}\delta(\mathbf{u}\cdot\mathbf{n})]ds + \int_{\partial S_0}[\bar{\mathbf{N}}\cdot\delta(\mathbf{P}\cdot\mathbf{u}) + \bar{\mathbf{M}}\cdot\delta\nabla(\mathbf{u}\cdot\mathbf{n})]dl\end{aligned} \tag{3.150}$$

where $\mathbf{f}$, $\bar{\mathbf{N}}$, and $\bar{\mathbf{M}}$ denote the body force resultant applied to the middle surface of the plate S_0, and the Cauchy traction resultant and moment applied to the boundary of the middle surface of the plate ∂S_0, respectively.

The kinetic energy of the plate is defined as the integral of the kinetic energy density over its volume, which is given by:

$$K = \int_{-\frac{h}{2}}^{\frac{h}{2}}\int_{S_0}\frac{1}{2}\rho\dot{\mathbf{u}}^2 dx_3 ds \tag{3.151}$$

where the superposed dot on a variable indicates time derivative (e.g., $\dot{\mathbf{u}} = \partial\mathbf{u}/\partial t$). The variation in kinetic energy, denoted by δK, can be derived by decomposing the displacement field $\mathbf{u}$ and using the chain rule of differentiation. Specifically, it can be expressed as:

$$\begin{aligned}\delta K &= \int_{-\frac{h}{2}}^{\frac{h}{2}}\int_{S_0}\rho\ddot{\mathbf{u}}\cdot\delta\mathbf{u}dx_3 ds \\ &= \int_{S_0}[(I_0\mathbf{P}\cdot\ddot{\mathbf{u}})\cdot\delta(\mathbf{P}\cdot\mathbf{u}) + [I_0(\ddot{\mathbf{u}}\cdot\mathbf{n}) - (I_2\nabla\cdot\nabla(\ddot{\mathbf{u}}\cdot\mathbf{n})]\delta(\mathbf{u}\cdot\mathbf{n}) + I_2\nabla\cdot(\nabla(\ddot{\mathbf{u}}\cdot\mathbf{n})\delta(\mathbf{u}\cdot\mathbf{n}))]ds\end{aligned} \tag{3.152}$$

where I_0 and I_2 are the mass moments of inertia and they can be calculated by

$$I_0 = \int_{-\frac{h}{2}}^{\frac{h}{2}}\rho dx_3, \quad I_2 = \int_{-\frac{h}{2}}^{\frac{h}{2}}\rho x_3^2 dx_3. \tag{3.153}$$

The dynamic version of the variational principle of total energy, which can be interpreted as

the minimization of the total potential energy with the inclusion of kinetic energy effects, is expressed as:

$$\delta\Pi = \int_0^T (\delta\Xi + \delta W - \delta K)dt = 0. \tag{3.154}$$

Expanding this integral, we obtain:

$$\begin{aligned}
&\int_0^T \int_{S_0} \{[\mathbf{f}_s - \nabla\cdot\mathbf{N}_s - I_0\mathbf{P}\cdot\ddot{\mathbf{u}}]\cdot\delta(\mathbf{P}\cdot\mathbf{u}) + [f_{x_3} - \nabla\cdot[\nabla_s\cdot(\mathbf{M}\cdot\mathbf{P})] - I_0(\ddot{\mathbf{u}}\cdot\mathbf{n}) + I_2\nabla\cdot\nabla(\ddot{\mathbf{u}}\cdot\mathbf{n})]\delta(\mathbf{u}\cdot\mathbf{n})\}dsdt \\
&+ \int_0^T \int_{S_0} \{\nabla\cdot[\mathbf{N}_s\cdot\delta(\mathbf{P}\cdot\mathbf{u})] - \nabla\cdot[\mathbf{P}\cdot\mathbf{M}\cdot\mathbf{P}\cdot\delta(\nabla(\mathbf{u}\cdot\mathbf{n}))] + \nabla\cdot[\nabla_S\cdot(\mathbf{M}\cdot\mathbf{P})] - I_2\nabla(\ddot{\mathbf{u}}\cdot\mathbf{n})]\delta(\mathbf{u}\cdot\mathbf{n})]\}dsdt \\
&+ \int_0^T \int_{\partial S_0} [\bar{\mathbf{N}}\cdot\delta(\mathbf{P}\cdot\mathbf{u}) + \bar{\mathbf{M}}\cdot\delta\nabla(\mathbf{u}\cdot\mathbf{n})]dldt = 0.
\end{aligned} \tag{3.155}$$

Before obtaining the boundary conditions in terms of displacements, forces, and moments along an edge, it is essential to precisely define the unit normal vector $\mathbf{m}$ of this edge. Applying the divergence theorem and Stokes's theorem, equation (3.155) can be reformulated as:

$$\begin{aligned}
&\int_0^T \int_{S_0} \{[\mathbf{f}_s - \nabla\cdot\mathbf{N}_s - I_0\mathbf{P}\cdot\ddot{\mathbf{u}}]\cdot\delta(\mathbf{P}\cdot\mathbf{u}) + [f_{x_3} - \nabla\cdot[\nabla_S\cdot(\mathbf{M}\cdot\mathbf{P})] - I_0(\ddot{\mathbf{u}}\cdot\mathbf{n}) + I_2\nabla\cdot\nabla(\ddot{\mathbf{u}}\cdot\mathbf{n})]\delta(\mathbf{u}\cdot\mathbf{n})\}dsdt \\
&+ \int_0^T \int_{\partial S_0} \{[(\mathbf{N}_s\cdot\mathbf{m} + \bar{\mathbf{N}})\cdot\delta(\mathbf{P}\cdot\mathbf{u})] - [((\mathbf{P}\cdot\mathbf{M}\cdot\mathbf{P})\cdot\mathbf{m} + \bar{\mathbf{M}})\cdot\delta(\nabla(\mathbf{u}\cdot\mathbf{n}))] + [\nabla_S\cdot(\mathbf{M}\cdot\mathbf{P}) \\
&- I_2\nabla(\ddot{\mathbf{u}}\cdot\mathbf{n})]\cdot\mathbf{m}\delta(\mathbf{u}\cdot\mathbf{n})\}dldt = 0.
\end{aligned} \tag{3.156}$$

In the given equation, the variables $\delta(\mathbf{P}\cdot\mathbf{u})$ and $\delta(\mathbf{u}\cdot\mathbf{n})$ are considered arbitrary. Consequently, we derive the following equilibrium equations:

$$\left.\begin{aligned}
\mathbf{f}_s - \nabla\cdot\mathbf{N}_s &= I_0\mathbf{P}\cdot\ddot{\mathbf{u}} \\
f_{x_3} - \nabla\cdot[\nabla_S\cdot(\mathbf{M}\cdot\mathbf{P})] &= I_0(\ddot{\mathbf{u}}\cdot\mathbf{n}) - I_2\nabla\cdot\nabla(\ddot{\mathbf{u}}\cdot\mathbf{n})
\end{aligned}\right\}. \tag{3.157}$$

For the second integral term of above equation, considering a more general case of a plate whose edges are not parallel to the x- and y-axes, as shown in **Fig.** 3.1, we introduce a rotation tensor $\mathbf{R}$ which relates Cartesian coordinates (x,y,z) to Coordinates (m,s,z) by

$$\begin{Bmatrix} x \\ y \\ z \end{Bmatrix} = \begin{bmatrix} cos\theta & -sin\theta & 0 \\ sin\theta & cos\theta & 0 \\ 0 & 0 & 1 \end{bmatrix} \begin{Bmatrix} m \\ s \\ z \end{Bmatrix} = \begin{bmatrix} m_x & -m_y & 0 \\ m_y & m_x & 0 \\ 0 & 0 & 1 \end{bmatrix} \begin{Bmatrix} m \\ s \\ z \end{Bmatrix}. \tag{3.158}$$

where θ is the rotation angle around the z -axis. Hence, the displacement (u_{0m}, u_{0s}, w) are related to (u_0, v_0, w) by the transformation

$$\begin{Bmatrix} u_0 \\ v_0 \\ w \end{Bmatrix} = \begin{bmatrix} cos\theta & -sin\theta & 0 \\ sin\theta & cos\theta & 0 \\ 0 & 0 & 1 \end{bmatrix} \begin{Bmatrix} u_{0m} \\ u_{0s} \\ w \end{Bmatrix}, \tag{3.159}$$

which can be expressed as

$$\mathbf{u} = \mathbf{R} \cdot \hat{\mathbf{u}}. \tag{3.160}$$

Similarly, the force tensor, the moment tensor and the normal derivative in the coordinate system (x, y, z) are related to those in the coordinate system (m,s,n) through the following transform expression

$$\mathbf{M} = \mathbf{R} \cdot \hat{\mathbf{M}} \cdot \mathbf{R}^T, \tag{3.161}$$

$$\mathbf{N}_s = \mathbf{R} \cdot \hat{\mathbf{N}}_s \cdot \mathbf{R}^T, \tag{3.162}$$

and

$$\nabla(\mathbf{u} \cdot \mathbf{n}) = \nabla(\mathbf{R} \cdot \hat{\mathbf{u}} \cdot \mathbf{n}). \tag{3.163}$$

Now we can rewrite the boundary expressions in equation (3.156) in terms of the displacements $\hat{\mathbf{u}}$

$$\begin{aligned} &\int_0^T \int_{\partial S_0} \{[\hat{\mathbf{N}}_s \cdot \mathbf{R}^T \cdot \mathbf{m} - \tilde{\mathbf{N}}] \cdot \delta(\mathbf{P} \cdot \hat{\mathbf{u}}) + [\hat{\mathbf{M}} \cdot \mathbf{R}^T \cdot \mathbf{m} - \tilde{\mathbf{M}}] \cdot \delta \nabla(\hat{\mathbf{u}} \cdot \mathbf{n}) \\ &- [\nabla \cdot \mathbf{M} - I_2 \nabla(\ddot{\mathbf{u}} \cdot \mathbf{n})] \cdot \mathbf{m} \delta(\mathbf{u} \cdot \mathbf{n})\} dl dt = 0, \end{aligned} \tag{3.164}$$

which gives the following corresponding boundary conditions:

$$\left.\begin{aligned} \hat{\mathbf{N}}_s \cdot \mathbf{R}^T \cdot \mathbf{m} - \tilde{\mathbf{N}} = 0 \\ \hat{\mathbf{M}} \cdot \mathbf{R}^T \cdot \mathbf{m} - \tilde{\mathbf{M}} = 0 \\ \nabla \cdot \mathbf{M} - I_2 \nabla(\ddot{\mathbf{u}} \cdot \mathbf{n}) = 0 \end{aligned}\right\}. \tag{3.165}$$

These boundary conditions provide constraints on the displacements, forces, and moments along the edge, offering further insights into the behavior of the system under consideration.

3.5.2 The Kirchhoff-Love Plate Theory

Consider a plate with uniform thickness h in a rectangular Cartesian coordinate system (x_1, x_2, x_3). The x_1-x_2-plane coincides with the plate's mid-plane, and the x_3-axis is oriented downward, as shown in **Fig.** 3.4.

The displacement field describing the time-dependent deformations of the middle surface is given by:

$$\mathbf{u}_0(\mathbf{x}, t) = \left\{\begin{array}{c} u_0(x_1, x_2, t) \\ v_0(x_1, x_2, t) \\ w(x_1, x_2, t) \end{array}\right\}, \tag{3.166}$$

where $u_0(x_1, x_2, t)$ and $v_0(x_1, x_2, t)$ are the in-plane displacements of a material point on the middle surface in the (x_1, x_2, x_3) coordinate directions, and $w(x_1, x_2, t)$ is the transverse displacement (or bending deflection) of the middle surface. For brevity, we denote these quantities as u_0, v_0, and w throughout this subsection. The deformed middle surface of the plate can be expressed as:

$$\Gamma = \{\boldsymbol{x} \in \mathbb{R}^3 \mid g(\mathbf{x}, t) = z - w(x_1, x_2, t) = 0\}. \tag{3.167}$$

Following Mindlin plate theory for small strains and rotations, the mid-surface deflection is significantly smaller than the plate thickness. This leads to negligible surface curvature, allowing us to approximate the normal vector as:

$$\mathbf{n} = \left\{\begin{array}{c} n_1 \\ n_2 \\ n_3 \end{array}\right\} = \left\{\begin{array}{c} -\frac{\partial w}{\partial x_1} \\ -\frac{\partial w}{\partial x_2} \\ 1 \end{array}\right\}. \tag{3.168}$$

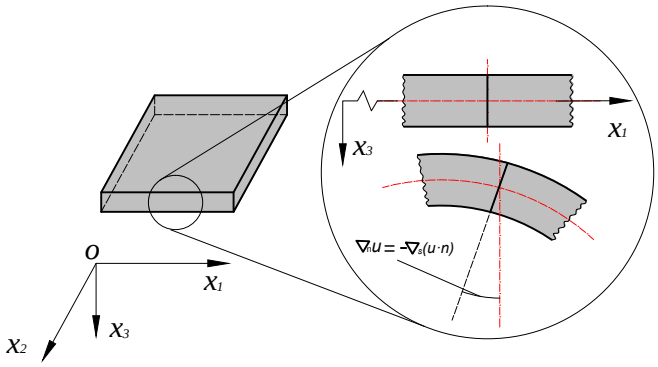

Figure 3.4: *The deformed configuration of a Kirchhoff-Love plate.*

Similarly, the complementary orthogonal projection operators $\mathbf{P}^{\perp}$ and $\mathbf{P}$ take the following forms:

$$\mathbf{P}^{\perp} = \begin{bmatrix} 0 & 0 & -\frac{\partial w}{\partial x_1} \\ 0 & 0 & -\frac{\partial w}{\partial x_2} \\ -\frac{\partial w}{\partial x_1} & -\frac{\partial w}{\partial x_2} & 1 \end{bmatrix}, \tag{3.169}$$

and

$$\mathbf{P} = \begin{bmatrix} 1 & 0 & \frac{\partial w}{\partial x_1} \\ 0 & 1 & \frac{\partial w}{\partial x_2} \\ \frac{\partial w}{\partial x_1} & \frac{\partial w}{\partial x_2} & 0 \end{bmatrix}. \tag{3.170}$$

As in the Mindlin-Reissner plate theory, the displacement field at any point within the plate can be formally expressed as:

$$\mathbf{u}(\mathbf{x},t) = \mathbf{u}_0(x_1,x_2,t) + x_3\phi(x_1,x_2,t), \quad \nabla_{\mathbf{n}}\mathbf{u} = \phi(x_1,x_2,t). \tag{3.171}$$

Starting from the assumption for the Kirchhoff-Love plate theory that the shear force is neglected, we have:

$$\mathbf{t} = (\mathbf{n}\cdot\mathbb{C}\cdot\mathbf{n})\cdot[\nabla_n\mathbf{u} + \nabla_S(\mathbf{u}\cdot\mathbf{n})] = \mathbf{0}. \tag{3.172}$$

Since $\mathbf{n}\cdot\mathbb{C}\cdot\mathbf{n}$ is positive definite and invertible, the equation above holds if and only if:

$$\nabla_{\mathbf{n}}\mathbf{u} + \nabla_S(\mathbf{u}\cdot\mathbf{n}) = \mathbf{0}. \tag{3.173}$$

By combining equations (3.168) and (3.171), and accounting for the definition of ∇_S, the ex-

pression for $\nabla_S(\mathbf{u}\cdot\mathbf{n})$ in this case is given as:

$$\nabla_S(\mathbf{u}\cdot\mathbf{n}) = \begin{Bmatrix} \frac{\partial w}{\partial x_1} \\ \frac{\partial w}{\partial x_2} \\ 0 \end{Bmatrix}. \tag{3.174}$$

It can be reduced from equation (3.173) that

$$\begin{Bmatrix} \phi_1(x_1,x_2,t) \\ \phi_2(x_1,x_2,t) \\ 0 \end{Bmatrix} = -\begin{Bmatrix} \frac{\partial w}{\partial x_1} \\ \frac{\partial w}{\partial x_2} \\ 0 \end{Bmatrix}. \tag{3.175}$$

Consequently, the displacement field at any point within the plate is given by:

$$\mathbf{u}(\mathbf{x},t) = \mathbf{u}_0(x_1,x_2,t) - x_3 \begin{Bmatrix} \frac{\partial w}{\partial x_1} \\ \frac{\partial w}{\partial x_2} \\ 0 \end{Bmatrix}. \tag{3.176}$$

Substituting equation (3.176) into equation (3.18) yields the explicit expression of the strain tensor $\boldsymbol{\varepsilon}_s$:

$$\boldsymbol{\varepsilon}_s = \begin{bmatrix} \frac{\partial u_0}{\partial x_1} & \frac{1}{2}(\frac{\partial u_0}{\partial x_2} + \frac{\partial v_0}{\partial x_1}) & 0 \\ \frac{1}{2}(\frac{\partial u_0}{\partial x_2} + \frac{\partial v_0}{\partial x_1}) & \frac{\partial v_0}{\partial x_2} & 0 \\ 0 & 0 & 0 \end{bmatrix}. \tag{3.177}$$

Similarly, substituting equation (3.176) into equation (3.27) yields the explicit expression for the curvature tensor $\boldsymbol{\kappa}$:

$$\boldsymbol{\kappa} = -\begin{bmatrix} \frac{\partial^2 w}{\partial x_1^2} & \frac{\partial^2 w}{\partial x_1 x_2} & 0 \\ \frac{\partial^2 w}{\partial x_1 x_2} & \frac{\partial^2 w}{\partial x_2^2} & 0 \\ 0 & 0 & 0 \end{bmatrix}. \tag{3.178}$$

3.5.3 Transversely Isotropic Material

For a plate with transversely isotropic maretial, the in-plane stress resultants $\mathbf{N}_s$ and moment resultants $\mathbf{M}$ are determined by substituting the transverse isotropic operators (2.144)-(2.151)

into equations (3.141)-(3.142). The explicit expressions for $\mathbf{N}_s$ and $\mathbf{M}$ are:

$$\mathbf{N}_s = \int_{-\frac{h}{2}}^{\frac{h}{2}} \left\{ \left(C_{12} - \frac{C_{13}^2}{C_{33}} \right) tr(\varepsilon_s)\mathbf{P} + (C_{11} - C_{12})\varepsilon_s \right\} dx_3, \tag{3.179}$$

$$\mathbf{M} = \int_{-\frac{h}{2}}^{\frac{h}{2}} \left\{ x_3^2 \left[\left(C_{12} - \frac{C_{13}^2}{C_{33}} \right) \mathrm{tr}(\kappa)\mathbf{P} + (C_{11} - C_{12})\kappa \right] \right\} dx_3. \tag{3.180}$$

Using the expressions for ε_s and $\mathbf{P}$ provided in equations (3.170) and (3.177), the representation of $\mathbf{N}_s$ in the matrix form is

$$\mathbf{N}_s = h\left(C_{12} - \frac{C_{13}^2}{C_{33}} \right) \begin{bmatrix} \frac{\partial u_0}{\partial x_1} + \frac{\partial v_0}{\partial x_2} & 0 & 0 \\ 0 & \frac{\partial u_0}{\partial x_1} + \frac{\partial v_0}{\partial x_2} & 0 \\ 0 & 0 & 0 \end{bmatrix} + h(C_{11} - C_{12}) \begin{bmatrix} \frac{\partial u_0}{\partial x_1} & \frac{1}{2}\left(\frac{\partial u_0}{\partial x_2} + \frac{\partial v_0}{\partial x_1}\right) & 0 \\ \frac{1}{2}\left(\frac{\partial u_0}{\partial x_2} + \frac{\partial v_0}{\partial x_1}\right) & \frac{\partial v_0}{\partial x_2} & 0 \\ 0 & 0 & 0 \end{bmatrix}.$$

According to the fundamental assumption of the Kirchhoff-Love plate theory, in which the thickness of the plate is considered unchanged during deformation, the modulus C_{33} is considered significantly large. This implies that C_{13}^2/C_{33} approaches zero, simplifying the expression for $\mathbf{N}_s$ reduces to:

$$\mathbf{N}_s = h \begin{bmatrix} C_{11}\frac{\partial u_0}{\partial x_1} + C_{12}\frac{\partial v_0}{\partial x_2} & \frac{(C_{11}-C_{12})}{2}\left(\frac{\partial u_0}{\partial x_2} + \frac{\partial v_0}{\partial x_1}\right) & 0 \\ \frac{(C_{11}-C_{12})}{2}\left(\frac{\partial u_0}{\partial x_2} + \frac{\partial v_0}{\partial x_1}\right) & C_{12}\frac{\partial u_0}{\partial x_1} + C_{11}\frac{\partial v_0}{\partial x_2} & 0 \\ 0 & 0 & 0 \end{bmatrix}. \tag{3.181}$$

By substituting the expressions for κ and $\mathbf{P}$ provided in (3.170) and (3.178)) into equation (3.180), the matrix representation of the moment tensor $\mathbf{M}$ is given by:

$$\mathbf{M} = \frac{h^3}{24}\left(C_{12} - \frac{C_{13}^2}{C_{33}} \right) \begin{bmatrix} -\frac{\partial^2 w}{\partial x_1^2} - \frac{\partial^2 w}{\partial x_2^2} & 0 & 0 \\ 0 & -\frac{\partial^2 w}{\partial x_1^2} - \frac{\partial^2 w}{\partial x_2^2} & 0 \\ 0 & 0 & 0 \end{bmatrix} + \frac{h^3}{24}(C_{11} - C_{12}) \begin{bmatrix} -\frac{\partial^2 w}{\partial x_1^2} & -\frac{\partial^2 w}{\partial x_1 \partial x_2} & 0 \\ -\frac{\partial^2 w}{\partial x_1 \partial x_2} & -\frac{\partial^2 w}{\partial x_2^2} & 0 \\ 0 & 0 & 0 \end{bmatrix}.$$

As before, since C_{13}^2/C_{33} approaches zero, $\mathbf{M}$ takes the following simple form:

$$\mathbf{M} = -\frac{h^2}{24} \begin{bmatrix} C_{11}\frac{\partial^2 w}{\partial x_1^2} + C_{12}\frac{\partial^2 w}{\partial x_2^2} & (C_{11} - C_{12})\frac{\partial^2 w}{\partial x_1 \partial x_2} & 0 \\ (C_{11} - C_{12})\frac{\partial^2 w}{\partial x_1 \partial x_2} & C_{12}\frac{\partial^2 w}{\partial x_1^2} + C_{11}\frac{\partial^2 w}{\partial x_2^2} & 0 \\ 0 & 0 & 0 \end{bmatrix}. \tag{3.182}$$

3.5.4 Isotropic Material

For an isotropic plate, the in-plane stress resultants $\mathbf{N}_s$ and moment resultants $\mathbf{M}$ can be determined by applying the isotropy operators (2.153)-(2.157) to equations (3.141)-(3.142). This yields:

$$\mathbf{N}_s = \frac{\partial E}{\partial \varepsilon_s} = \int_{-\frac{h}{2}}^{\frac{h}{2}} \left\{ \frac{2\mu\lambda}{\lambda+2\mu} tr(\varepsilon_s)\mathbf{P} + 2\mu\varepsilon_s \right\} dx_3, \tag{3.183}$$

$$\mathbf{M} = \frac{\partial E}{\partial \kappa} = \int_{-\frac{h}{2}}^{\frac{h}{2}} x_3^2 \left(\frac{2\mu\lambda}{\lambda+2\mu} \mathrm{tr}(\kappa)\mathbf{P} + 2\mu\kappa \right) dx_3. \tag{3.184}$$

By substituting equations (3.170) and (3.177) into equation (3.183), we can express $\mathbf{N}_s$ in the following matrix form:

$$\mathbf{N}_s = \frac{2h\mu\lambda}{\lambda+2\mu} \begin{bmatrix} \frac{\partial u_0}{\partial x_1} + \frac{\partial v_0}{\partial x_2} & 0 & 0 \\ 0 & \frac{\partial u_0}{\partial x_1} + \frac{\partial v_0}{\partial x_2} & 0 \\ 0 & 0 & 0 \end{bmatrix} + 2h\mu \begin{bmatrix} \frac{\partial u_0}{\partial x_1} & \frac{1}{2}\left(\frac{\partial u_0}{\partial x_2} + \frac{\partial v_0}{\partial x_1}\right) & 0 \\ \frac{1}{2}\left(\frac{\partial u_0}{\partial x_2} + \frac{\partial v_0}{\partial x_1}\right) & \frac{\partial v_0}{\partial x_2} & 0 \\ 0 & 0 & 0 \end{bmatrix}, \tag{3.185}$$

or equivalently,

$$\mathbf{N}_s = \frac{hE}{1-\nu^2} \begin{bmatrix} \frac{\partial u_0}{\partial x_1} + \nu\frac{\partial v_0}{\partial x_2} & \frac{(1-\nu)}{2}\left(\frac{\partial u_0}{\partial x_2} + \frac{\partial v_0}{\partial x_1}\right) & 0 \\ \frac{(1-\nu)}{2}\left(\frac{\partial u_0}{\partial x_2} + \frac{\partial v_0}{\partial x_1}\right) & \nu\frac{\partial u_0}{\partial x_1} + \frac{\partial v_0}{\partial x_2} & 0 \\ 0 & 0 & 0 \end{bmatrix}. \tag{3.186}$$

The moment tensor $\mathbf{M}$, determined by substituting equations (3.170) and (3.178) into equation (3.184), is given by:

$$\mathbf{M} = \frac{h^3\mu\lambda}{6(\lambda+2\mu)} \begin{bmatrix} -\frac{\partial^2 w}{\partial x_1^2} - \frac{\partial^2 w}{\partial x_2^2} & 0 & 0 \\ 0 & -\frac{\partial^2 w}{\partial x_1^2} - \frac{\partial^2 w}{\partial x_2^2} & 0 \\ 0 & 0 & 0 \end{bmatrix} + \frac{h^3\mu}{6} \begin{bmatrix} -\frac{\partial^2 w}{\partial x_1^2} & -\frac{\partial^2 w}{\partial x_1 \partial x_2} & 0 \\ -\frac{\partial^2 w}{\partial x_1 \partial x_2} & -\frac{\partial^2 w}{\partial x_2^2} & 0 \\ 0 & 0 & 0 \end{bmatrix} \tag{3.187}$$

or equivalently,

$$\mathbf{M} = \frac{h^3 E}{12(1-\nu^2)} \begin{bmatrix} -\frac{\partial^2 w}{\partial x_1^2} - \nu\frac{\partial^2 w}{\partial x_2^2} & -(1-\nu)\frac{\partial^2 w}{\partial x_1 \partial x_2} & 0 \\ -(1-\nu)\frac{\partial^2 w}{\partial x_1 \partial x_2} & -\nu\frac{\partial^2 w}{\partial x_1^2} - \frac{\partial^2 w}{\partial x_2^2} & 0 \\ 0 & 0 & 0 \end{bmatrix}. \tag{3.188}$$

3.5.5 Bernoulli Beam Theory

When the field in the x_2 direction vanishes and the fields in the x_1-direction and x_3-direction are independent of x_2, the Kirchhoff-Love plate reduces to a Bernoulli beam. For a beam with uniform thickness h and length L, the coordinates at any point $\mathbf{x}$ simplify to $\mathbf{x} \in \mathbb{R}^2$. Consistent with the Kirchhoff-Love plate, the coordinate system (x_1, x_3) is adopted, with x_1 aligned with the beam's centerline and x_3- positive downward (see **Fig.** 3.5). The displacement field governing the beam's time-dependent midline deformations is:

$$\mathbf{u}_0(\mathbf{x},t) = \begin{Bmatrix} u_0(x_1,t) \\ w(x_1,t) \end{Bmatrix}. \tag{3.189}$$

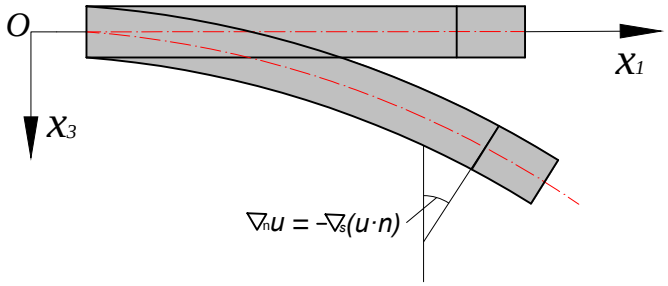

Figure 3.5: *The deformed configuration of a Bernoulli beam.*

The deformed midline curve of the beam is described by:

$$\Gamma = \{\mathbf{x} \in \mathbb{R}^2 \mid g(\mathbf{x}) = x_3 - w = 0\}. \tag{3.190}$$

The normal vector perpendicular to the deformed midline curve of the beam is given by:

$$\mathbf{n} = \begin{Bmatrix} n_1 \\ n_3 \end{Bmatrix} = \begin{Bmatrix} -\frac{\partial w}{\partial x_1} \\ 1 \end{Bmatrix}. \tag{3.191}$$

The complementary orthogonal projection operators $\mathbf{P}^{\perp}$ and $\mathbf{P}$ are

$$\mathbf{P}^{\perp} = \begin{bmatrix} 0 & -\frac{\partial w}{\partial x_1} \\ -\frac{\partial w}{\partial x_1} & 1 \end{bmatrix}, \tag{3.192}$$

and

$$\mathbf{P} = \begin{bmatrix} 1 & \frac{\partial w}{\partial x_1} \\ \frac{\partial w}{\partial x_1} & 0 \end{bmatrix}. \tag{3.193}$$

Therefore, the displacement is reduced to the following form:

$$\mathbf{u}(\mathbf{x},t) = \mathbf{u}_0(x_1,t) - x_3 \begin{Bmatrix} \frac{\partial w}{\partial x_1} \\ 0 \end{Bmatrix}. \tag{3.194}$$

The expressions for ε_s and κ can be determined as follows:

$$\varepsilon_s = \begin{bmatrix} \frac{\partial u_0}{\partial x_1} & 0 \\ 0 & 0 \end{bmatrix}, \tag{3.195}$$

$$\kappa = \begin{bmatrix} -\frac{\partial^2 w}{\partial x_1^2} & 0 \\ 0 & 0 \end{bmatrix}. \tag{3.196}$$

Assuming that the material of the beam is homogeneous and isotropic, the axial force N_s and bending moment M can be determined as follows:

$$N_s = \frac{Eh}{1-\nu^2}\frac{\partial u_0}{\partial x_1}, \tag{3.197}$$

$$M = -\frac{Eh^3}{12(1-\nu^2)}\frac{\partial^2 w}{\partial x_1^2}. \tag{3.198}$$

The equations of motion reduce to:

$$\frac{Eh}{1-\nu^2}\frac{\partial^2 u_0}{\partial x_1^2} + f_s = \rho h \frac{\partial^2 u_0}{\partial t^2}, \tag{3.199a}$$

$$\frac{Eh^3}{12(1-\nu^2)}\frac{\partial^4 w}{\partial x_1^4} - f_{x_3} = \frac{\rho h^2}{12}\frac{\partial^4 w}{\partial x_1^2 \partial t^2} - \frac{\partial^2 w}{\partial t^2}, \tag{3.199b}$$

for any $x_1 \in (0,L)$ and $t \in (0,T)$. Correspondingly, the boundary conditions are given by:

$$N_s = \bar{N}_s \quad \text{or} \quad u_0 = \bar{u}_0 \quad \text{at} \quad x_1 = 0 \quad \text{and} \quad x_1 = L, \tag{3.200a}$$

$$M = \bar{M} \quad \text{or} \quad w = \bar{w} \quad \text{at} \quad x_1 = 0 \quad \text{and} \quad x_1 = L. \tag{3.200b}$$

This formulation constitutes a boundary-initial value problem for determining u_0, w, governed by the system of differential equations in equations (3.199a-b) and the boundary conditions in equations (3.200a-b), with initial conditions at $t = 0$ and $t = T$. This establishes a non-classical Bernoulli-Euler beam model. Unlike the classical Bernoulli-Euler beam theory, the equations of motion in (3.199a-b) explicitly incorporate the Poisson effect. While this effect is often negligible for slender beams with significant aspect ratios (by setting $\nu = 0$), it becomes crucial for non-slender beams or materials with pronounced Poisson effects to ensure accurate results. Ignoring the Poisson effect reduces the model to the classical Bernoulli-Euler beam. Neglecting axial effects ($\nu = 0$) simplifies equations (3.199a) and boundary conditions (3.200a) to the classical model in Timoshenko [129]. For time-independent fields ($w = w(x_1)$), the model reduces to the quasistatic Bernoulli-Euler beam in Timoshenko [129].

3.6 Conclusion

Based on the theoretical frameworks established in Chapters 1 and 2, a comprehensive theoretical model for the strain energy of plate-shell structures has been developed. Employing a Taylor series expansion of displacements, a general strain energy expression in terms of mid-surface deformation metrics was derived. This enabled the introduction of a strain energy density function and subsequent derivation of conjugate stress measures. A variational approach systematically yielded the dynamic governing equations and boundary conditions for plate-shell structures.

The model was extended to scenarios neglecting coupling effects, leading to detailed formulations for corresponding stress measures, governing equations, and boundary conditions. For flat plates undergoing small deflections and rotations, the framework reduces to the well-known Mindlin plate and Timoshenko beam theories. Further simplification by neglecting both coupling and shear effects aligns the model with Kirchhoff plate and Bernoulli-Euler beam theories.

The framework accommodates anisotropic materials, as demonstrated by explicit formulations for transversely isotropic and isotropic cases. This expands the model's applicability to a wider range of structural materials.

The presented work provides a robust formulation for the analysis and design of advanced plate-shell structures. Accurate modeling and prediction of these structures under diverse load-

ing conditions are crucial for aerospace, civil, and mechanical engineering. The ability to accommodate complex material behaviors and structural configurations opens new avenues for efficient and resilient structural system development. This study offers valuable insights and tools for engineers and researchers at the forefront of structural analysis and design.

Chapter 4

Comparative Study of Homogenization Techniques Using Projection Operators for Laminated Plates

Laminated plates, renowned for their exceptional mechanical properties and high strength-to-weight ratio, are widely used across industries. These composites comprise multiple bonded layers, each typically homogeneous, contributing distinct mechanical properties. A characteristic feature of laminated plates is the zigzag (ZZ) displacement field, exhibiting abrupt slope changes at layer interfaces. This chapter introduces generalized zigzag theories, higher-order plate theories capturing transverse shear deformation and the zigzag phenomenon in laminated plate thickness.

Given the correspondence of the zigzag displacement effect with Hadamard's relation introduced in Chapter 1, and utilizing the operator introduced in Chapter 2, we have developed a homogenization method. This method ensures the continuity of transverse stresses at each layer interface. Additionally, analytical expressions are provided for the effective elastic tensor of transversely isotropic laminated plates.

The chapter further derives the 3D exact (H-Exact) and Kirchhoff plate (HK-LPT) solutions for the homogenized laminate. A comparative analysis of Zig-Zag, H-Exact, Classical Laminated Plate Theory (CPT), and HK-LPT methods for layered media is presented.

4.1 An Overview of Zigzag Theory in Analysis of Laminated Plates

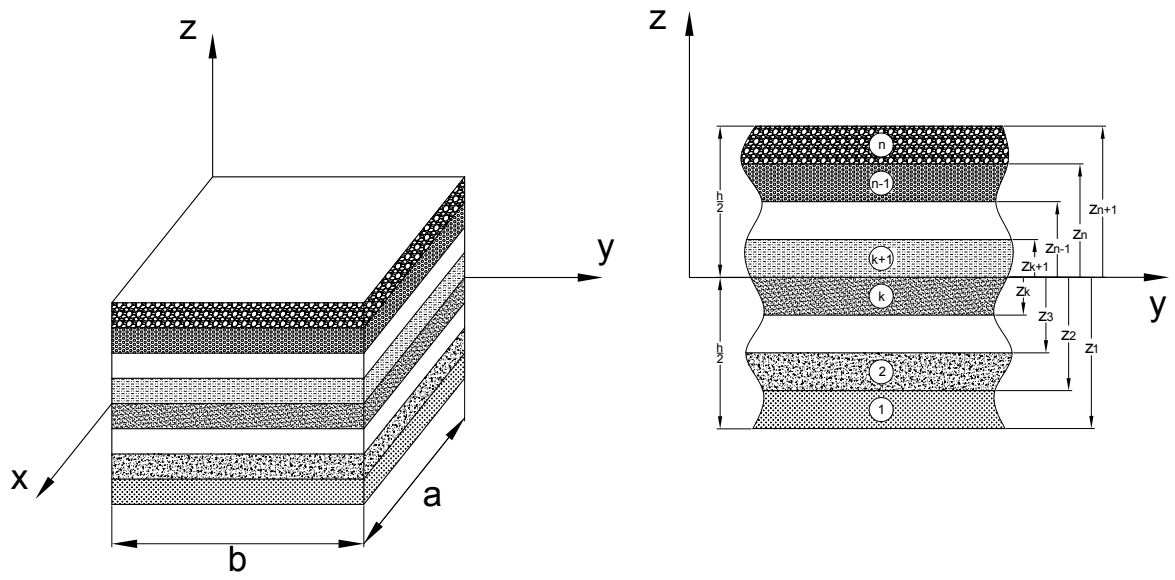

Figure 4.1: *Geometry and coordinate system of a laminate plate with n layers.*

Consider a laminated composite plate consisting of n parallel plane layers which, individually made of linearly elastic homogeneous materials, are perfectly bonded together. Let us introduce a system of Cartesian coordinates (x,y,z) such that the coordinates x and y are parallel to plane layers while the coordinate z is perpendicular to them (see **Fig.** 4.1). In particular, the bottom and top surfaces of the k-th layer with $1 \leq k \leq n$ are the corresponding coordinates z_k and z_{k+1} along the z-direction.

Let $\mathbf{u}^k$ denote the displacement vector defined within the k-th layer. According to the generalized zigzag theory of laminate plates [89, 92], the components (u^k, v^k, w^k) of $\mathbf{u}^k$ along the respective x, y and z axes are assumed to have the following expressions:

$$\begin{aligned} u^k(x,y,z) &= u_0^k(x,y) + u_1^k(x,y)z + u_2^k(x,y)z^2 + u_3^k(x,y)z^3 + u_4^k(x,y)z^4 + u_5^k(x,y)z^5 + \cdots, \\ v^k(x,y,z) &= v_0^k(x,y) + v_1^k(x,y)z + v_2^k(x,y)z^2 + v_3^k(x,y)z^3 + v_4^k(x,y)z^4 + v_5^k(x,y)z^5 + \cdots, \\ w^k(x,y,z) &= w_0(x,y). \end{aligned} \tag{4.1}$$

It is worth noting that in generalized zigzag theories, only zeroth- and first-order terms are considered in the expressions for the in-plane displacements. However, the displacement expres-

sions provided in the previous equations represent a more generalized theory, capable of incorporating higher-order terms depending on the chosen order of the zigzag theory. To clarify the derivation process, a third-order theory is chosen, extending the in-plane displacement up to the third order in z. Therefore, the displacement of the k-th layer can be expressed as:

$$\begin{aligned} u^k(x,y,z) &= u_0^k(x,y) + u_1^k(x,y)z + u_2^k(x,y)z^2 + u_3^k(x,y)z^3, \\ v^k(x,y,z) &= v_0^k(x,y) + v_1^k(x,y)z + v_2^k(x,y)z^2 + v_3^k(x,y)z^3, \\ w^k(x,y,z) &= w_0(x,y). \end{aligned} \tag{4.2}$$

The strain distribution within each layer, which is related to the displacement field, can be described by the following equation:

$$\varepsilon^k = \frac{1}{2}[\nabla \mathbf{u}^k + (\nabla \mathbf{u}^k)^T], \tag{4.3}$$

where ε^k represents the strain tensor in layer k, and the symbol ∇ denotes the gradient operator. The constitutive equation governing the behavior of the k-th layer orthotropic material is expressed in matrix form as:

$$\begin{Bmatrix} \sigma_x^k \\ \sigma_y^k \\ \sigma_z^k \\ \tau_{yz}^k \\ \tau_{xz}^k \\ \tau_{xy}^k \end{Bmatrix} = \begin{bmatrix} C_{11}^k & C_{12}^k & C_{13}^k & 0 & 0 & 0 \\ C_{12}^k & C_{22}^k & C_{23}^k & 0 & 0 & 0 \\ C_{13}^k & C_{23}^k & C_{33}^k & 0 & 0 & 0 \\ 0 & 0 & 0 & C_{44}^k & 0 & 0 \\ 0 & 0 & 0 & 0 & C_{55}^k & 0 \\ 0 & 0 & 0 & 0 & 0 & C_{66}^k \end{bmatrix} \begin{Bmatrix} \varepsilon_x^k \\ \varepsilon_y^k \\ \varepsilon_z^k \\ \gamma_{yz}^k \\ \gamma_{xz}^k \\ \gamma_{xy}^k \end{Bmatrix}. \tag{4.4}$$

Given the perfect bonding between layers in laminated plates, the continuity of in-plane displacement and transverse stress fields at the interface between adjacent layers is ensured. This continuity is mathematically expressed as follows:

$$\begin{aligned} &u^{k-1}\,|_{z=z_k} = u^k\,|_{z=z_k}, \quad v^{k-1}\,|_{z=z_k} = v^k\,|_{z=z_k}, \\ &\tau_{xz}^{k-1}\,|_{z=z_k} = \tau_{xz}^k\,|_{z=z_k}, \quad \tau_{yz}^{k-1}\,|_{z=z_k} = \tau_{yz}^k\,|_{z=z_k}, \quad (k = 2,3,\cdots,n). \end{aligned} \tag{4.5}$$

At the bottom ($z = z_1$) and top ($z = z_{n+1}$) surfaces of the laminate, the transverse shear stresses

τ_{xz} and τ_{yz} satisfy free shear traction conditions, which are expressed as follows:

$$\tau_{xz}^{1}(z_1) = 0, \quad \tau_{xz}^{n}(z_{n+1}) = 0, \quad \tau_{yz}^{1}(z_1) = 0, \quad \tau_{yz}^{n}(z_{n+1}) = 0. \tag{4.6}$$

In the framework of the generalized zigzag theory, the number of unknown variables increase proportionally with the number of layers in the laminate plate, depending on the assumed displacement. For instance, if we consider the displacement pattern described by equation (4.2), the total number of unknown variables for an n-layer laminated plate is given by 4n+5. However, it's essential to note that these 4n+5 unknown variables are not independent.The displacement is constrained by the necessity to satisfy 4(n-1) prescribed continuity conditions (i.e., equation (4.5)) and 4 specified free shear traction conditions (i.e., equation (4.6)), thereby resulting in a reduction of the total number of unknown variables to 5. Substituting equations (4.2), (4.3), and (4.4) into equations (4.5) and (4.6) yields the following set of equations:

$$\begin{aligned}
u_0^k &= u_0^1 + F_0^k u_1^1 + G_0^k w_{0,x}, \\
u_1^k &= F_1^k u_1^1 + G_1^k w_{0,x}, \\
u_2^k &= F_2^k u_1^1 + G_2^k w_{0,x}, \\
u_3^k &= F_3^k u_1^1 + G_3^k w_{0,x}, \\
v_0^k &= v_0^1 + H_0^k v_1^1 + I_0^k w_{0,y}, \\
v_1^k &= H_1^k v_1^1 + I_1^k w_{0,y}, \\
v_2^k &= H_2^k v_1^1 + I_2^k w_{0,y}, \\
v_3^k &= H_3^k v_1^1 + I_3^k w_{0,y}.
\end{aligned} \tag{4.7}$$

These equations demonstrate that the unknown variables in the assumed displacement (4.2) can be expressed in terms of five independent variables: u_0^1, u_1^1, v_0^1, v_1^1, and w_0. To facilitate subsequent discussions, we substitute u_0, u_1, v_0, v_1, and w_0 as the replacements for these five indepen-

dent variables. By introducing the following coefficients defined by

$$
\begin{aligned}
F_2 &= \frac{\alpha_3^n - 3\alpha_1^n z_1^2 + 3z_{n+1}^2}{-2\alpha_3^n z_1 + 3\alpha_2^n z_1^2 + 6z_1 z_{n+1}(z_1 - z_{n+1})},\\
G_2 &= \frac{\alpha_3^n - 3(1+\alpha_4^n) z_1^2 + 3z_{n+1}^2}{-2\alpha_3^n z_1 + 3\alpha_2^n z_1^2 + 6z_1 z_{n+1}(z_1 - z_{n+1})},\\
H_2 &= \frac{\beta_3^n - 3\beta_1^n z_1^2 + 3z_{n+1}^2}{-2\beta_3^n z_1 + 3\beta_2^n z_1^2 + 6z_1 z_{n+1}(z_1 - z_{n+1})},\\
I_2 &= \frac{\beta_3^n - 3(1+\beta_4^n) z_1^2 + 3z_{n+1}^2}{-2\beta_3^n z_1 + 3\beta_2^n z_1^2 + 6z_1 z_{n+1}(z_1 - z_{n+1})},\\
F_3 &= \frac{-\alpha_2^n + 2\alpha_1^n z_1 - 2z_{n+1}}{-2\alpha_3^n z_1 + 3\alpha_2^n z_1^2 + 6z_1 z_{n+1}(z_1 - z_{n+1})},\\
G_3 &= \frac{-\alpha_2^n + 2(z_1 + \alpha_4^n z_1 - z_{n+1})}{-2\alpha_3^n z_1 + 3\alpha_2^n z_1^2 + 6z_1 z_{n+1}(z_1 - z_{n+1})},\\
H_3 &= \frac{-\beta_2^n + 2\beta_1^n z_1 - 2z_{n+1}}{-2\beta_3^n z_1 + 3\beta_2^n z_1^2 + 6z_1 z_{n+1}(z_1 - z_{n+1})},\\
I_3 &= \frac{-\beta_2^n + 2(z_1 + \beta_4^n z_1 - z_{n+1})}{-2\beta_3^n z_1 + 3\beta_2^n z_1^2 + 6z_1 z_{n+1}(z_1 - z_{n+1})},
\end{aligned}
\tag{4.8}
$$

all coefficients in equation (4.7) are determined by laminate properties and coordinates as follows:

$$
\begin{aligned}
F_1^k &= \alpha_1^k + F_2\alpha_2^k + F_3\alpha_3^k,\\
G_1^k &= \alpha_4^k + G_2\alpha_2^k + G_3\alpha_3^k,\\
H_1^k &= \beta_1^k + H_2\beta_2^k + H_3\beta_3^k,\\
I_1^k &= \beta_4^k + I_2\beta_2^k + I_3\beta_3^k,\\
F_0^k &= \sum_{j=2}^{k} (F_1^{j-1} - F_1^j) z_j,\\
G_0^k &= \sum_{j=2}^{k} (G_1^{j-1} - G_1^j) z_j,\\
H_0^k &= \sum_{j=2}^{k} (H_1^{j-1} - H_1^j) z_j,\\
I_0^k &= \sum_{j=2}^{k} (I_1^{j-1} - I_1^j) z_j, \quad (k = 2,3,\cdots,n)
\end{aligned}
\tag{4.9}
$$

where α_i and β_i (i=1,2,3,4) can be calculated as follows:

$$\begin{aligned}
&\alpha_1^k = \tfrac{C_{55}^1}{C_{55}^k}, && \beta_1^k = \tfrac{C_{44}^1}{C_{44}^k},\\
&\alpha_2^k = \tfrac{2}{C_{55}^k}\textstyle\sum_{j=2}^{k}(C_{55}^{j-1} - 2C_{55}^{j-2} + C_{55}^{j})z_j, && \beta_2^k = \tfrac{2}{C_{44}^k}\textstyle\sum_{j=2}^{k}(C_{44}^{j-1} - 2C_{44}^{j-2} + C_{44}^{j})z_j,\\
&\alpha_3^k = \tfrac{3}{C_{55}^k}\textstyle\sum_{j=2}^{k}(C_{55}^{j-1} - 2C_{55}^{j-2} + C_{55}^{j})z_j^2, && \beta_3^k = \tfrac{3}{C_{44}^k}\textstyle\sum_{j=2}^{k}(C_{44}^{j-1} - 2C_{44}^{j-2} + C_{44}^{j})z_j^2,\\
&\alpha_4^k = \alpha_1^k - 1, && \beta_4^k = \beta_1^k - 1, \quad (k = 2,3,\cdots,n).
\end{aligned} \tag{4.10}$$

By examining equations (4.8) and (4.9), it becomes evident that the coefficients present in equation (4.7) are exclusively governed by the specific material properties and thickness of each layer in the laminated plate. Once these five independent unknown variables, as presented in equation (4.7), are determined, the displacements of individual layers within the laminate can be computed, thereby yielding the overall displacement of the laminated plate. To formulate the equilibrium equations governing these five independent variables and their corresponding boundary conditions, we utilize the principle of virtual work, which is expressed as follows:

$$\begin{aligned}
&\int_{-h/2}^{h/2}\int_{\Omega}(\sigma_x\delta\varepsilon_x + \sigma_y\delta\varepsilon_y + \sigma_z\delta\varepsilon_z + 2\tau_{xy}\delta\gamma_{xy} + 2\tau_{yz}\delta\gamma_{yz} + 2\tau_{xz}\delta\gamma_{xz})dAdz - \int_{\Omega}(q_{zz}\delta w)dA \qquad (4.11)\\
&= \int_{\Omega}[\sum_{k=1}^{n}\int_{z_k}^{z_{k+1}}(\sigma_x^k\delta\varepsilon_x^k + \sigma_y^k\delta\varepsilon_y + \sigma_z^k\delta\varepsilon_z^k + 2\tau_{xy}^k\delta\gamma_{xy}^k + 2\tau_{yz}^k\delta\gamma_{yz}^k + 2\tau_{xz}^k\delta\gamma_{xz}^k)dz - q_{zz}\delta w]dA = 0.
\end{aligned}$$

Substituting equations (4.7) into equation (4.11) and and considering the arbitrariness of the independent variables u_0, u_1, v_0, v_1, and w_0, the following equilibrium equations are obtained:

$$\begin{aligned}
\delta u_0: &\quad \frac{\partial N_x}{\partial x} + \frac{\partial N_{xy}}{\partial y} = 0,\\
\delta v_0: &\quad \frac{\partial N_{xy}}{\partial x} + \frac{\partial N_y}{\partial y} = 0,\\
\delta w_0: &\quad \frac{\partial^2 M_x}{\partial x^2} + 2\frac{\partial^2 M_{xy}}{\partial x\partial y} + \frac{\partial^2 M_y}{\partial y^2} + \frac{\partial R_{xz}}{\partial x} + \frac{\partial R_{yz}}{\partial y} + q_{zz} = 0,\\
\delta u_1: &\quad \frac{\partial P_x}{\partial x} + \frac{\partial P_{xy1}}{\partial y} + R_x = 0,\\
\delta v_1: &\quad \frac{\partial P_{xy2}}{\partial x} + \frac{\partial P_y}{\partial y} + R_y = 0,
\end{aligned} \tag{4.12}$$

with the corresponding boundary conditions related on:

$$
\begin{aligned}
&u_0 \quad or \quad N_x n_x + N_{xy} n_y, \\
&v_0 \quad or \quad N_{xy} n_x + N_y n_y, \\
&w_0 \quad or \quad M_{x,x} n_x + M_{x,y} n_y + M_{x,y} n_x + M_{y,y} n_y + R_{xz} n_x + R_{yz} n_y, \\
&u_1 \quad or \quad P_x n_x + P_{xy1} n_y, \\
&v_1 \quad or \quad P_{xy2} n_x + P_y n_y.
\end{aligned}
\tag{4.13}
$$

The resulting forces and moments in equation (4.12) are expressed as follows:

$$
\begin{aligned}
&(N_x, N_y, N_{xy}) = (\sum_{k=1}^{n} \int_{z_k}^{z_{k+1}} \sigma_x^k dz, \sum_{k=1}^{n} \int_{z_k}^{z_{k+1}} \sigma_y^k dz, \sum_{k=1}^{n} \int_{z_k}^{z_{k+1}} \sigma_{xy}^k dz), \\
&M_x = \sum_{k=1}^{n} [\int_{z_k}^{z_{k+1}} (G_0^k + G_1^k z + G_2 z^2 + G_3 z^3) \sigma_x^k dz], \\
&M_y = \sum_{k=1}^{n} [\int_{z_k}^{z_{k+1}} (I_0^k + I_1^k z + I_2 z^2 + I_3 z^3) \sigma_y^k dz], \\
&M_{xy} = \sum_{k=1}^{n} [\int_{z_k}^{z_{k+1}} (I_0^k + G_0^k + (I_1^k + G_1^k) z + (I_2^k + G_2) z^2 + (I_3^k + G_3) z^3) \tau_{xy}^k dz], \\
&R_{xz} = \sum_{k=1}^{n} [\int_{z_k}^{z_{k+1}} (1 + G_1^k + 2G_2 z + 3G_3 z^2) \tau_{xz}^k dz], \\
&R_{yz} = \sum_{k=1}^{n} [\int_{z_k}^{z_{k+1}} (1 + I_1^k + 2I_2 z + 3I_3 z^2) \tau_{yz}^k dz], \\
&P_x = \sum_{k=1}^{n} [\int_{z_k}^{z_{k+1}} (F_0^k + F_1^k z + F_2 z^2 + F_3 z^3) \sigma_x^k dz], \\
&P_y = \sum_{k=1}^{n} [\int_{z_k}^{z_{k+1}} (H_0^k + H_1^k z + H_2 z^2 + H_3 z^3) \sigma_x^k dz], \\
&P_{xy1} = \sum_{k=1}^{n} [\int_{z_k}^{z_{k+1}} (F_0^k + F_1^k z + F_2 z^2 + F_3 z^3) \tau_{xy}^k dz], \\
&P_{xy2} = \sum_{k=1}^{n} [\int_{z_k}^{z_{k+1}} (H_0^k + H_1^k z + H_2 z^2 + H_3 z^3) \tau_{xy}^k dz], \\
&R_x = \sum_{k=1}^{n} [\int_{z_k}^{z_{k+1}} (F_1^k + 2F_2 z + 3F_3 z^2) \tau_{xz}^k dz], \\
&R_y = \sum_{k=1}^{n} [\int_{z_k}^{z_{k+1}} (H_1^k + 2H_2 z + 3H_3 z^2) \tau_{yz}^k dz].
\end{aligned}
\tag{4.14}
$$

The equilibrium equations and corresponding boundary conditions are crucial for laminate anal-

ysis. Solving these equations under specific boundary conditions determines the laminate's displacement and stress distributions, providing insights into its response to external loads.

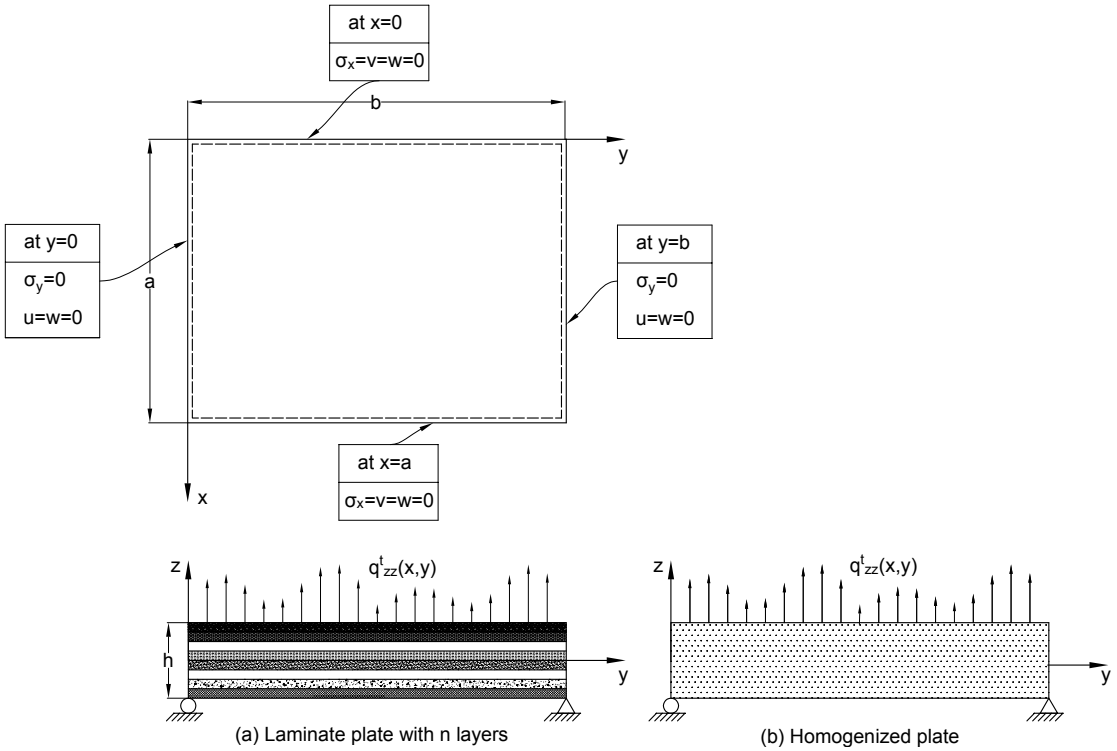

Figure 4.2: *Schematic illustration of simply supported boundary conditions for a laminate plate and homogenized rectangular plate under distributed load.*

Consider a rectangular laminate with orthogonal sides a and b, aligned with the x and y axes. The laminate is simply supported along all edges and subjected to a normal traction $q_{zz}(x,y)$ on its upper surface. The corresponding boundary conditions are:

$$\begin{aligned} &on\ x=0,\ a:\ v_0=w_0=N_x=M_x=0,\\ &on\ y=0,\ b:\ u_0=w_0=N_y=M_y=0. \end{aligned} \tag{4.15}$$

Under the prescribed boundary conditions, the solution of the governing differential equation (4.12) can be sought in the form of an infinite Fourier series, taking into account the orthogonal-

ity of the sine and cosine functions. The variables can be expressed as:

$$\begin{aligned} u_0 &= \sum_{n=1}^{\infty}\sum_{m=1}^{\infty} U_{mn}^{0}\ cospx\ sinqy \\ u_1 &= \sum_{n=1}^{\infty}\sum_{m=1}^{\infty} U_{mn}^{1}\ cospx\ sinqy \\ v_0 &= \sum_{n=1}^{\infty}\sum_{m=1}^{\infty} V_{mn}^{0}\ sinpx\ cosqy \\ v_1 &= \sum_{n=1}^{\infty}\sum_{m=1}^{\infty} V_{mn}^{1}\ sinpx\ cosqy \\ w_0 &= \sum_{n=1}^{\infty}\sum_{m=1}^{\infty} W_{mn}^{0} sinpx\ sinqy \end{aligned} \tag{4.16}$$

where p and q are determined by

$$p = \frac{n\pi}{a}, \tag{4.17}$$

$$q = \frac{m\pi}{b}. \tag{4.18}$$

The terms m and n represent the sequences of Fourier series utilized to expand the displacement functions. The sequence n corresponds to the Fourier series expansion in the x direction, while the sequence m corresponds to the Fourier series expansion in the y direction. In addition, the load can be expressed as a Fourier series:

$$q_{zz} = \sum_{n=1}^{\infty}\sum_{m=1}^{\infty} Q_{mn} sinpx\ sinqy, \tag{4.19}$$

where Q_{mn} are the coefficients determined by integrating the product of the load q_{zz} and the basis functions:

$$Q_{mn} = \frac{4}{ab}\int_0^b \int_0^a (q_{zz}\ sinpx\ sinqy) dxdy. \tag{4.20}$$

Substituting equations (4.16) and (4.19) into the equilibrium equation (4.12) yields a system of equations for the coefficients U_{mn}^{1}, V_{mn}^{0}, V_{mn}^{1}, and W_{mn}^{0} for each sequence m and n. Solving this system determines these coefficients, which define the displacement functions u_0, u_1, v_0, v_1, and w_0 for the given problem.

As evidenced by the preceding discussion, the Zigzag theory demonstrates flexibility and can accommodate various boundary conditions, making it suitable for a wide range of engineering applications. In addition, by increasing the order of the displacement polynomial (i.e., high-order Zigzag theories), as depicted in equation (4.1), these higher-order Zigzag theories demonstrate improved convergence towards the exact solutions for displacement and stress distributions. Consistent with the third-order Zigzag theory previously exhibited, the number of independent unknown variables in higher-order Zigzag theories is reduced by $4n$ compared to the assumed displacement variables, owing to continuity and free shear traction conditions. Additionally, the establishment of governing equations for independent unknown variables, accompanied by their respective boundary conditions, as well as the analytical framework for evaluating the response of laminated plates under specific boundary conditions, remains consistent with the third-order Zigzag theory presented previously.

However, escalating the order of the displacement polynomial significantly increases computational workload by expanding the degrees of freedom, especially in complex loading cases, which is crucial in practical engineering analyses employing higher-order Zigzag theory. As illustrated by equation (4.16), in complex loading cases, obtaining a closed-form solution of the displacement requires the Fourier expansion, which introduces numerous undetermined Fourier coefficients, leading to a significant increase in computational workload. On the other hand, as discussed in [92], the degree of convergence with the exact solution does not necessarily increase proportionally. This leads to limited practical applicability, particularly for the analysis of large and complex laminates. Striking a balance between accuracy and computational efficiency becomes crucial to ensure the feasibility and effectiveness of Zigzag theory in practical engineering analyses.

4.2 Homogenization of Laminated Plates

As previously discussed, the Zigzag effect and interfacial continuity conditions require the displacement function to satisfy C^0 continuity across the interfaces of the laminated composite. Moreover, the assumption of perfect bonding at the interface of laminates entails continuity of in-plane strain at the interface. Developing a comprehensive understanding of these effects is essential for designing and optimizing layered material systems that can attain desired me-

chanical and physical properties. Consequently, it is imperative to consider these effects while performing the equivalent homogenization of the laminate structure.

In accordance with the preceding discussion, each layer of the laminate is assumed to be composed of a material exhibiting linear elasticity, with the stress-strain relationship governed by Hooke's law as expressed in (2.66). In the absence of body forces, the stress tensor $\boldsymbol{\sigma}$ must satisfy the condition of being divergence-free, as provided in (2.70). In the process of homogenizing laminated plates, it is crucial to ensure the continuity of transverse stresses at the interfaces between distinct layers. Achieving this involves decomposing the second-order tensors $\boldsymbol{\varepsilon}$ and $\boldsymbol{\sigma}$ into their respective in-plane and transverse components. This decomposition process can be facilitated by introducing two extended orthogonal projection operators, $\mathbb{P}^{\perp}$ and $\mathbb{P}$, which project tensors onto the transverse and in-plane directions, respectively. The definitions and properties of these two projection operators are elaborated in detail in subsection (3.4), specifically in equations (2.79) through (2.84). Therefore, by employing the extended orthogonal projection operators $\mathbb{P}^{\perp}$ and $\mathbb{P}$, the strain tensor $\boldsymbol{\varepsilon}$ and stress tensor $\boldsymbol{\sigma}$ can be decomposed into their respective in-plane and transverse parts, as represented by:

$$\boldsymbol{\varepsilon} = \mathbb{P}^{\perp}\boldsymbol{\varepsilon} + \mathbb{P}\boldsymbol{\varepsilon}, \tag{4.21}$$

$$\boldsymbol{\sigma} = \mathbb{P}^{\perp}\boldsymbol{\sigma} + \mathbb{P}\boldsymbol{\sigma}. \tag{4.22}$$

By incorporating the above mentioned decompositions of stress and strain tensors into Hooke's law (2.66), and subsequently multiplying both sides by the projection tensor $\mathbb{P}^{\perp}$, the following expression is obtained:

$$\mathbb{P}^{\perp}\mathbb{C}\mathbb{P}^{\perp}\boldsymbol{\varepsilon} = \mathbb{P}^{\perp}\boldsymbol{\sigma} - \mathbb{P}^{\perp}\mathbb{C}\mathbb{P}\boldsymbol{\varepsilon}. \tag{4.23}$$

To simplify the aforementioned equation, we introduce the fourth-order tensor $\mathbb{B}$ as defined in (2.104). Recalling the properties of $\mathbb{B}$ provided in equation (2.105):

$$\mathbb{B}(\mathbb{P}^{\perp}\mathbb{C}\mathbb{P}^{\perp}) = (\mathbb{P}^{\perp}\mathbb{C}\mathbb{P}^{\perp})\mathbb{B} = \mathbb{P}^{\perp}, \quad \mathbb{B}\mathbb{P}^{\perp} = \mathbb{P}^{\perp}\mathbb{B} = \mathbb{B}. \tag{4.24}$$

These properties facilitate the simplification process by ensuring that $\mathbb{B}$ effectively interacts with the projections $\mathbb{P}^{\perp}$ and the material stiffness tensor $\mathbb{C}$. Therefore, we present them here once

again for clarity. Consequently, equation (4.23) can be transformed into a more concise form:

$$\boldsymbol{\varepsilon} = \mathbb{B}\boldsymbol{\sigma} + (\mathbb{I} - \mathbb{B}\mathbb{C})\mathbb{P}\boldsymbol{\varepsilon}. \tag{4.25}$$

Similarly, by introducing the previously mentioned decompositions of stress and strain tensors into equation (2.69) and following a similar procedure, we derive the relationship:

$$\boldsymbol{\sigma} = \mathbb{A}\boldsymbol{\varepsilon} + (\mathbb{I} - \mathbb{A}\mathbb{S})\mathbb{P}^{\perp}\boldsymbol{\sigma}, \tag{4.26}$$

where tensor $\mathbb{A}$ is defined in equation (2.99). In correspondence with equation (4.24), tensor $\mathbb{A}$ possesses the following properties:

$$\mathbb{A}(\mathbb{P}\mathbb{S}\mathbb{P}) = (\mathbb{P}\mathbb{S}\mathbb{P})\mathbb{A} = \mathbb{P}, \quad \mathbb{A}\mathbb{P} = \mathbb{P}\mathbb{A} = \mathbb{A}. \tag{4.27}$$

These properties facilitate the simplification process by ensuring that $\mathbb{A}$ effectively interacts with the projections $\mathbb{P}$ and the material compliance tensor $\mathbb{S}$. Additionally, the relationship between $\mathbb{A}$ and $\mathbb{B}$ can be established by using the following equations:

$$\mathbb{C}\mathbb{B} + \mathbb{A}\mathbb{S} = \mathbb{B}\mathbb{C} + \mathbb{S}\mathbb{A} = \mathbb{I}. \tag{4.28}$$

To further characterize the composite, we define the representative volume element (RVE) as a closed domain Ω of volume V, which encompasses the entire composite structure. The total thickness of the composite is denoted by h. Additionally, we define sub-domains $\Omega^{(k)}$, occupied by the kth-layered material, each characterized by volumes $V^{(k)}$ and thicknesses $h^{(k)}$. **Fig.** 4.1 illustrates the geometric configuration of the composite, with distinct layers and their corresponding sub-domains labeled. To enhance analytical clarity, we propose a redefinition of the coordinate system depicted in **Fig.** 4.1. Specifically, we employ a Cartesian coordinate framework featuring an orthonormal basis (e_1, e_2, e_3), where the unit vector perpendicular to all layers aligns with e_3 (i.e., $(x_1, x_2, x_3) \rightleftarrows (x, y, z)$). The individual thickness of each layer can be determined by evaluating the separation distance between the x_3-coordinates (i.e., z-coordinates) of adjacent interfaces. Specifically, the thickness of the kth-layer can be calculated using the

expression:

$$h^{(k)} = z_{k+1} - z_k. \tag{4.29}$$

Given that each layer has uniform thickness, the volume fraction f^k of the kth layer can be expressed as

$$f^{(k)} = \frac{h^{(k)}}{h}. \tag{4.30}$$

The constitutive equation governing the mechanical behavior of the kth-layer material is given by:

$$\boldsymbol{\sigma}^{(k)} = \mathbb{C}^{(k)}\boldsymbol{\varepsilon}^{(k)}, \tag{4.31}$$

where $\boldsymbol{\sigma}^{(k)}$ and $\boldsymbol{\varepsilon}^{(k)}$ denote the stress and strain tensors for the kth-layer material, respectively, with $\mathbb{C}^{(k)}$ representing the corresponding fourth-order elasticity tensor.

The assumption of perfect bonding between laminate layers ensures continuity. Additionally, we neglect end effects from the sides of the composite and consider uniform surface charges on the top and bottom surfaces. As a result, $\mathbb{P}^{\perp}\boldsymbol{\sigma}$ and $\mathbb{P}^{\parallel}\boldsymbol{\varepsilon}$ remain uniformly constant throughout all layers. More precisely,

$$\mathbb{P}^{\perp}\boldsymbol{\sigma}^{(1)} = \mathbb{P}^{\perp}\boldsymbol{\sigma}^{(2)} = \cdots = \mathbb{P}^{\perp}\boldsymbol{\sigma}^{(n)}, \quad \mathbb{P}\boldsymbol{\varepsilon}^{(1)} = \mathbb{P}\boldsymbol{\varepsilon}^{(2)} = \cdots = \mathbb{P}\boldsymbol{\varepsilon}^{(n)}. \tag{4.32}$$

We introduce the bracket notation $\langle\cdot\rangle$ and $\langle\cdot\rangle^{(k)}$ to denote the volume average of a quantity over the entire composite and kth-layer, respectively. The averages are defined as follows:

$$\langle\cdot\rangle = \frac{1}{V}\int_{\Omega}(\cdot)\mathrm{d}v, \quad \langle\cdot\rangle^{(k)} = \frac{1}{V^{(k)}}\int_{\Omega^{(k)}}(\cdot)^{(k)}\mathrm{d}v, \tag{4.33}$$

where $(\cdot)^{(k)}$ represents the value evaluated within the kth-layer. These notations are related by

$$\langle\cdot\rangle = \sum_{k=1}^{N} f^{(k)}\langle\cdot\rangle^{(k)}. \tag{4.34}$$

The macroscopic divergence-free fields $\boldsymbol{\sigma}^*$ and curl-free fields $\boldsymbol{\varepsilon}^*$ are defined as the volume averages of the microscopic quantities $\boldsymbol{\sigma}$ and $\boldsymbol{\varepsilon}$, respectively, as expressed by:

$$\boldsymbol{\sigma}^* = \langle\boldsymbol{\sigma}\rangle, \quad \boldsymbol{\varepsilon}^* = \langle\boldsymbol{\varepsilon}\rangle. \tag{4.35}$$

By substituting equations (4.25) and (4.26) into equation (4.35), and accounting for the continuity condition (4.32), we derive the following expressions:

$$\varepsilon^* = \langle \mathbb{S}\mathbb{A} \rangle \sigma^* + \langle \mathbb{B} \rangle \mathbb{P}^{\perp} \sigma^*, \tag{4.36}$$

$$\sigma^* = \langle \mathbb{A} \rangle \varepsilon^* + \langle \mathbb{C}\mathbb{B} \rangle \mathbb{P}^{\perp} \sigma^*. \tag{4.37}$$

Removing the term $\mathbf{P}^{\perp}\sigma^*$ from the expressions for σ^* and ε^*, as described above, yields the macroscopic constitutive relation:

$$\sigma^* = \mathbb{C}^* \varepsilon^*, \tag{4.38}$$

where the effective tensor $\mathbb{C}^*$ is defined as

$$\mathbb{C}^* = \langle \mathbb{C} - \mathbb{C}\mathbb{B}\mathbb{C} \rangle + \langle \mathbb{C}\mathbb{B} \rangle \langle \mathbb{P}^{\perp}\mathbb{C}\mathbb{P}^{\perp} \rangle \langle \mathbb{B}\mathbb{C} \rangle. \tag{4.39}$$

Once the parameters, including the number of laminated plate layers, their respective thicknesses, and the material properties of each layer, are determined, equation (4.39) can be utilized to compute the effective tensor $\mathbb{C}^*$ of the laminate. This equation provides a comprehensive framework for integrating these parameters into the calculation, thereby facilitating a thorough understanding of the process involved in determining the laminate's mechanical properties. Furthermore, the explicit matrix representation of $\mathbf{F}$, which is important in the homogenization process, can be derived utilizing the definitions outlined in equations (2.66) and (2.92). Specifically, we have:

$$\mathbf{F} = \begin{pmatrix} C_{i1j1}n_i n_j & C_{i1j2}n_i n_j & C_{i1j3}n_i n_j \\ C_{i2j1}n_i n_j & C_{i2j2}n_i n_j & C_{i2j3}n_i n_j \\ C_{i3j1}n_i n_j & C_{i3j2}n_i n_j & C_{i3j3}n_i n_j \end{pmatrix}^{-1}. \tag{4.40}$$

It is crucial to emphasize that when all layers exhibit transverse isotropy relative to the axis perpendicular to them, the expression for the fourth-order elastic tensor can be straightforwardly described by a specific mathematical formula, as shown in equation (2.141). Additionally, during the derivation of the effective modulus $\mathbb{C}^*$ for the homogenized material, important tensors such as $\mathbb{A}$, $\mathbb{B}$, and $\mathbf{F}$ are involved. Notably, in this case, these tensors possess explicit expressions, as presented in subsection (3.4). On this basis, the effective elasticity tensor $\mathbb{C}^*$ has a closed-form

expression.

Considering the expression (2.145) of tensor $\mathbf{F}$ as delineated in chapter 2.4, in conjunction with the definitions provided in equation (4.33) for the averages, we can formulate:

$$\langle \mathbf{F} \rangle = \left\langle \frac{1}{C_{44}} \right\rangle \left(\mathbf{I} - \left\langle \frac{C_{33} - C_{44}}{C_{33} C_{44}} \right\rangle \mathbf{P}^{\perp} \right). \tag{4.41}$$

By substituting the above equation into the method for inversion, as denoted by formula (2.143), the inverse of $\langle \mathbf{F} \rangle$ can be computed as follows:

$$\langle \mathbf{F} \rangle^{-1} = \frac{1}{\langle 1/C_{44} \rangle} \left(\mathbf{I} + \frac{\langle (C_{33} - C_{44})/(C_{33} C_{44}) \rangle}{\langle 1/C_{44} \rangle - \langle (C_{33} - C_{44})/(C_{33} C_{44}) \rangle} \mathbf{P}^{\perp} \right). \tag{4.42}$$

Considering the expression (2.147) of tensor $\mathbb{B}$ as delineated in subsection (3.4), the averages of $\mathbb{B}$ are given by:

$$\langle \mathbb{B} \rangle = \left\langle \frac{1}{2C_{44}} \right\rangle \left(\mathbb{P}^{\perp} - \left\langle \frac{C_{33} - 2C_{44}}{C_{33}} \right\rangle \mathbf{P}^{\perp} \otimes \mathbf{P}^{\perp} \right). \tag{4.43}$$

According to the properties provided by description (4.24) and the formula (2.143), the averages of $\mathbb{P}^{\perp} \mathbb{C} \mathbb{P}^{\perp}$ can be expressed as:

$$\langle \mathbb{P}^{\perp} \mathbb{C} \mathbb{P}^{\perp} \rangle = \frac{1}{\langle 1/(2C_{44}) \rangle} \left(\mathbb{P}^{\perp} + \frac{\langle (C_{33} - 2C_{44})/(2C_{33} C_{44}) \rangle}{1/\langle (2C_{44}) \rangle - \langle (C_{33} - 2C_{44})/(2C_{33} C_{44}) \rangle} \mathbf{P}^{\perp} \otimes \mathbf{P}^{\perp} \right). \tag{4.44}$$

According to equation (2.99) and (2.103), the average of tensor $\mathbb{C} - \mathbb{C}\mathbb{B}\mathbb{C}$, which appears in the computation of the effective elastic tensor $\mathbb{C}^*$, can be calculated as:

$$\langle \mathbb{C} - \mathbb{C}\mathbb{B}\mathbb{C} \rangle = \langle C_{11} - C_{12} \rangle \mathbb{P} + \left\langle \frac{C_{12} C_{33} - C_{13}^2}{C_{33}} \right\rangle \mathbf{P} \otimes \mathbf{P}. \tag{4.45}$$

Combining equations (2.141), (2.147), and (4.33), the averages of $\mathbb{B}\mathbb{C}$ and $\mathbb{C}\mathbb{B}$ can be computed as:

$$\langle \mathbb{C}\mathbb{B} \rangle = \mathbb{P}^{\perp} + \left\langle \frac{C_{13}}{C_{33}} \right\rangle \mathbf{P} \otimes \mathbf{P}^{\perp}, \tag{4.46}$$

$$\langle \mathbb{B}\mathbb{C} \rangle = \mathbb{P}^{\perp} + \left\langle \frac{C_{13}}{C_{33}} \right\rangle \mathbf{P}^{\perp} \otimes \mathbf{P}. \tag{4.47}$$

Therefore, the residual term in equation (4.39) for computing the effective elasticity tensor $\mathbb{C}^*$ can be calculated as:

$$\begin{aligned}\langle \mathbb{C}\mathbb{B} \rangle \langle \mathbb{P}^{\perp}\mathbb{C}\mathbb{P}^{\perp} \rangle \langle \mathbb{B}\mathbb{C} \rangle =& \frac{1}{\langle 1/(2C_{44}) \rangle} \left[\mathbb{P}^{\perp} + \frac{\langle (C_{33} - 2C_{44})/(2C_{33}C_{44}) \rangle}{1/\langle (2C_{44}) \rangle - \langle (C_{33} - 2C_{44})/(2C_{33}C_{44}) \rangle} \mathbf{P}^{\perp} \otimes \mathbf{P}^{\perp} \right] \\ &+ \left[\frac{(\langle C_{13}/C_{33} \rangle)^2}{\langle 1/(2C_{44}) \rangle} + \frac{(\langle C_{13}/C_{33} \rangle)^2 \langle (C_{33} - 2C_{44})/(2C_{33}C_{44}) \rangle}{\langle 1/(2C_{44}) \rangle - \langle (C_{33} - 2C_{44})/(2C_{33}C_{44}) \rangle} \right] \mathbf{P} \otimes \mathbf{P} \\ &+ 2 \left[\frac{\langle C_{13}/C_{33} \rangle}{\langle 1/(2C_{44}) \rangle} + \frac{\langle C_{13}/C_{33} \rangle \langle (C_{33} - 2C_{44})/(2C_{33}C_{44}) \rangle}{\langle 1/(2C_{44}) \rangle - \langle (C_{33} - 2C_{44})/(2C_{33}C_{44}) \rangle} \right] \mathbf{P}^{\perp} \otimes \mathbf{P}.\end{aligned} \tag{4.48}$$

Summing equations (4.45) and (4.48), we obtain the expression for computing $\mathbb{C}^*$ as:

$$\begin{aligned}\mathbb{C}^* =& \langle (C_{11} - C_{12}) \rangle \mathbb{P} + \frac{1}{\langle 1/(2C_{44}) \rangle} \left[\mathbb{P}^{\perp} + \frac{\langle (C_{33} - 2C_{44})/(2C_{33}C_{44}) \rangle}{1/\langle (2C_{44}) \rangle - \langle (C_{33} - 2C_{44})/(2C_{33}C_{44}) \rangle} \mathbf{P}^{\perp} \otimes \mathbf{P}^{\perp} \right] \\ &+ \left[\left\langle \frac{C_{12}C_{33} - C_{13}^2}{C_{33}} \right\rangle + \frac{(\langle C_{13}/C_{33} \rangle)^2}{\langle 1/(2C_{44}) \rangle} + \frac{(\langle C_{13}/C_{33} \rangle)^2 \langle (C_{33} - 2C_{44})/(2C_{33}C_{44}) \rangle}{\langle 1/(2C_{44}) \rangle - \langle (C_{33} - 2C_{44})/(2C_{33}C_{44}) \rangle} \right] \mathbf{P} \otimes \mathbf{P} \\ &+ 2 \left[\frac{\langle C_{13}/C_{33} \rangle}{\langle 1/(2C_{44}) \rangle} + \frac{\langle C_{13}/C_{33} \rangle \langle (C_{33} - 2C_{44})/(2C_{33}C_{44}) \rangle}{\langle 1/(2C_{44}) \rangle - \langle (C_{33} - 2C_{44})/(2C_{33}C_{44}) \rangle} \right] \mathbf{P}^{\perp} \otimes \mathbf{P}.\end{aligned} \tag{4.49}$$

Voigt notation is adopted for analytical clarity, considering the inherent symmetry of $\mathbb{C}^*$ as demonstrated by its general expression in equation (4.39) and the above specific closed-form computations for transversely isotropic materials, where $(I) \rightleftarrows [(ij) = (ji)]$. More Preciesely, $(1,2,3,4,5,6) \rightleftarrows [(11),(22),(33),(13,(12))]$. Furthermore, in Voigt notation, the matrix representation of the tensor $\mathbb{C}^*$ is as follows:

$$[\mathbb{C}^*] = \begin{bmatrix} C_{11}^* & C_{12}^* & C_{13}^* & 0 & 0 & 0 \\ C_{12}^* & C_{11}^* & C_{23}^* & 0 & 0 & 0 \\ C_{13}^* & C_{23}^* & C_{33}^* & 0 & 0 & 0 \\ 0 & 0 & 0 & C_{44}^* & 0 & 0 \\ 0 & 0 & 0 & 0 & C_{44}^* & 0 \\ 0 & 0 & 0 & 0 & 0 & \frac{1}{2}(C_{11}^* - C_{12}^*) \end{bmatrix}. \tag{4.50}$$

After obtaining the effective elastic tensor $\mathbb{C}^*$ of the laminate via homogenization, we can analyze the composite laminate as a homogeneous structure, thereby simplifying the analysis

of complex structures. This method provides a simplified and efficient way to determine the effective mechanical properties of the laminates, enabling the prediction of the mechanical behavior of the composite materials under different loading conditions. This is crucial for the design and optimization of the laminates. Moreover, the homogenization method is versatile and practical, as it can be applied to various types of laminated composites, including those with irregular shapes, non-uniform fiber orientations, and multiple layers. Therefore, the homogenization method has become an indispensable tool for the analysis and design of laminated composites, particularly in the aerospace and automotive industries.

4.3 The Bending Analysis of Homogenized Laminated Simply Supported Plates

4.3.1 3D Exact Solution for the Homogenized Laminate

For the purpose of comparison, the study systematically analyzes a composite material consisting of n parallel plane layers. Each layer is composed of a linearly elastic homogeneous material and is perfectly bonded to adjacent layers. Utilizing the homogenization approach previously outlined, we derive an equivalent homogenized laminate. The equivalent homogenized laminate is subjected to the same external loads, boundary conditions, and coordinate conditions as the original laminated rectangular structure, which is illustrated in **Fig.** 4.2.

Under these specified conditions, we derive 3D-exact analytical solutions for the equivalent homogenized laminate. The equations governing the equilibrium of stresses for the homogenized laminate are expressed as follows:

$$\nabla \cdot \boldsymbol{\sigma} + \mathbf{f} = \mathbf{0}. \tag{4.51}$$

where, $\mathbf{f}$ represents the external load, which, in this particular case, takes the form of a vector $\{q_{xz}, q_{yz}, q_{zz}\}^T$. The boundary conditions for the simply supported edges are defined as:

$$\begin{aligned} &on\ x = 0,\ a:\ \sigma_x = v = w = 0, \\ &on\ y = 0,\ b:\ \sigma_y = u = w = 0, \end{aligned} \tag{4.52}$$

where u, v, and w denote the displacement along the x, y, and z axes, respectively. In this case,

the solution of the governing differential equation, i.e., the expressions of the displacements, can be sought in the form of an infinite Fourier series, as follows:

$$\mathbf{u} = \begin{Bmatrix} u \\ v \\ w \end{Bmatrix} = \sum_{n=1}^{\infty} \sum_{m=1}^{\infty} \begin{Bmatrix} u_{mn}(z)\ cospx\ sinqy \\ v_{mn}(z)\ sinpx\ cosqy \\ w_{mn}(z)\ sinpx\ sinqy \end{Bmatrix}, \tag{4.53}$$

where values of p and q are determined by equations (4.17) and (4.18). The terms m and n represent sequences of Fourier series that are used to expand the displacement functions. Each sequence of Fourier series m and n dictates the number of harmonic terms comprising the series expansion, with the functions $u_{mn}(z)$, $v_{mn}(z)$, and $w_{mn}(z)$ formulated accordingly, as expressed below:

$$\begin{Bmatrix} u_{mn}(z) \\ v_{mn}(z) \\ w_{mn}(z) \end{Bmatrix} = \begin{Bmatrix} u^{\circ}_{mn} \\ v^{\circ}_{mn} \\ w^{\circ}_{mn} \end{Bmatrix} e^{sz}, \tag{4.54}$$

where u°_{mn}, v°_{mn}, w°_{mn} and s denote the unknown variables requiring determination. Upon substitution of equation (4.53), and the homogenized constitutive law for the laminated structure given by equation (4.39) into equation (4.51), a set of equations representing the system for the general solution is derived for each combination of the indices m and n. The equations can be compactly expressed in matrix form as follows:

$$\mathbf{M}\mathbf{u}^{\circ}_{mn} = \mathbf{0}, \tag{4.55}$$

where $\mathbf{M}$ is a 3×3 is coefficient matrix and $\mathbf{u}^{\circ}_{mn} = \{u^{\circ}_{mn}, v^{\circ}_{mn}, w^{\circ}_{mn}\}^T$ is the vector of unknown variables. The components of $\mathbf{M}$ are calculated as follows:

$$\begin{aligned}
M_{11} &= -C^*_{11}p^2 - C^*_{66}q^2 + C^*_{55}s^2, \\
M_{12} &= M_{21} = -(C^*_{12} + C^*_{66})pq, \\
M_{13} &= M_{31} = (C^*_{13} + C^*_{55})ps, \\
M_{22} &= -C^*_{22}q^2 - C^*_{66}p^2 + C^*_{44}s^2, \\
M_{23} &= -M_{32} = (C^*_{23} + C^*_{44})qs, \\
M_{33} &= -C^*_{55}p^2 - C^*_{44}q^2 + C^*_{33}s^2,
\end{aligned} \tag{4.56}$$

where C_{ij}^{*} represents the components of the effective elastic tensor after homogenization, following the Voigt notation mentioned previously.

To obtain nontrivial solutions for the unknown constants in the vector $\mathbf{u}_{mn}^{\circ}$, it is necessary for the determinant of the coefficient matrix $\mathbf{M}$ in the equation system to vanish for each combination of m and n. This requirement ensures the existence of nontrivial solutions to the governing equations of the structure under combined bending and axial loading. Solving the eigenvalue problem associated with the determinant of $\mathbf{M}$ yields six roots of this equation, defining six values of s and their corresponding eigenvectors. These eigenvectors describe the mode shapes of the homogenized laminated structure under combined bending and axial loading, representing the deformation and displacement patterns induced by the applied loading conditions. These eigenvectors can be expressed as:

$$\begin{Bmatrix} a_1(s_i) \\ a_2(s_i) \\ a_3(s_i) \end{Bmatrix} e^{s_i z}, \tag{4.57}$$

where s_i represents the i^{th} root of the characteristic equation, and $a_1(s_i)$, $a_2(s_i)$, and $a_3(s_i)$ are constants determined by:

$$\begin{aligned} a_1(s_i) &= [(C_{13}^{*}+C_{55}^{*})(-C_{22}^{*}q^2 - C_{66}^{*}p^2 + C_{44}^{*}s_i^2) + (C_{12}^{*}+C_{66}^{*})(C_{23}^{*}+C_{44}^{*})q^2]ps_i, \\ a_2(s_i) &= [(C_{23}^{*}+C_{44}^{*})(-C_{11}^{*}p^2 - C_{66}^{*}q^2 + C_{55}^{*}s_i^2) + (C_{12}^{*}+C_{66}^{*})(C_{13}^{*}+C_{55}^{*})p^2]qs_i \\ a_3(s_i) &= -(-C_{11}^{*}p^2 - C_{66}^{*}q^2 + C_{55}^{*}s_i^2)(-C_{22}^{*}q^2 - C_{66}^{*}p^2 + C_{44}^{*}s_i^2) + ((C_{12}^{*}+C_{66}^{*})pq)^2. \end{aligned} \tag{4.58}$$

Based on this, equation (4.54) can be explicitly written as:

$$\begin{Bmatrix} u_{mn}(z) \\ v_{mn}(z) \\ w_{mn}(z) \end{Bmatrix} = \sum_{i=1}^{6} \begin{Bmatrix} a_1(s_i) \\ a_2(s_i) \\ a_3(s_i) \end{Bmatrix} k_i e^{s_i z}. \tag{4.59}$$

The coefficient k_i is determined from the boundary conditions of the laminated structure. By substituting the above equation into equation (4.53), we can obtain a closed-form expression for the displacement $\mathbf{u}$ containing undetermined coefficients k_i. Subsequently, substituting this closed-form displacement into the homogenized constitutive relation (4.39) yields the following

expression for stresses:

$$
\begin{aligned}
\sigma_x &= \sum_{n=1}^{\infty}\sum_{m=1}^{\infty}[\sum_{i=1}^{6}(-C_{11}^{*}pa_1(s_i) - C_{12}^{*}qa_2(s_i) + C_{13}^{*}a_3(s_i)s_i)k_i e^{s_i z}]\ sinpx\ sinqy,\\
\sigma_y &= \sum_{n=1}^{\infty}\sum_{m=1}^{\infty}[\sum_{i=1}^{6}(-C_{12}^{*}pa_1(s_i) - C_{22}^{*}qa_2(s_i) + C_{23}^{*}a_3(s_i)s_i)k_i e^{s_i z}]\ sinpx\ sinqy,\\
\sigma_z &= \sum_{n=1}^{\infty}\sum_{m=1}^{\infty}[\sum_{i=1}^{6}(-C_{13}^{*}pa_1(s_i) - C_{23}^{*}qa_2(s_i) + C_{33}^{*}a_3(s_i)s_i)k_i e^{s_i z}]\ sinpx\ sinqy,\\
\tau_{xy} &= \sum_{n=1}^{\infty}\sum_{m=1}^{\infty}[C_{66}^{*}\sum_{i=1}^{6}(pa_1(s_i) + qa_2(s_i))k_i e^{s_i z}]\ cospx\ cosqy,\\
\tau_{xz} &= \sum_{n=1}^{\infty}\sum_{m=1}^{\infty}[C_{55}^{*}\sum_{i=1}^{6}(a_1(s_i)s_i + pa_3(s_i))k_i e^{s_i z}]\ cospx\ sinqy,\\
\tau_{yz} &= \sum_{n=1}^{\infty}\sum_{m=1}^{\infty}[C_{44}^{*}\sum_{i=1}^{6}(a_2(s_i)s_i + qa_3(s_i))k_i e^{s_i z}]\ sinpx\ cosqy.
\end{aligned}
\tag{4.60}
$$

To determine the coefficient k_i $(i = 1,2,\cdots,6)$, the stresses expression derived above is substituted into the boundary condition (4.52), resulting in a set of equations expressed in matrix form as:

$$
\begin{bmatrix}
\phi^1(\frac{h}{2}) & \phi^2(\frac{h}{2}) & \cdots & \phi^6(\frac{h}{2})\\
\varphi^1(\frac{h}{2}) & \varphi^1(\frac{h}{2}) & \cdots & \varphi^6(\frac{h}{2})\\
\chi^1(\frac{h}{2}) & \chi^2(\frac{h}{2}) & \cdots & \chi^6(\frac{h}{2})\\
\phi^1(-\frac{h}{2}) & \phi^2(-\frac{h}{2}) & \cdots & \phi^6(-\frac{h}{2})\\
\varphi^1(-\frac{h}{2}) & \varphi^1(-\frac{h}{2}) & \cdots & \varphi^6(-\frac{h}{2})\\
\chi^1(-\frac{h}{2}) & \chi^2(-\frac{h}{2}) & \cdots & \chi^6(-\frac{h}{2})
\end{bmatrix}
\begin{Bmatrix} k_1\\ k_2\\ k_3\\ k_4\\ k_5\\ k_6 \end{Bmatrix}
=
\begin{Bmatrix} Q_{zz}^{t}\\ Q_{xz}^{t}\\ Q_{yz}^{t}\\ Q_{zz}^{b}\\ Q_{xz}^{b}\\ Q_{yz}^{b} \end{Bmatrix},
\tag{4.61}
$$

where $\phi^i(z)$, $\varphi^i(z)$, and $\chi^i(z)$ are given by:

$$
\begin{aligned}
\phi^i(z) &= [-C_{13}^{*}pa_1(s_i) - C_{23}^{*}qa_2(s_i) + C_{33}^{*}a_3(s_i)s_i]e^{s_i z},\\
\varphi^i(z) &= C_{55}^{*}[a_1(s_i)s_i + pa_3(s_i)]e^{s_i z},\\
\chi^i(z) &= C_{44}^{*}[a_2(s_i)s_i + qa_3(s_i)]e^{s_i z}.
\end{aligned}
\tag{4.62}
$$

The Fourier coefficients Q_{ij} represent the distribution of the external load applied to the structure, calculated by integrating the traction vector components q_{ij} over the plate's surface using appropriate sine and cosine functions. Specifically, the six Fourier coefficients Q_{ij} are are calcu-

lated as follows:

$$
\begin{aligned}
Q^t_{zz} &= \frac{4}{ab}\int_0^b \int_0^a (q^t_{zz}\ sinpx\ sinqy)dxdy,\\
Q^t_{xz} &= \frac{4}{ab}\int_0^b \int_0^a (q^t_{xz}\ cospx\ sinqy)dxdy,\\
Q^t_{yz} &= \frac{4}{ab}\int_0^b \int_0^a (q^t_{yz}\ sinpx\ cosqy)dxdy,\\
Q^b_{zz} &= \frac{4}{ab}\int_0^b \int_0^a (q^b_{zz}\ sinpx\ sinqy)dxdy,\\
Q^b_{xz} &= \frac{4}{ab}\int_0^b \int_0^a (q^b_{xz}\ cospx\ sinqy)dxdy,\\
Q^b_{yz} &= \frac{4}{ab}\int_0^b \int_0^a (q^b_{yz}\ sinpx\ cosqy)dxdy,
\end{aligned}
\tag{4.63}
$$

where the superscript "t" and "b" in the Fourier coefficients denote the location of the physical quantity on the upper and lower surfaces, respectively. Hence, once the external loads are determined and substituted into equation (84), the system of linear equations (82) can be solved to determine the undetermined coefficients k_i $(i = 1, 2, \cdots, 6)$. This enables the computation of the displacement, providing a comprehensive representation of the plate's response to applied loads.

4.3.2 Kirchhoff-Love Plate Theory for the Homogenized Laminate

In Kirchhoff-Love plate theory, the deformation of a thin plate is described by a displacement field $\mathbf{u}(x,y)$ varying over its two-dimensional domain. This field is composed of three components: in-plane displacements u and v, representing displacements within the plane of the plate, and the out-of-plane displacement w describing deformation perpendicular to the plate. Mathematically, these displacement components are expressed as:

$$
\mathbf{u} = \begin{Bmatrix} u \\ v \\ w \end{Bmatrix} = \begin{Bmatrix} u_0(x,y) - z\frac{\partial w_0(x,y)}{\partial x} \\ v_0(x,y) - z\frac{\partial w_0((x,y)}{\partial y} \\ w_0(x,y) \end{Bmatrix},
\tag{4.64}
$$

where u_0, v_0, and w_0 respectively denote the displacements along the x, y, and z directions at the mid-plane of the homogenized plate. The equilibrium equations governing the displacement field of a homogenized orthotropic plate in relation to its elastic properties may be expressed as

follows in terms of the of the mid-plane displacements u_0, v_0, and w_0, as follows:

$$\begin{aligned}
&A_{11}\frac{\partial^2 u_0}{\partial x^2}+A_{12}\frac{\partial^2 v_0}{\partial x\partial y}+A_{66}(\frac{\partial^2 u_0}{\partial y^2}+\frac{\partial^2 v_0}{\partial x\partial y})-B_{11}\frac{\partial^3 w_0}{\partial x^3}-(B_{12}+B_{66})\frac{\partial^3 w_0}{\partial x\partial y^2}=0,\\
&A_{66}(\frac{\partial^2 u_0}{\partial x\partial y}+\frac{\partial^2 v_0}{\partial x^2})+A_{12}\frac{\partial^2 u_0}{\partial x\partial y}+A_{22}\frac{\partial^2 v_0}{\partial y^2}-(B_{12}+B_{66})\frac{\partial^3 w_0}{\partial x^2\partial y}-B_{22}\frac{\partial^3 w_0}{\partial y^3}=0,\\
&D_{11}\frac{\partial^4 w_0}{\partial x^4}+2(D_{12}+2D_{66})\frac{\partial^4 w_0}{\partial x^2\partial x^2}+D_{22}\frac{\partial^4 w_0}{\partial y^4}-B_{11}\frac{\partial^3 u_0}{\partial x^3}\\
&-(B_{12}+2B_{66})(\frac{\partial^3 u_0}{\partial x\partial y^2}+\frac{\partial^3 v_0}{\partial x^2\partial y})-B_{22}\partial^3\frac{\partial^3 v_0}{\partial y^3}=Q_0,
\end{aligned} \tag{4.65}$$

where the right-hand side of the third equation, Q_0, represents any applied loads or moments on the plate. The coefficients in the equations of equilibrium, which include the extensional stiffness coefficient A_{ij}, bending-extensional coupling coefficient B_{ij}, and bending stiffness coefficients D_{ij}, are determined through integrals involving the elastic constants of the plate. Specifically, they can be expressed as follows:

$$\begin{aligned}
(A_{11},B_{11},D_{11})&=\int_{\frac{-h}{2}}^{\frac{h}{2}} C_{11}^*(1,z,z^2)dz,\\
(A_{12},B_{12},D_{12})&=\int_{\frac{-h}{2}}^{\frac{h}{2}} C_{12}^*(1,z,z^2)dz,\\
(A_{22},B_{22},D_{22})&=\int_{\frac{-h}{2}}^{\frac{h}{2}} C_{22}^*(1,z,z^2)dz,\\
(A_{66},B_{66},D_{66})&=\int_{\frac{-h}{2}}^{\frac{h}{2}} C_{66}^*(1,z,z^2)dz.
\end{aligned} \tag{4.66}$$

In the case of a simple support edge condition, the following boundary conditions are prescribed:

$$\begin{aligned}
&on\ x=0,\ a:\ v_0=w_0=N_x=M_x=0,\\
&on\ y=0,\ b:\ u_0=w_0=N_y=M_y=0,
\end{aligned} \tag{4.67}$$

where N_x, N_y and M_x, M_y are the normal and moment components of the traction vector at the boundary, respectively. Similarly, the displacement field of the plate can be represented by a

general solution comprising a series of sinusoidal functions, as shown below:

$$\begin{aligned} u_0 &= \sum_{n=1}^{\infty}\sum_{m=1}^{\infty} U_{mn}\, cospx\, sinqy, \\ v_0 &= \sum_{n=1}^{\infty}\sum_{m=1}^{\infty} V_{mn}\, sinpx\, cosqy, \\ w_0 &= \sum_{n=1}^{\infty}\sum_{m=1}^{\infty} W_{mn} sinpx\, sinqy, \end{aligned} \tag{4.68}$$

where the coefficients U_{mn}, V_{mn}, and W_{mn} govern the amplitudes of the sinusoidal functions that constitute the general solution for the displacement field of the plate. Determining their values is essential for fully characterizing the displacement field. The substitution of equation (4.68) into equation (4.65) results in a system of equations concerning the coefficients U_{mn}, V_{mn}, and W_{mn}. These equations can be expressed in a more concise matrix form, as follows:

$$\mathbf{K}\mathbf{U}_{mn} = \begin{Bmatrix} 0 \\ 0 \\ Q_{mn} \end{Bmatrix} \tag{4.69}$$

where the vector $\mathbf{U}_{mn}$ represents the unknown variables, and the components of the coefficient matrix $\mathbf{K}$ are determined as follows:

$$\begin{aligned} K_{11} &= -A_{11}p^2 - A_{66}q^2, \\ K_{12} &= K_{21} = -(A_{12} + A_{66})pq, \\ K_{13} &= K_{31} = B_{11}p^3 + (B_{12} + B_{66})pq^2, \\ K_{22} &= -A_{66}p^2 - A_{22}q^2, \\ K_{23} &= K_{32} = (B_{12} + B_{66})p^2q + B_{22}q^3, \\ K_{33} &= D_{11}q^4 + 2(D_{12} + 2D_{66})p^2q^2 + D_{22}q^4. \end{aligned} \tag{4.70}$$

The values of Q_{mn} appearing on the right-hand side of the system of equations can be computed by evaluating the following double integral:

$$Q_{mn} = \frac{4}{ab}\int_0^b \int_0^a (Q_0\, sinpx\, sinqy)dxdy. \tag{4.71}$$

By solving the system of linear equations represented by equation (4.69), the displacement values corresponding to a particular load can be obtained. Therefore, the analytical expressions for in-plane stress can be derived by applying the stress-strain relationship to the obtained displacement field. Specifically, the stress components can be written as follows:

$$\begin{aligned}
\sigma_x &= \sum_{n=1}^{\infty}\sum_{m=1}^{\infty}[C_{11}^*(-U_{mn}p + zW_{mn}p^2) + C_{12}^*(-V_{mn}q + zW_{mn}q^2)]\ sinpx\ sinqy, \\
\tau_{xy} &= \sum_{n=1}^{\infty}\sum_{m=1}^{\infty}[C_{66}^*(U_{mn}q + V_{mn}p - 2zW_{mn}pq)]\ cospx\ cosqy, \\
\sigma_y &= \sum_{n=1}^{\infty}\sum_{m=1}^{\infty}[C_{12}^*(-U_{mn}p + zW_{mn}p^2) + C_{22}^*(-V_{mn}q + zW_{mn}q^2)]\ sinpx\ sinqy.
\end{aligned} \tag{4.72}$$

In Kirchhoff-Love plate theory, the plate is assumed to be thin and subjected to in-plane loads only, resulting in a planar stress state in the plate. The transverse stresses, which are perpendicular to the plane of the plate, can be obtained from the equilibrium equations, which require that the sum of the forces and moments in the z-direction be zero. By solving these equilibrium equations, the expressions for the transverse stresses can be obtained, as shown in the equations provided:

$$\begin{aligned}
\tau_{xz} = \sum_{n=1}^{\infty}\sum_{m=1}^{\infty}&[zU_{mn}(C_{11}^*p^2 + C_{66}^*q^2) + zV_{mn}(C_{12}^* + C_{66}^*)pq \\
&- \frac{1}{2}z^2W_{mn}(C_{11}^*p^3 + C_{12}^*pq^2 + 2C_{66}^*pq^2) + H_{mn}]\ cospx\ sinqy, \\
\tau_{yz} = \sum_{n=1}^{\infty}\sum_{m=1}^{\infty}&[zU_{mn}(C_{12}^* + C_{66}^*)pq + zV_{mn}(C_{66}^*p^2 + C_{22}^*q^2) \\
&- \frac{1}{2}z^2W_{mn}(C_{12}^*p^2q + C_{22}^*q^3 + 2C_{66}^*p^2q) + I_{mn}]\ sinpx\ cosqy, \\
\sigma_z = \sum_{n=1}^{\infty}\sum_{m=1}^{\infty}&[z(H_{mn}p + I_{mn}q) + \frac{1}{2}z^2U_{mn}(C_{11}^*p^3 + 2C_{66}^*pq^2 + C_{12}^*pq^2) \\
&+ \frac{1}{2}z^2V_{mn}(C_{1122}^*p^2q + 2C_{66}^*p^2q + C_{22}^*q^3) - \frac{1}{6}z^3W_{mn}(C_{11}^*p^4 \\
&+ 2C_{12}^*p^2q^2 + 4C_{66}^*p^2q^2 + C_{22}^*q^4) + J_{mn}]\ sinpx\ sinqy,
\end{aligned} \tag{4.73}$$

where the coefficients H_{mn}, I_{mn}, and J_{mn} in the expressions for the transverse stresses are unknown constants that are to be determined by satisfying the boundary conditions at the top and bottom surfaces of the plate.

4.4 Comparative Analysis of Displacement and Stress Predictions for Laminated Plates

To assess the predictive accuracy of the proposed method for predicting displacements and stresses in laminated plates, a comparative analysis is conducted against established theories, including 3D exact elasticity solution by Pagano (3D-Elasticity), classical laminated plate theory (CPT), and Zig-Zag theory (Zig-Zag) with a sixth-order polynomial approximation. The comparative study focuses on a rectangular symmetric laminate subjected to simply supported boundary conditions at x=0, a, and y=0, b.

Two distinct geometric configurations of laminated composite structures are investigated in this study. These configurations involve laminates composed of three, five, seven, and nine layers, all under uniform boundary conditions and consistent external loading conditions. The two primary configurations are delineated as follows:

(1) Unidirectional Fiber-Reinforced Laminate(Orthotropic Laminate): In this configuration, the laminate consists of multiple layers of unidirectional fiber-reinforced material. The layer material properties for this configuration are as follows:

$$\begin{aligned} E_L &= 25\times10^6 psi, \quad & E_T &= 10\times10^6 psi, \\ G_{LT} &= 0.5\times10^6 psi, \quad & G_{TT} &= 0.2\times10^6 psi, \\ \nu_{LT} &= \nu_{TT} = 0.25, \end{aligned} \tag{4.74}$$

where the symbol 'L' denotes the fiber-aligned direction, while 'T' corresponds to the direction perpendicular to the fiber orientation. To provide a more detailed description of the stacking structure of the laminate, the designation '0' indicates the alignment of fibers along the x-axis, whereas '90' denotes alignment along the y-axis. For example, in a three-layer laminate, if the central layer has fibers oriented along the y-axis while the top and bottom layers have fibers oriented along the x-axis, this configuration can be represented symbolically as '[0/90/0]'.

(2)Bidirectional Fiber-Reinforced Laminate: In this configuration, every layer exhibits in-plane isotropy, with uniform material properties within a plane perpendicular to the thickness direction. To achieve these configurations, we employed a combination of bidirectional plates (represented by '†') with fibers aligned along the x and y axes, and unidirectional plates (represented by '|') with fibers oriented along the z-axis direction. For example, a three-layer laminate

with the central layer as a unidirectional plate and the top and bottom layers as bidirectional plates can be symbolically denoted as '[†/|/†]'. The material properties of the unidirectional plates align with those specified in case 1. For the bidirectional plates in this configuration, the material properties are as follows:

$$\begin{aligned} E_L &= 25 \times 10^6 psi, \quad E_T = 10 \times 10^6 psi, \\ G_{LT} &= 0.5 \times 10^6 psi, \quad \nu_{LT} = \nu_{TT} = 0.25. \end{aligned} \tag{4.75}$$

The stacking sequences for these laminated structures were determined based on the specifications outlined in Table 4.1. Subsequently, these configurations and stacking sequences were analyzed using various methodologies to examine their responses under the specified boundary and loading conditions.

As previously mentioned, the load applied to the laminate can be decomposed into a double Fourier series, enabling its representation as a series of sinusoidal terms. In this study, we assume that the simply supported laminate is subjected to a sinusoidal transverse load $q_{zz}^t(x,y) = \sigma_0 sin(\frac{\pi x}{a}) sin(\frac{\pi y}{b})$ on its top surface, where σ_0 is a constant. Given the prescribed boundary conditions and assumptions, the displacement and stress of the laminate can be accurately determined and analyzed using various theoretical approaches. To facilitate a comprehensive comparison and analysis of predicted results obtained from different theoretical approaches, we implement the conventional approach of non-dimensionalization to normalize displacements and stresses. This involves introducing a set of rigorously defined dimensionless parameters, as follows:

$$\begin{aligned} (\bar{\sigma}_x, \bar{\sigma}_y, \bar{\sigma}_{xy}) &= \frac{1}{\sigma_0 S^2}(\sigma_x, \sigma_y, \sigma_{xy}), \\ (\bar{\tau}_{xz}, \bar{\tau}_{yz}, \bar{\sigma}_z) &= \frac{1}{\sigma_0 S}(\tau_{xz}, \tau_{yz}, \sigma_z), \\ \bar{u} = \frac{E_T u}{\sigma_0 h S^3}, \quad \bar{w} &= \frac{100 E_T w}{\sigma_0 h S^4}, \\ S = \frac{a}{h}, \quad \bar{z} &= \frac{z}{h}. \end{aligned} \tag{4.76}$$

Table 4.1 provides an comparative analysis of the performance of the Zig-Zag, H-Exact, CPT, and HK-LPT analyses, with respect to the 3D-Elasticity approach, which serves as the benchmark for this study. To accurately evaluate the convergence of each method, a global

convergence rate is introduced, defined as the L2-norm indicator given by:

$$err = \frac{\sqrt{\frac{1}{h}\int_{-\frac{h}{2}}^{\frac{h}{2}} \| p - p_0 \|^2 \, dz}}{\sqrt{\frac{1}{h}\int_{-\frac{h}{2}}^{\frac{h}{2}} \| p_0 \|^2 \, dz}} \tag{4.77}$$

where p_0 represents the value obtained by the 3D-Elasticity theory, while p represents the value obtained by the other theories. The global convergence rate quantifies the overall discrepancy across the entire thickness of a laminate between the 3D-Elasticity theory and alternative methods for approximating the solution of a given problem. As presented in Table 4.1, the maximum values and global convergence rates of stress components and in-plane displacements for four distinct laminated systems, acquired through various theories, have been provided. In some instances, as shown in **Fig.** 4.10(a), the maximum values of $\bar{\tau}_{yz}$ obtained through the 3D-Elasticity and Zig-Zag are not observed at $\bar{z} = 0$. In such cases, we have precisely annotated the coordinates of the maximum values and their corresponding locations on the graph for accuracy and completeness. The correlation between the maximum normalized deflection ($\bar{w}$) and the span-to-depth ratio (S) for both cases is visually presented in **Fig.** 4.3(a) and **Fig.** 4.3(b). It is evident that, particularly at lower S values in both cases, the CPT and the HK-LPT consistently underestimate the plate deflection. As the value of S increases, it becomes apparent that the approximations of the deflection computed using the CPT in both Case 1 and Case 2 progressively converge toward the exact solutions of deflection $\bar{w}$. And in Case 1, the HK-LPT demonstrates a gradual convergence of its computed approximate deflection towards the exact solution, while in Case 2, HK-LPT yields slightly higher deflection values relative to the exact solution. The Zigzag method provides a remarkably precise approximation of w that closely aligns with the true solution. The H-Exact method consistently provides highly accurate approximations of $\bar{w}$ in relation to the exact solution, except in the case of a large span-to-depth ratio S in Case 2, where it exhibits a slight tendency to overestimate $\bar{w}$ relative to the exact solution. Indeed, for large-span plates, deflection is primarily governed by flexural rigidity, which is closely linked to the z-direction elastic modulus. In the case of laminate plates, where the z-direction elastic moduli may not be uniform across each layer, the homogenization process that averages the z-direction elastic moduli can introduce some deviation between the computed deflection and the exact solution. Hence, in the case of large spans, particularly in Case 2, both the H-exact

Table 4.1: Comparison of 3D-Elasticity theory and alternative methods for multi-layer laminate analysis

case	$\bar{u}$		$\bar{\sigma}_x$		$\bar{\tau}_{xy}$		$\bar{\tau}_{xz}$		$\bar{\tau}_{yz}$		$\bar{\sigma}_z$	
	value $(0, \frac{b}{2}, -\frac{1}{2})$	err %	value $(\frac{a}{2}, \frac{b}{2}, \frac{1}{2})$	err %	value $(0, \frac{b}{2}, -\frac{1}{2})$	err %	value $(0, \frac{b}{2}, 0)$	err %	value $(\frac{a}{2}, 0, 0)$	err %	value $(\frac{a}{2}, \frac{b}{2}, \frac{1}{2})$	err %
	3D-Elasticity											
case1	0.00936	-	0.801	-	0.0505	-	0.256	-	0.217	-	0.25	-
	Zig-zag											
3layers	0.01030	22.4	0.842	17.2	0.0495	5.8	0.238	6.3	0.233	7.1	0.25	1.1
	H-Exact											
[0/90/0]	0.00882	53.4	0.517	43.9	0.0300	47.0	0.254	20.4	0.179	48.4	0.25	0.9
	CPT											
	0.00677	81.6	0.539	63.6	0.0213	50.4	0.395	38.2	0.0823	61.9	0.25	2.8
	HK-LPT											
	0.00670	81.0	0.367	60.3	0.0210	50.9	0.305	23.3	0.172	36.8	0.25	2.8
	0.00845	-	0.719	-	0.0408	-	0.268	-	0.208	-	0.25	-
5layers	0.00897	19.3	0.725	7.7	0.0376	10.7	0.259	2.9	0.223	6.47	0.25	0.8
[0/90/0	0.00902	43.1	0.479	39.5	0.0296	29.6	0.239	14.4	0.194	33.8	0.25	1.7
/90/0]	0.00677	60.0	0.539	43.2	0.0213	37.7	0.311	21.4	0.166	28.5	0.25	1.0
	0.00670	59.1	0.334	55.4	0.0210	38.2	0.279	17.9	0.199	25.6	0.25	1.0
	0.00818	-	0.694	-	0.0360	-	0.236	-	0.218	-	0.25	-
7layers	0.00890	21.5	0.717	16.5	0.0346	8.3	0.215	6.2	0.219	2.3	0.25	1.0
[0/90/0	0.00912	32.9	0.463	42.0	0.0296	18.5	0.232	12.0	0.200	25.0	0.25	1.3
/90/0/90	0.00677	47.0	0.539	34.4	0.0213	30.7	0.300	17.5	0.177	18.9	0.25	1.3
/0]	0.00670	46.1	0.319	57.0	0.0210	31.2	0.267	17.1	0.210	18.3	0.25	1.3
	0.00815	-	0.690	-	0.0336	-	0.237	-	0.211	-	0.25	-
9layers	0.00899	19.6	0.724	16.4	0.0334	7.5	0.223	5.9	0.210	17.0	0.25	1.1
[0/90/0	0.00917	26.1	0.453	45.7	0.0295	12.2	0.229	10.5	0.204	19.5	0.25	0.8
/90/0/90	0.00677	40.7	0.539	31.1	0.0213	27.9	0.281	15.7	0.197	14.5	0.25	1.6
/0/90/0]	0.00670	39.8	0.311	59.3	0.0210	28.3	0.261	16.3	0.217	14.0	0.25	1.6
case2	0.00374	-	0.430	-	0.0234	-	0.216	-	0.216	-	0.25	-
3layers	0.00400	10.2	0.422	5.8	0.0251	8.4	0.213	1.9	0.213	1.9	0.25	0.7
[†/|/†]	0.00520	45.1	0.407	15.2	0.0327	45.7	0.218	23.1	0.218	23.1	0.25	0.4
	0.00284	21.2	0.297	18.5	0.0178	20.6	0.222	45.1	0.222	45.1	0.25	1.3
	0.00390	45.7	0.279	25.9	0.0245	49.7	0.239	72.8	0.239	72.8	0.25	2.0
	0.00410	-	0.466	-	0.0258	-	0.195	-	0.195	-	0.25	-
5layers	0.00445	18.5	0.469	9.5	0.0280	12.5	0.186	3.0	0.186	3.0	0.25	1.1
[†/|/†	0.00556	35.8	0.390	31.7	0.0268	47.1	0.220	10.1	0.220	10.1	0.25	2.5
/|/†]	0.00340	21.8	0.356	14.9	0.0214	17.4	0.208	3.9	0.208	3.87	0.25	1.3
	0.00427	40.2	0.277	46.2	0.0350	58.8	0.239	17.1	0.239	17.1	0.25	4.5
	0.00445	-	0.503	-	0.0280	-	0.208	-	0.208	-	0.25	-
7layers	0.00485	13.8	0.512	9.9	0.0304	11.5	0.198	3.8	0.198	3.8	0.25	1.3
[†/|/†	0.00574	27.8	0.382	41.9	0.0361	48.8	0.221	10.8	0.221	10.8	0.25	2.5
/|/†/|	0.00376	21.1	0.393	16.3	0.0236	18.2	0.221	5.5	0.221	5.5	0.25	1.7
/†]	0.00445	33.8	0.276	53.8	0.0279	60.7	0.239	17.1	0.239	17.1	0.25	4.4
	0.00473	-	0.534	-	0.0297	-	0.204	-	0.204	-	0.25	-
9layers	0.00514	11.2	0.542	8.9	0.0323	10.1	0.196	3.5	0.196	3.5	0.25	1.2
[†/|/†	0.00584	20.8	0.379	47.9	0.0295	49.7	0.221	10.1	0.221	10.1	0.25	2.3
/|/†/|	0.00399	14.4	0.418	17.2	0.0251	18.8	0.219	6.1	0.219	6.1	0.25	1.7
/†/|/†]	0.00455	23.4	0.275	57.7	0.0286	61.1	0.239	16.0	0.239	16.0	0.25	4.1

and HK-LPT methods exhibit a degree of discrepancy in the computed deflection relative to the exact solution.

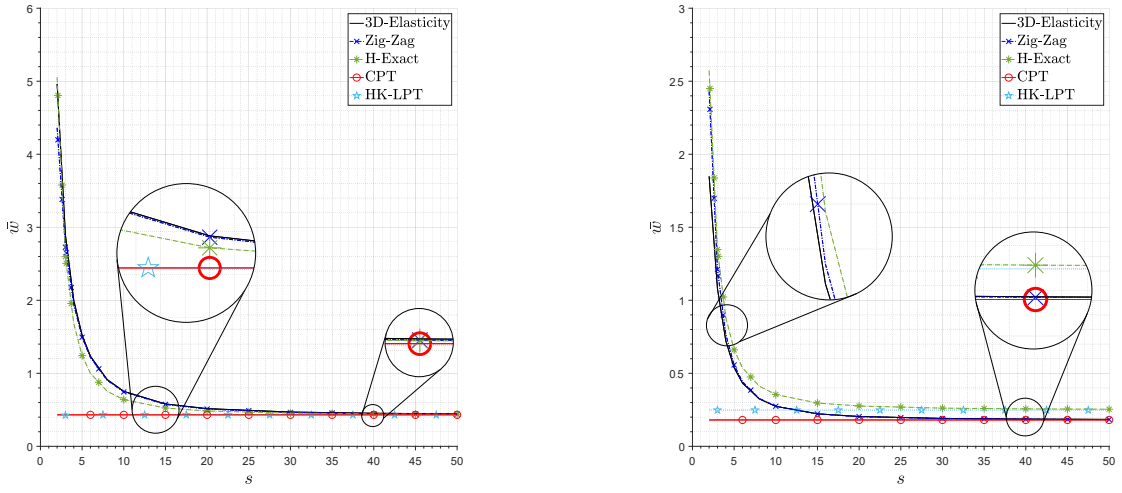

(a) (b)

Figure 4.3: *Comparison of normalized maximum deflection with varying span-to-depth ratio (S) for a three-layer laminate under sinusoidal transverse load: (a) case 1, (b) case 2.*

The **Fig.** 4.4 illustrates the comparison of normalized deflections at the thickness-center and width-center cross-sections along the lengthwise direction in a three-layer laminate, with a specified span-to-depth ratio ($S = 4$). Owing to the axial symmetry inherent in the structural configuration and the sinusoidal characteristics of the externally applied load, the deflection distribution demonstrates prominent symmetry. To enhance analytical efficiency, we have selectively illustrated a quarter (1/4) of the deflection profile along the longitudinal axis. It can be observed that the deflection distribution trends obtained through various approximation methods in both Case 1 and Case 2 align with those derived from the 3D-Elasticity. However, it is evident that the deflections obtained through the Zig-Zag method and H-Exact method closely approximate the values of the 3D-Exact solution at the respective positions along the $\bar{x}$-axis, conforming consistently to the comparisons illustrated in **Fig.** 4.3.

The distributions of displacements and stresses within 9-layer laminated plates for both Case 1 and Case 2, along with the stacking sequence detailed in Table 4.1, are illustrated in **Figs.** 4.5-4.10. Each figure shows the maximum value of a particular displacement or stress function along a vertical line across the laminate. **Fig.** 4.5 shows the variation of normalized in-plane displacement $\bar{u}$ through the thickness. With Table 4.1 as reference, it is evident that, for lam-

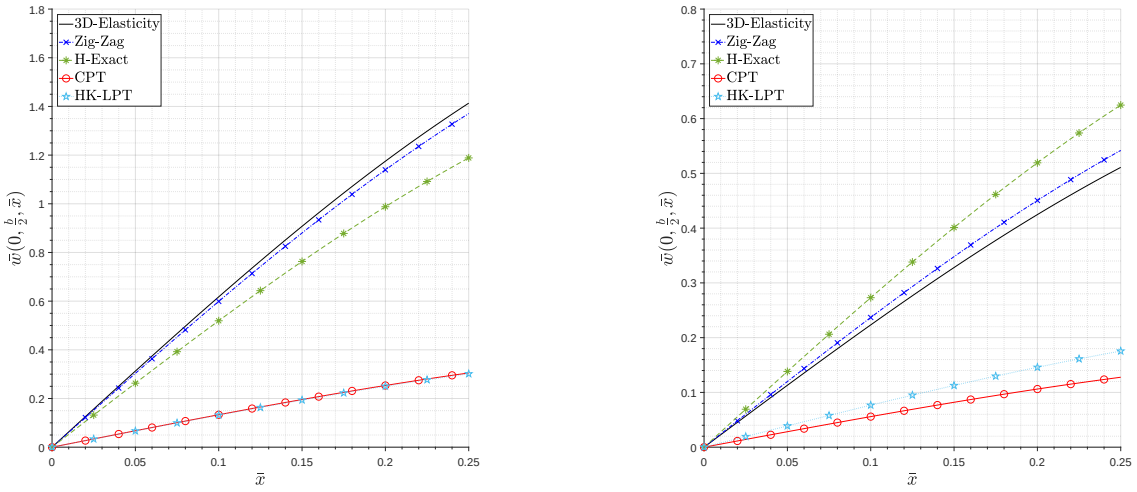

(a) (b)

Figure 4.4: *Comparing normalized deflections at the thickness-center and width-center cross-sections along the lengthwise direction in a three-layer laminate: : (a) case 1, (b) case 2.*

inated structures with identical total thickness, the distribution of the displacement $\bar{u}$ derived from the Zig-Zag, H-Exact, CPT, and HK-LPT, progressively converges towards the $\bar{u}$ obtained from 3D-Elasticity, with a corresponding decrease in the global error, as the number of layers in the laminate increases. This convergence can be attributed to a more uniform stress distribution throughout the laminate with an increase in the number of layers, resulting in reduced interlaminar shear stresses that may otherwise negatively affect the accuracy of the solutions. Notably, the H-Exact method exhibits a significant and consistent trend in the convergence of the $\bar{u}$ distribution, implying that it is capable of capturing the interlaminar shear stresses and their influence on the transverse deformation behavior of the laminate. As a result, it provides a precise prediction of the distribution of in-plane displacement and shear stresses. This assertion is further supported by the data presented in Table 4.1 and **Figs.** 4.7, 4.9, and 4.10, which illustrate the distribution of $\bar{\tau}_{xy}$, $\bar{\tau}_{xz}$, and $\bar{\tau}_{yz}$, respectively, along a vertical line across the laminate. Additionally, **Fig.**4.9 demonstrates that the H-Exact method provides a highly accurate estimation of the transverse stress $\bar{\sigma}_z$ compared to the value obtained by 3D-Elasticity.

Based on the obtained results, it can be inferred that the exact solution of the homogenized plate (H-Exact) has the potential to provide a reliable and accurate estimation of the elastic solution of the laminate (3D-Elasticity). Specifically, the degree of approximation achieved by the H-Exact method is observed to be comparable to that of the sixth-order Zig-Zag theory for mul-

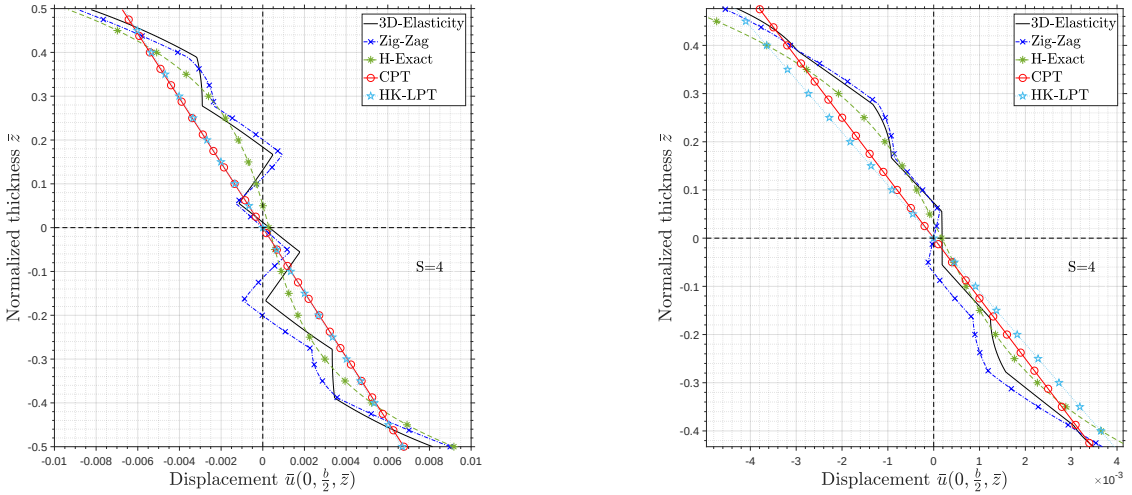

(a) (b)

Figure 4.5: *Variation of in-plane displacement $\bar{u}(0,\frac{b}{2},\bar{z})$ through the normalized thickness of a nine-layer laminate under sinusoidal transverse load: (a) case 1, 9 layers; (b)case 2, 9 layers.*

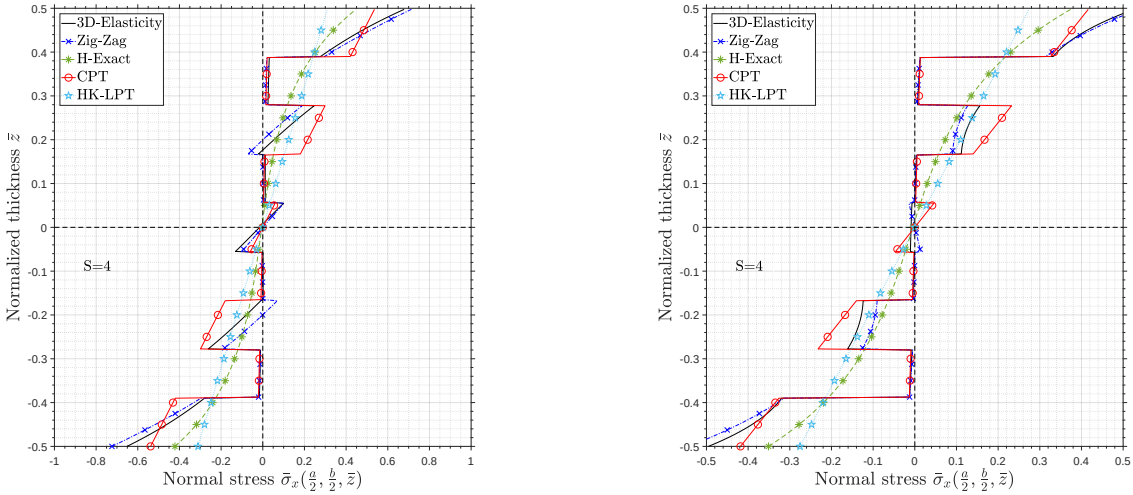

(a) (b)

Figure 4.6: *Variation of in-plane normal stress $\bar{\sigma}_x(\frac{a}{2},\frac{b}{2},\bar{z})$ through the normalized thickness of a nine-layer laminate under sinusoidal transverse load: (a) case 1, 9 layers; (b)case 2, 9 layers.*

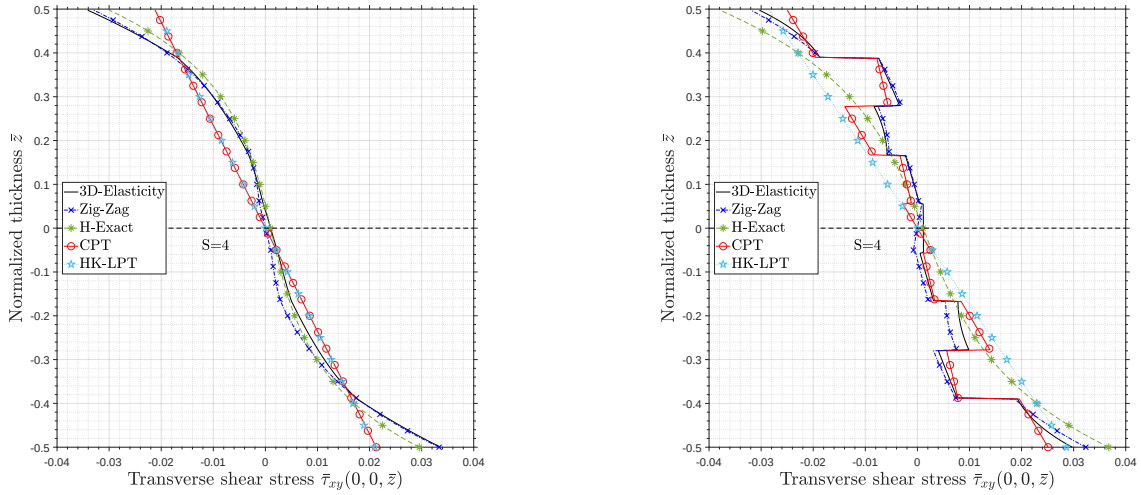

(a) (b)

Figure 4.7: *Variation of in-plane shear stress $\bar{\tau}_{xy}(0,0,\bar{z})$ through the normalized thickness of a nine-layer laminate under sinusoidal transverse load: (a) case 1, 9 layers; (b)case 2, 9 layers.*

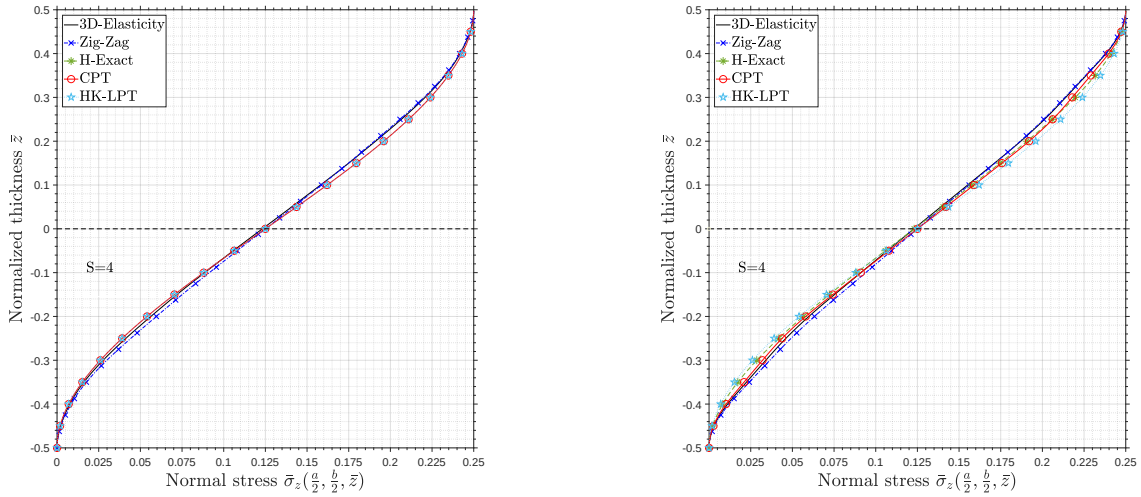

(a) (b)

Figure 4.8: *Variation of transverse normal stress $\bar{\sigma}_z(\frac{a}{2},\frac{b}{2},\bar{z})$ through the normalized thickness of a nine-layer laminate under sinusoidal transverse load: (a) case 1, 9 layers; (b)case 2, 9 layers.*

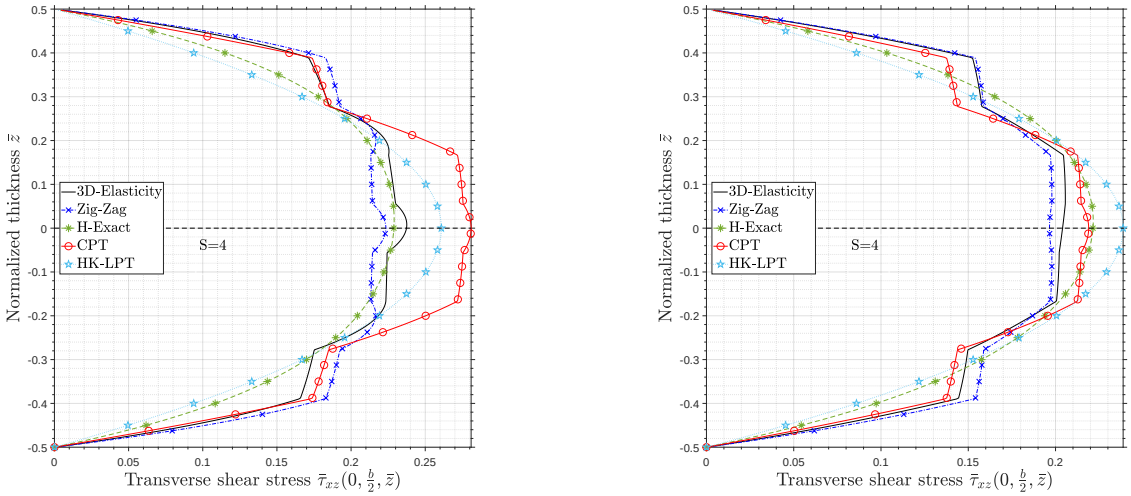

(a) (b)

Figure 4.9: *Variation of transverse shear stress* $\bar{\tau}_{xz}(0, \frac{b}{2}, \bar{z})$ *through the normalized thickness of a nine-layer laminate under sinusoidal transverse load: (a) case 1, 9 layers; (b)case 2, 9 layers.*

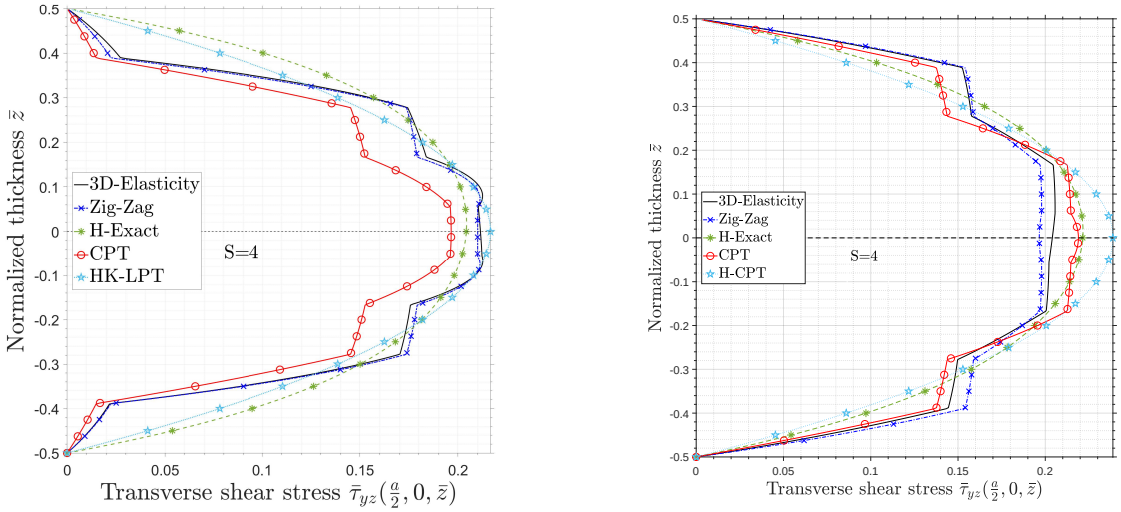

(a) (b)

Figure 4.10: *Variation of transverse shear stress* $\bar{\tau}_{yz}(\frac{a}{2}, 0, \bar{z})$ *through the normalized thickness of a nine-layer laminate under sinusoidal transverse load: (a) case 1, 9 layers; (b)case 2, 9 layers.*

tilayer laminates. Therefore, the H-Exact method can be considered as a promising alternative to existing theories for the analysis of laminated structures. Furthermore, the H-Exact method presents a promising approach for implementation in finite element analysis, particularly for modeling 3D elements of laminated structures encountered in practical engineering applications that often involve complex geometries, external loads, and boundary conditions. The accurate predictions of the displacement and stress distributions provided by the H-Exact method can enhance the reliability and efficiency of finite element simulations. Therefore, the incorporation of the H-Exact method into finite element models can lead to significant improvements in the design and optimization of laminated structures in various engineering fields. Specifically, the combination of H-exact method and finite element analysis is more suitable for thick and multi-layered laminated structure.

In contrast, certain local values, specifically the in-plane stress components $\bar{\sigma}x$ and $\bar{\tau}xy$, show significant differences. As previously noted, discontinuities in in-plane stresses may be inherent in solutions derived from 3D-Elasticity. However, the H-Exact and HK-LPT methods use homogenized equivalent structures, resulting in smoother, continuous in-plane stress curves. Interestingly, the overall in-plane stress distribution obtained from the H-Exact method closely approximates that derived from 3D-Elasticity. Simultaneously, within the distribution of transverse stresses, notable alignment is observed between the stress profiles derived from H-Exact and Zig-Zag theories and those obtained through 3D-Elasticity. Furthermore, the analysis presented in Table 1 highlights that the overall errors associated with these values are remarkably minimal, with their maximum magnitudes exhibiting close proximity. This consistent correspondence underscores the capacity of these methods to provide precise predictions for the comprehensive distribution of transverse stresses, strengthening their reliability in results analysis. Examination of these distribution plots and Table 4.1 reveals that, in comparison to the stress and displacement distributions obtained through Zig-Zag and H-Exact methods, the precision of the solution derived from the HK-LPT method exhibits a relatively modest level in comparison. It is noteworthy that HK-LPT employs an equivalent homogenized structure while simultaneously incorporating assumptions from Kirchhoff-Love plate theory. This dual approach involves a trade-off with respect to precision, yet yields a substantial improvement in computational efficiency. Furthermore, the analysis suggests that increasing the number of layers in the laminate improves the accuracy of predictions by both HK-LPT and CPT, when the total thickness of the

laminate is kept constant.

4.5 Conclusion

This chapter introduces generalized zigzag theories to capture transverse shear deformation and the zigzag phenomenon in laminated plates. A homogenization method, using Hadamard's relation and previously introduced operators, was developed to ensure continuous transverse stresses at layer interfaces. Analytical expressions for the effective elastic tensor of transversely isotropic laminates were derived.

Additionally, the 3D exact (H-Exact) and Kirchhoff plate (HK-LPT) solutions for homogenized laminates were presented. Comparative analyses between zigzag theory, H-Exact, Classical Laminated Plate Theory (CLPT), and Kirchhoff plate theory (KPT), benchmarked against 3D elasticity, demonstrated the improved zigzag theory's accuracy, comparable to sixth-order polynomials, in capturing laminated plate behavior.

For thick, multi-layered structures, combining H-Exact with finite element analysis offers a more efficient approach. This homogenization method effectively captures complex mechanical behavior due to transverse anisotropy and interfacial discontinuities, enabling simpler analysis through equivalent homogeneous material modeling.

In summary, the derived H-Exact and HK-LPT solutions provide a comprehensive analysis of laminated composites. While HK-LPT simplifies the model for practical applications, H-Exact offers a detailed approach. This work establishes a solid foundation for future research and practical applications in advanced laminated composite analysis and design.

Chapter 5

General Imperfect Interface Model for Poroelastic Composites and its Numerical Implementation Using XFEM

In Chapter 2, we presented Taylor expansions for both scalar and vector fields. Building upon this foundation, the current chapter extends these expansions to scenarios where both types of fields coexist. This extension forms the basis for developing an imperfect interface model aimed at replacing the transition layer in porous composites. Specifically, this model conceptualizes the transition layer, which connects the matrix and inclusion phase with a uniform slight thickness h, as a zero-thickness interface. Leveraging coordinate-free interfacial operators introduced earlier in Chapter 2, we derive precise jump relations that describe the discontinuities in physical fields at both ends of this transition layer. These relations provide a rigorous and concise mathematical framework for understanding the behavior across imperfect interfaces.

In the context of isotropic material configurations, explicit forms of jump relations for imperfect interfaces are provided and extensively discussed. Special attention is given to scenarios where the transition layer material itself is isotropic, further refining the theoretical underpinnings.

To showcase the efficiency of our numerical methods, we employ the principle of virtual work to derive weak forms that address the complex coupled boundary conditions typical of particulate composites. Within the eXtended Finite Element Method (XFEM) framework, we introduce enrichment functions designed to enhance the accuracy of interpolation functions in

capturing discontinuous relations. These weak forms are then discretized to obtain equilibrium equations, which serve as a robust theoretical basis for our numerical simulations.

Moreover, we utilize the level set function defined in Chapter 1 to effectively trace the imperfect interface within the composite material. This approach categorizes elements divided by the imperfect interface into different types, each requiring specific integration strategies. We have developed a sophisticated computational program tailored to solve the practical problem of a spherical inclusion embedded in an infinite matrix via a generalized imperfect interface under prescribed boundary conditions. Furthermore, rigorous analytical solutions are derived for benchmarking purposes, allowing us to thoroughly assess the accuracy and convergence of our numerical method.

Lastly, the Generalized Self-Consistent Scheme (GSCS) has been extensively employed to estimate effective poroelastic properties, underscoring its broad applicability and relevance in the field of composite materials characterization and analysis.

5.1 Theoretical Modeling Approach for General Imperfect Interface in Poroelastic Composites

We first focus on creating a comprehensive imperfect interface model to replace the transition layer discussed in this document. Then, we conduct theoretical analyses to outline the structural and physical attributes of this model through mathematical deduction. Specifically: (i) The interphase $\Omega^{(1)}$ is perfectly bonded to its neighboring phases $\Omega^{(1)}$ and $\Omega^{(2)}$ by the interface S_1 and S_2 in three-phase configuration , as shown in **Fig.** 5.1. Initially, we replace the transition layer with a zero-thickness imperfect interface S_0 located in the middle of the transition layer geometrically. The materials surrounding the transition layer, $\Omega^{(1)}$ and $\Omega^{(2)}$ are extended to the imperfect interface S_0 while the perfect interfaces S_1 and S_2 as shown in **Fig.** 5.2. Thus, the transition from a three-phase configuration to the corresponding two-phase configuration is geometrically achieved. (ii) To characterize the physical properties of the transition layer, it is essential to express the relationship between the physical fields on both surfaces S_1 and S_2 of the transition layer in the three-phase configuration. Subsequently, we derive relevant discontinuity relations that the physical fields across the imperfect interface exhibit equivalently in the two-phase configuration.

5.1.1 Governing Equations

Let us consider that the material constituting the three-phase configuration exhibits linearly poroelastic behavior for each phase. This assumption serves as the basis for introducing a constitutive law, which provides a rigorous framework for understanding the mechanical behavior of porous materials under the influence of fluid pressure in isothermal conditions. This law, essential to our analysis, can be expressed concisely as follows:

$$\boldsymbol{\sigma} = \mathbb{C}\boldsymbol{\varepsilon} + \boldsymbol{\theta} p, \quad \boldsymbol{\varepsilon} = \mathbb{S}(\boldsymbol{\sigma} - \boldsymbol{\theta} p) \tag{5.1}$$

where, $\boldsymbol{\sigma}$ represents the stress tensor, $\boldsymbol{\varepsilon}$ denotes the strain tensor, and p signifies the fluid pressure. The tensors $\mathbb{C}$ and $\mathbb{S} = \mathbb{C}^{-1}$ characterize the elastic properties of the porous medium, representing the fourth-order stiffness and compliance elasticity tensors, respectively. These tensors possess symmetric components C_{ijkl} and M_{ijkl} satisfying the minor and major symmetries $C_{ijkl} = C_{jikl} = C_{klij}$ and $S_{ijkl} = S_{jikl} = S_{klij}$. Additionally, they exhibit positive definiteness. The term $\boldsymbol{\theta}$ denotes the Biot-Willis tensor, accounting for the interaction between the solid skeleton and the fluid phase. Similarly, the Biot-Willis tensor $\boldsymbol{\theta}$ is also symmetric, such as $\theta_{ij} = \theta_{ji}$. The infinitesimal strain tensor $\boldsymbol{\varepsilon}$ is determined by the displacement vector $\mathbf{u}$ as follows:

$$\boldsymbol{\varepsilon} = \frac{1}{2}[\nabla \mathbf{u} + (\nabla \mathbf{u})^T] \tag{5.2}$$

where, the symbol ∇ represents the gradient operator, while $(\cdot)^T$ denotes the transpose operation. In the absence of body forces, the stress tensor $\boldsymbol{\sigma}$ adheres to the equilibrium equation, expressed mathematically as:

$$\mathrm{div}\boldsymbol{\sigma} = 0. \tag{5.3}$$

The velocity vector $\mathbf{w}$, denoting the relative velocity of the fluid, follows the mass conservation equation:

$$\mathrm{div}\mathbf{w} = -\boldsymbol{\theta} : \dot{\boldsymbol{\varepsilon}} + \frac{\dot{p}}{\eta}. \tag{5.4}$$

Here, η denotes the Biot's modulus, and the dot indicates the time derivative. The relationship between the velocity vector $\mathbf{w}$ and the pore pressure p can be described by the Darcy law as

follows:

$$\mathbf{w} = -\mathbf{K}\nabla p, \tag{5.5}$$

where $\mathbf{K}$ represents the permeability tensor of the porous material.

The extended orthogonal projection operators $\mathbb{P}^{\perp}$ and $\mathbb{P}$ facilitate the decomposition of the strain tensor $\boldsymbol{\varepsilon}$ and the stress tensor $\boldsymbol{\sigma}$ into their respective in-plane and transverse components as follows:

$$\boldsymbol{\varepsilon} = \mathbb{P}^{\perp}\boldsymbol{\varepsilon} + \mathbb{P}\boldsymbol{\varepsilon}, \tag{5.6}$$

$$\boldsymbol{\sigma} = \mathbb{P}^{\perp}\boldsymbol{\sigma} + \mathbb{P}\boldsymbol{\sigma}. \tag{5.7}$$

Substituting these decompositions into the first part of the constitutive law (5.1) gives:

$$\mathbb{P}^{\perp}\boldsymbol{\sigma} + \mathbb{P}\boldsymbol{\sigma} = \mathbb{C}\mathbb{P}^{\perp}\boldsymbol{\varepsilon} + \mathbb{C}\mathbb{P}\boldsymbol{\varepsilon} + \boldsymbol{\theta}p. \tag{5.8}$$

Multiplying both sides by $\mathbb{P}^{\perp}$ and utilizing the properties (2.84) results in:

$$\mathbb{P}^{\perp}\mathbb{C}\mathbb{P}^{\perp}\boldsymbol{\varepsilon} = \mathbb{P}^{\perp}\boldsymbol{\sigma} - \mathbb{P}^{\perp}\mathbb{C}\mathbb{P}\boldsymbol{\varepsilon} - \mathbb{P}^{\perp}\boldsymbol{\theta}p. \tag{5.9}$$

Introducing the fourth-order tensor $\mathbb{B}$ as defined in (2.104) and considering its properties (2.105), the above equation is simplified to:

$$\mathbb{P}^{\perp}\boldsymbol{\varepsilon} = \mathbb{B}\boldsymbol{\sigma} - \mathbb{B}\mathbb{C}\mathbb{P}\boldsymbol{\varepsilon} - \mathbb{B}\boldsymbol{\theta}p. \tag{5.10}$$

By adding $\mathbb{P}\boldsymbol{\varepsilon}$ to both sides and applying the complementary property (4.28), the equation is transformed into:

$$\boldsymbol{\varepsilon} = \mathbb{B} : (\boldsymbol{\sigma} - \boldsymbol{\theta}p) + \mathbb{S} : \mathbb{A} : \boldsymbol{\varepsilon}. \tag{5.11}$$

Similarly, by substituting the decomposed forms of $\boldsymbol{\varepsilon}$ and $\boldsymbol{\sigma}$ into the second part of constitutive law (5.1), the following is obtained:

$$\mathbb{P}^{\perp}\boldsymbol{\varepsilon} + \mathbb{P}\boldsymbol{\varepsilon} = \mathbb{S}\mathbb{P}^{\perp}\boldsymbol{\sigma} + \mathbb{S}\mathbb{P}\boldsymbol{\sigma} - \mathbb{S}\boldsymbol{\theta}p. \tag{5.12}$$

Multiplying both sides by $\mathbb{P}$ and using the properties (2.84) yields:

$$\mathbb{PSP}\boldsymbol{\sigma} = \mathbb{P}\boldsymbol{\varepsilon} - \mathbb{PSP}^{\perp}\boldsymbol{\sigma} + \mathbb{PS}\boldsymbol{\theta}p \tag{5.13}$$

Introducing the fourth-order tensor $\mathbb{A}$ as defined in (2.99) and recalling its properties in (2.102), the above equation is rewritten as:

$$\mathbb{P}\boldsymbol{\sigma} = \mathbb{A}\boldsymbol{\varepsilon} - \mathbb{ASP}^{\perp}\boldsymbol{\sigma} + \mathbb{AS}\boldsymbol{\theta}p \tag{5.14}$$

Adding $\mathbb{P}^{\perp}\boldsymbol{\sigma}$ to both sides and applying the complementary property (4.28) results in:

$$\boldsymbol{\sigma} = \mathbb{A} : \boldsymbol{\varepsilon} + \mathbb{C} : \mathbb{B} : \boldsymbol{\sigma} + \mathbb{A} : \mathbb{S} : \boldsymbol{\theta}p. \tag{5.15}$$

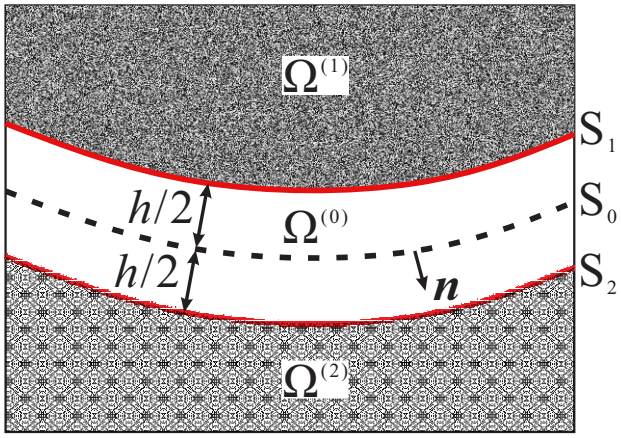

Figure 5.1: *The interphase $\Omega^{(0)}$ is bonded perfectly to its two neighboring phase $\Omega^{(1)}$ and $\Omega^{(2)}$ in three-phase configuration.*

5.1.2 The Relations for Perfect Interfaces and Imperfect Interfaces

As illustrated in **Fig.** 5.1, the domain of $\mathbb{R}^3$ is divided into three sub-domains, $\Omega^{(0)}$, $\Omega^{(1)}$, and $\Omega^{(2)}$, by a curved interphase with uniform thickness h. The notation $\Omega^{(i)}$ $(i = 0, 1, 2)$ designates the sub-domain occupied by different materials, such as the interphase ($\Omega^{(0)}$) and phase 1 ($\Omega^{(1)}$). The behavior of materials within these sub-domains is linear and governed by equations (5.11) and (5.15). The interphase is assumed to bond the phase 1 and phase 2 perfectly, namely the surface S_1 and S_2 are both perfect. To continue the derivation, we introduce the discontinuity re-

lation proposed by Hadamard [57] regarding a function that remains continuous across a surface $S_i(i=1,2)$ within its domain Ω but lacks continuous differentiability at S_i. For illustrative purposes, we discuss the case at S_1, where the functions confined within $\Omega^{(1)}$ and $\Omega^{(0)}$ are denoted as $(\cdot)^{(1)}$ and $(\cdot)^{(0)}$ respectively. Analogous considerations hold for S_2. The Hadamard relations for the scalar function φ and the vector function $\mathbf{g}$, presumed to be continuously and piecewise continuously differentiable over $\Omega^{(i)}$ $(i=0,1)$ but not necessarily continuously differentiable at S_1, are expressed as follows:

$$\nabla_S \varphi^{(1)} = \nabla_S \varphi^{(0)} \qquad \text{on} \quad S_1, \tag{5.16}$$

$$\nabla_S \mathbf{g}^{(1)} = \nabla_S \mathbf{g}^{(0)} \qquad \text{on} \quad S_1, \tag{5.17}$$

$$\mathrm{div}_S \mathbf{g}^{(1)} = \mathrm{div}_S \mathbf{g}^{(0)} \qquad \text{on} \quad S_1. \tag{5.18}$$

Consider an interface S_0, parallel to the surface S_1 and S_2, which geometrically lies midway between S_1 and S_2 [100]. The distance of a point $\mathbf{x} \in S_0$ to S_1 and S_2 are both equal to $h/2$. The connections of S_0 to S_1 and S_2 at point x can be established by the distance h, described mathematically as follows:

$$\begin{cases} S_0 = \{\mathbf{x} \in \Omega | f(\mathbf{x}) = 0\}; \\ S_1 = \{\mathbf{y} \in \mathbb{R}^3 | \mathbf{y} = \mathbf{x} - h\mathbf{n}(\mathbf{x}), \mathbf{x} \in S_0\}; \\ S_2 = \{\mathbf{y} \in \mathbb{R}^3 | \mathbf{y} = \mathbf{x} + h\mathbf{n}(\mathbf{x}), \mathbf{x} \in S_0\}. \end{cases} \tag{5.19}$$

It is evident that S_i $(i=0,1,2)$ represent perfect interfaces, with certain fields demonstrating continuity across them, as specified in equations (2.29), (2.30), (2.73), and (2.75). They can be uniformly represented as:

$$(\cdot)^{(+)}|_{S_i} = (\cdot)^{(-)}|_{S_i}. \tag{5.20}$$

Here, $(\cdot)^{(+)}$ and $(\cdot)^{(-)}$ denote the physical quantities involved in equations (2.29), (2.30), (2.73), and (2.75) on the respective sides of the interface. In this section, the following physical quanti-

ties are considered:

$$\begin{cases} p^{(+)}|_{S_i} = p^{(-)}|_{S_i}, & \mathbf{u}^{(+)}|_{S_i} = \mathbf{u}^{(-)}|_{S_i}, \\ \nabla_S p^{(+)}|_{S_i} = \nabla_S p^{(-)}|_{S_i}, & (\mathbf{w}\cdot\mathbf{n})^{(+)}|_{S_i} = (\mathbf{w}\cdot\mathbf{n})^{(-)}|_{S_i}, \\ \mathbb{P}\boldsymbol{\varepsilon}^{(+)}|_{S_i} = \mathbb{P}\boldsymbol{\varepsilon}^{(-)}|_{S_i}, & \mathbb{P}^{\perp}\boldsymbol{\sigma}^{(+)}|_{S_i} = \mathbb{P}^{\perp}\boldsymbol{\sigma}^{(-)}|_{S_i}. \end{cases} \tag{5.21}$$

On these basic, the displacement vector $\mathbf{u}$ on the middle surface S_0 of the three-phase composite can be approximated by its quantity on the adjacent surface S_1 or surface S_2 with a Taylor expansion:

$$\begin{aligned} \mathbf{u}^{(0)}|_{S_0} &= \mathbf{u}^{(0)}|_{S_2} - \frac{h}{2}(\nabla\mathbf{u}^{(0)}\cdot\mathbf{n})|_{S_2} + \mathbf{0}(h^2), \\ \mathbf{u}^{(0)}|_{S_0} &= \mathbf{u}^{(0)}|_{S_1} + \frac{h}{2}(\nabla\mathbf{u}^{(0)}\cdot\mathbf{n})|_{S_1} + \mathbf{0}(h^2). \end{aligned} \tag{5.22}$$

The following equation is derived by subtracting the two preceding equations and applying the properties of the perfect surfaces S_1 and S_2, specifically the conditions related to $\mathbf{u}$ as detailed in equation (5.21):

$$\mathbf{u}^{(2)}|_{S_2} - \mathbf{u}^{(1)}|_{S_1} = \frac{h}{2}[(\boldsymbol{\varepsilon}^{(0)}\cdot\mathbf{n})|_{S_2} + (\boldsymbol{\varepsilon}^{(0)}\cdot\mathbf{n})|_{S_1}] + \mathbf{0}(h^2). \tag{5.23}$$

By substituting the first part of the recast constitutive equation (5.11) into the above equation and applying the properties of the perfect surface S_1 and S_2 (5.21), we obtain:

$$\begin{aligned} \mathbf{u}^{(2)}|_{S_2} - \mathbf{u}^{(1)}|_{S_1} =& \frac{h}{2}(\mathbb{B}^{(0)} : \boldsymbol{\sigma}^{(2)} - \mathbb{B}^{(0)} : \boldsymbol{\theta}^{(0)} p^{(2)} + \mathbb{S}^{(0)} : \mathbb{A}^{(0)} : \boldsymbol{\varepsilon}^{(2)})|_{S_2}\cdot\mathbf{n} \\ &+ \frac{h}{2}(\mathbb{B}^{(0)} : \boldsymbol{\sigma}^{(1)} - \mathbb{B}^{(0)} : \boldsymbol{\theta}^{(0)} p^{(1)} + \mathbb{S}^{(0)} : \mathbb{A}^{(0)} : \boldsymbol{\varepsilon}^{(1)})|_{S_1}\cdot\mathbf{n} + \mathbf{0}(h^2). \end{aligned} \tag{5.24}$$

It is worth noting that, in the derivation above, we have utilized the properties of the operators $\mathbb{B}$ and $\mathbb{A}$, specifically $\mathbb{B}\mathbb{P}^{\perp} = \mathbb{B}$ and $\mathbb{A}\mathbb{P} = \mathbb{A}$.

The stress vector $\mathbf{t} = \boldsymbol{\sigma}\cdot\mathbf{n}$ mentioned previously is continuity when it across the perfect interface. The stress vector $\mathbf{t}$ on the middle surface S_0 of the three-phase composite can be ap-

proximated by its value on either the adjacent surface S_1 or surface S_2 using a Taylor expansion:

$$\begin{aligned}\mathbf{t}^{(0)}|_{S_0} &= \mathbf{t}^{(0)}|_{S_2} - \frac{h}{2}(\nabla\mathbf{t}^{(0)}\cdot\mathbf{n})|_{S_2} + \mathbf{0}(h^2),\\ \mathbf{t}^{(0)}|_{S_0} &= \mathbf{t}^{(0)}|_{S_1} + \frac{h}{2}(\nabla\mathbf{t}^{(0)}\cdot\mathbf{n})|_{S_1} + \mathbf{0}(h^2).\end{aligned} \tag{5.25}$$

Subtracting the first expression from the second yields:

$$\mathbf{t}^{(2)}|_{S_2} - \mathbf{t}^{(1)}|_{S_1} = \frac{h}{2}[(\nabla\mathbf{t}^{(0)}\cdot\mathbf{n})|_{S_2} + (\nabla\mathbf{t}^{(0)}\cdot\mathbf{n})|_{S_1}] + \mathbf{0}(h^2). \tag{5.26}$$

Based on the previous definition of stress vector $\mathbf{t}$, the term $\nabla\mathbf{t}\cdot\mathbf{n}$ can be further expanded as:

$$\nabla\mathbf{t}\cdot\mathbf{n} = \nabla(\boldsymbol{\sigma}\cdot\mathbf{n}) = (\nabla\boldsymbol{\sigma}\cdot\mathbf{n})\cdot\mathbf{n} + \boldsymbol{\sigma}\cdot(\nabla\mathbf{n}\cdot\mathbf{n}). \tag{5.27}$$

Given the fact that $\nabla\mathbf{n}\cdot\mathbf{n} = \mathbf{0}$, it follows that:

$$\nabla\mathbf{t}\cdot\mathbf{n} = \nabla\boldsymbol{\sigma} : \mathbf{N} = div_N\boldsymbol{\sigma}. \tag{5.28}$$

Since the stress tensor $\boldsymbol{\sigma}$ is divergence-free, and recognizing that the divergence can be decomposed as $\mathrm{div}\boldsymbol{\sigma} = \mathrm{div}_N\boldsymbol{\sigma} + \mathrm{div}_S\boldsymbol{\sigma}$, we derive the important relation:

$$\nabla\mathbf{t}\cdot\mathbf{n} = -\mathrm{div}_S\boldsymbol{\sigma}. \tag{5.29}$$

By substituting the second part of the recast constitutive equation (5.15) into the preceding equation, we obtain the following result:

$$\nabla\mathbf{t}\cdot\mathbf{n} = -div_S(\mathbb{A} : \boldsymbol{\varepsilon} + \mathbb{C} : \mathbb{B} : \boldsymbol{\sigma} + \mathbb{A} : \mathbb{S} : \boldsymbol{\theta}p). \tag{5.30}$$

By incorporating this expression into equation (5.25) and applying the properties of the perfect surface S_1 and S_2 (5.21), we obtain the following relation for the stress vector:

$$\begin{aligned}\mathbf{t}^{(2)}|_{S_2} - \mathbf{t}^{(1)}|_{S_1} = &-\frac{h}{2}\mathrm{div}_S(\mathbb{A}^{(0)} : \boldsymbol{\varepsilon}^{(2)} + \mathbb{C}^{(0)} : \mathbb{B}^{(0)} : \boldsymbol{\sigma}^{(2)} + \mathbb{A}^{(0)} : \mathbb{S}^{(0)} : \boldsymbol{\theta}^{(0)}p^{(2)})|_{S_2}\\ &-\frac{h}{2}\mathrm{div}_S(\mathbb{A}^{(0)} : \boldsymbol{\varepsilon}^{(1)} + \mathbb{C}^{(0)} : \mathbb{B}^{(0)} : \boldsymbol{\sigma}^{(1)} + \mathbb{A}^{(0)} : \mathbb{S}^{(0)} : \boldsymbol{\theta}^{(0)}p^{(1)})|_{S_1} + \mathbf{0}(h^2).\end{aligned} \tag{5.31}$$

Similarly, the pore pressure p on the middle surface S_0 of the three-phase composite can be

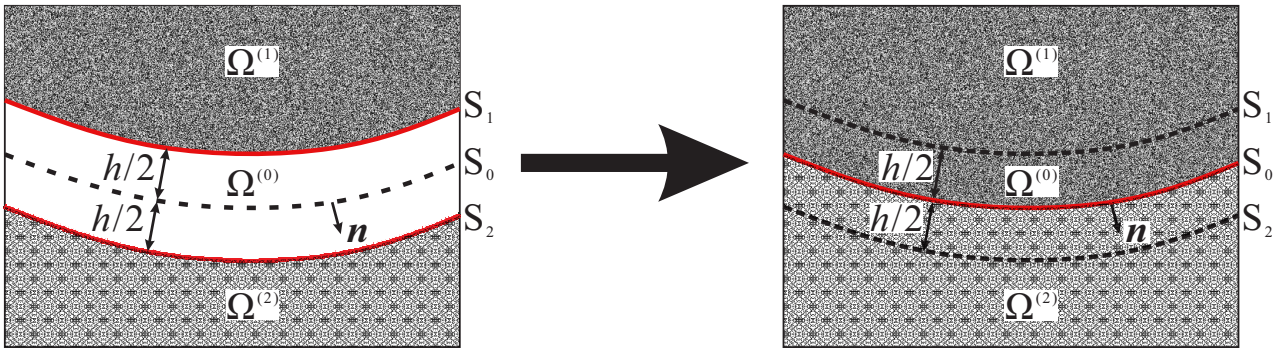

Figure 5.2: *The transformation of three-phase configuration into two-phase configuration by replacing the interphase $\Omega^{(0)}$ with the imperfect interface S_0.*

approximated using a Taylor series expansion around the adjacent surfaces S_1 and S_2, leading to the following expressions:

$$\begin{aligned} p^{(0)}|_{S_0} &= p^{(0)}|_{S_2} - \frac{h}{2}(\nabla p^{(0)} \cdot \mathbf{n})|_{S_2} + 0(h^2), \\ p^{(0)}|_{S_0} &= p^{(0)}|_{S_1} + \frac{h}{2}(\nabla p^{(0)} \cdot \mathbf{n})|_{S_1} + 0(h^2). \end{aligned} \tag{5.32}$$

By subtracting these two equations and taking into account the continuity of p across the perfect interface, the following result is obtained:

$$p^{(2)}|_{S_2} - p^{(1)}|_{S_1} = \frac{h}{2}[(\nabla p^{(0)} \cdot \mathbf{n})|_{S_2} + (\nabla p^{(0)} \cdot \mathbf{n})|_{S_1}] + 0(h^2). \tag{5.33}$$

While the normal fluid flux w_n on the middle surface S_0 of a three-phase composite can be approximated by a Taylor series expansion around the adjacent surfaces S_1 and S_2, yielding:

$$\begin{aligned} w_n^{(0)}|_{S_0} &= w_n^{(0)}|_{S_2} - \frac{h}{2}(\nabla w_n^{(0)} \cdot \mathbf{n})|_{S_2} + 0(h^2), \\ w_n^{(0)}|_{S_0} &= w_n^{(0)}|_{S_1} + \frac{h}{2}(\nabla w_n^{(0)} \cdot \mathbf{n})|_{S_1} + 0(h^2). \end{aligned} \tag{5.34}$$

Considering the continuity of w_n across the perfect interface and subtracting the previous two equations yields:

$$w_n^{(2)}|_{S_2} - w_n^{(1)}|_{S_1} = \frac{h}{2}[(\nabla w_n^{(0)} \cdot \mathbf{n})|_{S_2} + (\nabla w_n^{(0)} \cdot \mathbf{n})|_{S_1}] + 0(h^2). \tag{5.35}$$

5.1.3 Jumps Across the Imperfect Interface in the Two-Phase Configuration

As mentioned before, in the two-phase configuration, the transition layer is replaced by the imperfect surface S_0 with the neighboring phases 1 and 2 being extended to the surface S_0. The domain $\mathbb{R}^3$ is regarded as divided into two sub-domains $\Omega^{(-)}$ and $\Omega^{(+)}$ by the surface S_0 as shown in Figure 5.2. To physically equivalent the three-phase configuration with the two-phase configuration, the physical fields across the imperfect interface S_0 must satisfy certain discontinuous relations that characterize the jump of the physical field across the domain restricted by the surfaces S_1 and S_2 in the three-phase configuration.

Applying the Taylor expansion, the displacement vector $\mathbf{u}$ on the surfaces S_1 and S_2 can be conveyed by the vector $\mathbf{u}$ on the imperfect interface with an error of order $0(h^2)$

$$\begin{aligned}\mathbf{u}^{(2)}|_{S_2} &= \mathbf{u}^{(+)} + \frac{h}{2}(\nabla\mathbf{u}^{(+)}\cdot\mathbf{n}) + \mathbf{0}(h^2),\\ \mathbf{u}^{(1)}|_{S_1} &= \mathbf{u}^{(-)} - \frac{h}{2}(\nabla\mathbf{u}^{(-)}\cdot\mathbf{n}) + \mathbf{0}(h^2),\end{aligned} \tag{5.36}$$

where $(\cdot)^{(+)}$ denotes the physical parameter evaluated on the phase 2 side of S_0 and the value $(\cdot)^{(-)}$ is on the phase 1 side of S_0. By subtracting these two equations, we obtain the following relation:

$$\mathbf{u}^{(2)}|_{S_2} - \mathbf{u}^{(1)}|_{S_1} = [\![\mathbf{u}]\!] + \frac{h}{2}(\boldsymbol{\varepsilon}^{(+)}\cdot\mathbf{n} + \boldsymbol{\varepsilon}^{(-)}\cdot\mathbf{n}) + \mathbf{0}(h^2), \tag{5.37}$$

where, the jump operator $[\![\cdot]\!]$ is defined as $[\![\cdot]\!] = (\cdot)^{(+)} - (\cdot)^{(-)}$ denoting the discontinuity of the quantity $(\cdot)$ across the interface S_0. Substituting equation (5.24) into this expression yields the following result:

$$\begin{aligned}[\![\mathbf{u}]\!] =& \frac{h}{2}[(\mathbb{B}^{(0)} : \boldsymbol{\sigma}^{(2)} - \mathbb{B}^{(0)} : \boldsymbol{\theta}^{(0)} p^{(2)} + \mathbb{S}^{(0)} : \mathbb{A}^{(0)} : \boldsymbol{\varepsilon}^{(2)})\cdot\mathbf{n}]|_{S_2}\\ &+ \frac{h}{2}[(\mathbb{B}^{(0)} : \boldsymbol{\sigma}^{(1)} - \mathbb{B}^{(0)} : \boldsymbol{\theta}^{(0)} p^{(1)} + \mathbb{S}^{(0)} : \mathbb{A}^{(0)} : \boldsymbol{\varepsilon}^{(1)})\cdot\mathbf{n}]|_{S_1}\\ &- \frac{h}{2}(\boldsymbol{\varepsilon}^{(+)} + \boldsymbol{\varepsilon}^{(-)})\cdot\mathbf{n} + \mathbf{0}(h^2).\end{aligned} \tag{5.38}$$

Next, applying the Taylor expansion gives the following expressions:

$$\begin{aligned}&(\mathbb{B}^{(0)}:\boldsymbol{\sigma}^{(2)}-\mathbb{B}^{(0)}:\boldsymbol{\theta}^{(0)}p^{(2)}+\mathbb{S}^{(0)}:\mathbb{A}^{(0)}:\boldsymbol{\varepsilon}^{(2)})|_{S_2}\\&=\mathbb{B}^{(0)}:\boldsymbol{\sigma}^{(+)}-\mathbb{B}^{(0)}:\boldsymbol{\theta}^{(0)}p^{(+)}+\mathbb{S}^{(0)}:\mathbb{A}^{(0)}:\boldsymbol{\varepsilon}^{(+)}+\mathbf{0}(h),\end{aligned}\tag{5.39}$$

and

$$\begin{aligned}&(\mathbb{B}^{(0)}:\boldsymbol{\sigma}^{(1)}-\mathbb{B}^{(0)}:\boldsymbol{\theta}^{(0)}p^{(1)}+\mathbb{S}^{(0)}:\mathbb{A}^{(0)}:\boldsymbol{\varepsilon}^{(1)})|_{S_1}\\&=\mathbb{B}^{(0)}:\boldsymbol{\sigma}^{(-)}-\mathbb{B}^{(0)}:\boldsymbol{\theta}^{(0)}p^{(-)}+\mathbb{S}^{(0)}:\mathbb{A}^{(0)}:\boldsymbol{\varepsilon}^{(-)}+\mathbf{0}(h).\end{aligned}\tag{5.40}$$

Utilizing equation (5.11), we establish the following relationship:

$$\begin{aligned}\boldsymbol{\varepsilon}^{(+)}+\boldsymbol{\varepsilon}^{(-)}=&\mathbb{S}^{(2)}:\mathbb{A}^{(2)}:\boldsymbol{\varepsilon}^{(+)}+\mathbb{B}^{(2)}:\boldsymbol{\sigma}^{(+)}-\mathbb{B}^{(2)}:\boldsymbol{\theta}^{(2)}p^{(+)}\\&+\mathbb{S}^{(1)}:\mathbb{A}^{(1)}:\boldsymbol{\varepsilon}^{(-)}+\mathbb{B}^{(1)}:\boldsymbol{\sigma}^{(-)}-\mathbb{B}^{(1)}:\boldsymbol{\theta}^{(1)}p^{(-)}.\end{aligned}\tag{5.41}$$

Substituting equations (5.39)-(5.41) into equation (5.38), we obtain the following jump condition

$$\begin{aligned}[\![\mathbf{u}]\!]=&\frac{h}{2}[(\mathbb{S}^{(0)}:\mathbb{A}^{(0)}-\mathbb{S}^{(2)}:\mathbb{A}^{(2)}):\boldsymbol{\varepsilon}^{(+)}+(\mathbb{S}^{(0)}:\mathbb{A}^{(0)}-\mathbb{S}^{(1)}:\mathbb{A}^{(1)}):\boldsymbol{\varepsilon}^{(-)}]\cdot\mathbf{n}\\&-\frac{h}{2}[(\mathbb{B}^{(0)}:\boldsymbol{\theta}^{(0)}-\mathbb{B}^{(2)}:\boldsymbol{\theta}^{(2)})p^{(+)}+(\mathbb{B}^{(0)}:\boldsymbol{\theta}^{(0)}-\mathbb{B}^{(1)}:\boldsymbol{\theta}^{(1)})p^{(-)}]\cdot\mathbf{n}\\&+\frac{h}{2}[(\mathbb{B}^{(0)}-\mathbb{B}^{(2)})\boldsymbol{\sigma}^{(+)}+(\mathbb{B}^{(0)}-\mathbb{B}^{(1)})\boldsymbol{\sigma}^{(+)}]\cdot\mathbf{n}+\mathbf{0}(h^2).\end{aligned}\tag{5.42}$$

Using equation (2.104), we observe that $\mathbf{n}\mathbb{B}\boldsymbol{\sigma}=\mathbf{F}\cdot\mathbf{t}$. Substituting this relation into the previous expression, the equation can be reformulated as follows:

$$\begin{aligned}[\![\mathbf{u}]\!]=&\frac{h}{2}[(\mathbb{S}^{(0)}:\mathbb{A}^{(0)}-\mathbb{S}^{(2)}:\mathbb{A}^{(2)}):\boldsymbol{\varepsilon}^{(+)}+(\mathbb{S}^{(0)}:\mathbb{A}^{(0)}-\mathbb{S}^{(1)}:\mathbb{A}^{(1)}):\boldsymbol{\varepsilon}^{(-)}]\cdot\mathbf{n}\\&-\frac{h}{2}[(\mathbb{B}^{(0)}:\boldsymbol{\theta}^{(0)}-\mathbb{B}^{(2)}:\boldsymbol{\theta}^{(2)})p^{(+)}+(\mathbb{B}^{(0)}:\boldsymbol{\theta}^{(0)}-\mathbb{B}^{(1)}:\boldsymbol{\theta}^{(1)})p^{(-)}]\cdot\mathbf{n}\\&+\frac{h}{2}[(\mathbf{F}^{(0)}-\mathbf{F}^{(2)})\cdot\mathbf{t}^{(+)}+(\mathbf{F}^{(0)}-\mathbf{F}^{(1)})\cdot\mathbf{t}^{(-)}]+\mathbf{0}(h^2).\end{aligned}\tag{5.43}$$

For the traction vector $\mathbf{t}$ in the two-phase configuration, we can derive the following using Taylor expansion:

$$\mathbf{t}^{(2)}|_{S_2}-\mathbf{t}^{(1)}|_{S_1}=[\![\mathbf{t}]\!]+\frac{h}{2}(\nabla\mathbf{t}^{(+)}\cdot\mathbf{n}+\nabla\mathbf{t}^{(-)}\cdot\mathbf{n})+\mathbf{0}(h^2).\tag{5.44}$$

Incorporating equations (5.31) and (5.30) into the preceding expression, we obtain:

$$\begin{aligned}[\![\mathbf{t}]\!] =& -\frac{h}{2}\mathrm{div}_S(\mathbb{A}^{(0)}:\boldsymbol{\varepsilon}^{(2)}+\mathbb{C}^{(0)}:\mathbb{B}^{(0)}:\boldsymbol{\sigma}^{(2)}+\mathbb{A}^{(0)}:\mathbb{S}^{(0)}:\boldsymbol{\theta}^{(0)}p^{(2)})|_{S_2}\\ &-\frac{h}{2}\mathrm{div}_S(\mathbb{A}^{(0)}:\boldsymbol{\varepsilon}^{(1)}+\mathbb{C}^{(0)}:\mathbb{B}^{(0)}:\boldsymbol{\sigma}^{(1)}+\mathbb{A}^{(0)}:\mathbb{S}^{(0)}:\boldsymbol{\theta}^{(0)}p^{(1)})|_{S_1}\\ &+\frac{h}{2}\mathrm{div}_S(\mathbb{A}^{(2)}:\boldsymbol{\varepsilon}^{(+)}+\mathbb{C}^{(2)}:\mathbb{B}^{(2)}:\boldsymbol{\sigma}^{(+)}+\mathbb{A}^{(2)}:\mathbb{S}^{(2)}:\boldsymbol{\theta}^{(2)}p^{(+)})\\ &+\frac{h}{2}\mathrm{div}_S(\mathbb{A}^{(1)}:\boldsymbol{\varepsilon}^{(-)}+\mathbb{C}^{(1)}:\mathbb{B}^{(1)}:\boldsymbol{\sigma}^{(-)}+\mathbb{A}^{(1)}:\mathbb{S}^{(1)}:\boldsymbol{\theta}^{(1)}p^{(-)})+\mathbf{0}(h^2).\end{aligned} \tag{5.45}$$

Using Taylor expansion, we can express the following:

$$\begin{aligned}&(\mathbb{A}^{(0)}:\boldsymbol{\varepsilon}^{(2)}+\mathbb{C}^{(0)}:\mathbb{B}^{(0)}:\boldsymbol{\sigma}^{(2)}+\mathbb{A}^{(0)}:\mathbb{S}^{(0)}:\boldsymbol{\theta}^{(0)}p^{(2)})|_{S_2}\\ &=\mathbb{A}^{(0)}:\boldsymbol{\varepsilon}^{(+)}+\mathbb{C}^{(0)}:\mathbb{B}^{(0)}:\boldsymbol{\sigma}^{(+)}+\mathbb{A}^{(0)}:\mathbb{S}^{(0)}:\boldsymbol{\theta}^{(0)}p^{(+)}+\mathbf{0}(h),\end{aligned} \tag{5.46}$$

and

$$\begin{aligned}&(\mathbb{A}^{(0)}:\boldsymbol{\varepsilon}^{(1)}+\mathbb{C}^{(0)}:\mathbb{B}^{(0)}:\boldsymbol{\sigma}^{(1)}+\mathbb{A}^{(0)}:\mathbb{S}^{(0)}:\boldsymbol{\theta}^{(0)}p^{(1)})|_{S_1}\\ &=\mathbb{A}^{(0)}:\boldsymbol{\varepsilon}^{(-)}+\mathbb{C}^{(0)}:\mathbb{B}^{(0)}:\boldsymbol{\sigma}^{(-)}+\mathbb{A}^{(0)}:\mathbb{S}^{(0)}:\boldsymbol{\theta}^{(0)}p^{(-)}+\mathbf{0}(h).\end{aligned} \tag{5.47}$$

Thus, substituting these expressions into equation (5.45) yields:

$$\begin{aligned}[\![\mathbf{t}]\!] =&\frac{h}{2}\mathrm{div}_S[(\mathbb{A}^{(2)}:\mathbb{S}^{(2)}:\boldsymbol{\theta}^{(2)}-\mathbb{A}^{(0)}:\mathbb{S}^{(0)}:\boldsymbol{\theta}^{(0)})p^{(+)}+(\mathbb{A}^{(1)}:\mathbb{S}^{(1)}:\boldsymbol{\theta}^{(1)}-\mathbb{A}^{(0)}:\mathbb{S}^{(0)}:\boldsymbol{\theta}^{(0)})p^{(-)}]\\ &+\frac{h}{2}\mathrm{div}_S[(\mathbb{C}^{(2)}:\mathbb{B}^{(2)}-\mathbb{C}^{(0)}:\mathbb{B}^{(0)}):\boldsymbol{\sigma}^{(+)}+(\mathbb{C}^{(1)}:\mathbb{B}^{(1)}-\mathbb{C}^{(0)}:\mathbb{B}^{(0)}):\boldsymbol{\sigma}^{(-)}]\\ &+\frac{h}{2}\mathrm{div}_S[(\mathbb{A}^{(2)}-\mathbb{A}^{(0)}):\boldsymbol{\varepsilon}^{(+)}+(\mathbb{A}^{(1)}-\mathbb{A}^{(0)}):\boldsymbol{\varepsilon}^{(-)}]+\mathbf{0}(h^2).\end{aligned} \tag{5.48}$$

While for the pore pressure p in the two-phase configuration, we can derive the following using Taylor expansion:

$$\begin{aligned}p^{(2)}|_{S_2} &= p^{(+)}+\frac{h}{2}(\nabla p^{(+)}\cdot\mathbf{n})+0(h^2),\\ p^{(1)}|_{S_1} &= p^{(-)}-\frac{h}{2}(\nabla p^{(-)}\cdot\mathbf{n})+0(h^2),\end{aligned} \tag{5.49}$$

By subtracting the above two equations, the following relation is obtained:

$$p^{(2)}|_{S_2}-p^{(1)}|_{S_1}=[\![p]\!]+\frac{h}{2}(\nabla p^{(+)}\cdot\mathbf{n}+\nabla p^{(-)}\cdot\mathbf{n})+0(h^2). \tag{5.50}$$

Substituting (5.33) into the above equation yields:

$$[\![p]\!] = \frac{h}{2}[(\nabla p^{(0)} \cdot \mathbf{n})|_{S_2} + (\nabla p^{(0)} \cdot \mathbf{n})|_{S_1} - (\nabla p^{(+)} \cdot \mathbf{n} + \nabla p^{(-)} \cdot \mathbf{n})] + 0(h^2). \tag{5.51}$$

Recalling Darcy's law (5.5), we can decompose the normal fluid flux $w_n = \mathbf{w} \cdot \mathbf{n}$ as follows:

$$\mathbf{w} \cdot \mathbf{n} = -(\mathbf{K} \cdot \nabla p) \cdot \mathbf{n} = -[\mathbf{K} \cdot (\mathbf{T} + \mathbf{N}) \cdot \nabla p] \cdot \mathbf{n}, \tag{5.52}$$

which can be further rewritten as:

$$w_n = \mathbf{n} \cdot \mathbf{K} \cdot \nabla_S p - (\mathbf{n} \cdot \mathbf{K}\mathbf{n}) \nabla p \cdot \mathbf{n}. \tag{5.53}$$

Considering the positive definiteness of $\mathbf{K}$, which implies that $\mathbf{n} \cdot \mathbf{K}\mathbf{n} \neq 0$, we can derive from the above expression that:

$$\nabla p \cdot \mathbf{n} = -\frac{w_n}{\mathbf{n} \cdot \mathbf{K}\mathbf{n}} - \frac{\mathbf{n} \cdot \mathbf{K}}{\mathbf{n} \cdot \mathbf{K}\mathbf{n}} \cdot \nabla_S p. \tag{5.54}$$

We introduce the following definitions:

$$k_{nn} = \mathbf{n} \cdot \mathbf{K}\mathbf{n}, \quad \mathbf{s} = \frac{\mathbf{n} \cdot \mathbf{K}}{\mathbf{n} \cdot \mathbf{K}\mathbf{n}}. \tag{5.55}$$

Substituting these definitions into (5.54), the expression simplifies to:

$$\nabla p \cdot \mathbf{n} = -\frac{w_n}{k_{nn}} - \mathbf{s} \nabla_S p. \tag{5.56}$$

Applying the Taylor expansion, we obtain:

$$\begin{aligned} (-\frac{w_n^{(0)}}{k_{nn}^{(0)}} - \mathbf{s}^{(0)} \nabla_S p^{(0)})|_{S_2} &= -\frac{w_n^{(+)}}{k_{nn}^{(0)}} - \mathbf{s}^{(0)} \nabla_S p^{(+)} + 0(h), \\ (-\frac{w_n^{(0)}}{k_{nn}^{(0)}} - \mathbf{s}^{(0)} \nabla_S p^{(0)})|_{S_1} &= -\frac{w_n^{(-)}}{k_{nn}^{(0)}} - \mathbf{s}^{(0)} \nabla_S p^{(-)} + 0(h). \end{aligned} \tag{5.57}$$

According formula (5.56), it follows that

$$\nabla p^{(+)} \cdot \mathbf{n} + \nabla p^{(-)} \cdot \mathbf{n} = -\frac{w_n^{(+)}}{k_{nn}^{(2)}} - \mathbf{s}^{(2)} \nabla_S p^{(+)} - \frac{w_n^{(+)}}{k_{nn}^{(1)}} - \mathbf{s}^{(1)} \nabla_S p^{(+)}. \tag{5.58}$$

By substituting (5.57) and (5.58) into (5.51), we derive the pressure jump $[\![p]\!]$ as follows:

$$[\![p]\!] = \frac{h}{2}\left[\frac{w_n^{(+)}}{k_{nn}^{(2)}} + \frac{w_n^{(-)}}{k_{nn}^{(1)}} - \frac{w_n^{(+)}}{k_{nn}^{(0)}} - \frac{w_n^{(-)}}{k_{nn}^{(0)}}\right] - \frac{h}{2}\left[(\mathbf{s}^{(0)} - \mathbf{s}^{(1)})\nabla_S p^{(-)} + (\mathbf{s}^{(0)} - \mathbf{s}^{(2)})\nabla_S p^{(+)}\right] + 0(h^2). \tag{5.59}$$

And for the normal fluid flux in the two-phase configuration, the following can be derived using a Taylor expansion:

$$\begin{aligned} w_n^{(2)}|_{S_2} &= w_n^{(+)} + \frac{h}{2}(\nabla w_n^{(+)} \cdot \mathbf{n}) + 0(h^2), \\ w_n^{(1)}|_{S_1} &= w_n^{(-)} - \frac{h}{2}(\nabla w_n^{(-)} \cdot \mathbf{n}) + 0(h^2). \end{aligned} \tag{5.60}$$

Subtracting the above two equations yields the following relation:

$$w_n^{(2)}|_{S_2} - w_n^{(1)}|_{S_1} = [\![w_n]\!] + \frac{h}{2}(\nabla w_n^{(+)} \cdot \mathbf{n} + \nabla w_n^{(-)} \cdot \mathbf{n}) + 0(h^2), \tag{5.61}$$

Substituting equation (5.35) into the above expression results in:

$$[\![w_n]\!] = \frac{h}{2}[(\nabla w_n^{(0)} \cdot \mathbf{n})|_{S_2} + (\nabla w_n^{(0)} \cdot \mathbf{n})|_{S_1} - (\nabla w_n^{(+)} \cdot \mathbf{n} + \nabla w_n^{(-)} \cdot \mathbf{n})] + 0(h^2). \tag{5.62}$$

Recalling the definition of w_n and the fact that $\nabla \mathbf{n} \cdot \mathbf{n} = 0$, we obtain:

$$\nabla w_n \cdot \mathbf{n} = \nabla \mathbf{w} : \mathbf{N} + \mathbf{w} \cdot (\nabla \mathbf{n}) \cdot \mathbf{n} = \mathrm{div}_N \mathbf{w}. \tag{5.63}$$

According to equation (5.4), it follows that:

$$\mathrm{div}_N \mathbf{w} = -\mathrm{div}_S \mathbf{w} - \boldsymbol{\theta} : \dot{\boldsymbol{\varepsilon}} + \frac{\dot{p}}{\eta}. \tag{5.64}$$

The term $\mathrm{div}_S\mathbf{w}$ can be expanded as:

$$\mathrm{div}_S\mathbf{w} = -\nabla(\mathbf{K}\cdot(\mathbf{N}+\mathbf{T})p) : \mathbf{T} = -\mathrm{div}_S(\mathbf{K}\cdot\nabla_S p) - \nabla[(\mathbf{K}\cdot\mathbf{n})(\nabla p\cdot\mathbf{n})] : \mathbf{T}. \tag{5.65}$$

Applying the expression for $\nabla p\cdot\mathbf{n}$ from equation (5.54), we get:

$$\begin{aligned}\nabla[(\mathbf{K}\cdot\mathbf{n})(\nabla p\cdot\mathbf{n})] : \mathbf{T} &= \nabla[-\frac{\mathbf{Kn}}{\mathbf{n}\cdot\mathbf{Kn}}w_n - \frac{(\mathbf{Kn})\otimes(\mathbf{n}\cdot\mathbf{K})}{\mathbf{n}\cdot\mathbf{Kn}}\nabla_S p] : \mathbf{T} \\ &= \mathrm{div}_S[-\mathbf{s}w_n - \frac{(\mathbf{Kn})\otimes(\mathbf{n}\cdot\mathbf{K})}{\mathbf{n}\cdot\mathbf{Kn}}\nabla_S p].\end{aligned} \tag{5.66}$$

Substituting equations (5.65) and (5.66) into (5.64) and defining $\mathbf{D} = \mathbf{K} - \frac{(\mathbf{Kn})\otimes(\mathbf{n}\cdot\mathbf{K})}{\mathbf{n}\cdot\mathbf{Kn}}$, yields:

$$\nabla w_n\cdot\mathbf{n} = \mathrm{div}_S(-\mathbf{s}w_n + \mathbf{D}\cdot\nabla_S p) - \boldsymbol{\theta} : \dot{\varepsilon} + \frac{\dot{p}}{\eta}. \tag{5.67}$$

By applying the Taylor expansion, the following expressions are obtained:

$$\begin{aligned}&[\mathrm{div}_S(-\mathbf{s}^{(0)}w_n^{(0)} + \mathbf{D}^{(0)}\cdot\nabla_S p^{(0)}) - \boldsymbol{\theta}^{(0)} : \dot{\varepsilon}^{(0)} + \frac{\dot{p}^{(0)}}{\eta^{(0)}}]|_{S_2} \\ &= \mathrm{div}_S(-\mathbf{s}^{(0)}w_n^{(+)} + \mathbf{D}^{(\mathbf{0})}\cdot\nabla_S p^{(+)}) - \boldsymbol{\theta}^{(0)} : \dot{\varepsilon}^{(+)} + \frac{\dot{p}^{(+)}}{\eta^{(0)}} + 0(h),\end{aligned} \tag{5.68}$$

and

$$\begin{aligned}&[\mathrm{div}_S(-\mathbf{s}^{(0)}w_n^{(0)} + \mathbf{D}^{(0)}\cdot\nabla_S p^{(0)}) - \boldsymbol{\theta}^{(0)} : \dot{\varepsilon}^{(0)} + \frac{\dot{p}^{(0)}}{\eta^{(0)}}]|_{S_1} \\ &= \mathrm{div}_S(-\mathbf{s}^{(0)}w_n^{(-)} + \mathbf{D}^{(0)}\cdot\nabla_S p^{(-)}) - \boldsymbol{\theta}^{(0)} : \dot{\varepsilon}^{(-)} + \frac{\dot{p}^{(-)}}{\eta^{(0)}} + 0(h).\end{aligned} \tag{5.69}$$

According to equation (5.67), the expression for $\nabla w_n^{(+)}\cdot\mathbf{n} + \nabla w_n^{(-)}\cdot\mathbf{n}$ becomes:

$$\begin{aligned}\nabla w_n^{(+)}\cdot\mathbf{n} + \nabla w_n^{(-)}\cdot\mathbf{n} =& \mathrm{div}_S(-\mathbf{s}^{(2)}w_n^{(+)} - \mathbf{s}^{(1)}w_n^{(-)} + \mathbf{D}^{(2)}\cdot\nabla_S p^{(+)} + \mathbf{D}^{(1)}\cdot\nabla_S p^{(-)}) \\ &- \boldsymbol{\theta}^{(2)} : \dot{\varepsilon}^{(+)} + \frac{\dot{p}^{(+)}}{\eta^{(2)}} - \boldsymbol{\theta}^{(1)} : \dot{\varepsilon}^{(-)} + \frac{\dot{p}^{(-)}}{\eta^{(1)}}.\end{aligned} \tag{5.70}$$

To obtain the expression for the normal fluid flux jump $[\![w_n]\!]$, substitute equations (5.68) and

(5.70) into (5.62), yielding:

$$\begin{aligned}\llbracket w_n \rrbracket =& \frac{h}{2}\mathrm{div}_S[(\mathbf{D}^{(0)}-\mathbf{D}^{(1)})\cdot\nabla_S p^{(-)}+(\mathbf{D}^{(0)}-\mathbf{D}^{(2)})\cdot\nabla_S p^{(+)}]-\frac{h}{2}\mathrm{div}_S[(\mathbf{s}^{(0)}-\mathbf{s}^{(1)})w_n^{(-)}+(\mathbf{s}^{(0)}-\mathbf{s}^{(2)})w_n^{(+)}]\\ &-\frac{h}{2}\left[(\boldsymbol{\theta}^{(0)}-\boldsymbol{\theta}^{(1)}):\dot{\boldsymbol{\varepsilon}}^{(-)}+(\boldsymbol{\theta}^{(0)}-\boldsymbol{\theta}^{(2)}):\dot{\boldsymbol{\varepsilon}}^{(+)}-\left(\frac{1}{\eta^{(0)}}-\frac{1}{\eta^{(1)}}\right)\dot{p}^{(-)}-\left(\frac{1}{\eta^{(0)}}-\frac{1}{\eta^{(2)}}\right)\dot{p}^{(+)}\right]+0(h^2).\end{aligned} \tag{5.71}$$

To display the discontinuity expression more compact, several computational symbols are defined as follows:

$$(\cdot)^{(\pm)}=[\frac{1}{2}((\cdot)^{(+)}+(\cdot)^{(-)})\pm\frac{1}{2}((\cdot)^{(+)}-(\cdot)^{(-)})]=\langle\cdot\rangle\pm\frac{1}{2}\llbracket\cdot\rrbracket, \tag{5.72}$$

where, the symbol $\langle\cdot\rangle=\frac{1}{2}((\cdot)^{(+)}+(\cdot)^{(-)})$ denotes the average of the quantity $(\cdot)$ across the interface S_0. Utilizing the established symbols, the jump relations across the imperfect interface can be systematically formulated into concise and efficient equations, as shown below:

$$\begin{aligned}\llbracket\mathbf{u}\rrbracket &= \frac{h}{2}\Big\{[(2\mathbb{S}^{(0)}:\mathbb{A}^{(0)}-\mathbb{S}^{(2)}:\mathbb{A}^{(2)}-\mathbb{S}^{(1)}:\mathbb{A}^{(1)}):\langle\boldsymbol{\varepsilon}\rangle]\cdot\mathbf{n}+(2\mathbf{F}^{(0)}-\mathbf{F}^{(2)}-\mathbf{F}^{(1)})\cdot\langle\mathbf{t}\rangle\\ &\quad-(2\mathbb{B}^{(0)}:\boldsymbol{\theta}^{(0)}-\mathbb{B}^{(2)}:\boldsymbol{\theta}^{(2)}-\mathbb{B}^{(1)}:\boldsymbol{\theta}^{(1)})\langle p\rangle\cdot\mathbf{n}\Big\}+\mathbf{0}(h^2),\end{aligned} \tag{5.73}$$

$$\begin{aligned}\llbracket\mathbf{t}\rrbracket &= \frac{h}{2}\mathrm{div}_S[(\mathbb{A}^{(2)}+\mathbb{A}^{(1)}-2\mathbb{A}^{(0)}):\langle\boldsymbol{\varepsilon}\rangle+(\mathbb{C}^{(2)}:\mathbb{B}^{(2)}+\mathbb{C}^{(1)}:\mathbb{B}^{(1)}-2\mathbb{C}^{(0)}:\mathbb{B}^{(0)}):\langle\boldsymbol{\sigma}\rangle\\ &\quad+(\mathbb{A}^{(2)}:\mathbb{S}^{(2)}:\boldsymbol{\theta}^{(2)}+\mathbb{A}^{(1)}:\mathbb{S}^{(1)}:\boldsymbol{\theta}^{(1)}-2\mathbb{A}^{(0)}:\mathbb{S}^{(0)}:\boldsymbol{\theta}^{(0)})\langle p\rangle]+\mathbf{0}(h^2),\end{aligned} \tag{5.74}$$

$$\llbracket p\rrbracket = \frac{h}{2}\left[\left(\frac{1}{k_{nn}^{(2)}}+\frac{1}{k_{nn}^{(1)}}-\frac{2}{k_{nn}^{(0)}}\right)\langle w_n\rangle\right]-\frac{h}{2}\left[(2\mathbf{s}^{(0)}-\mathbf{s}^{(1)}-\mathbf{s}^{(2)})\cdot\nabla_s\langle p\rangle\right]+0(h^2), \tag{5.75}$$

$$\begin{aligned}\llbracket w_n\rrbracket &= \frac{h}{2}\mathrm{div}_S[(2\mathbf{D}^{(0)}-\mathbf{D}^{(1)}-\mathbf{D}^{(2)})\cdot\nabla_S\langle p\rangle]-\frac{h}{2}\mathrm{div}_S[(2\mathbf{s}^{(0)}-\mathbf{s}^{(1)}-\mathbf{s}^{(2)})\langle w_n\rangle]\\ &\quad-\frac{h}{2}\left[(2\boldsymbol{\theta}^{(0)}-\boldsymbol{\theta}^{(1)}-\boldsymbol{\theta}^{(2)}):\langle\dot{\boldsymbol{\varepsilon}}\rangle-\left(\frac{2}{\eta^{(0)}}-\frac{1}{\eta^{(1)}}-\frac{1}{\eta^{(2)}}\right)\langle\dot{p}\rangle\right]+0(h^2).\end{aligned} \tag{5.76}$$

5.1.4 General Isotropic Interface Model and Extreme Particular Interface Models

When all phases within the three-phase configuration are isotropic, the elastic stiffness and compliance tensors assume simplified forms. Specifically, they can be expressed as:

$$\mathbb{C}^{(i)} = 2\mu^{(i)}\mathbb{I} + \left(\frac{3\kappa^{(i)} - 2\mu^{(i)}}{3}\right)\mathbf{I}\otimes\mathbf{I}, \quad \mathbb{S}^{(i)} = \frac{1}{2\mu^{(i)}}\mathbb{I} + \left(\frac{2\mu^{(i)} - 3\kappa^{(i)}}{18\kappa^{(i)}\mu^{(i)}}\right)\mathbf{I}\otimes\mathbf{I}, \tag{5.77}$$

where $\kappa^{(i)}$ and $\mu^{(i)}$ denote the bulk modulus and shear modulus, respectively, of phase i ($i = 0, 1,$ or 2). Under isotropic conditions, where material properties remain uniform in all directions, the coupling between strain and fluid pressure is homogeneous across all directions. Additionally, the material's permeability remains constant irrespective of orientation. Consequently, this enables us to express the Biot's tensor $\boldsymbol{\theta}$ and the permeability tensor $\mathbf{K}$ as follows:

$$\boldsymbol{\theta}^{(i)} = \theta^{(i)}\mathbf{I}, \quad \mathbf{K}^{(i)} = K^{(i)}\mathbf{I}, \tag{5.78}$$

where $\theta^{(i)}$ and $K^{(i)}$ denote scalar coefficients. By substituting equation (5.77) into equations (2.153)-(2.158), the following relations can be inferred:

$$\mathbf{G}^{(i)} = \mu^{(i)}\mathbf{P} + \left(\frac{4\mu^{(i)} + 3\kappa^{(i)}}{3}\right)\mathbf{P}^{\perp}, \tag{5.79}$$

$$\mathbf{F}^{(i)} = \frac{1}{\mu^{(i)}}\mathbf{P} + \left(\frac{3}{4\mu^{(i)} + 3\kappa^{(i)}}\right)\mathbf{P}^{\perp}, \tag{5.80}$$

$$\mathbb{B}^{(i)} = \frac{1}{2\mu^{(i)}}\left(\mathbb{P}^{\perp} + \frac{2\mu^{(i)} - 3\kappa^{(i)}}{4\mu^{(i)} + 3\kappa^{(i)}}\mathbf{P}^{\perp}\otimes\mathbf{P}^{\perp}\right), \tag{5.81}$$

$$\mathbb{A}^{(i)} = 2\mu^{(i)}\left(\mathbb{P} - \frac{2\mu^{(i)} - 3\kappa^{(i)}}{4\mu^{(i)} + 3\kappa^{(i)}}\mathbf{P}\otimes\mathbf{P}\right). \tag{5.82}$$

Combining the tensors obtained above along with equations (5.77) and (5.78), and substituting them into equations (5.73)-(5.76), we derive the interfacial jump relations in the isotropic case:

$$\begin{aligned}
[\![\mathbf{u}]\!] &= \frac{h}{2}[c_1(\mathbf{P}\colon\langle\boldsymbol{\varepsilon}\rangle)\cdot\mathbf{n}+(c_2\mathbf{P}^{\perp}+c_3\mathbf{P})\cdot\langle\mathbf{t}\rangle+c_4\langle p\rangle\mathbf{n}]+0(h^2), && (5.83)\\
[\![\mathbf{t}]\!] &= \frac{h}{2}\mathrm{div}_S[(c_5\mathbb{P}+c_6\mathbf{P}\otimes\mathbf{P}):\langle\boldsymbol{\varepsilon}\rangle+(c_1\mathbf{P}^{\perp}\colon\langle\boldsymbol{\sigma}\rangle)\mathbf{P}+c_7\langle p\rangle\mathbf{P}]+0(h^2), && (5.84)\\
[\![p]\!] &= \frac{h}{2}c_8\langle w_n\rangle+0(h^2), && (5.85)\\
[\![w_n]\!] &= \frac{h}{2}c_9\Delta_S\langle p\rangle-\frac{h}{2}[c_{10}\mathrm{tr}\langle\dot{\boldsymbol{\varepsilon}}\rangle-c_{11}\langle\dot{p}\rangle]+0(h^2), && (5.86)
\end{aligned}$$

where the material parameters c_i $(i=1,2,...,9)$ are detailed in Appendix A, while $\Delta_S\langle p\rangle$ denotes the surface Laplacian of $\langle p\rangle$, computed as $\Delta_S\langle p\rangle=\mathrm{div}_S(\nabla_S\langle p\rangle)$.

Analyzing the general interface model in the two opposite extreme cases, where the interphase exhibits significantly higher or lower rigidity and permeability compared to that of the surrounding phases, is crucial for understanding imperfect interface. To facilitate the analysis of these two cases, we introduce a small dimensionless parameter $\varsigma=h/h_0\ll 1$, with h_0 representing a reference length on the same order as the geometrical dimensions of the inhomogeneities within a composite material. Subsequently, we can express the extreme cases as follows:

Case 1 - high rigidity and permeability of interphase

$$\begin{aligned}
&\mathbb{C}^{(0)}=\frac{\widehat{\mathbb{C}}^{(0)}}{\varsigma}, && \mathbb{C}^{(2)}=\widehat{\mathbb{C}}^{(2)}, && \mathbb{C}^{(1)}=\widehat{\mathbb{C}}^{(1)},\\
&\theta^{(0)}=\frac{\widehat{\theta}^{(0)}}{\varsigma}, && \theta^{(2)}=\widehat{\theta}^{(2)}, && \theta^{(1)}=\widehat{\theta}^{(1)}, && (5.87)\\
&\mathbf{K}^{(0)}=\frac{\widehat{\mathbf{K}}^{(0)}}{\varsigma}, && \mathbf{K}^{(2)}=\widehat{\mathbf{K}}^{(2)}, && \mathbf{K}^{(1)}=\widehat{\mathbf{K}}^{(1)},\\
&\frac{1}{\eta^{(0)}}=\frac{1}{\varsigma\widehat{\eta}^{(0)}}, && \frac{1}{\eta^{(2)}}=\frac{1}{\widehat{\eta}^{(2)}}, && \frac{1}{\eta^{(1)}}=\frac{1}{\widehat{\eta}^{(1)}};
\end{aligned}$$

Case 2 - low rigidity and permeability of interphase

$$
\begin{aligned}
&\mathbb{C}^{(0)} = \varsigma\widehat{\mathbb{C}}^{(0)}, && \mathbb{C}^{(2)} = \widehat{\mathbb{C}}^{(2)}, && \mathbb{C}^{(1)} = \widehat{\mathbb{C}}^{(1)},\\
&\boldsymbol{\theta}^{(0)} = \varsigma\widehat{\boldsymbol{\theta}}^{(0)}, && \boldsymbol{\theta}^{(2)} = \widehat{\boldsymbol{\theta}}^{(2)}, && \boldsymbol{\theta}^{(1)} = \widehat{\boldsymbol{\theta}}^{(1)},\\
&\mathbf{K}^{(0)} = \varsigma\widehat{\mathbf{K}}^{(0)}, && \mathbf{K}^{(2)} = \widehat{\mathbf{K}}^{(2)}, && \mathbf{K}^{(1)} = \widehat{\mathbf{K}}^{(1)},\\
&\frac{1}{\eta^{(0)}} = \frac{\varsigma}{\widehat{\eta}^{(0)}}, && \frac{1}{\eta^{(2)}} = \frac{1}{\widehat{\eta}^{(2)}}, && \frac{1}{\eta^{(1)}} = \frac{1}{\widehat{\eta}^{(1)}}.
\end{aligned}
\tag{5.88}
$$

Here, $\widehat{\mathbb{C}}^{(i)}$, $\widehat{\boldsymbol{\theta}}^{(i)}$, $\widehat{\mathbf{K}}^{(i)}$, and $\widehat{\eta}^{(i)}$ $(i = 1,2,3)$denote the reference stiffness tensors, Biot's tensors, permeability tensors, and Biot's modulus, respectively, each of which is of the same order.

In the first case, considering the material relations (5.87) within the jump relations (5.73)-(5.76), it can be demonstrated that, with an error of the order of $\mathbf{0}(h)$ or $0(h)$,

$$\llbracket \mathbf{u} \rrbracket = \mathbf{0}, \tag{5.89}$$

$$\llbracket \mathbf{t} \rrbracket = -h_0 \mathrm{div}_S \left[\widehat{\mathbb{A}}^{(0)} : \langle \boldsymbol{\varepsilon} \rangle + \widehat{\mathbb{A}}^{(0)} : \widehat{\mathbb{S}}^{(0)} : \widehat{\boldsymbol{\theta}}^{(0)} \langle p \rangle \right], \tag{5.90}$$

$$\llbracket p \rrbracket = 0, \tag{5.91}$$

$$\llbracket w_n \rrbracket = h_0 \left[\mathrm{div}_S(\widehat{\mathbf{D}}^{(0)} : \nabla_S \langle p \rangle) - \widehat{\boldsymbol{\theta}}^{(0)} : \langle \dot{\boldsymbol{\varepsilon}} \rangle + \frac{\langle \dot{p} \rangle}{\widehat{\eta}^{(0)}} \right]. \tag{5.92}$$

In this case, it is clear that both the displacement vector and fluid pressure maintain continuity across the interface, with an error of order $\mathbf{0}(h)$ or $0(h)$. Conversely, the traction vector and normal fluid flux display a discontinuous behavior. These relations characterize the poroelastic coherent imperfect interface model, which can be viewed as the extension to poroelasticity of the well-known Gurtin-Murdoch model. According to the subsection (5.1.4), when the interphase exhibits isotropy, the jump relations (5.90) and (5.92) can be simplified as follows:

$$\llbracket \mathbf{t} \rrbracket = -\mathrm{div}_S \left[\lambda_s \mathrm{tr}(\boldsymbol{\varepsilon}_s)\mathbf{P} + 2\mu_s \boldsymbol{\varepsilon}_s + p\theta_s \mathbf{P} \right], \tag{5.93}$$

$$\llbracket w_n \rrbracket = \left[K_{s1} \Delta_S p - h_0 \widehat{\theta}^{(0)} \mathrm{tr}(\langle \dot{\boldsymbol{\varepsilon}} \rangle) + \frac{h_0}{\widehat{\eta}^{(0)}} \dot{p} \right], \tag{5.94}$$

with

$$\boldsymbol{\varepsilon}_s = \mathbb{P} : \boldsymbol{\varepsilon}^{(+)} = \mathbb{P} : \boldsymbol{\varepsilon}^{(-)}, \qquad p = p^{(+)} = p^{(-)}, \qquad \dot{p} = \dot{p}^{(+)} = \dot{p}^{(-)}, \tag{5.95}$$

$$\lambda_s = \frac{2h_0\widehat{\mu}^{(0)}(2\widehat{\mu}^{(0)} - 3\widehat{\kappa}^{(0)})}{4\widehat{\mu}^{(0)} + 3\widehat{\kappa}^{(0)}}, \quad \mu_s = h_0\widehat{\mu}^{(0)}, \quad \theta_s = \frac{6h_0\widehat{\mu}^{(0)}\widehat{\theta}^{(0)}}{4\widehat{\mu}^{(0)} + 3\widehat{\kappa}^{(0)}}, \quad K_{s1} = h_0\widehat{K}^{(0)}. \tag{5.96}$$

In the second case, taking into account material relations (5.88) in jump relations (5.73)-(5.76), it can be shown that, with an error of the order of $\mathbf{0}(h)$ or $0(h)$,

$$[\![\mathbf{u}]\!] = h_0\widehat{\mathbf{F}}^{(0)}\mathbf{t}, \tag{5.97}$$

$$[\![\mathbf{t}]\!] = \mathbf{0}, \tag{5.98}$$

$$[\![p]\!] = -\frac{h_0}{\widehat{k}_{nn}^{(0)}}w_n, \tag{5.99}$$

$$[\![w_n]\!] = 0, \tag{5.100}$$

with

$$\mathbf{t} = \mathbf{t}^{(+)} = \mathbf{t}^{(-)}, \qquad w_n = w_n^{(+)} = w_n^{(-)}. \tag{5.101}$$

In this case, it is evident that the traction vector and normal fluid flux maintain continuity across the interface, with an error of order $\mathbf{0}(h)$ or $0(h)$. Conversely, the displacement vector and fluid pressure exhibit a jump across the same interface. These relations characterize the poroelastic coherent imperfect interface model, which can be regarded as an extension of the widely recognized spring-layer interface model to the realm of poroelasticity. When the interphase demonstrates isotropy, the jump relations (5.97) and (5.99) can be reduced to the following form:

$$[\![\mathbf{u}]\!] = (\alpha_t\mathbf{P} + \alpha_n\mathbf{P}^{\perp})\mathbf{t}, \tag{5.102}$$

$$[\![p]\!] = -K_{s2}w_n, \tag{5.103}$$

$$\tag{5.104}$$

with

$$\alpha_t = \frac{3h_0}{4\widehat{\mu}^{(0)} + 3\widehat{\kappa}^{(0)}}, \qquad \alpha_n = \frac{h_0}{\widehat{\mu}^{(0)}}, \qquad K_{s2} = \frac{h_0}{\widehat{K}^{(0)}}. \tag{5.105}$$

5.2 Numerical Implementation with XFEM

The discontinuous relations governing a general imperfect interface, which is equivalent to the interphase embedded in the matrix and the inclusion phase of a composite material, have been rigorously derived. In this section, our focus lies on elaborating an effective numerical method specific to dealing with imperfect interfaces. We center our attention on the analysis of porous composites, thoroughly illustrating the numerical calculation process, thereby providing a valuable reference for the numerical analysis of composite materials. To facilitate the implementation of numerical methods and reduce complexity, we proceed to simplify the discontinuous relations (5.73) and (5.74) as follows:

$$[\![\mathbf{u}]\!] = \frac{h}{2}[(\mathbf{n}\cdot\mathbb{F}):\langle\varepsilon\rangle - (\mathbf{n}\cdot\mathbf{R})\langle p\rangle + \mathbf{H}\cdot\langle\mathbf{t}\rangle] + 0(h^2), \tag{5.106}$$

$$[\![\mathbf{t}]\!] = \frac{h}{2}\mathrm{div}_S[\mathbf{S}\langle p\rangle + (\mathbb{Y}\cdot\mathbf{n})\langle\mathbf{t}\rangle + \mathbb{Z}:\langle\varepsilon\rangle] + 0(h^2). \tag{5.107}$$

The symbols appearing in the two simplified equations above are specifically defined as follows:

$$\begin{aligned}
\mathbb{F} &= 2\mathbb{S}^{(0)}:\mathbb{A}^{(0)} - \mathbb{S}^{(2)}:\mathbb{A}^{(2)} - \mathbb{S}^{(1)}:\mathbb{A}^{(1)}, && (5.108)\\
\mathbf{R} &= 2\mathbb{B}^{(0)}:\boldsymbol{\theta}^{(0)} - \mathbb{B}^{(2)}:\boldsymbol{\theta}^{(2)} - \mathbb{B}^{(1)}:\boldsymbol{\theta}^{(1)}, && (5.109)\\
\mathbf{H} &= 2\mathbf{F}^{(0)} - \mathbf{F}^{(2)} - \mathbf{F}^{(1)}, && (5.110)\\
\mathbf{S} &= \mathbb{A}^{(2)}:\mathbb{S}^{(2)}:\boldsymbol{\theta}^{(2)} + \mathbb{A}^{(1)}:\mathbb{S}^{(1)}:\boldsymbol{\theta}^{(1)} - 2\mathbb{A}^{(0)}:\mathbb{S}^{(0)}:\boldsymbol{\theta}^{(0)}, && (5.111)\\
\mathbb{Y} &= \mathbb{C}^{(2)}:\mathbb{B}^{(2)} + \mathbb{C}^{(1)}:\mathbb{B}^{(1)} - 2\mathbb{C}^{(0)}:\mathbb{B}^{(0)}, && (5.112)\\
\mathbb{Z} &= \mathbb{A}^{(2)} + \mathbb{A}^{(1)} - 2\mathbb{A}^{(0)}. && (5.113)
\end{aligned}$$

In accordance with the conversion relation $\mathbb{C}:\mathbb{B} + \mathbb{A}:\mathbb{S} = \mathbb{I}$, we can deduce the following expression:

$$\mathbb{F} = \mathbb{B}^{(2)}:\mathbb{C}^{(2)} + \mathbb{B}^{(1)}:\mathbb{C}^{(1)} - 2\mathbb{B}^{(0)}:\mathbb{C}^{(0)} = \mathbb{Y}^T. \tag{5.114}$$

Additionally, it is imperative to acknowledge these computational properties: $\mathbb{P}:\mathbf{S} = \mathbf{S}$, $\mathbb{F}:\mathbb{P} = \mathbb{F}$, $\mathbb{Z}:\mathbb{P} = \mathbb{Z}$, and $\mathbb{Y}:\mathbb{P}^{\perp} = \mathbb{Y}$, owing to the relations $\mathbb{A}:\mathbb{P} = \mathbb{A}$ and $\mathbb{B}:\mathbb{P} = \mathbb{B}$.

5.2.1 Strong and Weak Formulations for Boundary Value Problems

The discontinuities obtained above are initially expressed as differential equations (strong formulations), which should be converted into the corresponding integral equations (weak formulations) to suit the discretization within the extended finite element method (XFEM) framework. For computational efficiency without sacrificing essential properties, a poroelastic composite comprising only one matrix and one inclusion phase is selected as the computational model (see **Fig.** 5.3). The symbol Ω denotes the entire analysis domain of the composite, bounded by

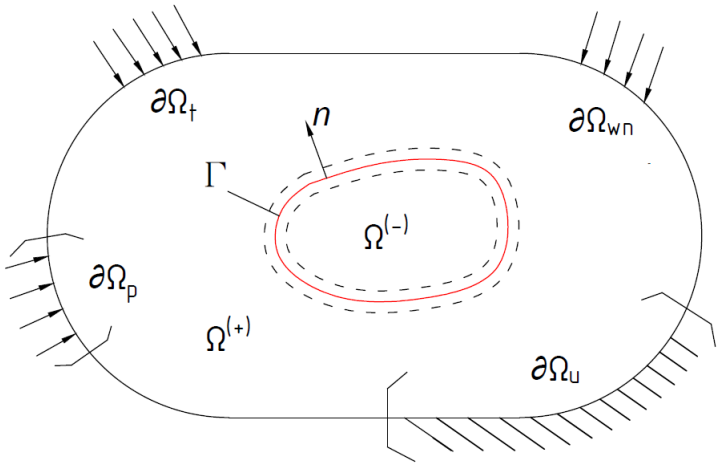

Figure 5.3: *The boundary condition of the inclusion phase embeds in matrix phase bonded by a general imperfect interface.*

a surface $\partial\Omega$. The sub-domains occupied by the matrix and inclusion phases are represented as $\Omega^{(+)}$ and $\Omega^{(-)}$, respectively. The general imperfect interface, characterized by equations (5.73), (5.74), (5.75), and (5.76), which divides the analysis domain into $\Omega^{(+)}$ and $\Omega^{(-)}$, is denoted by Γ. Thus, $\Omega = \Omega^{(-)} \cup \Omega^{(+)} \cup \Gamma$. The external boundary conditions are specified as follows:

$$\mathbf{u} = \bar{\mathbf{u}} \quad \text{on} \quad \partial\Omega_u, \quad \mathbf{t} = \bar{\mathbf{t}} \quad \text{on} \quad \partial\Omega_t, \tag{5.115}$$

$$p = \overline{p} \quad \text{on} \quad \partial\Omega_p, \quad w_n = \overline{w}_n \quad \text{on} \quad \partial\Omega_{w_n}. \tag{5.116}$$

The external boundary conditions adhere to the conditions where $\partial\Omega_u \cup \partial\Omega_t = \partial\Omega_p \cup \partial\Omega_{w_n} = \partial\Omega$, and $\partial\Omega_u \cap \partial\Omega_t = \partial\Omega_p \cap \partial\Omega_{w_n} = \emptyset$. Here, $\bar{\mathbf{u}}$, $\bar{\mathbf{t}}, \overline{p}$, and $\overline{w}_n$ represent the corresponding imposed physical quantities at the boundary. The boundary of the sub-domain $\Omega^{(-)}$ comprises the closed imperfect interface Γ, while that of $\Omega^{(+)}$ is formed by $\partial\Omega$ and Γ.

Employing a piecewise differentiable virtual displacement field $\delta\mathbf{u}$ defined over Ω as an independent control variable, the weak formulation for the boundary value problem is derived as follows, with the virtual work principle imposed on $\Omega^{(-)}$ and $\Omega^{(+)}$

$$\int_{\Omega^{(2)}} \boldsymbol{\sigma} : \delta\varepsilon dv = \int_{\partial\Omega_t} \bar{\mathbf{t}} \cdot \delta\mathbf{u} - \int_S \mathbf{t}^{(+)} \cdot \delta\mathbf{u}^{(+)} ds, \tag{5.117}$$

$$\int_{\Omega^{(1)}} \boldsymbol{\sigma} : \delta\varepsilon dv = \int_\Gamma \mathbf{t}^{(-)} \cdot \delta\mathbf{u}^{(-)} ds, \tag{5.118}$$

where $\delta\varepsilon$ represents the virtual strain tensor determined by $\delta\varepsilon = \nabla(\delta\mathbf{u})$, with the condition $\delta\mathbf{u} = 0$ on Ω_u. By combining equations (5.117) and (5.118), the weak form of the entire composite can be expressed as follows:

$$\int_\Omega \boldsymbol{\sigma} : \delta\varepsilon dv + \int_\Gamma [\![\mathbf{t} \cdot \delta\mathbf{u}]\!] ds = \int_{\partial\Omega_t} \bar{\mathbf{t}} \cdot \delta\mathbf{u} ds. \tag{5.119}$$

Making a difference between equations (5.106) and (5.107) the second term on the right-hand side of the equation above can be obtained using the surface divergence (or Stokes) theorem:

$$\begin{aligned} \int_\Gamma [\![\mathbf{t} \cdot \delta\mathbf{u}]\!] ds &= \frac{h}{2} \int_\Gamma [\langle \mathbf{t} \rangle \cdot \mathbf{H} \langle \delta\mathbf{t} \rangle - \langle \delta\varepsilon \rangle : \mathbb{Z} \langle \varepsilon \rangle] ds \\ &- \frac{h}{2} \int_\Gamma [\langle \mathbf{t} \rangle \cdot (\mathbf{n} \cdot \mathbf{R}) \langle \delta p \rangle + \langle \delta\varepsilon \rangle : \mathbf{S} \langle p \rangle] ds. \end{aligned} \tag{5.120}$$

To ensure that the weak formulations involve only the control variables $\mathbf{u}$ and p, we utilize equation (5.106) to express the traction vector $\mathbf{t}$ and the virtual traction vector $\delta\mathbf{t}$ in terms of the displacement vector $\mathbf{u}$, the virtual displacement vector $\delta\mathbf{u}$, and the strain gradient ε, as follows:

$$\langle \mathbf{t} \rangle = \frac{2}{h} \mathbf{H}^{-1} [\![\mathbf{u}]\!] + \mathbf{H}^{-1} (\mathbf{n} \cdot \mathbf{R}) \langle p \rangle - \mathbf{H}^{-1} (\mathbf{n} \cdot \mathbb{F}) \langle \varepsilon \rangle, \tag{5.121}$$

$$\langle \delta\mathbf{t} \rangle = \frac{2}{h} \mathbf{H}^{-1} [\![\delta\mathbf{u}]\!] + \mathbf{H}^{-1} (\mathbf{n} \cdot \mathbf{R}) \langle \delta p \rangle - \mathbf{H}^{-1} (\mathbf{n} \cdot \mathbb{F}) \langle \delta\varepsilon \rangle. \tag{5.122}$$

Finally, the concrete expression of the weak form is obtained through rigorous mathematical

calculation, yielding:

$$\int_\Omega \varepsilon : \mathbb{C}\delta\varepsilon dv + \int_\Omega p\boldsymbol{\theta} : \delta\varepsilon dv - \frac{h}{2}\int_\Gamma [\langle\delta\varepsilon\rangle : \mathbb{Z}\langle\varepsilon\rangle] ds - \frac{h}{2}\int_\Gamma [\langle\delta\varepsilon\rangle : \mathbf{S}\langle p\rangle] ds + \frac{2}{h}\int_\Gamma [\![\mathbf{u}]\!]\cdot\mathbf{H}^{-1}[\![\delta\mathbf{u}]\!] ds$$
$$- \int_\Gamma [\![\mathbf{u}]\!]\cdot\mathbf{H}^{-1}(\mathbf{n}\cdot\mathbb{F})\langle\delta\varepsilon\rangle ds + \int_\Gamma [\![\delta\mathbf{u}]\!]\cdot\mathbf{H}^{-1}(\mathbf{n}\cdot\mathbf{R})\langle p\rangle ds - \frac{h}{2}\int_\Gamma \langle p\rangle(\mathbf{R}^T\mathbf{n})\cdot\mathbf{H}^{-1}(\mathbf{n}\cdot\mathbb{F})\langle\delta\varepsilon\rangle ds$$
$$- \int_\Gamma [\![\delta\mathbf{u}]\!]\cdot\mathbf{H}^{-1}(\mathbf{n}\cdot\mathbb{F})\langle\varepsilon\rangle ds + \frac{h}{2}\int_\Gamma \langle\varepsilon\rangle : (\mathbb{F}^T\cdot\mathbf{n})\cdot\mathbf{H}^{-1}(\mathbf{n}\cdot\mathbb{F})\langle\delta\varepsilon\rangle ds = \int_{\partial\Omega_t}\bar{\mathbf{t}}\cdot\delta\mathbf{u} ds. \tag{5.123}$$

For the fluid phase, we apply a similar method and procedure to derive the weak form within the composite. The weak form for the fluid phase is expressed as follows:

$$-\int_\Omega \mathbf{K}\nabla p\cdot\nabla(\delta p) dv + \int_\Gamma [\![p]\!]\left(\frac{1}{k_{nn}^{(2)}} + \frac{1}{k_{nn}^{(1)}} - \frac{2}{k_{nn}^{(0)}}\right)^{-1}\left(\frac{2[\![\delta p]\!]}{h} + (2\mathbf{s}^{(0)} - \mathbf{s}^{(1)} - \mathbf{s}^{(2)})\cdot\nabla_S\langle\delta p\rangle\right) ds$$
$$+\frac{h}{2}\int_\Gamma \left(\frac{1}{k_{nn}^{(2)}} + \frac{1}{k_{nn}^{(1)}} - \frac{2}{k_{nn}^{(0)}}\right)^{-1}\nabla_S\langle p\rangle\cdot(2\mathbf{s}^{(0)} - \mathbf{s}^{(1)} - \mathbf{s}^{(2)})\left(\frac{2[\![\delta p]\!]}{h} + (2\mathbf{s}^{(0)} - \mathbf{s}^{(1)} - \mathbf{s}^{(2)})\cdot\nabla_S\langle\delta p\rangle\right) ds$$
$$-\frac{h}{2}\int_\Gamma \left[(2\boldsymbol{\theta}^{(0)} - \boldsymbol{\theta}^{(1)} - \boldsymbol{\theta}^{(2)}) : \langle\dot{\varepsilon}\rangle\langle\delta p\rangle - \left(\frac{2}{\eta^{(0)}} - \frac{1}{\eta^{(1)}} - \frac{1}{\eta^{(2)}}\right)\langle\dot{p}\rangle\langle\delta p\rangle\right] ds \tag{5.124}$$
$$-\frac{h}{2}\int_\Gamma (2\mathbf{D}^{(0)} - \mathbf{D}^{(1)} - \mathbf{D}^{(2)})\nabla_S\langle p\rangle\cdot\nabla_S\langle\delta p\rangle ds = \int_\Omega \left(\boldsymbol{\theta} : \dot{\varepsilon} - \frac{\dot{p}}{\eta}\right)\delta p dv + \int_{\partial\Omega_{w_n}} \overline{w}_n\cdot\delta p ds.$$

5.2.2 Level Set Function and Enriched Shape Functions

In the analysis of inclusion problems, the Extended Finite Element Method (XFEM) introduces additional degrees of freedom and modifies the form of basis functions within discontinuous regions (i.e., elements intersected by imperfect interfaces), thereby facilitating improved accommodation of discontinuities. By incorporating additional degrees of freedom and adjusting the basis functions, XFEM efficiently accommodates discontinuous features without excessive reliance on grid refinement or interpolation techniques. This intrinsic flexibility enables XFEM to provide highly accurate numerical solutions for problems involving interface discontinuities while optimizing computational resources and enhancing overall efficiency. The level set method (LSM) is highly effective in offering accurate and adaptable portrayal of imperfect interface positions and geometries. By employing an additional scalar function, known as the level set function, LSM represents the position of an interface. This function defines a surface in a higher-dimensional space, where points on the surface directly correspond to points on the

interface. The numerical values assigned to these points denote their signed distances from the interface. Specifically, the imperfect interface S is represented as the zero level-set of a function, defined as:

$$S = \{\boldsymbol{x} \in \mathbb{R}^3 \mid \phi(\boldsymbol{x}) = 0\}. \tag{5.125}$$

The interface S divides the solution domain Ω into two subdomains: $\Omega^{(-)}$ and $\Omega^{(+)}$. In $\Omega^{(-)}$, the level set function $\phi(\boldsymbol{x})$ is negative ($\phi(\boldsymbol{x}) < 0$), indicating points inside the interface. Conversely, in $\Omega^{(+)}$, $\phi(\boldsymbol{x})$ is positive ($\phi(\boldsymbol{x}) > 0$), representing points outside the interface. The value $\phi(\boldsymbol{x})$ at any point within an element can be approximated by a linear combination of the shape functions and the level set function values at the nodes of that element. This approximation is expressed as:

$$\phi(\boldsymbol{x}) \approx \sum_{i=1}^{n} N_i(\boldsymbol{x})\phi_i(\boldsymbol{x}), \tag{5.126}$$

where $N_i(\boldsymbol{x})$ represents the shape function associated with the standard finite element, and $\phi_i(\boldsymbol{x})$ denotes the value of the level set function at the nodes of the element. The unit normal vector $\mathbf{n}(\boldsymbol{x})$ at a point $\boldsymbol{x}$ on the interface S is computed as follows:

$$\mathbf{n}(\boldsymbol{x}) = \frac{\nabla\phi(\boldsymbol{x})}{\|\nabla\phi(\boldsymbol{x})\|}. \tag{5.127}$$

When elements are cut by imperfect interfaces, adjustments in form and degrees of freedom are essential for capturing displacement and pore pressure jumps accurately. Introducing additional degrees of freedom and modifying the basis function form enables solutions to effectively represent discontinuities across interfaces, thereby facilitating a more appropriate depiction and precise capture of such phenomena. In the XFEM, the displacement and pore pressure approximate expressions are decomposed into three parts, with the first part capturing continuous behavior, while the second and third parts are designed to address strong and weak discontinuities, respectively. Specifically, the expressions are formulated as follows:

$$\mathbf{u}(\boldsymbol{x}) \approx \sum_{i=1}^{n} N_i^u(\boldsymbol{x})\mathbf{u}_i + \sum_{j=1}^{m} N_j^u(\boldsymbol{x})\chi_j(\boldsymbol{x})\overline{\mathbf{c}}_j + \sum_{j=1}^{m} N_j^u(\boldsymbol{x})\Psi_j(\boldsymbol{x})\overline{\overline{\mathbf{c}}}_j, \tag{5.128a}$$

$$p(\boldsymbol{x}) \approx \sum_{i=1}^{n} N_i^p(\boldsymbol{x})p_i + \sum_{j=1}^{m} N_j^p(\boldsymbol{x})\chi_j(\boldsymbol{x})\overline{g}_j + \sum_{j=1}^{m} N_j^p(\boldsymbol{x})\Psi_j(\boldsymbol{x})\overline{\overline{g}}_j. \tag{5.128b}$$

In the expressions above, $\mathbf{u}(\boldsymbol{x})$ and $p(\boldsymbol{x})$ denote the displacement and pore pressure fields, respectively, evaluated at arbitrary points within an element. The symbols $N_i^{(\cdot)}$ ($\cdot$ =u or p) represent the shape functions of the standard finite element, while $\mathbf{u}_i$ and p_i denote the displacement and pore pressure at the i^{th} node of this element. $\bar{\mathbf{c}}_j$, $\bar{\bar{\mathbf{c}}}_j$, $\bar{g}_j$, and $\bar{\bar{g}}_j$ denote the enriched degrees of freedom (DOFs) for displacement and pore pressure, respectively. Here, n represents the number of nodes in a standard finite element, while m indicates the number of enriched nodes. It is essential to emphasize that the value of m is determined by the type of the enriched element and must adhere to the condition $m \leqslant n$. Additionally, $\chi_j(\boldsymbol{x})$ and $\Psi_j(\boldsymbol{x})$ represent enrichment functions employed to characterize strong and weak discontinuities within elements cut by the imperfect interface, respectively. They are defined as follows:

$$\chi_j(\boldsymbol{x}) = \text{sign}(\phi(\boldsymbol{x})) - \text{sign}(\phi_j(\boldsymbol{x})), \tag{5.129}$$

$$\Psi_j(\boldsymbol{x}) = \sum_{i=1}^{n} N_i(\boldsymbol{x})|\phi_i| - |\sum_{i=1}^{n} N_i(\boldsymbol{x})\phi_i|, \tag{5.130}$$

where the function $sign(\phi(\boldsymbol{x}))$ yields a value of 1, 0, or -1 depending on whether $\phi(\boldsymbol{x})$ is positive, zero, or negative, respectively. The derivative expressions of these two enrichment functions are as follows:

$$\frac{\partial \chi_j(\boldsymbol{x})}{\partial \boldsymbol{x}} = 0, \tag{5.131}$$

$$\frac{\partial \Psi_j(\boldsymbol{x})}{\partial \boldsymbol{x}} = \sum_{i=1}^{n} \{ \frac{\partial N_i(\boldsymbol{x})}{\partial \boldsymbol{x}} [|\phi_i| - sign(\sum_{i=1}^{n} N_i(\boldsymbol{x})\phi_i)\phi_i] \}. \tag{5.132}$$

The enrichment functions $\chi_j(\boldsymbol{x})$ and $\Psi_j(\boldsymbol{x})$ play crucial roles in capturing discontinuities within the finite element framework. Specifically, $\chi_j(\boldsymbol{x})$ exhibits a clear discontinuity across the imperfect interface, with its derivatives uniformly zero throughout the domain Ω. In contrast, $\Psi_j(\boldsymbol{x})$ demonstrates continuity across the same interface, yet its derivative lacks continuity. Through the implementation of enrichment functions (5.129) and (5.130), both strong and weak discontinuities can be effectively represented, providing a comprehensive approach to handling interface-related phenomena within the XFEM.

5.2.3 Parameters of Discrete Control Equations

Substituting the approximate expressions for displacement and pore pressure, given by (5.128b) and (5.128a), into the weak formulations (5.123) and (5.125), and considering the arbitrariness of node variations, yields the governing equation of the discrete system as follows:

$$[\mathbf{Q}_{up}+\mathbf{Q}_{us}]\{\dot{\mathbf{u}}\}+[\mathbf{Q}_{pp}+\mathbf{Q}_{ps}]\{\dot{p}\}+[\mathbf{H}_{pp}+\mathbf{H}_{ps}]\{p\}=\{\mathbf{f}_p\}, \tag{5.133}$$

$$[\mathbf{W}_{uu}+\mathbf{W}_{us}]\{\mathbf{u}\}+[\mathbf{W}_{up}+\mathbf{W}_{sp}]\{p\}=\{\mathbf{f}_u\}, \tag{5.134}$$

where, the vector $\{p\}$ includes both the classic DOFs (p_i) and the enriched DOFs ($\overline{g}_j, \overline{\overline{g}}_j$), while the vector $\{\mathbf{u}\}$ consists of the classic DOFs u as well as the enriched DOFs ($\overline{c}$, $\overline{\overline{c}}$). The symbols $\dot{p}$ and $\dot{\mathbf{u}}$ denote the time derivatives of the vectors p and $\mathbf{u}$, respectively, indicating the rates of change of the DOFs with respect to time. Through the utilization of a time integration technique such as the Newmark method, these derivatives undergo discretization. Consequently, the time derivatives of primary variables at the current time step are determined in relation to known values from the preceding time step, in accordance with the iterative nature inherent in numerical methods. This process follows a progression as outlined below:

$$\begin{aligned}\{\dot{\mathbf{u}}\}^{n+1} &= a_0(\{\mathbf{u}\}^{n+1}-\{\mathbf{u}\}^n)-a_1\{\dot{\mathbf{u}}\}^n \\ \{\dot{p}\}^{n+1} &= a_2(\{p\}^{n+1}-\{p\}^n)-a_3\{\dot{p}\}^n\end{aligned} \tag{5.135}$$

where $a_0=\frac{\gamma}{\beta\Delta t}$, $a_1=\frac{\gamma}{\beta}-1$, and $a_2=\frac{\gamma}{\beta}-1$. The constants γ and β denote the Newmark constants, while Δt represents the time step. Furthermore, the computation of the matrices related

to material properties in equations (5.133) and (5.134) is elaborated as follows:

$$
\begin{aligned}
&\mathbf{Q}_{up} = \int_{\Omega} \mathbf{N}_p^T \mathbf{m} \boldsymbol{\theta}^{(r)} \mathbf{B}_u dv, && \mathbf{Q}_{us} = \tfrac{h}{2} \int_{\Gamma} \widetilde{\mathbf{N}}_p^T \mathbf{m} \tilde{\boldsymbol{\theta}} \widetilde{\mathbf{B}}_u dv, \\
&\mathbf{Q}_{pp} = -\int_{\Omega} \mathbf{N}_p^T \tfrac{1}{\eta^{(r)}} \mathbf{N}_p ds, && \mathbf{Q}_{ps} = -\tfrac{h}{2} \int_{\Gamma} \widetilde{\mathbf{N}}_p^T \tilde{\boldsymbol{\eta}} \widetilde{\mathbf{N}}_p^T ds, \\
&\mathbf{H}_{pp} = \int_{\Omega} \mathbf{B}_p^T \mathbf{K}^{(r)} \mathbf{B}_p dv, && \mathbf{H}_{ps} = \mathbf{H}_{ps_1} + \mathbf{H}_{ps_2} + \mathbf{H}_{ps_3} + \mathbf{H}_{ps_4} + \mathbf{H}_{ps_5}, \\
&\mathbf{H}_{ps_1} = -\tfrac{2}{h} \int_{\Gamma} \overline{\mathbf{N}}_p^T \bar{k}_{nn} \overline{\mathbf{N}}_p ds, && \mathbf{H}_{ps_2} = -\int_{\Gamma} \bar{k}_{nn} \overline{\mathbf{N}}_p^T \mathbf{m} \tilde{\mathbf{s}} \widetilde{\mathbf{B}}_p ds, \\
&\mathbf{H}_{ps_3} = -\int_{\Gamma} \bar{k}_{nn} \widetilde{\mathbf{B}}_p^T \tilde{\mathbf{s}} \mathbf{m}^T \overline{\mathbf{N}}_p ds, && \mathbf{H}_{ps_4} = -\tfrac{h}{2} \int_{\Gamma} \bar{k}_{nn} \widetilde{\mathbf{B}}_p^T \tilde{\mathbf{s}} \tilde{\mathbf{s}}^T \widetilde{\mathbf{B}}_p ds, \\
&\mathbf{H}_{ps_5} = \tfrac{h}{2} \int_{\Gamma} \widetilde{\mathbf{B}}_p^T \tilde{\mathbf{D}} \widetilde{\mathbf{B}}_p ds, && \mathbf{f}_p = \int_{\partial \Omega_{w_n}} \mathbf{N}_p^T \overline{w}_n ds, \\
&\mathbf{W}_{uu} = \int_{\Omega} \mathbf{B}_u^T \mathbb{L}^{(r)} \mathbf{B}_u dv, && \mathbf{W}_{us} = \mathbf{W}_{us_1} + \mathbf{W}_{us_2} + \mathbf{W}_{us_3} + \mathbf{W}_{us_4}, \\
&\mathbf{W}_{us_1} = \tfrac{2}{h} \int_{\Gamma} \overline{\mathbf{N}}_u^T \mathbf{H}^{-1} \overline{\mathbf{N}}_u ds, && \mathbf{W}_{us_2} = -\tfrac{h}{2} \int_{\Gamma} \widetilde{\mathbf{B}}_u^T [\mathbb{Z} - (\mathbb{F}^T \cdot \mathbf{n}) \cdot \mathbf{H}^{-1} \cdot (\mathbf{n} \cdot \mathbb{F})] \widetilde{\mathbf{B}}_u ds, \\
&\mathbf{W}_{us_3} = -\int_{\Gamma} \overline{\mathbf{N}}_u^T [\mathbf{H}^{-1} \cdot (\mathbf{n} \cdot \mathbb{F})] \widetilde{\mathbf{B}}_u ds, && \mathbf{W}_{up} = \int_{\Omega} \mathbf{B}_u^T \boldsymbol{\theta}^{(r)} \mathbf{m}^T \mathbf{N}_p dv, \\
&\mathbf{W}_{sp} = \mathbf{W}_{sp_1} + \mathbf{W}_{sp_2} + \mathbf{W}_{sp_3}, && \mathbf{W}_{sp_1} = \int_{\Gamma} \overline{\mathbf{N}}_u^T [\mathbf{H}^{-1} \cdot (\mathbf{n} \cdot \mathbf{R})] \mathbf{m}^T \widetilde{\mathbf{N}}_p ds, \\
&\mathbf{W}_{sp_2} = -\tfrac{h}{2} \int_{\Gamma} \widetilde{\mathbf{B}}_u^T \mathbf{S} \mathbf{m}^T \widetilde{\mathbf{N}}_p ds, && \mathbf{W}_{sp_3} = -\tfrac{h}{2} \int_{\Gamma} \widetilde{\mathbf{B}}_u^T [(\mathbb{F}^T \cdot \mathbf{n}) \cdot \mathbf{H}^{-1} \cdot (\mathbf{n} \cdot \mathbf{R})] \mathbf{m}^T \widetilde{\mathbf{N}}_p ds, \\
&\mathbf{f}_u = \int_{\partial \Omega_t} \mathbf{N}_u^T \bar{\mathbf{t}} ds.
\end{aligned}
\tag{5.136}
$$

Here $(\cdot)^{(r)}$ (with $r = 1, 2$) denotes the physical quantities associated with the material properties of the inclusion and matrix phases, respectively. The vector $\mathbf{m}$ is represented as $[1\ 1\ 1]$. Detailed calculation formulas for the effective scalar $\bar{\eta}$, $\bar{k}_{nn}$, effective vector $\tilde{\mathbf{s}}$, and effective tensors $\tilde{\boldsymbol{\theta}}$ and $\tilde{\mathbf{T}}$ are provided in Appendix (B). Additionally, symbols $\mathbf{N}_p$, $\overline{\mathbf{N}}_p$, and $\widetilde{\mathbf{N}}_p$ represent the shape function matrices associated with variables p, $[\![p]\!]$, and $\langle p \rangle$, respectively. The derivatives of these shape function matrices, denoted as $\mathbf{B}p$, $\overline{\mathbf{B}}_p$, and $\widetilde{\mathbf{B}}_p$, are defined through the mathematical rela-

tionships $\nabla p = \mathbf{B}_p p^e$, $\nabla[\![p]\!] = \overline{\mathbf{B}}_p p^e$, and $\nabla\langle p\rangle = \widetilde{\mathbf{B}}_p p^e$, which correspond to the form functions $\mathbf{N}_p$, $\overline{\mathbf{N}}_p$, and $\widetilde{\mathbf{N}}_p$. More precisely, the formulations for these relationships are as follows:

$$\begin{aligned} p &= \mathbf{N}_p p^e, \quad & \mathbf{B}_p &= \mathbf{L}_p \mathbf{N}_p, \\ [\![p]\!] &= \overline{\mathbf{N}}_p p^e, \quad & \overline{\mathbf{B}}_p &= \mathbf{L}_p \overline{\mathbf{N}}_p, \\ \langle p\rangle &= \widetilde{\mathbf{N}}_p p^e, \quad & \widetilde{\mathbf{B}}_p &= \mathbf{L}_p \widetilde{\mathbf{N}}_p, \end{aligned} \tag{5.137}$$

where, the vector p^e represents the pressure values at the nodes, while the matrix $\mathbf{L}_p$ represents a symbolic matrix operator composed of partial derivative operators. In the specific context of solving a three-dimensional problem, $\mathbf{L}_p$ assumes the following form:

$$\mathbf{L}_p = \begin{bmatrix} \frac{\partial}{\partial x_1} \\ \frac{\partial}{\partial x_2} \\ \frac{\partial}{\partial x_3} \end{bmatrix}. \tag{5.138}$$

Similarly, the shape functions, denoted as $\mathbf{N}_u$, $\overline{\mathbf{N}}_u$, and $\widetilde{\mathbf{N}}_u$, correspondingly relate to distinct displacement fields $\mathbf{u}$, $[\![\mathbf{u}]\!]$, and $\langle\mathbf{u}\rangle$. The strain matrices $\mathbf{B}_u$, $\overline{\mathbf{B}}_u$, and $\widetilde{\mathbf{B}}_u$ represent the derivatives of these shape functions, i.e., $\mathbf{N}u$, $\overline{\mathbf{N}}u$, and $\widetilde{\mathbf{N}}u$, and are interconnected through the computational relations $\nabla\mathbf{u} = \mathbf{B}_u\mathbf{u}^e$, $\nabla[\![\mathbf{u}]\!] = \overline{\mathbf{B}}_u\mathbf{u}^e$, and $\nabla\langle\mathbf{u}\rangle = \widetilde{\mathbf{B}}_u\mathbf{u}^e$. The specific computational framework is detailed as follows:

$$\begin{aligned} \mathbf{u} &= \mathbf{N}_u \mathbf{u}^e, \quad & \mathbf{B}_u &= \mathbf{L}_u \mathbf{N}_u, \\ [\![\mathbf{u}]\!] &= \overline{\mathbf{N}}_u \mathbf{u}^e, \quad & \overline{\mathbf{B}}_u &= \mathbf{L}_u \overline{\mathbf{N}}_u, \\ \langle\mathbf{u}\rangle &= \widetilde{\mathbf{N}}_u \mathbf{u}^e, \quad & \widetilde{\mathbf{B}}_u &= \mathbf{L}_u \widetilde{\mathbf{N}}_u, \end{aligned} \tag{5.139}$$

where the vector $\mathbf{u}^e$ represents the displacement values at the nodes, while the matrix $\mathbf{L}_u$ denotes a symbolic matrix operator comprising partial derivative operators as its elements. Particularly,

for three-dimensional problem computations, its formulation can be expressed as:

$$\mathbf{L}_u = \begin{bmatrix} \frac{\partial}{\partial x_1} & 0 & 0 \\ 0 & \frac{\partial}{\partial x_2} & 0 \\ 0 & 0 & \frac{\partial}{\partial x_3} \\ \frac{\partial}{\partial x_2} & \frac{\partial}{\partial x_1} & 0 \\ 0 & \frac{\partial}{\partial x_3} & \frac{\partial}{\partial x_2} \\ \frac{\partial}{\partial x_3} & 0 & \frac{\partial}{\partial x_1} \end{bmatrix}. \tag{5.140}$$

5.2.4 Element Types and Numerical Integration Strategies

As stated in equations (5.128a) and (5.128b), the value of m is determined by the type of the enriched element. Moreover, within XFEM, varying integration strategies are implemented for different types of elements. Therefore, the classification of elements plays a crucial role within the XFEM framework. The determination of element types relies on assessing the spatial relationship between the element and the interface, facilitated by the LSM primarily through evaluating the level set function value of nodes within the element. To describe the type of element in a visualized way, We establish a two-dimensional model that is divided by triangular elements as schematically illustrated in **Fig.** 5.4. In this instance, the elements can be classified into three types through the geometric position relationship between the elements and the interface.

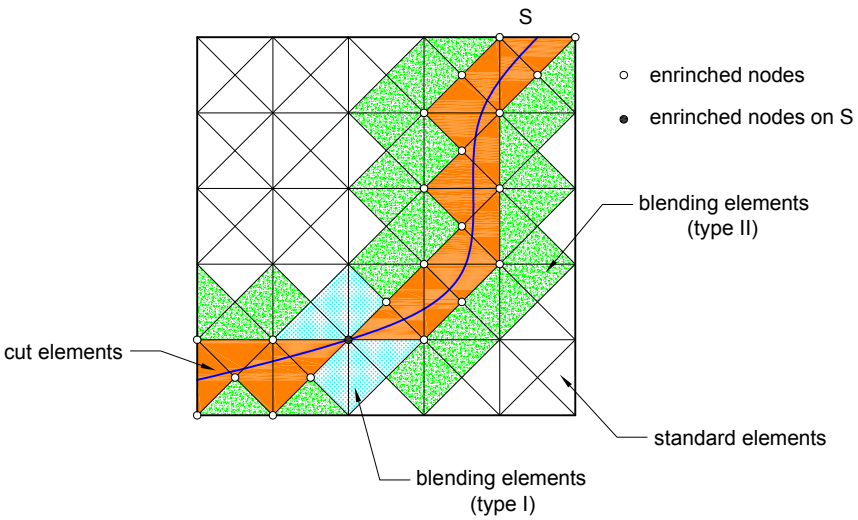

Figure 5.4: *2D representation of the different kinds of element generated by the interface* **S** *intersecting the standard triangular elements.*

(i) Standard finite elements These elements lack enriched nodes and are implemented using the standard finite element method.

(ii) Fully cut elements When elements are divided by the interface, resulting in two parts, they are categorized as fully cut elements. In this case, all nodes within the element are enriched.

(iii) Blending elements These elements have some nodes enriched, and there are two subtypes. Blending elements type I have nodes located directly on the interface, while Blending elements type II are positioned near the cut element and share only some nodes with it.

To obtain the values of the coefficient matrices associated with the unknown vector $\mathbf{u}$ and p as displayed in equation (5.136), numerical integration techniques need to be applied. This entails calculating volume and area integrals, typically estimated using numerical integration methods or approximation techniques. Among numerical integration methods, Gauss quadrature, chosen for its efficiency with polynomial or nearly polynomial functions, plays a pivotal role in computing characteristic matrices of elements. In XFEM, different numerical integration strategies are employed for various element types. For standard elements, the integration procedure is similar to that of classical finite element methods. Conversely, for blending elements, the integral points are adjusted depending on the specific characteristics of each element type. For the cutting elements, wherein physical fields exhibit piecewise continuity due to the presence of interfaces, a specialized integration approach becomes essential to ensure precision and effectively characterize field discontinuities across these interfaces. Specifically, when an element intersects with an imperfect interface, it undergoes a detailed subdivision into multiple sub-elements, each possessing edges that closely approximate the interface geometry. This subdivision process guarantees the continuity of fields within each sub-element, thereby facilitating individualized integration over these sub-regions. Meanwhile, the number and types of generated sub-elements vary based on the different types of intersection between interfaces and elements, as illustrated in Figure 4 for tetrahedral elements. The intersection types between interfaces and elements can be discerned by evaluating the level set function values of nodes within the elements. The strategies for determining intersection types and generating sub-elements are implemented in the computational program. The Gauss quadrature method is based on selecting suitable weights and integration points to ensure exact integration of the highest possible polynomial. To ensure calculation accuracy, the following integral schemes are used to compute the

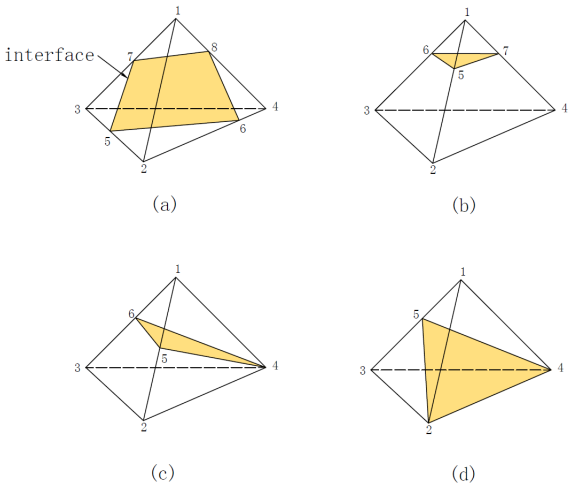

Figure 5.5: *The type that the tetrahedral elements cut by the imperfect interface.*

coefficient matrices:

(1) For standard elements without enrichment nodes, a single Gauss integral point is employed.

(2) For blending elements, four Gauss integral points are adopted.

(3) In cut elements, 15 Gauss integral points are applied for each sub-element, and seven Gauss integral points are used on the imperfect interface.

5.3 Validation and Discussion of Imperfect Interface Model and Numerical Method

In this section, we consider the case of a steady state in which the solution of a two-phase poroelastic composite with general imperfect interface can be first obtained analytically and exactly. This solution is then used as a benchmark to compare with the numerical solution derived by applying the numerical method established in the previous section. This comparison aims to illustrate the correctness and effectiveness of the numerical method as well as the general imperfect interface model.

5.3.1 Analytical Solutions to Boundary Value Problems

First of all, we recall that a steady state in poroelasticity can be characterized by the fact that the derivative with respect to time of any quantity will vanish, i.e. $\dot{\boldsymbol{\varepsilon}} = \mathbf{0}$ and $\dot{p} = 0$. To obtain the analysis benchmark, we consider first the two-phase configuration in which a spherical inclusion $\Omega^{(1)}$ of radius R embedded in an infinite matrix $\Omega^{(2)}$. The interface S between the matrix and inclusion is described by a general imperfect interface model in which the discontinuities of the physical fields across the interface are specified by equations (5.73), (5.74), (5.75) and (5.76). A cartesian coordinate system of which the origin coincides with the geometric center of the spherical inclusion is introduced. The materials forming both the inclusion and matrix domains are assumed to be linearly poroelastic and isotropic.

Let the poroelastic composite Ω be subjected to the following prescribed uniform pressure and linear displacement boundary conditions on its external surface $\partial\Omega$:

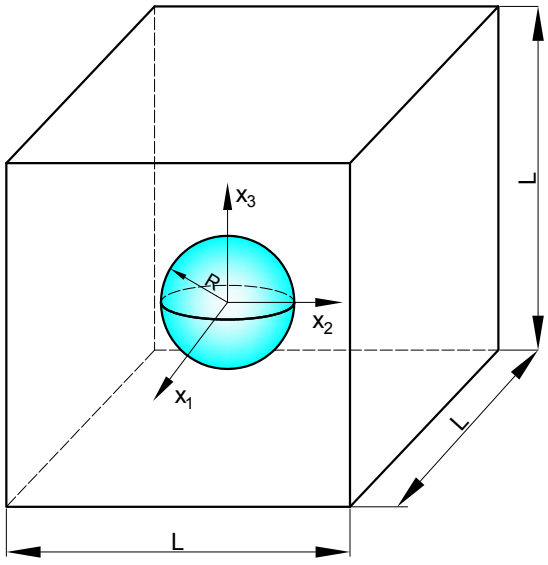

Figure 5.6: *The spherical inclusion embeds in a hexahedron matrix bonded by a general imperfect interface.*

$$\bar{p} = \beta_0, \tag{5.141}$$

$$\bar{\mathbf{u}} = \boldsymbol{\varepsilon}_0 \mathbf{x} \tag{5.142}$$

where β_0 and $\boldsymbol{\varepsilon}_0$ are two prescribed constants. Starting from the spherical symmetry of the

problem, we look for the pressure and displacement fields in the inclusion and matrix phases in the following forms:

$$p^{(r)} = \beta_0, \tag{5.143}$$

$$\mathbf{u}^{(r)}(\mathbf{x}) = F^{(r)}\mathbf{x} + G^{(r)}\frac{\mathbf{x}}{||\mathbf{x}||^3} \tag{5.144}$$

where $F^{(r)}$ and $G^{(r)}$ are two constants to be determined from the boundary and interfacial conditions and the value of the superscript is $r = 1$ evaluated at $\mathbf{x} \in \Omega^{(1)}$ or $r = 2$ evaluated at $\mathbf{x} \in \Omega^{(2)}$. The requirement for finiteness of the displacement at the center $\mathbf{x} = \mathbf{0}$ of the spherical inclusion $\Omega^{(1)}$ implies that $G^{(1)} = 0$. Employing the remote boundary conditions (5.142), $F^{(2)} = \varepsilon_0$ can be deduced. Therefore, we obtain

$$p^{(1)} = p^{(2)} = \beta_0, \tag{5.145}$$

$$\mathbf{u}^{(1)} = F^{(1)}\mathbf{x}, \tag{5.146}$$

$$\mathbf{u}^{(2)} = \left(\varepsilon_0 + \frac{G^{(2)}}{||\mathbf{x}||^3}\right)\mathbf{x}. \tag{5.147}$$

Consequently, the resulting strain tensor $\varepsilon^{(1)}$ of the matrix phase $\Omega^{(1)}$ can be determined by

$$\varepsilon^{(1)} = \frac{1}{2}(\nabla\mathbf{u}^{(1)} + \nabla^T\mathbf{u}^{(1)}) = F^{(1)}\mathbf{I}. \tag{5.148}$$

Similarly, the strain tensor $\varepsilon^{(2)}$ of the matrix phase $\Omega^{(2)}$ is given by

$$\varepsilon^{(2)} = \frac{1}{2}(\nabla\mathbf{u}^{(2)} + \nabla^T\mathbf{u}^{(2)}) = \left(\varepsilon_0 + \frac{G^{(2)}}{||\mathbf{x}||^3}\right)\mathbf{I} - \frac{3G^{(2)}}{||\mathbf{x}||^5}\mathbf{x}\otimes\mathbf{x}. \tag{5.149}$$

As mentioned previously, the materials forming the inclusion, matrix and interphase are linearly poroelastic and isotropic. Consequently, the governing equation (1) takes therefore the following simple form

$$\boldsymbol{\sigma} = (\kappa - \frac{2}{3}\mu)\mathrm{Tr}(\varepsilon)\mathbf{I} + 2\mu\varepsilon + \theta p\mathbf{I} \tag{5.150}$$

where κ and μ are the bulk modulus and shear modulus respectively and θ represents the Biot

coefficient. Introducing (5.148) and (5.149) into the constitutive equation (5.150), the stress tensors $\boldsymbol{\sigma}^{(1)}$ and $\boldsymbol{\sigma}^{(2)}$ evaluated at the domain $\Omega^{(1)}$ and $\Omega^{(2)}$ can be obtained as follows:

$$\boldsymbol{\sigma}^{(1)} = (\kappa^{(1)} - \frac{2}{3}\mu^{(1)})(3F^{(1)}\mathbf{I}) + 2\mu^{(1)}F^{(1)}\mathbf{I} + \theta^{(1)}p^{(1)}\mathbf{I} = 3\kappa^{(1)}F^{(1)}\mathbf{I} + \theta^{(1)}\beta_0\mathbf{I}, \tag{5.151}$$

$$\boldsymbol{\sigma}^{(2)} = 3\varepsilon_0\kappa^{(2)}\mathbf{I} + \frac{2\mu^{(2)}G^{(2)}}{||\mathbf{x}||^3}\left(\mathbf{I} - 3\frac{\mathbf{x}\otimes\mathbf{x}}{||\mathbf{x}||^2}\right) + \theta^{(2)}\beta_0\mathbf{I}. \tag{5.152}$$

Then, the traction vectors evaluated on the two sides of the imperfect interface S characterized by $||\mathbf{x}|| = R$ are given by

$$\mathbf{t}^{(-)} = \boldsymbol{\sigma}^{(1)}\cdot\mathbf{n} = (3\kappa^{(1)}F^{(1)} + \theta^{(1)}\beta_0)\mathbf{n}, \tag{5.153}$$

$$\mathbf{t}^{(+)} = \boldsymbol{\sigma}^{(2)}\cdot\mathbf{n} = \left(3\kappa^{(2)}\varepsilon_0 + \theta^{(2)}\beta_0 - \frac{4\mu^{(2)}G^{(2)}}{R^3}\right)\mathbf{n}. \tag{5.154}$$

According to the above calculation, the jumping relationships of the displacement and stress vector fields $\mathbf{u}$ and $\mathbf{t}$ across the interface can be worked out, which contain unknown parameters $F^{(1)}$ and $G^{(2)}$. If the two unknown parameters are solved, the displacement field of the whole domain can be clearly expressed. Recalling the discontinuity relations previously derived, the two unknowns parameters, with which the displacement field of the whole domain can be clearly expressed, can be solved.

Introducing the expressions (5.146), (5.147), (5.153) and (5.154) into relations (5.73) and (5.74), the jump relations of the traction vector $\mathbf{t}$ and displacement field $\mathbf{u}$ across the general imperfect interface model take the following forms:

$$\begin{aligned}
&3\kappa^{(2)}\varepsilon_0 + \theta^{(2)}\beta_0 - \frac{4\mu^{(2)}G^{(2)}}{R^3} - 3\kappa^{(1)}F^{(1)} - \theta^{(1)}\beta_0 = \left(\frac{4\mu^{(0)}\theta^{(0)}}{\lambda^{(0)}+2\mu^{(0)}} - \frac{2\mu^{(1)}\theta^{(1)}}{\lambda^{(1)}+2\mu^{(1)}} - \frac{2\mu^{(2)}\theta^{(2)}}{\lambda^{(2)}+2\mu^{(2)}}\right)\frac{\beta_0 h}{R} \\
&+\left(\frac{\lambda^{(0)}}{\lambda^{(0)}+2\mu^{(0)}} - \frac{\lambda^{(1)}}{2(\lambda^{(1)}+2\mu^{(1)})} - \frac{\lambda^{(2)}}{2(\lambda^{(2)}+2\mu^{(2)})}\right)\left(3\kappa^{(1)}F^{(1)} + (\theta^{(1)}+\theta^{(2)})\beta_0 + 3\kappa^{(2)}\varepsilon_0 - 4\mu^{(2)}\frac{G^{(2)}}{R^3}\right)\frac{h}{R} \\
&+\left(\frac{4\mu^{(0)}\lambda^{(0)}}{\lambda^{(0)}+2\mu^{(0)}} - \frac{2\mu^{(1)}\lambda^{(1)}}{\lambda^{(1)}+2\mu^{(1)}} - \frac{2\mu^{(2)}\lambda^{(2)}}{\lambda^{(2)}+2\mu^{(2)}} + 2\mu^{(0)} - \mu^{(1)} - \mu^{(2)}\right)\left(F^{(1)} + \varepsilon_0 + \frac{G^{(2)}}{R^3}\right)\frac{h}{R},
\end{aligned} \tag{5.155}$$

$$\varepsilon_0 R + \frac{G^{(2)}}{R^2} - F^{(1)} R = -\left(\frac{\theta^{(0)}}{\lambda^{(0)} + 2\mu^{(0)}} - \frac{\theta^{(1)}}{2(\lambda^{(1)} + 2\mu^{(1)})} - \frac{\theta^{(2)}}{2(\lambda^{(2)} + 2\mu^{(2)})} \right) h\beta_0 \tag{5.156}$$
$$+ \left(\frac{1}{2(\lambda^{(0)} + 2\mu^{(0)})} - \frac{1}{4(\lambda^{(2)} + 2\mu^{(2)})} - \frac{1}{4(\lambda^{(1)} + 2\mu^{(1)})} \right) \left(3\kappa^{(1)} F^{(1)} + (\theta^{(1)} + \theta^{(2)})\beta_0 + 3\kappa^{(2)} \varepsilon_0 \right.$$
$$\left. - \frac{4\mu^{(2)} G^{(2)}}{R^3} \right) h + \left(\frac{\lambda^{(2)}}{2(\lambda^{(2)} + 2\mu^{(2)})} + \frac{\lambda^{(1)}}{2(\lambda^{(1)} + 2\mu^{(1)})} - \frac{\lambda^{(0)}}{\lambda^{(0)} + 2\mu^{(0)}} \right) \left(F^{(1)} + \varepsilon_0 + \frac{G^{(2)}}{R^3} \right) h$$

where $\lambda^{(r)} = \kappa^{(r)} - \frac{2}{3}\mu^{(r)}$ denote the Lamé coefficient. By solving the system of two equations (5.155) and (5.156) with two unknown constants $F^{(1)}$ and $G^{(2)}$, we obtain first $F^{(1)}$ and $G^{(2)}$ and derive then the displacement, strain and stress fields in the matrix and inclusion phases as well as the jumps of the displacement and traction fields through the general imperfect interface.

When the three-phase matrix/interphase/inclusion configuration is concerned, under the same boundary conditions (5.141) and (5.142), the pressure and displacement fields in the inclusion and matrix phases take the same expressions as in the two-phase matrix/inclusion configuration while the pressure and displacement fields in the interphase are given by

$$p^{(0)} = \beta_0, \tag{5.157}$$

$$\mathbf{u}^{(0)} = \left(F_0 + \frac{G^{(0)}}{||\mathbf{x}||^3} \right) \mathbf{x}. \tag{5.158}$$

Owing to the fact that the interface S_1 ($||\mathbf{x}|| = R - \frac{h}{2}$) between the inclusion and interphase and the interface S_2 ($||\mathbf{x}|| = R + \frac{h}{2}$) between the matrix and interphase are both perfect, the displacement and stress vectors are therefore continuous across these interfaces S_1 and S_2, or equivalently

$$F^{(0)} + \frac{G^{(0)}}{(R - \frac{h}{2})^3} = F^{(1)}, \tag{5.159}$$

$$3\kappa^{(0)} F^{(0)} - \frac{4\mu^{(0)} G^{(0)}}{(R - \frac{h}{2})^3} + \theta^{(0)} \beta_0 = 3\kappa^{(1)} F^{(1)} + \theta^{(1)} \beta_0, \tag{5.160}$$

$$F_0 + \frac{G^{(0)}}{(R+\frac{h}{2})^3} = \varepsilon_0 + \frac{G^{(2)}}{(R+\frac{h}{2})^3}, \tag{5.161}$$

$$3\kappa^{(0)}F_0 - \frac{4\mu^{(0)}G^{(0)}}{(R+\frac{h}{2})^3} + \theta^{(0)}\beta_0 = 3\kappa^{(1)}\varepsilon_0 - \frac{4\mu^{(2)}G^{(2)}}{(R+\frac{h}{2})^3} + \theta^{(2)}\beta_0. \tag{5.162}$$

We obtain another system of 4 linear equations (5.176)-(5.177) with 4 unknown constants $F^{(1)}$, $F^{(0)}$, $G^{(0)}$ and $G^{(2)}$. The resolution of this system of 4 linear equations implies the pressure, displacement, strain and stress fields in the matrix, interphase and inclusion phases.

5.3.2 Convergence Analysis

The validity and accuracy of the proposed numerical procedure can be verified through convergence analysis, which calculates the error of the approximate numerical results with respect to the corresponding analytic exact solution. To conduct this analysis, a cube with a side length l is extracted from the infinite matrix. Within this cube, a spherical inclusion with a radius $R = \frac{1}{4}l$ is embedded at the center, and both are divided into tetrahedra with a side length h_e. To examine the effect of interface thickness on convergence, interfaces with varying thickness are selected for the convergence analysis.

The displacement fields within the inclusion and matrix phase as well as on the interface of the cube are given by the analytical exact expression (5.146) in conjunction with (5.147). To enhance the precision of the convergence analysis, the global convergence rate is employed, defined by the following L^2-norm indicator:

$$e = \frac{\sqrt{\frac{1}{vol(\Omega)}\int_\Omega \parallel \mathbf{u}^{h_e} - \mathbf{u} \parallel^2 dV + \frac{1}{area(S)}\int_S \parallel [\![\mathbf{u}]\!]^{h_e} - [\![\mathbf{u}]\!] \parallel^2 dS}}{\sqrt{\frac{1}{vol(\Omega)}\int_\Omega \parallel \mathbf{u} \parallel^2 dV + \frac{1}{area(S)}\int_S \parallel [\![\mathbf{u}]\!] \parallel^2 dS}} \tag{5.163}$$

where the $\mathbf{u}^{h_e}$ represents the displacement vector of numerical solution by XFEM and the $\mathbf{u}$ indicates the quantity of analytic exact solution. $vol(\Omega)$ is the volume of the cube matrix and $area(S)$ denotes the area of imperfect interface between the cube and the spherical inclusion.

The granite is selected as the research object. The parameters used in our analysis are shown in Table 5.1. To illustrate the applicability and generality of the general imperfect interface above, the Young's modulus of the interphase is set to vary from 50 MPa to 5×10^6 MPa while the

Poisson's ratios of the inclusion, matrix and interphase are kept constant with $\nu^{(1)} = \nu^{(0)} = 0.2$ and $\nu^{(2)} = 0.23$.

Table 5.1: Parameters used for the analysis

Set no.	$E^{(1)}(MPa)$	$E^{(2)}(MPa)$	$E^{(0)}(MPa)$	interphase thichness
1	4×10^4	9×10^4	$50 \sim 5 \times 10^7$	$10^{-3}l$
2	4×10^4	9×10^4	$50 \sim 5 \times 10^7$	$10^{-4}l$

As the element size h_e decreases, the results of the convergence analysis are plotted in **Fig.** 5.7. We can notice that, with the element size h_e diminishes, the relative error e decreases. As shown, they also reflect that the numerical solutions converge to the corresponding analytical exact solution. Meanwhile, the convergence rates with a smaller value of the interphase thickness h are better than those with a larger value. Indeed, the interphase thickness h involved in the weak form (5.123) and (5.125) plays a central role in the process of establishing the imperfect interface model and numeric implementation. Note that in these processes, some of the higher order infinitesimal quantities about h are treated as zero. Thus, when the interphase thickness h increases, the convergence rates are smaller.

5.3.3 Analysis of Numerical and Analytical Results

In addition, we deeply discuss the effectiveness of the discontinuities across the general imperfect interfaces by analyzing the distribution of the displacement and stress fields. The previous model with the same material and geometric parameters, as shown in **Fig.** 5.6, is employed for analysis. The whole model domain is meshed with 296595 tetrahedron elements and 64000 nodes. In order to characterize the effect of interface thickness on discontinuity, we choose the interphase with different thickness for analysis.

To ensure that the physical fields of the numerical method model are consistent with those of the theoretical method model, the displacement field on the surface of the cube is provided by the the analytical exact expression (5.155) together with (5.156). Along the direction of the x_3-axis, a straight line normal to the $x_1 - x_2$ plane is selected in the origin of the analysis model. In this straight line, 20 points are evenly chosen, then the displacement component u_3 and stress component σ_{33} along the x_3-axis of these point are drawn. The comparison of the numerical result obtained by the XFEM-based implementation proposed and the analytical results are

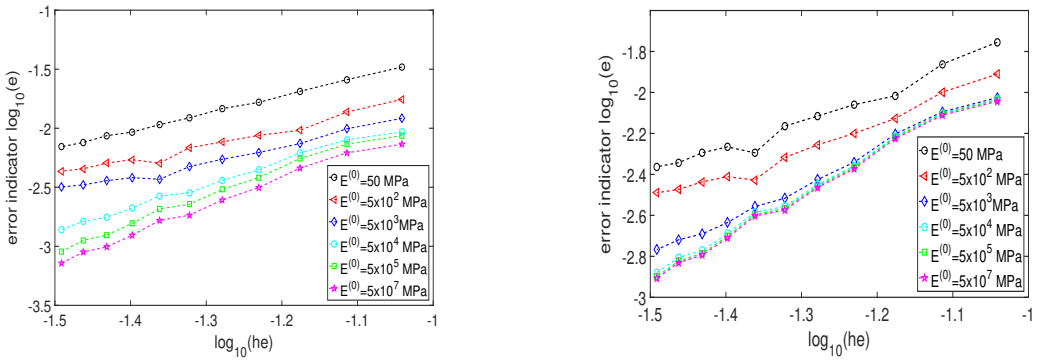

(a) (b)

Figure 5.7: *Convergence analysis for the spherical inclusion problem with the general interface.*

exhibited in Figure 5.8 and Figure 5.9. The comparison chars show that the the displacement

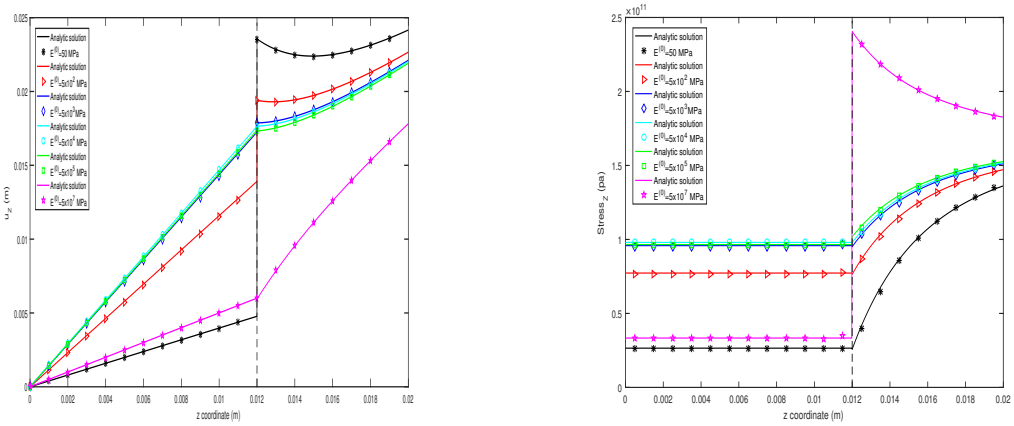

(a) Displacement field along x_3-axis (b) Stress field along x_3-axis

Figure 5.8: *Comparison of the numerical and analytical results for the displacement component u_3 and stress component σ_{33} along the x_3-axis with the thickness $10^{-3}l$ of the interphase.*

component u_3 and stress component σ_{33} of the numerical method accord with that of the analytical method. The displacement field is continuous in the solution domain except the imperfect interface. From these figures, when the Young's modulus of the interphase is much smaller than that of the surrounding phase, displacement at the imperfect interface suffers a very significant jump. As the Young's modulus of the interphase increases, the displacement jump at the interface diminishes. When the Young's modulus of the interphase is much larger than that of the surrounding phases, the displacement field at the imperfect interface converts into continuous. From the distribution of the stress component in the whole domain, it is continuous at the inter-

face when the Young's modulus of the interphase is several orders of magnitude smaller than that of the matrix phase and inclusion phase. When the Young's modulus of the interphase becomes larger than that of the surrounding phases, the stress component begin to become discontinuous at the interface. The distribution of these fields varying with the different Young's modulus of the interphase consistent with the properties of the imperfect interface introduced previously. E-specially the cases that the Young's modulus of the interphase is much larger or smaller than that of the surrounding phases correspond to the spring-layer model or the coherent interface model. The foregoing discussions clearly indicate that the proposed numerical method is applicable and universal for the analysis of the saturated porous composites. It is available to handle various interface cases across which the physical fields suffer the strong and weak discontinuities.

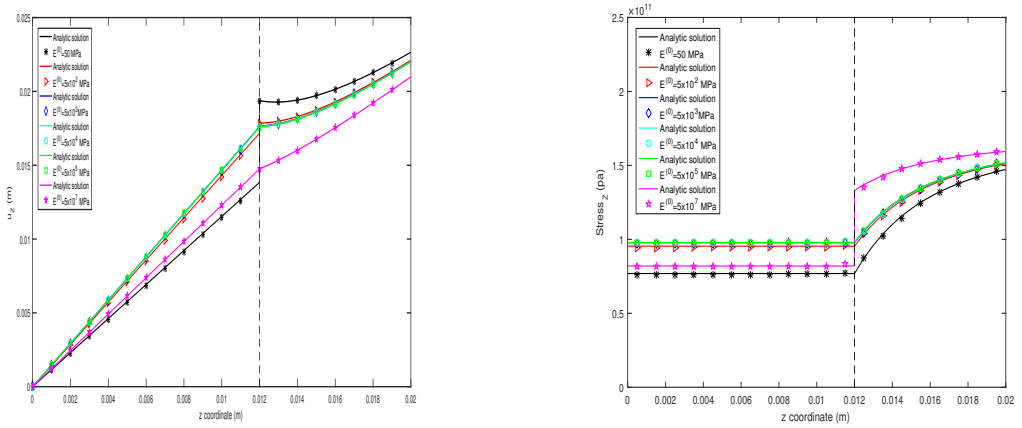

(a) (b)

Figure 5.9: *Comparison of the numerical and analytical results for the displacement component u_3 and stress component σ_{33} along the x_3-axis with the thickness $10^{-4}l$ of the interphase.*

Comparing the **Fig.** 5.8 and **Fig.** 5.9, we can see that the thickness of the interphase has a significant influence on the interface effect. Indeed, distribution of these fields of the numerical results and theoretical results are obviously different with the two different thickness of the interphase. As the thickness of the interphase increases, there is a more remarkable jump of the physical fields at the interface.

5.4 Generalized Self-Consistent Scheme (GSCS) for Estimating Effective Poroelastic Properties

In order to determine the effective poroelastic properties of the composite constituted by a poroelastic matrix reinforced by spherical poroelastic inclusions, a micromechanical model based on the generalized self-consistent scheme is now proposed. The matrix and inclusion phases are assumed to be both isotropic, and the interface between them is described by a general imperfect interface model. This model is an extension to poroelastic materials with general imperfect interfaces of the classical GSCS, which was initiated by Van der Poel [110], improved by Smith [123, 124], and completed by Christensen and Lo [27].

According to this model, we first consider an infinite body Ω^∞ made of the effective homogeneous medium, which is subjected to the same uniform boundary conditions as shown in Eqs. (5.141) and (5.142). Due to the linearity of the local constitutive laws of each phase and to that of the imperfect interface, the corresponding effective behavior remains isotropic and linearly poroelastic and takes the form

$$\sigma^* = \left(\kappa^* - \frac{2}{3}\mu^*\right)\mathrm{tr}(\varepsilon^*)\mathbf{I} + 2\mu^*\varepsilon^* + \theta^* p^*\mathbf{I} \tag{5.164}$$

where κ^*, μ^* and θ^* are the effective bulk and shear modulus and the effective Biot's coefficient. Under the uniform boundary conditions Eqs. (5.141) and (5.142), the following displacements, pressure, strain and stress tensors, traction vector are given in Ω^∞

$$\begin{aligned} &\mathbf{u}^*(\mathbf{x}) = \varepsilon_0\mathbf{x}, \quad \theta^*(\mathbf{x}) = \beta_0, \quad \varepsilon^*(\mathbf{x}) = \varepsilon_0\mathbf{I}, \\ &\sigma^*(\mathbf{x}) = (3\kappa^*\varepsilon_0 + \theta^*\beta_0)\mathbf{I}, \quad \mathbf{t}^* = (3\kappa^*\varepsilon_0 + \theta^*\beta_0)\mathbf{n}. \end{aligned} \tag{5.165}$$

The free energy of Ω^∞ takes the following form

$$U_0(\varepsilon_0, \beta_0) = \frac{1}{2} vol(\Omega^\infty)\left(9\kappa^*\varepsilon_0^2 + 6\theta^*\varepsilon_0\beta_0 - \frac{\beta_0^2}{\eta^*}\right) \tag{5.166}$$

where η^* represents the effective Biot's modulus.

Next, we cut a sphere out of the foregoing infinite effective medium Ω^∞ and substitute back a composite sphere Ω while imposing the same boundary condition on $\partial\Omega^\infty$ as before. The

interface between the composite sphere and outside medium is assumed perfectly bonded. The core of this composite sphere is made of the inclusion phase 1 and is surrounded by a concentric shell consisting of the matrix phase 2. The radii of the core and coating, symbolized by R and ρ are chosen so as to be compatible with its prescribed phase volume fractions

$$c_1 = 1 - c_2 = \left(\frac{R}{\rho}\right)^3. \tag{5.167}$$

The spherical interface S between the matrix and inclusion is formulated by the general imperfect interface model as described in Section 2. Starting the spherical symmetry of the problem and taking account to the boundary condtions Eqs. (5.141) and (5.142), we seek the pressure and displacement fields within the inclusion (phase 1), matrix (phase 2) and effective medium (phase e) in the following forms:

$$p^{(1)} = p^{(2)} = p^{(e)} = \beta_0, \tag{5.168}$$

$$\begin{aligned}
\mathbf{u}^{(1)} &= (F^{(1)}\varepsilon_0 + f^{(1)}\beta_0)\mathbf{x}, \\
\mathbf{u}^{(2)} &= \left(F^{(2)}\varepsilon_0 + f^{(2)}\beta_0 + \frac{G^{(2)}\varepsilon_0 + g^{(2)}\beta_0}{||\mathbf{x}||^3}\right)\mathbf{x}, \\
\mathbf{u}^{(e)} &= \left(\varepsilon_0 + \frac{G^{(e)}\varepsilon_0 + g^{(e)}\beta_0}{||\mathbf{x}||^3}\right)\mathbf{x}.
\end{aligned} \tag{5.169}$$

Here, $F^{(1)}$, $F^{(2)}$, $G^{(2)}$ and $G^{(e)}$ are unknown constants associated with the displacement loading ε_0 while $f^{(1)}$, $f^{(2)}$, $g^{(2)}$ and $g^{(e)}$ are unknown constants connected with the pressure loading β_0.

The resulting strain and stress tensors are given by

$$
\begin{aligned}
\boldsymbol{\varepsilon}^{(1)} &= (F^{(1)}\boldsymbol{\varepsilon}_0 + f^{(1)}\boldsymbol{\beta}_0)\mathbf{I}, \\
\boldsymbol{\varepsilon}^{(2)} &= \left(F^{(2)}\boldsymbol{\varepsilon}_0 + f^{(2)}\boldsymbol{\beta}_0 + \frac{G^{(2)}\boldsymbol{\varepsilon}_0 + g^{(2)}\boldsymbol{\beta}_0}{||\mathbf{x}||^3}\right)\mathbf{I} - \frac{3(G^{(2)}\boldsymbol{\varepsilon}_0 + g^{(2)}\boldsymbol{\beta}_0)}{||\mathbf{x}||^5}\mathbf{x}\otimes\mathbf{x}, \\
\boldsymbol{\varepsilon}^{(e)} &= \left(\boldsymbol{\varepsilon}_0 + \frac{G^{(e)}\boldsymbol{\varepsilon}_0 + g^{(e)}\boldsymbol{\beta}_0}{||\mathbf{x}||^3}\right)\mathbf{I} - \frac{3(G^{(e)}\boldsymbol{\varepsilon}_0 + g^{(e)}\boldsymbol{\beta}_0)}{||\mathbf{x}||^5}\mathbf{x}\otimes\mathbf{x}, \qquad (5.170) \\
\boldsymbol{\sigma}^{(1)} &= 3\kappa^{(1)}(F^{(1)}\boldsymbol{\varepsilon}_0 + f^{(1)}\boldsymbol{\beta}_0)\mathbf{I} + \theta^{(1)}\boldsymbol{\beta}_0\mathbf{I}, \\
\boldsymbol{\sigma}^{(2)} &= 3\kappa^{(2)}(F^{(2)}\boldsymbol{\varepsilon}_0 + f^{(2)}\boldsymbol{\beta}_0)\mathbf{I} + \frac{2\mu^{(2)}(G^{(2)}\boldsymbol{\varepsilon}_0 + g^{(2)}\boldsymbol{\beta}_0)}{||\mathbf{x}||^3}\left(\mathbf{I} - 3\frac{\mathbf{x}\otimes\mathbf{x}}{||\mathbf{x}||^2}\right) + \theta^{(2)}\boldsymbol{\beta}_0\mathbf{I}, \\
\boldsymbol{\sigma}^{(e)} &= 3\boldsymbol{\varepsilon}_0\kappa^*\mathbf{I} + \frac{2\mu^*(G^{(e)}\boldsymbol{\varepsilon}_0 + g^{(e)}\boldsymbol{\beta}_0)}{||\mathbf{x}||^3}\left(\mathbf{I} - 3\frac{\mathbf{x}\otimes\mathbf{x}}{||\mathbf{x}||^2}\right) + \theta^*\boldsymbol{\beta}_0\mathbf{I}. \qquad (5.171)
\end{aligned}
$$

The traction vectors, $\mathbf{t}^{(-)}$ and $\mathbf{t}^{(+)}$, evaluated on the two sides of the imperfect interface S, characterized by $||\mathbf{x}|| = R$, are specified by

$$
\mathbf{t}^{(-)} = \boldsymbol{\sigma}^{(1)}\cdot\mathbf{n} = [3\kappa^{(1)}(F^{(1)}\boldsymbol{\varepsilon}_0 + f^{(1)}\boldsymbol{\beta}_0) + \theta^{(1)}\boldsymbol{\beta}_0]\mathbf{n}, \qquad (5.172)
$$

$$
\mathbf{t}^{(+)} = \boldsymbol{\sigma}^{(2)}\cdot\mathbf{n} = \left[3\kappa^{(2)}(F^{(2)}\boldsymbol{\varepsilon}_0 + f^{(2)}\boldsymbol{\beta}_0) + \theta^{(2)}\boldsymbol{\beta}_0 - \frac{4\mu^{(2)}(G^{(2)}\boldsymbol{\varepsilon}_0 + g^{(2)}\boldsymbol{\beta}_0)}{R^3}\right]\mathbf{n}. \qquad (5.173)
$$

The traction vector $\mathbf{t}$ on the interface $\partial\Omega$ with $||\mathbf{x}|| = \rho$ between the matrix and effective medium is expressed by

$$
\mathbf{t} = \left[3\kappa^{(2)}(F^{(2)}\boldsymbol{\varepsilon}_0 + f^{(2)}\boldsymbol{\beta}_0) + \theta^{(2)}\boldsymbol{\beta}_0 - \frac{4\mu^{(2)}(G^{(2)}\boldsymbol{\varepsilon}_0 + g^{(2)}\boldsymbol{\beta}_0)}{\rho^3}\right]\mathbf{n}. \qquad (5.174)
$$

Across the general imperfect interface S, the jump relations of the traction vector $\mathbf{t}$ and displace-

ment field $\mathbf{u}$ can be rewritten in the following form

$$
\begin{aligned}
&3\kappa^{(2)}(F^{(2)}\varepsilon_0+f^{(2)}\beta_0)+\theta^{(2)}\beta_0-\frac{4\mu^{(2)}(G^{(2)}\varepsilon_0+g^{(2)}\beta_0)}{R^3}-3\kappa^{(1)}(F^{(1)}\varepsilon_0+f^{(1)}\beta_0)-\theta^{(1)}\beta_0\\
&=\left(\frac{4\mu^{(0)}\theta^{(0)}}{\lambda^{(0)}+2\mu^{(0)}}-\frac{2\mu^{(1)}\theta^{(1)}}{\lambda^{(1)}+2\mu^{(1)}}-\frac{2\mu^{(2)}\theta^{(2)}}{\lambda^{(2)}+2\mu^{(2)}}\right)\frac{\beta_0 h}{R}+\left(\frac{\lambda^{(0)}}{\lambda^{(0)}+2\mu^{(0)}}-\frac{\lambda^{(1)}}{2(\lambda^{(1)}+2\mu^{(1)})}\right.\\
&\left.-\frac{\lambda^{(2)}}{2(\lambda^{(2)}+2\mu^{(2)})}\right)\left((\theta^{(1)}+\theta^{(2)})\beta_0+3\kappa^{(1)}(F^{(1)}\varepsilon_0+f^{(1)}\beta_0)+3\kappa^{(2)}(F^{(2)}\varepsilon_0+f^{(2)}\beta_0)\right.\\
&\left.-4\mu^{(2)}\frac{(G^{(2)}\varepsilon_0+g^{(2)}\beta_0)}{R^3}\right)\frac{h}{R}+\left(2\mu^{(0)}-\mu^{(1)}-\mu^{(2)}+\frac{4\mu^{(0)}\lambda^{(0)}}{\lambda^{(0)}+2\mu^{(0)}}-\frac{2\mu^{(1)}\lambda^{(1)}}{\lambda^{(1)}+2\mu^{(1)}}\right.\\
&\left.-\frac{2\mu^{(2)}\lambda^{(2)}}{\lambda^{(2)}+2\mu^{(2)}}\right)\left(F^{(1)}\varepsilon_0+f^{(1)}\beta_0+F^{(2)}\varepsilon_0+f^{(2)}\beta_0+\frac{(G^{(2)}\varepsilon_0+g^{(2)}\beta_0)}{R^3}\right)\frac{h}{R},
\end{aligned}
\tag{5.175}
$$

$$
\begin{aligned}
&(F^{(2)}\varepsilon_0+f^{(2)}\beta_0)R+\frac{(G^{(2)}\varepsilon_0+g^{(2)}\beta_0)}{R^2}-(F^{(1)}\varepsilon_0+f^{(1)}\beta_0)R=-\left(\frac{\theta^{(0)}}{\lambda^{(0)}+2\mu^{(0)}}-\frac{\theta^{(1)}}{2(\lambda^{(1)}+2\mu^{(1)})}\right.\\
&\left.-\frac{\theta^{(2)}}{2(\lambda^{(2)}+2\mu^{(2)})}\right)h\beta_0+\left(\frac{1}{2(\lambda^{(0)}+2\mu^{(0)})}-\frac{1}{4(\lambda^{(2)}+2\mu^{(2)})}-\frac{1}{4(\lambda^{(1)}+2\mu^{(1)})}\right)\left(3\kappa^{(1)}(F^{(1)}\varepsilon_0+f^{(1)}\beta_0)\right.\\
&\left.+(\theta^{(1)}+\theta^{(2)})\beta_0+3\kappa^{(2)}(F^{(2)}\varepsilon_0+f^{(2)}\beta_0)-\frac{4\mu^{(2)}(G^{(2)}\varepsilon_0+g^{(2)}\beta_0)}{R^3}\right)h+\left(\frac{\lambda^{(2)}}{2(\lambda^{(2)}+2\mu^{(2)})}\right.\\
&\left.+\frac{\lambda^{(1)}}{2(\lambda^{(1)}+2\mu^{(1)})}-\frac{\lambda^{(0)}}{\lambda^{(0)}+2\mu^{(0)}}\right)\left(F^{(1)}\varepsilon_0+f^{(1)}\beta_0+F^{(2)}\varepsilon_0+f^{(2)}\beta_0+\frac{(G^{(2)}\varepsilon_0+g^{(2)}\beta_0)}{R^3}\right)h.
\end{aligned}
\tag{5.176}
$$

Across the perfect bonded interface $\partial\Omega$, the continuity conditions of the traction vector $\mathbf{t}$ and displacement field $\mathbf{u}$ read

$$
\begin{aligned}
&3\kappa^{(2)}(F^{(2)}\varepsilon_0+f^{(2)}\beta_0)-\frac{4\mu^{(2)}(G^{(2)}\varepsilon_0+g^{(2)}\beta_0)}{\rho^3}+\theta^{(2)}\beta_0\\
&=3\kappa^{*}\varepsilon_0-\frac{4\mu^{*}(G^{(e)}\varepsilon_0+g^{(e)}\beta_0)}{\rho^3}+\theta^{*}\beta_0,
\end{aligned}
\tag{5.177}
$$

$$
(F^{(2)}\varepsilon_0+f^{(2)}\beta_0)\rho+\frac{(G^{(2)}\varepsilon_0+g^{(2)}\beta_0)}{\rho^2}=\varepsilon_0\rho+\frac{(G^{(e)}\varepsilon_0+g^{(e)}\beta_0)}{\rho^2}.
\tag{5.178}
$$

Due to the presence of the composite sphere in the effective medium, the initially uniform strain and stress fields of the latter are disturbed. It is shown in Appendix that the free energy $U(\varepsilon_0,\beta_0)$

of Ω^{∞} after inserting the composite sphere Ω is given by the following formula:

$$U = U_0 + \frac{1}{2}\int_{\partial\Omega}(\mathbf{t}\cdot\mathbf{u}^* - \mathbf{t}^*\cdot\mathbf{u})ds + \frac{1}{2}\int_{\Omega}\left(\beta_0\theta\mathrm{tr}(\varepsilon) - \frac{\beta_0^2}{\eta}\right)dv - \frac{1}{2}\left(3\theta^*\varepsilon_0\beta_0 - \frac{\beta_0^2}{\eta^*}\right)vol(\Omega). \tag{5.179}$$

Here, $\mathbf{u}^*$ and $\mathbf{t}^*$ are the initial traction and displacement vectors on $\partial\Omega$; $\mathbf{u}$ and $\mathbf{t}$ are the traction and displacement vectors on $\partial\Omega$ when the composite sphere has been introduced; ε is the strain field in the composite sphere. Compared with the classical formulas of Eshelby [38], Eq. (5.179) can be viewed as a poroelastic extension. As in the GSCS of Christensen and Lo [27], the effective poroelastic properties of the effective medium are required to be such that the presence of the composite sphere does not change the initial free energy. Thus, the self-consistency condition reads

$$\begin{aligned}&\int_{\partial\Omega}(\mathbf{t}\cdot\mathbf{u}^* - \mathbf{t}^*\cdot\mathbf{u})ds + \int_{\Omega}\left(\beta_0\theta\mathrm{tr}(\varepsilon) - \frac{\beta_0^2}{\eta}\right)dv - \left(3\theta^*\varepsilon_0\beta_0 - \frac{\beta_0^2}{\eta^*}\right)vol(\Omega)\\ &+\int_S\left(\theta^{(0)}\beta_0[\![u_i]\!]n_i - \frac{h\beta_0^2}{\eta^{(0)}}\right)ds = 0.\end{aligned} \tag{5.180}$$

Note that when $\beta_0 = 0$, the self-consistency condition (5.180) reduces to that of Christensen and Lo [27].

Firstly, we introduce the expressions of $\mathbf{u}^*$, $\mathbf{t}^*$ given by Eq. (5.165), and of the strain field ε provided by Eq. (5.170) into Eq. (5.180). Accounting for Eqs. (5.177) and (5.178) implies that the self-consistency condition (5.180) holds for any ε_0 and β_0 if and only if

$$G^{(e)} = 0, \tag{5.181}$$

$$\theta^* = c_1\theta^{(1)}F^{(1)} + c_2\theta^{(2)}F^{(2)} + c_1\theta^{(0)}\left(F^{(2)} + \frac{G^{(2)}}{R^3} - F^{(1)}\right) - (3\kappa^* + 4\mu^*)\left(\frac{g^{(e)}}{\rho^3}\right), \tag{5.182}$$

$$\begin{aligned}\frac{1}{\eta^*} &= 3\theta^*\left(\frac{g^{(e)}}{\rho^3}\right) + c_1\left(\frac{1}{\eta^{(1)}} - 3\theta^{(1)}f^{(1)}\right) + c_2\left(\frac{1}{\eta^{(2)}} - 3\theta^{(2)}f^{(2)}\right)\\ &\quad + 3c_1\left[\frac{h}{R\eta^{(0)}} - \theta^{(0)}\left(f^{(2)} + \frac{g^{(2)}}{R^3} - f^{(1)}\right)\right].\end{aligned} \tag{5.183}$$

Secondly, setting $\beta_0 = 0$, $G^{(e)} = 0$, and $\varepsilon_0 = 1$ into Eqs. (5.175)-(5.178), we obtain a system of four linear equations for the four unknowns $F^{(1)}$, $F^{(2)}$, $G^{(2)}$, and κ^*. The resolution of this system of four linear equations allows us to calculate the effective compressibility modulus κ^*

as well as the values of $F^{(1)}$, $F^{(2)}$ and $G^{(2)}$.

Thirdly, introducing Eq. (5.182) and setting $\beta_0 = 1$ and $\varepsilon_0 = 0$ into Eqs. (5.175)-(5.178) yield a new system of four linear equations for the four unknowns $f^{(1)}$, $f^{(2)}$, $g^{(2)}$, and $g^{(e)}$. By solving this system of four linear equations, we obtain the values of unknown constants $f^{(1)}$, $f^{(2)}$ and $g^{(2)}$. Moreover, we can also show that

$$g^{(e)} = 0. \tag{5.184}$$

Consequently, the effective Biot's coefficient θ^* given by Eq. (5.182) takes therefore a simple form:

$$\theta^* = c_1\theta^{(1)}F^{(1)} + c_2\theta^{(2)}F^{(2)} + c_1\theta^{(0)}\left(F^{(2)} + \frac{G^{(2)}}{R^3} - F^{(1)}\right). \tag{5.185}$$

Finally, by using Eq. (5.183) and by taking into account Eq. (5.184), we can calculate the effective Biot modulus η^* by

$$\begin{aligned}\eta^* = \Bigg\{ & c_1\left(\frac{1}{\eta^{(1)}} - 3\theta^{(1)}f^{(1)}\right) + c_2\left(\frac{1}{\eta^{(2)}} - 3\theta^{(2)}f^{(2)}\right) \\ & + 3c_1\left[\frac{h}{R\eta^{(0)}} - \theta^{(0)}\left(f^{(2)} + \frac{g^{(2)}}{R^3} - f^{(1)}\right)\right]\Bigg\}^{-1}.\end{aligned} \tag{5.186}$$

Table 5.2: Material parameters used for the analysis

Material parameters	Inclusion	Interphase	Matrix
Young modulus (Pa)	$E^{(1)} = 9\times10^6$	$E^{(0)} = 5\times10^3$ to 5×10^9	$E^{(1)} = 2\times10^6$
Poisson's ratio	$\nu^{(1)} = 0.4$	$\nu^{(0)} = 0.35$	$\nu^{(2)} = 0.3$
Biot's coefficient	$\theta^{(1)} = 0.8$	$\theta^{(0)} = 0.5$	$\theta^{(2)} = 0.45$
Biot's modulus (Pa)	$\eta^{(1)} = 2\times10^6$	$\eta^{(0)} = 2\times10^3$ to 2×10^9	$\eta^{(2)} = 10^6$

To numerically illustrate the results obtained above for the effective poroelastic properties of composites with general imperfect interfaces, we consider a composite consisting of a host matrix phase reinforced by spherical inclusions. The material properties of the inclusion, interphase, and matrix phases are given the same values as in the previous section and are provided in Table 5.2. In **Figs.** 5.10, 5.11, and 5.12, we plot the variations of the effective properties κ^*, θ^*, and η^* in terms of the volume fraction of inclusions c_1.

It can be seen from **Figs.** 5.10 and 5.12 that when the interphase is not very soft with respect

to the matrix and inclusion phases, due to the fact that the inclusion phase is stiffer than the matrix, the effective compressibility modulus κ^* and Biot's modulus η^* increase as the volume fraction of inclusions c_1 increases. This is because the effect of the imperfect interface on the effective properties is weak.

However, when the interphase is very soft with respect to the matrix and inclusion phases, **Figs.** 5.10 and 5.12 show that the effective compressibility modulus κ^* and Biot's modulus η^* decrease even as the volume fraction of inclusions c_1 increases. This indicates that the effect of the imperfect interface on the effective compressibility modulus κ^* and effective Biot's modulus η^* becomes important.

In contrast to the observations from **Figs.** 5.10 and 5.12, we can observe from **Fig.** 5.11 that, despite the variation in the interphase's properties, the effective Biot's coefficient θ^* always increase as the volume fraction of inclusions c_1 increases.

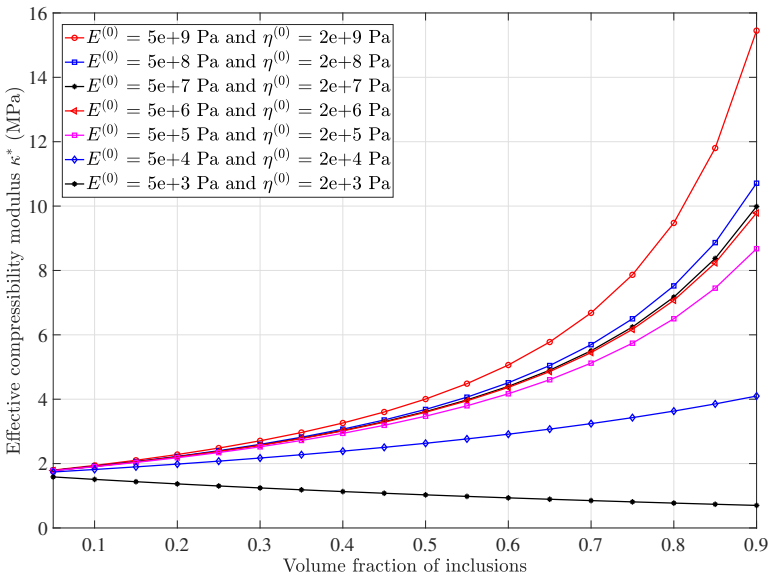

Figure 5.10: *The effective compressibilty modulus κ^* versus the volume fraction of inclusions c_1.*

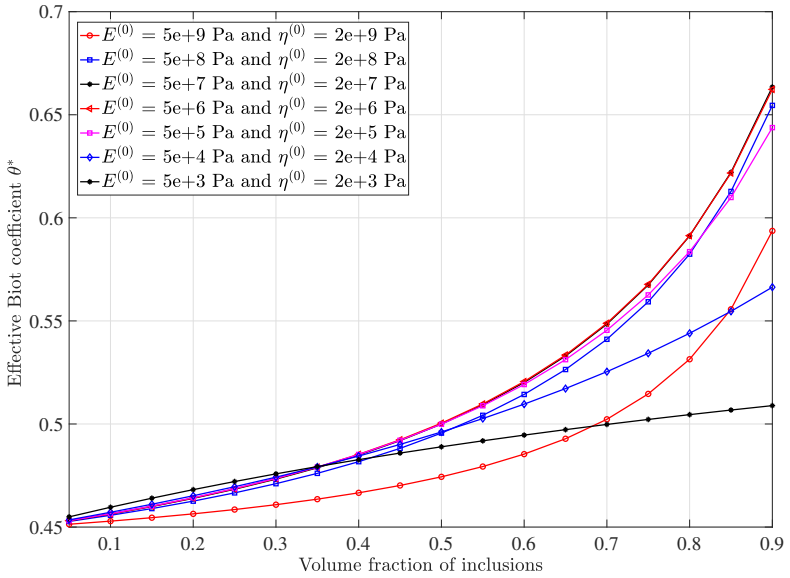

Figure 5.11: *The effective Biot's coefficient θ^* versus the volume fraction of inclusions c_1.*

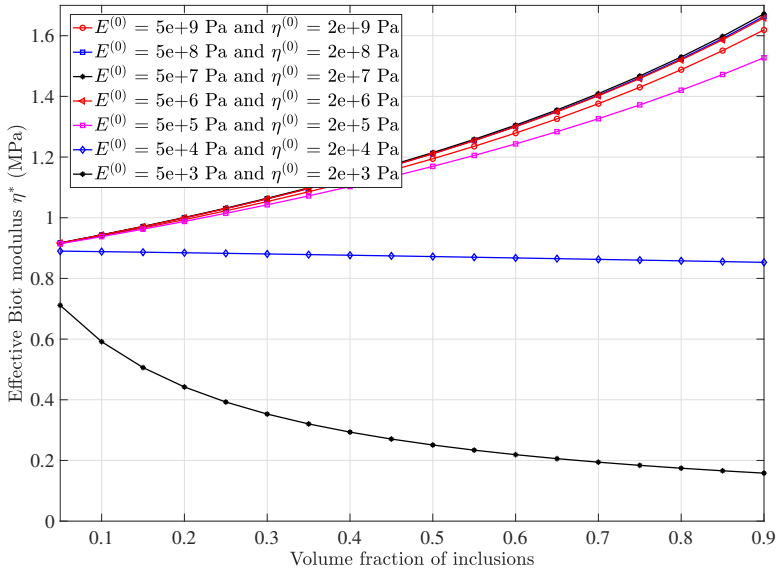

Figure 5.12: *The effective Biot's modulus η^* versus the volume fraction of inclusions c_1.*

5.5 Conclusion

In this work, we have successfully established a comprehensive imperfect interface model for poroelastic composites through theoretical analysis. Our approach involves deriving and expressing the discontinuities of the fields across the interface in a coordinate-free and compact manner. This has laid the groundwork for an efficient numerical method to analyze these models. By formulating the governing equations and weak forms for composites with imperfect interfaces, we provided a robust theoretical foundation for numerical implementation.

Utilizing the framework of the Extended Finite Element Method (XFEM), we introduced approximate interpolation functions enriched with appropriate functions to characterize both strong and weak discontinuities. The numerical solutions of the model were computed using a Matlab program, demonstrating the method's capability to handle coupled boundary conditions. The results of our numerical simulations were validated against analytical solutions, highlighting the applicability and generality of the imperfect interface model.

Our numerical method is not only capable of capturing strong and weak discontinuities but also serves as a powerful tool for homogenizing poroelastic composites and determining size-dependent effective properties of composites with complex microstructures. This work paves the way for future studies that could incorporate the effects of temperature, thereby addressing more realistic engineering scenarios where temperature influences material properties.

Further extensions of this study could explore composites with multiple irregular-shaped inclusions, moving beyond the single spherical inclusion embedded in an infinite matrix analyzed here. The theoretical and numerical framework developed in this work, supported by rigorous jump relations and effective use of the level set function for interface tracking, provides a solid basis for ongoing research.

Additionally, the application of the Generalized Self-Consistent Scheme (GSCS) underscores the broad relevance and utility of our methods in estimating the effective poroelastic properties of composites. This work contributes significantly to the field of composite materials characterization and analysis, offering both theoretical insights and practical numerical tools for handling complex material interfaces.

Conclusions

This thesis has made significant contributions to the modeling and analysis of shell-like structures in composite materials and structures, primarily in the following three aspects:

Firstly, this study develops a systematic and coordinate-independent asymptotic analysis method for characterizing scalar or vector functions within shell-like structures. The primary advantage of this approach lies in its independence from any specific coordinate system, facilitating straightforward conversion to Cartesian coordinates. Moreover, it allows for the representation of scalar or vector functions at arbitrary points within the shell-like structure, even when these functions are piecewise continuous. This adaptability ensures broad applicability in modeling plates, shells, and interfaces. By accurately capturing the intrinsic material properties of these structures, this innovative approach significantly enhances the precision and reliability of their modeling. Consequently, it offers a robust framework for advancing the understanding and simulation of complex structural behaviors, making it invaluable for future research in this field.

Secondly, this study has utilized variational methods to derive the comprehensive governing equations of motion and associated boundary conditions for plates in a unified and succinct framework. Building upon an asymptotic analysis that is free from dependency on any specific coordinate system and rooted in differential geometry, this approach effectively tackles the complexities arising from significant material anisotropy in plates. Moreover, this method significantly expands the classical plate theory's applicability to plates featuring interfaces of diverse geometries. By integrating variational principles with asymptotic techniques and differential geometry, this research not only enhances the theoretical foundations but also provides practical tools for modeling and analyzing complex plate structures. The systematic formulation of governing equations and boundary conditions underscores the method's robustness in capturing the intricate behavior of plates with varying material properties and interface configurations. Furthermore, a homogenization approach is established utilizing operators introduced

in the process of asymptotic expansion of vector functions and the continuity relations discussed for perfect interfaces.

Thirdly, this study has developed a general imperfect interface model with an accuracy of $O(h^2)$ for poroelastic composite materials. By specifically addressing critical scenarios such as extreme cases involving transition layer materials and isotropic constituents, this model greatly enhances the capabilities for modeling and practical application in the analysis of poroelastic composites. Integration of this model with advanced computational techniques such as XFEM and GSCS enables robust numerical simulations and homogenization analyses. This combined approach not only strengthens the theoretical foundation of poroelasticity but also provides a powerful framework for studying complex material interactions and structural behaviors in heterogeneous media.

Building upon the foundation laid in this research work, the following new research directions can be initiated:

Firstly, the asymptotic analysis method utilized in this study proves to be equally effective in the modeling of shells. By combining it with variational methods, one can systematically derive the governing equations and boundary conditions that govern the motion of shells in a unified and compact manner. This approach not only ensures a rigorous theoretical foundation but also facilitates the efficient computation of shell behaviors under various conditions. The integration of asymptotic analysis and variational techniques enables a comprehensive exploration of shell dynamics, addressing complex interactions between geometry, material properties, and external forces.

Secondly, in Chapter 3, which focuses on plate theory, has primarily examined examples characterized by linear behavior-specifically, small deflections and modest rotational angles. However, it is essential to extend our analysis and validation to encompass scenarios involving large deflections or significant rotational angles. The nonlinear behavior exhibited by plates under substantial deformations necessitates a more comprehensive investigation. To address these challenges, a rigorous exploration of the nonlinear aspects of plate mechanics is imperative. This involves revisiting the fundamental equations governing plate deformation to accurately capture nonlinear effects, such as deriving normal vectors pertaining to the mid-surface and orthogonal projection operators, alongside various geometric equations involving deformation metrics. Furthermore, the validation of theoretical predictions through experimental or numerical simu-

lations is crucial to ensuring the reliability and applicability of the proposed models under real-world conditions. By enhancing our understanding of plate mechanics under large deflections and rotations, we contribute to advancing structural analysis and design methodologies, thereby fostering innovation in engineering applications. Furthermore, the interface models established in this study are linear. However, when a nonlinear intermediate phase exists between nonlinear phases, the derivation of interface models remains largely unresolved. Extending the methods developed in this paper to address this issue represents a critically important research direction. Additionally, this chapter discusses plate modeling starting with the elastic field, which is the most fundamental physical model, primarily focusing on the deformation and stress distribution of materials under external forces. However, in practical applications, materials and structures are subjected not only to mechanical forces but also to other physical fields such as electric, magnetic, and thermal fields. Therefore, plate modeling needs to be extended to multi-field coupling, for example, considering piezoelectric and flexoelectric effects. This requires incorporating multi-field coupling physical models, expanding the constitutive relations of materials to include electric fields and electric displacement, and formulating coupled governing equations through asymptotic and variational methods. This approach allows for a more accurate representation of the multi-physical interactions in engineering applications, providing a theoretical foundation for the design and optimization of multifunctional materials and structures.

Thirdly, in Chapter 2, the asymptotic expansions of the physical fields in shell-like structures have focused on linear geometric and constitutive equations. These developments can be extended to nonlinear scenarios, particularly within the framework of large deformations. The linear geometric and constitutive equations discussed provide a foundational understanding applicable to initial analyses. However, for practical applications involving shell-like structures experiencing significant deformations, nonlinear formulations are essential. Extending the asymptotic expansions to incorporate nonlinear geometric effects and material behavior under large deformation conditions is crucial for accurately predicting the structural response. By advancing towards nonlinear asymptotic analyses, we can better capture complex phenomena such as geometric nonlinearity and material plasticity, which are pivotal in engineering design and structural integrity assessments. This progression enhances our capability to model and analyze shell-like structures more realistically, thereby facilitating advancements in the field of structural mechanics and design optimization.

Furthermore, integrating these established models with advanced numerical methods remains a crucial area of research. For example, combining finite element methods and proposing suitable elements such as plate, shell, or interface elements to streamline analysis is imperative. This approach represents a pivotal advancement in enhancing the computational efficiency and accuracy of structural and material simulations. By utilizing and extending advanced numerical methods, we can broaden the applicability of the developed models to effectively address real-world complexities. This integration not only enhances the predictive capabilities of structural analysis but also fosters exploration into innovative design possibilities across engineering applications.

Appendix

Appendix A: The expression of the material parameters c_i.

The explicit expressions of the material parameters c_i in the isotropic case, derived in chapter 5.1.4, are as follows:

$$
\begin{aligned}
c_1 &= \frac{2\mu^{(2)}-3\kappa^{(2)}}{4\mu^{(2)}+3\kappa^{(2)}}+\frac{2\mu^{(1)}-3\kappa^{(1)}}{4\mu^{(1)}+3\kappa^{(1)}}-2\frac{2\mu^{(0)}-3\kappa^{(0)}}{4\mu^{(0)}+3\kappa^{(0)}},\\
c_2 &= \frac{6}{4\mu^{(0)}+3\kappa^{(0)}}-\frac{3}{4\mu^{(2)}+3\kappa^{(2)}}-\frac{3}{4\mu^{(1)}+3\kappa^{(1)}},\\
c_3 &= \frac{2}{\mu^{(0)}}-\frac{2}{\mu^{(2)}}-\frac{2}{\mu^{(1)}},\\
c_4 &= \frac{3\theta^{(2)}}{4\mu^{(2)}+3\kappa^{(2)}}+\frac{3\theta^{(1)}}{4\mu^{(1)}+3\kappa^{(1)}}-\frac{6\theta^{(0)}}{4\mu^{(0)}+3\kappa^{(0)}},\\
c_5 &= 2\mu^{(2)}+2\mu^{(1)}-4\mu^{(0)},\\
c_6 &= \frac{2\mu^{(2)}(2\mu^{(2)}-3\kappa^{(2)})}{4\mu^{(2)}+3\kappa^{(2)}}+\frac{2\mu^{(1)}(2\mu^{(1)}-3\kappa^{(1)})}{4\mu^{(1)}+3\kappa^{(1)}}-\frac{4\mu^{(0)}(2\mu^{(0)}-3\kappa^{(0)})}{4\mu^{(0)}+3\kappa^{(0)}},\\
c_7 &= \frac{6\mu^{(2)}\theta^{(2)}}{4\mu^{(2)}+3\kappa^{(2)}}+\frac{6\mu^{(1)}\theta^{(1)}}{4\mu^{(1)}+3\kappa^{(1)}}-\frac{12\mu^{(0)}\theta^{(0)}}{4\mu^{(0)}+3\kappa^{(0)}},\\
c_8 &= \frac{1}{K^{(2)}}+\frac{1}{K^{(1)}}-\frac{2}{K^{(0)}},\\
c_9 &= 2K^{(0)}-K^{(1)}-K^{(2)},\\
c_{10} &= 2\theta^{(0)}-\theta^{(2)}-\theta^{(1)},\\
c_{11} &= \frac{2}{\eta^{(0)}}-\frac{1}{\eta^{(1)}}-\frac{1}{\eta^{(2)}}.
\end{aligned}
\tag{A.1}
$$

Appendix B: The effective coefficient appearing in equation Eq. (5.136).

$$\tilde{\eta} = \frac{2}{\eta^{(0)}} - \frac{1}{\eta^{(1)}} - \frac{1}{\eta^{(2)}}, \quad \bar{k}_{nn} = \left(\frac{1}{k_{nn}^{(2)}} + \frac{1}{k_{nn}^{(1)}} - \frac{2}{k_{nn}^{(0)}} \right)^{-1},$$
$$\tilde{\theta} = 2\theta^{(0)} - \theta^{(1)} - \theta^{(2)}, \quad \tilde{\mathbf{D}} = 2\mathbf{D}^{(0)} - \mathbf{D}^{(1)} - \mathbf{D}^{(2)}, \tag{B.1}$$
$$\tilde{\mathbf{s}} = 2\mathbf{s}^{(0)} - \mathbf{s}^{(1)} - \mathbf{s}^{(2)}.$$

Appendix C: The derivation of Eq. (5.179)

First, the free energy of Ω^{∞} containing a composite sphere takes, by definition, the following form

$$\begin{aligned} U =& \frac{1}{2}\int_{\Omega^{\infty}} \left(\varepsilon_{ij} L_{ijkl} \varepsilon_{kl} + 2\theta \varepsilon_{kk} \beta_0 - \frac{\beta_0^2}{\eta} \right) dv + \frac{1}{2}\int_S [\![\sigma_{ij} u_i]\!] n_j ds \\ &+ \frac{1}{2}\int_S \left(\theta^{(0)} \beta_0 [\![u_i]\!] n_i - \frac{h\beta_0^2}{\eta^{(0)}} \right) ds. \end{aligned} \tag{C-1}$$

where the second and third terms on the right hand side is related to the discontinuities of the stress and displacement vectors across the imperfect interface S_0.

Next, using the constitutive law equation (5.1), we calculate $2(U-U_0)$ as follows:

$$\begin{aligned} 2(U-U_0) &= \int_{\Omega^{\infty}} \left(\sigma_{ij}\varepsilon_{ij} + \theta\varepsilon_{kk}\beta_0 - \frac{\beta_0^2}{\eta} \right) dv + \int_S [\![\sigma_{ij}u_i]\!] n_j ds + \int_S \left(\theta^{(0)}\beta_0 [\![u_i]\!] n_i - \frac{h\beta_0^2}{\eta^{(0)}} \right) ds \\ &- \frac{1}{2}\int_{\Omega^{\infty}} \left(\sigma_{ij}^* \varepsilon_{ij}^* + \theta \varepsilon_{kk}^* \beta_0 - \frac{\beta_0^2}{\eta^*} \right) dv \\ &= \int_{\Omega^{\infty}} \left(\sigma_{ij} u_{i,j} + \theta\varepsilon_{kk}\beta_0 - \frac{\beta_0^2}{\eta} \right) dv + \int_S [\![\sigma_{ij}u_i]\!] n_j ds + \int_S \left(\theta^{(0)}\beta_0 [\![u_i]\!] n_i - \frac{h\beta_0^2}{\eta^{(0)}} \right) ds \\ &- \frac{1}{2}\int_{\Omega^{\infty}} \left(\sigma_{ij}^*, u_{i,j}^* + \theta \varepsilon_{kk}^* \beta_0 - \frac{\beta_0^2}{\eta^*} \right) dv. \end{aligned} \tag{C-2}$$

Applying the integration by parts, divergence theorem, and equilibrium equation (5.3), it can be

shown from equation (C-2) that

$$\begin{aligned} 2(U-U_0) &= \int_\Omega \left(\sigma_{ij}u^*_{i,j} - \sigma^*_{ij}u_{i,j}\right) dv + \int_S \left([\![\sigma_{ij}]\!]n_j u^*_i - \sigma^*_{ij}n_j[\![u_i]\!]\right) ds \\ &+ \int_\Omega \left(\theta\varepsilon_{kk}\beta_0 - \frac{\beta_0^2}{\eta} - \theta^*\varepsilon^*_{kk}\beta_0 + \frac{\beta_0^2}{\eta^*}\right) dv + \int_{\partial\Omega^\infty} (\sigma_{ij}+\sigma^*_{ij})(u_i - u^*_i)n_j ds \\ &+ \int_{\Omega^\infty\setminus\Omega} \left(\sigma_{ij}\varepsilon^*_{ij} + \theta\varepsilon_{kk}\beta_0 - \frac{\beta_0^2}{\eta} - \sigma^*_{ij}\varepsilon_{ij} - \theta^*\varepsilon^*_{kk}\beta_0 + \frac{\beta_0^2}{\eta^*}\right) dv \\ &+ \int_S \left(\theta^{(0)}\beta_0[\![u_i]\!]n_i - \frac{h\beta_0^2}{\eta^{(0)}}\right) ds. \end{aligned} \tag{C-3}$$

By accounting for the boundary conditions (5.141) and (5.142), it is immediate that

$$\int_{\partial\Omega^\infty} (\sigma_{ij}+\sigma^*_{ij})(u_i - u^*_i)n_j ds = 0. \tag{C-4}$$

It follows from the integration by parts, divergence theorem and equilibrium equation (5.3) that

$$\int_\Omega \left(\sigma_{ij}u^*_{i,j} - \sigma^*_{ij}u_{i,j}\right) dv + \int_S \left([\![\sigma_{ij}]\!]n_j u^*_i - \sigma^*_{ij}n_j[\![u_i]\!]\right) ds = \int_{\partial\Omega} (\mathbf{t}\cdot\mathbf{u}^* - \mathbf{t}^*\cdot\mathbf{u}) ds. \tag{C-5}$$

Due to the fact that the effective outside medium $\Omega^\infty \setminus \Omega$ is homogeneous with the effective constitutive laws given by

$$\boldsymbol{\sigma}^* = \left(\kappa^* - \frac{2}{3}\mu^*\right)\mathrm{tr}(\boldsymbol{\varepsilon}^*)\mathbf{I} + 2\mu^*\boldsymbol{\varepsilon}^* + \theta^*\beta_0\mathbf{I}, \quad \boldsymbol{\sigma} = \left(\kappa^* - \frac{2}{3}\mu^*\right)\mathrm{tr}(\boldsymbol{\varepsilon})\mathbf{I} + 2\mu^*\boldsymbol{\varepsilon} + \theta^*\beta_0\mathbf{I}, \tag{C-6}$$

and $\theta = \theta^*$, it can be demonstrated that

$$\int_{\Omega^\infty\setminus\Omega} \left(\sigma_{ij}\varepsilon^*_{ij} + \theta\varepsilon_{kk}\beta_0 - \frac{\beta_0^2}{\eta} - \sigma^*_{ij}\varepsilon_{ij} - \theta^*\varepsilon^*_{kk}\beta_0 + \frac{\beta_0^2}{\eta^*}\right) dv = 0. \tag{C-7}$$

Finally, by introducing equations (C-4)-(C-7) into equation (C-3), we obtain

$$\begin{aligned} 2(U-U_0) = &\int_{\partial\Omega} (\mathbf{t}\cdot\mathbf{u}^* - \mathbf{t}^*\cdot\mathbf{u}) ds + \int_\Omega \left(\theta\varepsilon_{kk}\beta_0 - \frac{\beta_0^2}{\eta} - \theta^*\varepsilon^*_{kk}\beta_0 + \frac{\beta_0^2}{\eta^*}\right) dv \\ &+ \int_S \left(\theta^{(0)}\beta_0[\![u_i]\!]n_i - \frac{h\beta_0^2}{\eta^{(0)}}\right) ds. \end{aligned} \tag{C-8}$$

This equation allows us to express the free energy U of the effective medium with the composite sphere as specified in equation (5.179).

Bibliography

[1] Achenbach, J. D., & Zhu, H. (1989). Effect of interfacial zone on mechanical behavior and failure of fiber-reinforced composites. *Journal of the Mechanics and Physics of Solids*, *37*, 381–393.

[2] Adamson, A. W., Gast, A. P. et al. (1967). *Physical chemistry of surfaces* volume 150. Interscience Publishers New York.

[3] Aghalovyan, L. A. (2015). *Asymptotic theory of anisotropic plates and shells*. World Scientific.

[4] Altenbach, H. (1998). Theories for laminated and sandwich plates: A review. *Mechanics of Composite Materials*, *34*, 243–252.

[5] Altenbach, H., & Eremeyev, V. A. (2011). *Shell-like structures: non-classical theories and applications* volume 15. Springer Science & Business Media.

[6] Barbero, E. J., Reddy, J. N., & Teply, J. (1990). An accurate determination of stresses in thick laminates using a generalized plate theory. *International Journal for Numerical Methods in Engineering*, *29*, 1–14.

[7] Belytschko, T., Krongauz, Y., Organ, D., Fleming, M., & Krysl, P. (1996). Meshless methods: an overview and recent developments. *Computer Methods in Applied Mechanics and Engineering*, *139*, 3–47.

[8] Benveniste, Y. (1985). The effective mechanical behaviour of composite materials with imperfect contact between the constituents. *Mechanics of Materials*, *4*, 197–208.

[9] Benveniste, Y. (2006). A general interface model for a three-dimensional curved thin anisotropic interphase between two anisotropic media. *Journal of the Mechanics and Physics of Solids*, *54*, 708–734.

[10] Benveniste, Y. (2006). An o (hn) interface model of a three-dimensional curved interphase in conduction phenomena. *Proceedings of the Royal Society A: Mathematical, Physical and Engineering Sciences*, *462*, 1593–1617.

[11] Benveniste, Y., & Baum, G. (2007). An interface model of a graded three-dimensional anisotropic curved interphase. *Proceedings of the Royal Society A: Mathematical, Physical and Engineering Sciences*, *463*, 419–434.

[12] Benveniste, Y., & Miloh, T. (2001). Imperfect soft and stiff interfaces in two-dimensional elasticity. *Mechanics of Materials*, *33*, 309–323.

[13] Bövik, P. (1994). On the modelling of thin interface layers in elastic and acoustic scattering problems. *The Quarterly Journal of Mechanics and Applied Mathematics*, *47*, 17–42.

[14] Bravo-Castillero, J., Rodríguez-Ramos, R., Mechkour, H., Otero, J. A., & Sabina, F. J. (2008). Homogenization of magneto-electro-elastic multilaminated materials. *The Quarterly Journal of Mechanics & Applied Mathematics*, *61*, 311–332.

[15] Caillerie, D. (1978). Sur le comportement limite d'une inclusion mince de grande rigidité. *Comptes Rendus de l'Académie des Sciences de Paris A*, *287*, 675–678.

[16] Carrera, E. (1997). Cz requirements-models for the two dimensional analysis of multilayered structures. *Composite Structures*, *37*, 373–383.

[17] Carrera, E. (2003). Historical review of zig-zag theories for multilayered plates and shells. *Applied Mechanics Reviews*, *56*, 287–308.

[18] Carrera, E., & Brischetto, S. (2009). A survey with numerical assessment of classical and refined theories for the analysis of sandwich plates. *Applied Mechanics Reviews*, *62*.

[19] Carrera, E., Brischetto, S., & Nali, P. (2011). *Plates and shells for smart structures: classical and advanced theories for modeling and analysis* volume 36. John Wiley & Sons.

[20] Cauchy, A.-L. (1828). Sur l'equilibre et le mouvement d'une plaque solide. *Exercises de Matematique*, *3*, 328–355.

[21] Cermelli, P., & Gurtin, M. E. (1994). The dynamics of solid-solid phase transitions 2. incoherent interfaces. *Archive for Rational Mechanics and Analysis*, *127*, 41–99.

[22] Chen, T. Y., & Dvorak, G. J. (2006). Fibrous nanocomposites with interface stress: Hill's and levin's connections for effective moduli. *Applied Physics Letters*, *88*.

[23] Chen, T. Y., Dvorak, G. J., & Yu, C. C. (2007). Size-dependent elastic properties of unidirectional nano-composites with interface stresses. *Acta Mechanica*, *188*, 39–54.

[24] Chen, T. Y., Dvorak, G. J., & Yu, C. C. (2007). Solids containing spherical nano-inclusions with interface stresses: effective properties and thermal–mechanical connections. *International Journal of Solids and Structures*, *44*, 941–955.

[25] Chen, Z. R., Yu, S. W., Meng, L., & Lin, Y. (2002). Effective properties of layered magneto-electro-elastic composites. *Composite Structures*, *57*, 177–182.

[26] Cho, M., & Parmerter, R. R. (1993). Efficient higher order composite plate theory for general lamination configurations. *AIAA Journal*, *31*, 1299–1306.

[27] Christensen, R. M., & Lo, K. (1979). Solutions for effective shear properties in three phase sphere and cylinder models. *Journal of the Mechanics and Physics of Solids*, *27*, 315–330.

[28] Ciarlet, P. G. (2005). An introduction to differential geometry with applications to elasticity. *Journal of Elasticity*, *78*, 1–215.

[29] Cuenot, S., Frétigny, C., Demoustier-Champagne, S., & Nysten, B. (2004). Surface tension effect on the mechanical properties of nanomaterials measured by atomic force microscopy. *Physical Review B*, *69*, 165410.

[30] Di Sciuva, M. (1986). Bending, vibration and buckling of simply supported thick multilayered orthotropic plates: an evaluation of a new displacement model. *Journal of Sound and Vibration*, *105*, 425–442.

[31] Dingreville, R., Qu, J. M., & Cherkaoui, M. (2005). Surface free energy and its effect on the elastic behavior of nano-sized particles, wires and films. *Journal of the Mechanics and Physics of Solids*, *53*, 1827–1854.

[32] Discher, D. E., Boal, D. H., & Boey, S. K. (1998). Simulations of the erythrocyte cytoskeleton at large deformation. ii. micropipette aspiration. *Biophysical Journal*, *75*, 1584–1597.

[33] Do Carmo, M. P. (2016). *Differential geometry of curves and surfaces: revised and updated second edition*. Courier Dover Publications.

[34] Duan, H. L., Wang, J. X., Huang, Z. P., & Karihaloo, B. L. (2005). Eshelby formalism for nano-inhomogeneities. *Proceedings of the Royal Society A: Mathematical, Physical and Engineering Sciences*, *461*, 3335–3353.

[35] Duan, H. L., Wang, J. X., Huang, Z. P., & Karihaloo, B. L. (2005). Size-dependent effective elastic constants of solids containing nano-inhomogeneities with interface stress. *Journal of the Mechanics and Physics of Solids*, *53*, 1574–1596.

[36] Duan, H. L., Wang, J. X., Huang, Z. P., & Karihaloo, B. L. (2005). Size-dependent effective elastic constants of solids containing nano-inhomogeneities with interface stress. *Journal of the Mechanics and Physics of Solids*, *53*, 1574–1596.

[37] Duan, H. L., Wang, J. X., & Karihaloo, B. L. (2009). Theory of elasticity at the nanoscale. *Advances in applied mechanics*, *42*, 1–68.

[38] Eshelby, J. D. (1956). The continuum theory of lattice defects. In *Solid State Physics* (pp. 79–144). Elsevier volume 3.

[39] Euler, L. (1766). De motu vibratorio tympanorum. *Novi Commentarii Academiae Scientiarum Petropolitanae*, (pp. 243–260).

[40] Fan, J. R., & Ye, J. Q. (1990). An exact solution for the statics and dynamics of laminated thick plates with orthotropic layers. *International Journal of Solids and Structures*, *26*, 655–662.

[41] Fish, J., & Belytschko, T. (2007). *A first course in finite elements* volume 1. Wiley New York.

[42] Ganghoffer, J. F., & Schultz, J. (1996). Geometrically non-linear modelling of contact problems involving thin elastic layers. *Journal of the Mechanics and Physics of Solids*, *44*, 1103–1127.

[43] Gay, D. (2022). *Composite materials: design and applications*. CRC Press.

[44] Germain, S. (1826). *Remarques sur la nature, les bornes et l'éntendue de la question des surfaces élastiques, et équation générale de ces surfaces*. Huzard-Courcier.

[45] Geymonat, G., Krasucki, F., & Lenci, S. (1999). Mathematical analysis of a bonded joint with a soft thin adhesive. *Mathematics and Mechanics of Solids*, *4*, 201–225.

[46] Giordano, S., Goueygou, M., Tiercelin, N., Talbi, A., Pernod, P., & Preobrazhensky, V. (2014). Magneto-electro-elastic effective properties of multilayered artificial multiferroics with arbitrary lamination direction. *International Journal of Engineering Science*, *78*, 134–153.

[47] Grenestedt, J. L., & Bassinet, F. (2000). Influence of cell wall thickness variations on elastic stiffness of closed-cell cellular solids. *International Journal of Mechanical Sciences*, *42*, 1327–1338.

[48] Gu, S. T., & He, Q. C. (2011). Interfacial discontinuity relations for coupled multifield phenomena and their application to the modeling of thin interphases as imperfect interfaces. *Journal of the Mechanics and Physics of Solids*, *59*, 1413–1426.

[49] Gu, S. T., & He, Q. C. (2015). Compact closed-form micromechanical expressions for the effective uncoupled and coupled linear properties of layered composites. *Philosophical Magazine*, *95*, 2793–2816.

[50] Gu, S. T., Liu, J. T., & He, Q. C. (2014). Piezoelectric composites: Imperfect interface models, weak formulations and benchmark problems. *Computational Materials Science*, *94*, 182–190.

[51] Gu, S. T., Liu, J. T., & He, Q. C. (2014). The strong and weak forms of a general imperfect interface model for linear coupled multifield phenomena. *International Journal of Engineering Science*, *85*, 31–46.

[52] Gurtin, M. E. (1993). The dynamics of solid-solid phase transitions 1. coherent interfaces. *Archive for Rational Mechanics and Analysis*, *123*, 305–335.

[53] Gurtin, M. E. (1993). *Thermomechanics of evolving phase boundaries in the plane*.

[54] Gurtin, M. E. (1999). *Configurational forces as basic concepts of continuum physics* volume 137. Springer Science & Business Media.

[55] Gurtin, M. E., & Murdoch, A. I. (1975). A continuum theory of elastic material surfaces. *Archive for Rational Mechanics and Analysis*, *57*, 291–323.

[56] Gurtin, M. E., Weissmüller, J., & Larche, F. (1998). A general theory of curved deformable interfaces in solids at equilibrium. *Philosophical Magazine A*, *78*, 1093–1109.

[57] Hadamard, J. (1903). *Leçons sur la propagation des ondes et les équations de l'hydrodynamique*. Hermann, Paris.

[58] Hashin, Z. (1990). Thermoelastic properties and conductivity of carbon/carbon fiber composites. *Mechanics of Materials*, *8*, 293–308.

[59] Hashin, Z. (1991). The spherical inclusion with imperfect interface. *Journal of Applied Mechanics*, *58*, 444–449.

[60] Hashin, Z. (1992). Extremum principles for elastic heterogenous media with imperfect interfaces and their application to bounding of effective moduli. *Journal of the Mechanics and Physics of Solids*, *40*, 767–781.

[61] Hashin, Z. (2001). Thin interphase/imperfect interface in conduction. *Journal of Applied Physics*, *89*, 2261–2267.

[62] Hashin, Z. (2002). Thin interphase/imperfect interface in elasticity with application to coated fiber composites. *Journal of the Mechanics and Physics of Solids*, *50*, 2509–2537.

[63] He, Q. C. (2006). *Mécanique de l'interface*. Cours de DEA de l'Université Gustave Eiffel.

[64] He, Q. C., & Curnier, A. (1995). A more fundamental approach to damaged elastic stress-strain relations. *International Journal of Solids and Structures*, *32*, 1433–1457.

[65] He, Q. C., & Feng, Z. Q. (2012). Homogenization of layered elastoplastic composites: Theoretical results. *International journal of non-linear mechanics*, *47*, 367–376.

[66] He, Q. C., Telega, J. J., & Curnier, A. (1996). Unilateral contact of two solids subject to large deformations: formulation and existence results. *Proceedings of the Royal Society of London. Series A: Mathematical, Physical and Engineering Sciences*, *452*, 2691–2717.

[67] Hencky, H. (1921). Der spanngszustand in rechteckigen platten (diss.), z. *Angew Math und Mech*, *1*.

[68] Hill, R. (1961). Discontinuity relations in mechanics of solids. *Progress in Solid Mechanics*, *2*, 245–276.

[69] Hill, R. (1983). Interfacial operators in the mechanics of composite media. *Journal of the Mechanics and Physics of Solids*, *31*, 347–357.

[70] Huber, M. T. (1929). *Probleme der Statik technisch wichtiger orthotroper Platten*.

[71] Hutchinson, J. R. (2001). Shear coefficients for timoshenko beam theory. *Journal of Applied Mechanics*, *68*, 87–92.

[72] Huy, H. P., & Sánchez-Palencia, E. (1974). Phénomčnes de transmission ā travers des couches minces de conductivitéélevée. *Journal of Mathematical Analysis and Applications*, *47*, 284–309.

[73] Ibach, H. (2006). *Physics of surfaces and interfaces* volume 12. Springer.

[74] Kapania, R. K., & Raciti, S. (1989). Recent advances in analysis of laminated beams and plates. part i-sheareffects and buckling. *AIAA Journal*, *27*, 923–935.

[75] Kármán, T. V. (1907). Festigkeitsprobleme im maschinenbau. *Encycl der Math Wiss*, (pp. 311–385).

[76] Kelvin, W. T. B., & Tait, P. G. (1888). *Treatise on Natural Philosophy* volume 1. At the University Press.

[77] Kim, J. Y. (2011). Micromechanical analysis of effective properties of magneto-electro-thermo-elastic multilayer composites. *International Journal of Engineering Science*, *49*, 1001–1018.

[78] Kirchhoff, G. (1850). Über das gleichgewicht und die bewegung einer elastischen scheibe. *Journal für die reine und angewandte Mathematik (Crelles Journal)*, *1850*, 51–88.

[79] Klarbring, A. (1991). Derivation of a model of adhesively bonded joints by the asymptotic expansion method. *International Journal of Engineering Science*, *29*, 493–512.

[80] Klarbring, A., & Movchan, A. B. (1998). Asymptotic modelling of adhesive joints. *Mechanics of Materials*, *28*, 137–145.

[81] Lagrange, J. L. (1828). Note communiquée aux commissaires pour le prix de la surface élastique décembre 1811. *Annales de Chimie et de Physique*, *39*, 1828.

[82] Le Quang, H., & He, Q. C. (2007). Size-dependent effective thermoelastic properties of nanocomposites with spherically anisotropic phases. *Journal of the Mechanics and Physics of Solids*, *55*, 1899–1931.

[83] Le Quang, H., & He, Q. C. (2008). Variational principles and bounds for elastic inhomogeneous materials with coherent imperfect interfaces. *Mechanics of Materials*, *40*, 865–884.

[84] Le Quang, H., & He, Q. C. (2009). Estimation of the effective thermoelastic moduli of fibrous nanocomposites with cylindrically anisotropic phases. *Archive of Applied Mechanics*, *79*, 225–248.

[85] Lee, K. H., Senthilnathan, N. R., Lim, S. P., & Chow, S. T. (1990). An improved zig-zag model for the bending of laminated composite plates. *Composite Structures*, *15*, 137–148.

[86] Lekhnitskii, S. G. (1968). *Anisotropic plates*. Technical Report Foreign Technology Div Wright-Patterson Afb Oh.

[87] Lemrabet, K., & LIONS, J. L. R. (1987). Le problème de ventcel pour le système de l'élasticité dans un domaine de ir3. *Comptes rendus de l'Académie des sciences. Série 1, Mathématique*, *304*, 151–154.

[88] Li, J. Y., & Dunn, M. L. (1998). Micromechanics of magnetoelectroelastic composite materials: average fields and effective behavior. *Journal of Intelligent Material Systems and Structures*, *9*, 404–416.

[89] Li, X., & Liu, D. (1995). Zigzag theory for composite laminates. *AIAA Journal*, *33*, 1163–1165.

[90] Librescu, L., & Hause, T. (2000). Recent developments in the modeling and behavior of advanced sandwich constructions: a survey. *Composite Structures*, *48*, 1–17.

[91] Lim, C. T., Zhou, E. H., & Quek, S. T. (2006). Mechanical models for living cells-a review. *Journal of Biomechanics*, *39*, 195–216.

[92] Liu, D., & Li, X. (1996). An overall view of laminate theories based on displacement hypothesis. *Journal of Composite Materials*, *30*, 1539–1561.

[93] Liu, J. T., Gu, S. T., & He, Q. C. (2015). A computational approach for evaluating the effective elastic moduli of non-spherical particle reinforced composites with interfacial displacement and traction jumps. *International Journal for Multiscale Computational Engineering*, *13*.

[94] Liu, J. T., Gu, S. T., Monteiro, E., & He, Q. C. (2014). A versatile interface model for thermal conduction phenomena and its numerical implementation by xfem. *Computational Mechanics*, *53*, 825–843.

[95] Liu, J. T., Xu, Y., & He, Q. C. (2020). Modeling and simulating the effects of a general imperfect interface in fibrous piezoelectric composites. *International Journal of Engineering Science*, *157*, 103379.

[96] Lo, K. H., Christensen, R. M., & Wu, E. M. (1977). A high-order theory of plate deformation-part 1: Homogeneous plates. *Journal of Applied Mechanics*, *45*, 663–668.

[97] Love, A. E. H. (1888). Xvi. the small free vibrations and deformation of a thin elastic shell. *Philosophical Transactions of the Royal Society of London.(A.)*, (pp. 491–546).

[98] Mindlin, R. D. (1951). Influence of rotatory inertia and shear on flexural motions of isotropic, elastic plates, .

[99] Mitrushchenkov, A., Chambaud, G., Yvonnet, J., & He, Q. C. (2010). Towards an elastic model of wurtzite aln nanowires. *Nanotechnology*, *21*, 255702.

[100] Moës, N., Cloirec, M., Cartraud, P., & Remacle, J. F. (2003). A computational approach to handle complex microstructure geometries. *Computer Methods in Applied Mechanics and Engineering*, *192*, 3163–3177.

[101] Mogilevskaya, S. G., Crouch, S. L., & Stolarski, H. K. (2008). Multiple interacting circular nano-inhomogeneities with surface/interface effects. *Journal of the Mechanics and Physics of Solids*, *56*, 2298–2327.

[102] Mogilevskaya, S. G., Crouch, S. L., Stolarski, H. K., & Benusiglio, A. (2010). Equivalent inhomogeneity method for evaluating the effective elastic properties of unidirectional multi-phase composites with surface/interface effects. *International Journal of Solids and Structures*, *47*, 407–418.

[103] Murakami, H. (1986). Laminated composite plate theory with improved in-plane responses, . *53*, 661–666.

[104] Murdoch, A. I. (1976). A thermodynamical theory of elastic material interfaces. *The Quarterly Journal of Mechanics and Applied Mathematics*, *29*, 245–275.

[105] Murdoch, A. I. (2005). Some fundamental aspects of surface modelling. *Journal of Elasticity*, *80*, 33–52.

[106] Noor, A. K., & Burton, W. S. (1989). Assessment of shear deformation theories for multilayered composite plates, . *42*, 1–13.

[107] Oswald, J., Gracie, R., Khare, R., & Belytschko, T. (2009). An extended finite element method for dislocations in complex geometries: Thin films and nanotubes. *Computer Methods in Applied Mechanics and Engineering*, *198*, 1872–1886.

[108] Pagano, N. J. (1969). Exact solutions for composite laminates in cylindrical bending. *Journal of Composite Materials*, *3*, 398–411.

[109] Pagano, N. J. (1970). Exact solutions for rectangular bidirectional composites and sandwich plates. *Journal of Composite Materials*, *4*, 20–34.

[110] Van der Poel, C. (1958). On the rheology of concentrated dispersions. *Rheologica Acta*, *1*, 198–205.

[111] Poisson, S.-D. (1828). *Mémoire sur l'équilibre et le mouvement des corps élastiques*. F. Didot.

[112] Qu, J. M. (1993). The effect of slightly weakened interfaces on the overall elastic properties of composite materials. *Mechanics of Materials*, *14*, 269–281.

[113] Reddy, J. N. (2003). *Mechanics of laminated composite plates and shells: theory and analysis*. CRC press.

[114] Reddy, J. N. (2006). *Theory and analysis of elastic plates and shells*. CRC Press.

[115] Reissner, E. (1945). The effect of transverse shear deformation on the bending of elastic plates. *Journal of Applied Mechanics*, *12*, A69–A77.

[116] Ren, J. G. (1986). Bending theory of laminated plate. *Composites Science and Technology*, *27*, 225–248.

[117] Ren, S. C., Liu, J. T., Gu, S. T., & He, Q. C. (2014). An xfem-based numerical procedure for the analysis of poroelastic composites with coherent imperfect interface. *Computational Materials Science*, *94*, 173–181.

[118] Sab, K., & Lebée, A. (2015). *Homogenization of heterogeneous thin and thick plates*. John Wiley & Sons.

[119] Sánchez-Palencia, E. (1970). Comportement limite d'un probleme de transmissiona travers une plaque faiblement conductrice. *Comptes Rendus de l'Académie des Sciences -Paris Series A*, *270*, 1026–1028.

[120] Sharma, P., & Ganti, S. (2004). Size-dependent eshelby's tensor for embedded nano-inclusions incorporating surface/interface energies. *Journal of Applied Mechanics*, *71*, 663–671.

[121] Sharma, P., Ganti, S., & Bhate, N. (2003). Effect of surfaces on the size-dependent elastic state of nano-inhomogeneities. *Applied Physics Letters*, *82*, 535–537.

[122] Shenoy, V. B. (2002). Size-dependent rigidities of nanosized torsional elements. *International Journal of Solids and Structures*, *39*, 4039–4052.

[123] Smith, J. C. (1974). Correction and extension of van der poel's method for calculating the shear modulus of a particulate composite. *Journal of research of the National Bureau of Standards. Section A, Physics and chemistry*, *78*, 355.

[124] Smith, J. C. (1975). Simplification of van der poel's formula for the shear modulus of a particulate composite. *Journal of research of the National Bureau of Standards. Section A, Physics and chemistry*, *79*, 419.

[125] Steigmann, D. J., & Ogden, R. (1999). Elastic surface-substrate interactions. *Proceedings of the Royal Society of London. Series A: Mathematical, Physical and Engineering Sciences*, *455*, 437–474.

[126] Sukumar, N., Chopp, D. L., Moës, N., & Belytschko, T. (2001). Modeling holes and inclusions by level sets in the extended finite-element method. *Computer Methods in Applied Mechanics and Engineering*, *190*, 6183–6200.

[127] Timoshenko, S. (1913). *Sur la stabilité des systèmes élastiques*. A. Dumas.

[128] Timoshenko, S. (1953). History of strength of materials mcgraw-hill book company. *Inc., New York/Toronto/London*, .

[129] Timoshenko, S. (1983). *History of strength of materials: with a brief account of the history of theory of elasticity and theory of structures*. Courier Corporation.

[130] Timoshenko, S., & Woinowsky-Krieger, S. (1959). *Theory of plates and shells* volume 2. McGraw-hill New York.

[131] Todt, M., Rammerstorfer, F. G., Hartmann, M. A., Paris, O., & Fischer, F. D. (2011). Shell-models for multi-layer carbon nano-particles. *Shell-like Structures: Non-classical Theories and Applications*, (pp. 585–602).

[132] Torquato, S. (2005). Theory of random heterogeneous materials. In *Handbook of Materials Modeling: Methods* (pp. 1333–1357). Springer.

[133] Truesdell, C. (2012). *Essays in the History of Mechanics*. Springer Science & Business Media.

[134] Ventsel, E., Krauthammer, T., & Carrera, E. (2002). Thin plates and shells: theory, analysis, and applications. *Appllied Mechanics Reviews*, *55*, B72–B73.

[135] Vol'mir, A. S. (1967). *A translation of flexible plates and shells*. Air Force Flight Dynamics Laboratory, Research and Technology Division, Air Force Systems Command.

[136] Von Kármán, T., Sechler, E. E., & Donnell, L. H. (1932). The strength of thin plates in compression. *Transactions of the American Society of Mechanical Engineers*, *54*, 53–56.

[137] Voronkova, E. B., Bauer, S. M., & Eriksson, A. (2011). Nonclassical theories of shells in application to soft biological tissues. *Shell-like Structures: Non-classical Theories and Applications*, (pp. 647–654).

[138] Wang, B. R., Liu, J. T., Gu, S. T., & He, Q. C. (2015). Numerical evaluation of the effective conductivities of composites with interfacial weak and strong discontinuities. *International Journal of Thermal Sciences*, *93*, 1–20.

[139] Wang, C. M. (1995). Timoshenko beam-bending solutions in terms of euler-bernoulli solutions. *Journal of Engineering Mechanics*, *121*, 763–765.

[140] Wang, X., Pan, E., Albrecht, J. D., & Feng, W. J. (2009). Effective properties of multilayered functionally graded multiferroic composites. *Composite Structures*, *87*, 206–214.

[141] Weissmüller, J., & Cahn, J. W. (1997). Mean stresses in microstructures due to interface stresses: A generalization of a capillary equation for solids. *Acta Materialia*, *45*, 1899–1906.

[142] Yang, F. (2004). Size-dependent effective modulus of elastic composite materials: spherical nanocavities at dilute concentrations. *Journal of Applied Physics*, *95*, 3516–3520.

[143] Yvonnet, J., He, Q. C., & Toulemonde, C. (2008). Numerical modelling of the effective conductivities of composites with arbitrarily shaped inclusions and highly conducting interface. *Composites Science and Technology*, *68*, 2818–2825.

[144] Yvonnet, J., He, Q. C., Zhu, Q. Z., & Shao, J. F. (2011). A general and efficient computational procedure for modelling the kapitza thermal resistance based on xfem. *Computational Materials Science*, *50*, 1220–1224.

[145] Yvonnet, J., Le Quang, H., & He, Q. C. (2008). An xfem/level set approach to modelling surface/interface effects and to computing the size-dependent effective properties of nanocomposites. *Computational Mechanics*, *42*, 119–131.

[146] Yvonnet, J., Le Quang, H., Toulemonde, C., & He, Q. C. (2008). Thermo-mechanical modelling of materials containing micro/nano inclusions with imperfect interfaces. *International Journal of Material Forming*, *1*, 1139–1142.

[147] Zhu, Q. Z., Gu, S. T., Yvonnet, J., Shao, J. F., & He, Q. C. (2011). Three-dimensional numerical modelling by xfem of spring-layer imperfect curved interfaces with applications to linearly elastic composite materials. *International Journal for Numerical Methods in Engineering*, *88*, 307–328.